

TECH LIBRARY KAFB, NM



0060102



NASA CR-891

LOAN

RI

# NASA CONTRACTOR REPORT

NASA CR-891

## ENGINEERING CRITERIA FOR SPACECRAFT CABIN ATMOSPHERE SELECTION

*by M. S. Bonura, W. G. Nelson, et al.*

*Prepared by*  
DOUGLAS AIRCRAFT COMPANY, INC.

Santa Monica, Calif.

*for*

## FEDD DOCUMENT

Note that this document bears the label "FEDD," an acronym for "FOR EARLY DOMESTIC DISSEMINATION." The FEDD label is affixed to documents that may contain information having high commercial potential.

The FEDD concept was developed as a result of the desire to maintain U.S. leadership in world trade markets and encourage a favorable balance of trade. Since the availability of tax-supported U.S. technology to foreign business interests could represent an unearned benefit, ~~research results that may have high commercial potential~~ are being distributed to U.S. industry in advance of general release.

The recipient of this report must treat the information it contains according to the conditions of the FEDD label on the front cover.



**ENGINEERING CRITERIA FOR SPACECRAFT CABIN  
ATMOSPHERE SELECTION**

By M. S. Bonura, W. G. Nelson, et al.

Distribution of this report is provided in the interest of information exchange. Responsibility for the contents resides in the author or organization that prepared it.

Prepared under Contract No. NASw-1371 by  
**DOUGLAS AIRCRAFT COMPANY, INC.**  
Santa Monica, Calif.

for

**NATIONAL AERONAUTICS AND SPACE ADMINISTRATION**

## FOREWORD

In this study, new test data were obtained and analyses completed to allow evaluation of the engineering criteria associated with the selection of space cabin atmospheres. The work described in this report was conducted by the Advance Biotechnology and Power Department of the Douglas Aircraft Company, Inc., Missile and Space Systems Division (MSSD), Santa Monica, California, under Contract NASw-1371. This project was completed for Walton L. Jones, M.D., Director of Biotechnology and Human Research Division and J. N. Pecoraro, under the direction of A. L. Ingelfinger of the Office of Advanced Research and Technology, Headquarters, the National Aeronautics and Space Administration, Washington, D.C. M. S. Bonura was the Principal Investigator and W. G. Nelson was Deputy Principal Investigator for Douglas, MSSD. Valuable assistance from W. W. Guy, Crew Systems Division, NASA Manned Spacecraft Center, is acknowledged.

Those who assisted in preparation of this report are as follows:

M. S. Bonura  
W. G. Nelson  
M. Adelberg  
R. S. Barker  
R. L. Blakely  
G. V. Colombo  
J. K. Jackson  
O. C. Ledford  
P. P. Mader  
E. S. Mills  
S. W. Nicol  
M. Price  
D. E. Richardson  
T. C. Secord  
B. N. Taylor  
E. C. Thomas  
M. M. Yakut



## ABSTRACT

Tests and analyses were completed to help evaluate the engineering influences of cabin atmosphere selection on the life support system design of advanced spacecraft. The following areas have been considered:

- **Comfort Zone:** Test data indicate that comfort zones are 5° to 7°F higher in helium-oxygen atmospheres than in nitrogen-oxygen.
- **Leakage:** Test data and theory indicate that the normal leakage from the space cabin involves a higher weight flow rate when nitrogen is the diluent. In the event of an emergency puncture, an atmosphere with a helium diluent will have a more rapid pressure decay.
- **Airlock:** Systems analysis indicates a pump-down system for atmosphere conservation will be advantageous from a weight standpoint if used more than 3 to 6 times per mission.
- **Heat and Mass Transfer:** Data show that heat exchangers, condensers, and absorption beds will require approximately equal weight and power for equal heat loads and operating temperatures.
- **System Weight:** The overall effect of atmosphere selection on life support system penalty was evaluated for a typical orbital laboratory and comparative weights of systems using helium and nitrogen as atmospheric diluents are presented. At 7 psia design pressure, the He-O<sub>2</sub> system is 14 percent lighter than an equivalent N<sub>2</sub>-O<sub>2</sub> system.
- **Fire Propagation:** Data on ignition and combustion of cotton cloth and insulated wires under various typical atmospheres are included. Comparison of pure oxygen, N<sub>2</sub>-O<sub>2</sub> and He-O<sub>2</sub> atmospheres is covered. Increasing diluent concentration, in general, results in decreased burning rates. Increased oxygen partial pressure decreases ignition temperature.



## CONTENTS

FIGURES	ix
TABLES	xiii
NOMENCLATURE	xv
INTRODUCTION	xxi
SECTION 1 - SUMMARY	1
SECTION 2 - COMFORT ZONE	17
Comfort Zone Analytical Consideration	19
Comfort Zone Test Procedure	25
Data Correlation	31
Conclusions and Recommendations	40
References	42
SECTION 3 - LEAKAGE	43
Orifice Flow, Capillary Flow, and Laminar Pipe Flow Theory	45
Steady-State and Transient Leakage Test Procedure	57
Transient and Steady-State Leakage Data	57
Helium Leakage into Electronic Components	61
Leakage Penalty	71
Conclusions and Recommendations	75
References	79
SECTION 4 - AIRLOCK SYSTEM	81
Airlock System Operation, Usage, and Theory	86
Comparison of Airlock Penalty for Different Atmospheric Conditions and Airlock Designs	102
Conclusions and Recommendations	115
References	116
SECTION 5 - ATMOSPHERIC SUPPLY SYSTEM	117
High-Pressure Gaseous Storage	118
Supercritical Storage	118
Subcritical Storage	124
Conclusions and Recommendations	130
References	137
SECTION 6 - THE EFFECT OF ATMOSPHERE SELECTION ON COMPONENT HEAT AND MASS TRANSFER	139
Heat Exchanger and Condenser Evaluation	140
Heat Exchanger Theory	140
Heat Exchanger Pressure Drop	143
Heat Exchanger Test Description	144
Heat Exchanger Correlation Data	144
Heat Exchanger Penalty Comparison	146

Adsorption Bed Tests and Evaluation	151
Adsorption Bed Heat Transfer Theory	151
Adsorption Bed Mass Transfer Theory	153
Adsorption Bed Pressure Drop Theory	154
Adsorption Bed Test Description and Procedure	155
Adsorption Bed Data Correlation	157
Application of Experimental Data to Adsorption Bed Design	165
Conclusions and Recommendations	184
References	188
SECTION 7 - THE EFFECT OF ATMOSPHERE SELECTION ON LIFE SUPPORT SYSTEM PENALTY	189
Methodology for Penalty Evaluation	190
Atmospheric Supply and Pressurization System	190
Thermal Control System	190
Atmospheric Purification and Control System	201
Example Problem Comparing Life Support System Penalty for Different Cabin Atmospheres	202
Atmosphere Supply and Pressurization System	203
Atmosphere Purification System and Thermal Control System	203
Summary of Penalty Comparison for Different Atmospheres	215
Conclusions and Recommendations	215
References	219
SECTION 8 - COMPARISON OF ATMOSPHERES FOR FIRE PREVENTION	221
A Discussion of Fire Theory	223
Gravity and Convection Effects on Ignition	223
Low Gravity Burning Characteristics	232
Ignition and Burning Test Procedure and Data	239
Atmospheric Effect on Ignition Temperature	239
Atmospheric Effect on Ignition and Burning of Cloth in One g	243
Atmosphere Effects on Burning of Insulated Wire in One g	261
Null Gravity Fire Test Procedure and Data	267
Conclusions and Recommendations	278
References	281

## FIGURES

1-1	Comfort Temperature Data Comparison	2
1-2	Life Support System Weight Trend	7
1-3	Ignition Temperature for Cotton Cloth & Wire Insulation	10
1-4	Flame Propagation Rates Relative to Rate in Air at 14.7 psia	11
1-5	Representative Null Gravity Test of Cotton Cloth	13
1-6	Relative Time to Smoking and Burn-Through, Single Insulated Wire	14
1-7	Relative Time to Smoking and to Burn-Through, One Wire in Bundle of Insulated Wires	16
2-1	Insensible Heat Loss	21
2-2	Radiation Heat Loss	23
2-3	Effect of Gas Composition on Clothing Thermal Resistance	24
2-4	Comfort Simulator Configuration	26
2-5	Space Cabin Simulator Looking Toward Command Center	27
2-6	Comfort Simulator in the Space Cabin	28
2-7	Space Cabin Simulator Pressure Profile	29
2-8	Thermal Comfort Zone Representative Test Run	30
2-9	Comfort Temperature Data for Nitrogen-Oxygen Atmospheres	34
2-10	Comfort Temperature Data for Helium-Oxygen Atmosphere	35
2-11	Comfort Zones	36
2-12	Comfort Zones	37
2-13	Comfort Zones	38
3-1	Pressure Decay Characteristics	47
3-2	Outlet Pressure of Laminar Flow Leak	53
3-3	Leakage Rate From Laminar Flow Leak	54
3-4	Effect of Diluent Selection on Laminar Leakage Rate	55
3-5	Test Arrangement for Steady-State Leakage	58
3-6	Steady-State Leakage Data	60

3-7	Pressure Decay Test for 5 psia and 0.5-Inch Hole	62
3-8	Pressure Decay Data for 5 psia and 1.0-Inch Diameter Hole	63
3-9	Pressure Decay Data for 5 psia Pure Oxygen	64
3-10	Pressure Decay Data for 7 psia and 0.5-Inch Diameter Hole	65
3-11	Pressure Decay Data for 7 psia and 1.0-Inch Diameter Hole	66
3-12	Pressure Decay Test for 10 psia and 0.5-Inch Diameter Hole	67
3-13	Pressure Decay Data for 10 psia and 1.0-Inch Diameter Hole	68
3-14	Typical Temperature Decay During Pressure Decay Test	69
3-15	Flow Coefficients for Pressure Decay Tests	70
3-16	Representative Leakage Weight Penalty	73
3-17	Representative Leakage Weight Penalty	74
3-18	Safe Times for Cabin Pressure Decay	76
4-1	Representative Airlock Expendable Gas Systems	82
4-2	Representative Airlock Pump-Down Systems	83
4-3	Expendable-Gas Airlock System Penalty Including Cryogenic Storage Penalty	91
4-4	Average Airlock Pump Power Required	97
4-5	Maximum Airlock Pump Power Required	98
4-6	Ratio of Final Cabin Pressure to Initial Cabin Pressure	99
4-7	Final Cabin Temperature	100
5-1	High-Pressure Gas Storage-Gas Supply Subsystem Diagram	119
5-2	Weight Penalties of Spherical High-Pressure Oxygen and Nitrogen Tanks	120
5-3	Volume Penalties of Spherical High-Pressure Oxygen and Nitrogen Tanks	121
5-4	Volume and Weight Penalties of Spherical High-Pressure Helium Tanks	122
5-5	Supercritical Cryogenic Fluid Storage	125
5-6	Supercritical Oxygen Storage Penalty	126
5-7	Supercritical Nitrogen Storage Penalty	127
5-8	Estimated Heat Leaks for Supercritical Tanks	128
5-9	Supercritical Helium Storage Penalty	129
5-10	Two-Phase Storage With Vapor Delivery	131
5-11	Subcritical Oxygen Storage Penalty	132
5-12	Subcritical Nitrogen Storage Penalty	133
6-1	Correlated Heat Transfer Data for Heat Exchanger	145

6-2	Correlated Friction Data for Heat Exchanger	147
6-3	Heat Transfer Data for Silica-Gel and Zeolite Pellets	158
6-4	Mass Transfer Data for Zeolite Pellets	159
6-5	Zeolite Adsorption Bed Data for 14.7 psia Air	161
6-6	Pressure Drop Data for Davidson, Grade 40, 6-12 Mesh Silica-Gel	162
6-7	Pressure Drop Data for Linde, Type 5A, 1/8-Inch Zeolite Pellets	163
6-8	Fanning Friction Data for Silica-Gel and Zeolite Pellets	164
6-9	Heat or Mass Transfer in a Packed Bed	175
6-10	Carbon Dioxide Isotherm Test Data for Linde 5A, 1/16-Inch Diameter Pellets	178
6-11	CO <sub>2</sub> Loading for Molecular Sieve Example--Calculated using Figure 6-9	180
6-12	Weight of CO <sub>2</sub> Adsorbed Versus Bed Length for Molecular Sieve Example	182
7-1	Thermal and Atmospheric Control System	191
7-2	Single-Pass Crossflow Heat Exchanger Performance	192
7-3	Fan Overall Efficiency Versus Hydraulic Power	199
7-4	Fan Overall Weight Versus Volumetric Flow Rate	200
7-5	Cabin Thermal Control Weight and Power Requirements-- 5 psia O <sub>2</sub>	204
7-6	Cabin Thermal Control Weight and Power Requirements-- 5 psia N <sub>2</sub> -O <sub>2</sub>	205
7-7	Cabin Thermal Control Weight and Power Requirements-- 5 psia He-O <sub>2</sub>	206
7-8	Cabin Thermal Control Weight and Power Requirements-- 10 psia N <sub>2</sub> -O <sub>2</sub>	207
7-9	Cabin Thermal Control Weight and Power Requirements-- 10 psia He-O <sub>2</sub>	208
7-10	Heat Exchanger Outlet Temperature	214
7-11	Total Thermal Control Loop Weight Penalty	217
8-1	Cotton Cloth and Ignition Wire	224
8-2	Heating Rates of Wire and Cloth	225
8-3	Temperature Profiles (No Convection)	226
8-4	Gas Density Profiles (No Convection-Evolved Gases Considered Negligible)	228
8-5	Oxygen Concentration Profiles (No Convection, Neglecting Evolved Gases)	229

8-6	Oxygen Concentration Profiles (No Convection)	230
8-7	Ignition Process With No Convection Present	231
8-8	Temperature Profiles (Free and/or Forced Convection)	233
8-9	Oxygen Concentration Profiles (Free and/or Forced Convection)	234
8-10	Ignition Process With Convection Present	235
8-11	Variations of Critical Convective Velocity as a Function of Critical Gravitational Acceleration	240
8-12	Plate and Furnace Test Apparatus Inside the Space Cabin Simulator	241
8-13	First Ignition of Cotton Cloth Specimen	242
8-14	Minimum Ignition Temperatures of Specific Test Specimens	244
8-15	Ignition Temperature for Cotton Cloth and Wire Insulation	245
8-16	Average Minimum Ignition Temperatures	246
8-17	Test Schematic	247
8-18	Comparison of Ignition and Burning Time for Cotton Cloth in Various Atmospheric Compositions (Constant Wire Temperature)	250
8-19	Comparison of Ignition and Burning Time for Cotton Cloth in Various Atmospheric Compositions (Constant Power Input)	251
8-20	Effect of Increasing Diluent Partial Pressure on Flame Propagation Rate	254
8-21	Correlation of Flame Propagation Rate in Different Gas Mixtures	256
8-22	Burning Times of Cotton Cloth in Different Atmospheres With Free and Forced Convection	259
8-23	Bell Jar and Wire Test Apparatus	262
8-24	Smoking and Burn-Through of Single Insulated Wire in Different Atmospheres	264
8-25	Smoking and Burn-Through of an Exposed Wire in a Wire Bundle in Different Atmospheres	266
8-26	Zero Gravity Test Apparatus	268
8-27	Representative Null Gravity Test of Cotton Cloth	274

## TABLES

1-I	Mean Values of Steady State Leakage Data	3
1-II	Sources of Leakage	5
1-III	Heat Exchanger Data--Weight, Pressure Drop, and Power Ratios	8
2-I	Representative Data for Upper and Lower Limits and Comfort Zone for Each Subject as a Function of Atmospheric Composition, Pressure and CLO Value	32
2-II	Comfort Zone Test Conditions and Results	33
3-I	Ratio of Nitrogen-Oxygen to Helium-Oxygen Leak Rates by Weight for Sonic Flow	45
3-II	Ratio of Nitrogen-Oxygen to Helium-Oxygen Leak Rates by Weight of Capillary Flow	48
3-III	Ratio of Nitrogen-Oxygen to Helium-Oxygen Leak Rates, by Weight, for Laminar Flow in Small Capillaries	56
3-IV	Results of Steady-State Leakage Tests	59
3-V	Leakage Sources and Orders of Magnitude	72
3-VI	Mean Values of Steady-State Leakage Data	73
3-VII	Relative Penalty Difference	77
4-I	Comparison of Airlock System Configurations	85
4-II	Airlock Pump-Down Penalty	101
4-III	Airlock System Atmosphere Penalty Comparisons	112
5-I	Properties of Cryogenic Fluids and Supercritical Storage Vessel Design Data	123
6-I	Effect of Atmospheric Composition and Pressure on Three Man Adiabatic Molecular Sieve Bed Design	167
6-II	Effect of Atmospheric Composition and Pressure on Nine Man Adiabatic Molecular Sieve Bed Design	169
6-III	Effect of Atmospheric Composition, Pressure, and Molecular Sieve Design on a Three Man Adiabatic Silica Gel Bed Design	171
6-IV	Effect of Atmospheric Composition, Pressure, and Molecular Sieve Design on a Three Man Isothermal Silica Gel Bed Design	172
6-V	Total Weight Penalty Trends for a Three Man Adiabatic Molecular Sieve and Silica Gel Bed Designs	174

6-VI	Mass Transfer Data for a 7-psia N <sub>2</sub> -O <sub>2</sub> Molecular Sieve Bed from Figure 6-9	181
6-VII	Comparison of Molecular Sieve Bed Lengths	183
6-VIII	Comparison of Silica Gel Bed Lengths	184
6-IX	Effect of Cabin Atmosphere on Typical Components for a Three Man System	186
7-I	Atmosphere and Heat Exchanger Properties	194
7-II	Heat Exchanger Optimization Data	195
7-III	Weight Requirements for Stored Atmospheric Constituents	209
7-IV	Weight and Power Requirements for Airlock Operation	210
7-V	Condenser Loop Weight and Power Requirements	211
7-VI	Carbon Dioxide Adsorption Subsystem Weight and Power Requirements	212
7-VII	Life Support System Weights for Example Problem	216
8-I	Cotton Cloth Burn Data for Various Atmospheric Compositions	249
8-II	Effects of Different Atmospheres on the Combustion Rate of Cotton Cloth	253
8-III	Heat Capacities of Gas Mixtures at 25°C	255
8-IV	Two by Two Inch Cotton Cloth Burn Data for Various Atmospheric Compositions With Free and Forced Convection	258
8-V	Oxygen Starvation Test Results for Two by Two Cotton Cloth	260
8-VI	Smoke Development and Burn-Through Data for Insulated Wire Specimens	263
8-VII	Null Gravity Test Results	270
8-VIII	Burning Trends in One g and Null Gravity	272

## NOMENCLATURE

<u>Symbols</u>	<u>Definition</u>	<u>Units</u>
a	thermal diffusivity, $k/(C_p \rho)$	ft <sup>2</sup> /hr
a <sub>v</sub>	surface area per unit volume	ft <sup>2</sup> /ft <sup>3</sup>
A	area	ft <sup>2</sup>
A <sub>F</sub>	frontal area of bed	ft <sup>2</sup>
A <sub>f</sub>	heat exchanger fin area	ft <sup>2</sup>
A <sub>HX</sub>	heat exchanger size parameter, (UA)K <sub>j</sub> F <sub>j</sub> /j	lb
b	heat exchanger power parameter, f(PPF)K <sub>f</sub> F <sub>f</sub>	dimensionless
C	specific heat; C <sub>b</sub> , specific heat of crewman; C <sub>p</sub> , specific heat at constant pressure; C <sub>v</sub> , specific heat at constant volume	Btu/lb °F
C	flow capacitance	Btu/hr - °F
C <sub>D</sub>	flow coefficient	dimensionless
CLO	clothing value (1 CLO = 0.88hr °F ft <sup>2</sup> /Btu)	hr °F ft <sup>2</sup> /Btu
CO <sub>2</sub>	oxygen concentration	moles/liter
CO <sub>2</sub> <sup>amb</sup>	oxygen concentration at ambient conditions	moles/liter
c	constant	dimensionless
d	diameter; d <sub>i</sub> , inner diameter	ft; in.
D	diameter; D <sub>H</sub> , hydraulic diameter; D <sub>p</sub> , particle diameter	μ; ft
D <sub>v</sub>	mass diffusivity	ft
e	exponential function or base of natural logarithm	dimensionless
E	heat exchanger effectiveness	dimensionless
f.	Fanning friction factor	dimensionless
f'	modified Fanning friction factor	dimensionless
F	cryogenic storage factor	dimensionless
F <sub>A</sub>	view factor	dimensionless
F <sub>E</sub>	emissivity factor	dimensionless
F <sub>f</sub>	fluid power parameter, $\mu^2/2 g \rho^2$	lb-ft <sup>2</sup> /hr
F <sub>j</sub>	fluid heat transfer parameter, $1/k(Pr)^{1/3}$	ft-hr - °F/Btu
F <sub>ty</sub>	tensile yield stress	psi
g	gravitational constant	ft/sec <sup>2</sup>

$g_c$	critical acceleration of gravity	ft/sec <sup>2</sup>
Gr	Grashof number, $\beta g L^3 \Delta T / \nu^2$ ; Gr <sub>D</sub> , Grashof number based on diameter $D$ , $\beta g D^3 T / \nu^2$	dimensionless
$G_e$	superficial mass velocity	lb/hr-ft <sup>2</sup>
G	Gaussian error function	dimensionless
h	convective heat transfer film coefficient	Btu/hr °F ft <sup>2</sup>
h	specific enthalpy	Btu/lb
H	enthalpy	Btu
$H_v$	heat of vaporization	Btu
j	Colburn modulus, $h(\text{Pr})^{2/3} / G_s C_p$	dimensionless
j'	modified Colburn modulus	dimensionless
$j_h$	Colburn heat transfer modulus	dimensionless
$j_m$	Colburn mass transfer modulus	dimensionless
k	thermal conductivity	Btu/hr ft °F
$k_G$	mass transfer coefficient	lb-mole/hr-ft <sup>2</sup> -atm
$K_c$	ratio of total canister weight, including HX surface, to bed material weight	dimensionless
$K_f$	core power parameter, $1/K_m D^3$	1/lb-ft
$K_j$	core heat transfer parameter, $K_m D / \eta$	lb/ft
$K_m$	material surface density of heat exchanger core	lb/ft <sup>2</sup>
$K_v$	ratio of airlock to receiver volume	dimensionless
$K'$	constant for gas diffusion through glass	ft <sup>3</sup> -ft-ft <sup>2</sup> / sec-ft <sup>2</sup> -lb-sec
$K_i$	constant for entrance effects	dimensionless
$K_e$	constant for exit effects	dimensionless
$l$	tube or fin length	ft
L	length	ft
$L_B$	total bed length in flow direction	ft
$L_C$	capillary length	cm
m	mass or weight of gas; or crewman	lb
$\dot{m}$	propagation rate	in/sec
M	molecular weight; $M_G$ , molecular weight of carrier gas; $M_A$ , molecular weight of absorbate	lb/lb-mole
$M'$	molecular weight (M) divided by 32	dimensionless
$M_p$	ratio of receiver to cabin pressure	dimensionless
$M_a$	Mach number	dimensionless

n	number of heat exchanger passes	dimensionless
NTU	number of transfer units	dimensionless
Nu	Nusselt number, $hL/k$ ; $Nu_D$ , Nusselt number based on diameter, $hD/k$	dimensionless
p	bed porosity	dimensionless
p'	partial gas pressure; $p'_{Bm}$ , logarithmic mean partial pressure of component B in gas mixture	lb/ft <sup>2</sup> ; psia
P	absolute pressure	lb/ft <sup>2</sup> ; psia
P <sub>ag</sub>	pressure of the adsorbate in the carrier gas	atm
P <sub>ab</sub>	pressure of the adsorbate at the surface of the bed material	atm
P <sub>G</sub>	pressure of the carrier gas	atm
P <sub>H<sub>2</sub>O</sub>	pressure of water vapor	psia
P'	pressure (P) divided by 14.7	dimensionless
Pr	Prandtl number, $C_p\mu/k$	dimensionless
PEN	penalty	lb
PPF	power penalty factor	lb/ft-lb/hr
PWR	power	kW
q	heat input	Btu
$\dot{q}$	rate of heat flow	Btu/hr
Q	volume flow rate	$\mu$ liter/sec
Q <sub>G</sub>	gas flow	ft <sup>3</sup> /min
r	radius; $r_1$ , inner radius; $r_F$ , radius of fuel molecule; $r_{O_2}$ , radius of oxygen molecule	in.
R	gas constant	ft-lb/lb <sup>o</sup> R
Re	Reynold's number, $VL\rho/\mu$ ; $Re_D$ , Reynold's number based on diameter, $VD\rho/\mu$	dimensionless
R <sub>u</sub>	universal gas constant (1545 ft-lb/ <sup>o</sup> R mole)	ft-lb/ <sup>o</sup> R mole
Sc	Schmidt number, $\mu/\rho D_v$	dimensionless
SE	specific energy	Btu/lb
SF	safety factor	dimensionless
Sh	Sherwood number, $kR_u T p'_{Bm} L$	dimensionless
t	time	sec; hr
t <sub>f</sub>	fin thickness	ft
t <sub>m</sub>	duration	days
t <sub>w</sub>	wall thickness	in.

T	temperature; $T_o$ , ambient temperature; $T_l$ , local temperature, $T_\infty$ , temperature of flame front; $T_b$ , temperature at cloth surface; $T_w$ , wall temperature	$^{\circ}\text{R}$ , $^{\circ}\text{F}$
$T'$	temperature (T) divided by $527^{\circ}\text{R}$	dimensionless
U	mean velocity	ft/sec
UA	heat exchanger overall heat transfer coefficient and area product	Btu/hr - $^{\circ}\text{F}$
$U_t$	total number of airlock uses	dimensionless
v	gas specific volume	ft <sup>3</sup> /lb
V	gas volume	ft <sup>3</sup>
$V_c$	critical convective velocity	ft/sec
$\dot{v}$	volume flow rate	cu ft/min
$\dot{w}$	weight flow rate	lb/sec
$\dot{w}_A$	adsorption rate of the adsorbate gas	lb/hr
$W_A$	actual work	Btu
$W'$	ideal adiabatic work	Btu
WT	weight	lb
$X_c$	critical diffusion length	in.
Z	thermal capacity ratio	dimensionless

<u>Greek Symbols</u>	<u>Definition</u>	<u>Units</u>
$\beta$	temperature coefficient of volumetric expansion	1/ $^{\circ}\text{F}$
$\gamma$	ratio of specific heats ( $C_p/C_v$ )	dimensionless
$\delta$	area ratio, free flow area/frontal area	dimensionless
$\Delta$	incremental	dimensionless
$\eta_o$	overall fin effectiveness for heat exchanger core	dimensionless
$\eta_f$	fin effectiveness for heat exchanger core fins	dimensionless
$\eta_F$	fan efficiency	%
$\eta_P$	pump efficiency	%
$\theta_c$	time (critical)	sec
$\theta_P$	pumping time	min
$\mu$	absolute viscosity	lb/hr-ft, lb/sec-ft

$\mu'$	viscosity ( $\mu$ ) divided by 0.046	dimensionless
$\nu$	kinematic viscosity	ft <sup>2</sup> /hr
$\rho$	fluid density	lb/ft <sup>3</sup>
$\rho_{amb}$	fluid density at ambient conditions	lb/ft <sup>3</sup>
$\rho_{RM}$	density of receiver material	lb/in <sup>3</sup>
$\sigma$	Stefan-Boltzman constant	dimensionless
$\sigma_g$	density ratio, $\rho_g/0.076$	dimensionless
$\phi$	power penalty factor	lb/kW
$\phi'$	power penalty factor	lb/kW-hr
$\phi_s$	shape factor for non-spherical particles	dimensionless

### Subscripts

a	airlock gas
avg	average conditions
b	body of crewman
c	condenser
C	convection
d	diluent (He or N <sub>2</sub> )
ex	expended atmosphere
E	electrical
f	final condition
F	fan
g	gas
gen	generation rate
h	hydrogen
H	hydraulic
He	helium-oxygen mixture
i	initial or inlet condition
in	inside condition
ins	insensible
k	cabin gas
l	liquid
m	metabolic
M	mean value

max	maximum conditions
min	minimum conditions
mr	mean radiation
$N_2-O_2$	nitrogen-oxygen mixture
o	oxygen or outlet condition
P	pump
p	total pressure
po	power system
pri	primary, gas side of condenser or heat exchanger
r	radiation
R	receiver gas
S	body surface
sec	secondary, liquid side of condenser or heat exchanger
sw	sweat rate
sk	skin
sys	system
T	total
V	vapor
v	volume
w	work

## INTRODUCTION

Planned manned orbital laboratories and interplanetary spacecraft will have increased mission durations that make a two-gas atmosphere system desirable from the physiological standpoint. The addition of an inert diluent provides less severe constraints for future experiment selection and eases the materials selection problem particularly for longer duration spacecraft. The pressure level for two-gas atmospheres has been proposed between 5 and 7 psia to minimize vehicle weight penalty, and to decrease the potential of bends associated with the transition from higher pressures to the suit loop one-gas system or in case of an emergency cabin decompression. Nitrogen, helium, argon, and neon have been proposed as inert diluents for spacecraft two-gas systems. Neither argon nor neon appears to have any distinct advantages from an engineering standpoint as diluents over helium or nitrogen when the physical properties are considered. Nitrogen is the best understood and helium has favorable weight and heat transfer properties. Therefore, the two most promising proposed diluents are nitrogen and helium.

Results of tests and supporting analyses conducted to compare the effects of atmosphere selection on life support system design are presented as follows:

- (1) Summary
- (2) Comfort Zone
- (3) Leakage
- (4) Airlock System
- (5) Atmosphere Supply System
- (6) The Effect of Atmosphere Selection on Component Heat and Mass Transfer
- (7) The Effect of Atmosphere Selection on Life Support System Penalty
- (8) Comparison of Atmospheres for Fire Prevention.

## Section 1 SUMMARY

A summary of tests, analysis and results for each presented section is given below:

### COMFORT ZONE

Comfort data from 79 test runs were completed in 18 days of continuous tests with a crew of four working at an average metabolic rate of 480 Btu/hr/man in a small comfort simulator. These runs provided data to establish average comfort temperatures but did not allow evaluation of comfort zone width. The test data indicate that only minor temperature differences exist in different atmospheric mixtures for a crewman with very little or no clothing. Figure 1-1 presents representative test data illustrating this point. This may explain why statements have been made to the effect that the difference in temperature for comfort in helium-oxygen mixtures, as compared to nitrogen-oxygen mixtures is negligible, because past tests have been conducted with subjects wearing little or no clothing. However, test results for crewmen wearing light to medium clothing show an appreciable difference in comfort temperatures between helium-oxygen and nitrogen-oxygen atmospheres as shown in Figure 1-1. For the 5 psia tests, the temperature level for comfort was 5°F higher for helium-oxygen than for nitrogen-oxygen. At 7 psia, a 7°F increase in comfort temperature resulted.

Besides the above 18 days of controlled tests with a small comfort simulator, full-scale testing was performed under a random work-rest cycle and vehicle operating conditions in the 4000 cu ft space cabin simulator. These tests included 30 days at 7 psia nitrogen-oxygen and 5 days at 5 psia helium-oxygen. The crewmen were allowed to select the most comfortable temperature during each test run while performing a work-rest cycle from full sleep to full exercise. The average cabin temperature selected for comfort was 78°F for nitrogen-oxygen at 7 psia and 85°F for helium-oxygen at 5 psia. The above data are in agreement with controlled tests previously discussed.

It is concluded that the difference in heat transfer effect between nitrogen-oxygen and helium-oxygen is small for light clothing weights, but becomes quite large for normal clothing values. The two effects that are present are: (1) convection heat transfer, and (2) the resistance to heat flow in the clothing. Both these effects are increased by the higher thermal conductivity of the He-O<sub>2</sub> atmosphere. The thermal resistance of clothing appeared to be directly proportional to the thermal conductivity of the atmospheric gas entrapped in the clothing.

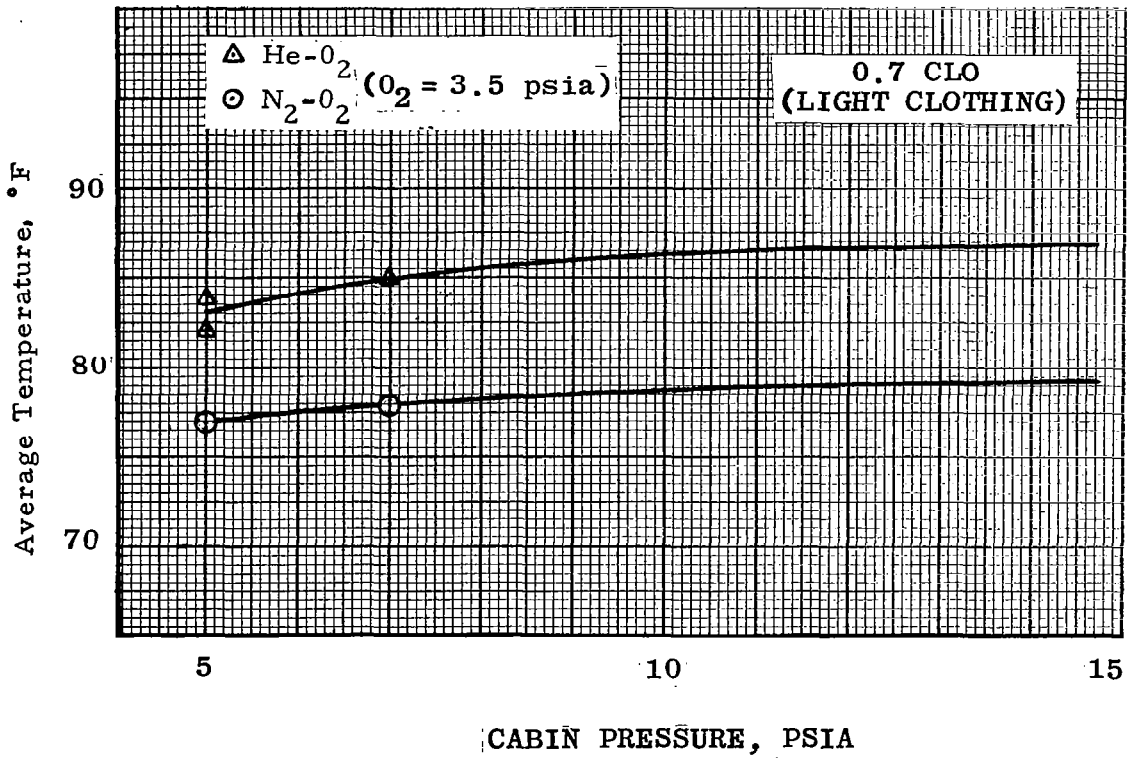
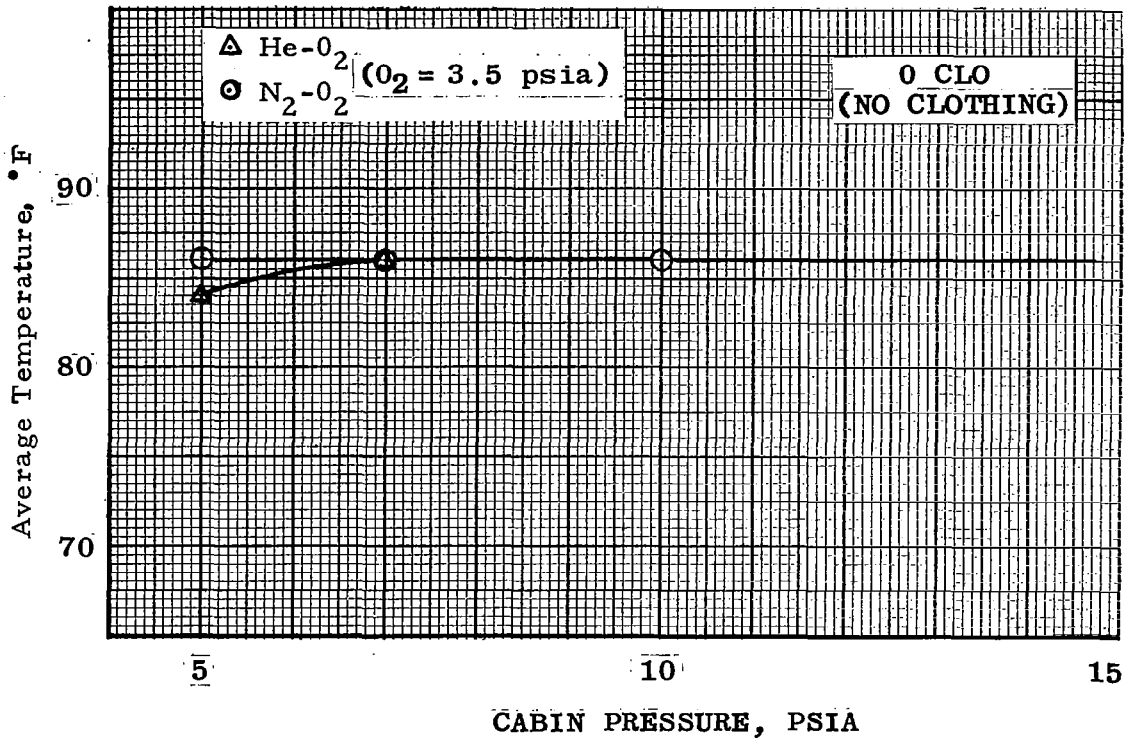


Figure 1-1 Comfort Temperature Data Comparison

The exploratory comfort tests completed provide significant comfort zone data for determining thermal control system and other life support subsystem penalties, particularly when the atmospheric temperatures are close to the cabin wall temperature. Additional comfort zone tests with more subjects and a greater variety of clothing weight must be completed to further refine the permissible cabin temperature level for comfort in helium-oxygen. Tests should also be completed for the condition where the cabin wall temperature is significantly different from that of the atmosphere to verify or modify the presented data for predicting the temperature for comfort. Tests must be completed for accurately determining clothing resistance and thermal conductivity of clothing samples in various gas mixtures to establish the effect of entrapped gas.

### LEAKAGE DATA AND ANALYSIS

The atmospheric storage system weight difference is very important in the total weight penalty resulting for the life support system. The penalty contributed by leakage must be added to that for metabolic use, for repressurization, and for airlock usage to enable an evaluation of the total penalty. Transient and steady-state leakage tests were performed to verify the methods to be used to obtain a penalty for leakage. Test procedures, results, and a correlation with theory are presented in Section 3. Test data and theory for steady and transient conditions were in good agreement for helium-oxygen and nitrogen-oxygen atmospheric compositions.

The two basic types of vehicle atmospheric leakage considered in the test program were: (1) Steady-state leakage of the type which cannot be avoided in space-cabin design and must be continuously supported by a make-up supply, and (2) emergency leakage of sufficient magnitude to cause cabin pressure decay, such as that caused by a meteoroid impact. Most designers engaged in future spacecraft studies have used leakage rates that range from 1 to 5 lb/day, depending on vehicle size and design. Major leakage, in most instances, has been through hatch and/or hangar seals. Total vehicle leakage has been accounted for by carrying sufficient supply gas to compensate for normal steady-state leakage and to provide for at least one complete compartment or vehicle repressurization for emergency conditions. Table 1-I shows the experimentally determined ratios of leakage flow rates, by weight, for nitrogen-oxygen and helium-oxygen atmospheres at 5, 7, and 10 psia. These data agree well with theory presented in Section 3.

TABLE 1-I  
MEAN VALUES OF STEADY-STATE LEAKAGE DATA

Total Pressure (psia)	Ratio of N <sub>2</sub> -O <sub>2</sub> to He-O <sub>2</sub> (by weight)
5	1.23
7	1.66
10	1.80

The test results on cabin pressure decay closely followed adiabatic decompression theory. A flow coefficient of 0.60 with the assumption of adiabatic decompression will yield satisfactory results for transient pressures for both helium-oxygen and nitrogen-oxygen mixtures. However, temperature changes were much less than predicted.

Tests and analyses indicated that the loss of oxygen through leakage is higher when helium diluent is used rather than nitrogen. However, the total weight of gas loss and the respective weight for equivalent types of storage is less for the helium-oxygen atmosphere.

A comparative analysis of the effect of transient and steady-state leakage on the weight penalty for a typical space vehicle is presented in Section 3, Table 3-VII. The configuration studied was for a 90-day mission with 4 to 9 men in a cabin having a volume of 5360 cu ft and 7 psia pressure. A baseline leakage rate of 2 lb per day in a 7 psia nitrogen-oxygen atmosphere was assumed. The leakage weight penalty included steady-state leakage plus one cabin repressurization plus weight of storage tanks required for the oxygen and diluent used. The total weight penalty for leakage was 525 lb for nitrogen-oxygen and 411 lb for helium-oxygen atmospheres.

The major leakage source should occur through hatches or hangar seals, except for the emergency situation of a meteoroid penetration, seal failure, or other type of sudden failure. Therefore, criteria were established to approximate normal leakage that can be anticipated for future vehicles. Actual seal leakage test data were obtained for a flight-type airlock by Douglas under NASA Contract NAS1-3983. A number of different hatch seals were used on the airlock; however, in all cases seal leakage was negligible. The air lock was tested with air at a one-atmosphere pressure with the space side exposed to vacuum on the order of  $10^{-6}$  mm Hg. Maximum leakage for an inflatable seal after 50 hatch operations was 17.3 cc per 24 hr, which amounts to  $2.85 \times 10^{-5}$  lb/day/in. A typical design value for seal leakage is  $7 \times 10^{-3}$  lb/day/in; which appears to be a safe value for design purposes with nitrogen-oxygen and pure oxygen at 7 psia. The equivalent leakage rate for helium-oxygen would be  $4.21 \times 10^{-3}$  lb/day/in. Other sources of leakage and estimated order of magnitude based on a 7 psia nitrogen-oxygen atmosphere are presented in Table I-II.

During testing in the space cabin simulator, premature failure of some types of electronic equipment was noted. One pertinent finding was that seven vidicon television monitoring tubes failed in the helium-oxygen space cabin atmosphere. During 13 days of testing, with three tubes installed in the cabin, deterioration of tube performance indicated an average tube life of 60 hr. It appeared that helium diffused either through the glass or through the tube seal between the electrode and the glass portion of the tube. Helium gas entered the tube and raised its internal pressure causing a gaseous tube condition.

No failures occurred during any of the 42 days of tests with nitrogen diluent, nor during the 2-day checkout test with helium-oxygen. In addition, a subsequent 5-day test was performed with a helium-oxygen atmosphere of 5 psia. Electronic equipment installed in the cabin consisted of three television monitor cameras. Lights in the cabin consisted of 40 W fluorescent

TABLE 1-II  
SOURCES OF LEAKAGE

Leakage Source	Order of Magnitude
Hatches and hangar door seals	$2.85 \times 10^{-5}$ to $7 \times 10^{-3}$ lb per day/in.
Electrical leads	$10^{-7}$ lb/day/in. (negligible)
O-ring seal (replaceable)	$10^{-9}$ lb/day/in. (negligible)
Valves	$10^{-3}$ lb/day/valve (negligible)
Seams and joints (welded)	$10^{-4}$ lb/day (negligible)
Diffusion through vehicle skin	$10^{-14}$ lb/day (negligible)

overhead lights, a 100 W incandescent bulb, and 1/25 W miniature neon bulbs. New vidicon tubes and one new light in each area were installed prior to the test. No vidicon tube failures occurred during the 5-day test as had occurred during the previous test. No failure or decrease in brightness occurred with the fluorescent, incandescent, or neon lights. The longer test had included operation at 5, 7 and 10 psia. The higher partial pressure of helium during this test may account for the apparent increase in tube failure rate. Helium concentration in several components was measured with a mass spectrometer after the 5-day space cabin simulator test. The incandescent bulb and the fluorescent light had considerable helium that had entered the component. No helium was measured in equivalent new bulbs, and the manufacturer stated that essentially no helium should be present in new bulbs. Helium contamination of evacuated glass tubes appears to be a definite problem. At the present, it is not known whether the leakage occurs through the glass or through the metal-to-glass seals. Additional testing is necessary to determine the nature of the leakage and to define satisfactory solutions to the problem.

#### AIRLOCK PENALTY ASSOCIATED WITH ATMOSPHERE SELECTION

The penalty of the atmosphere loss in airlock operation must be determined to size the atmosphere supply and storage system if extravehicular activity is to be significant during the mission. A procedure is presented in Section 4 for evaluating the penalty associated with an expendable gas airlock configuration where the atmosphere is exhausted overboard and resupplied from stored gas for each usage, and a system configuration that conserves the atmosphere by pumping it into the cabin or into a storage tank for re-use.

The selection of atmospheric composition and pressure has only a secondary effect on airlock penalty difference. The primary concern is whether the airlock is an expendable or pump-down type, the required number of uses, and the associated power penalty for pumping.

Although an expendable atmosphere system is relatively simple, it is costly from a penalty standpoint when used more than a few times. The exact break-even point between an expendable gas and pump-down for conservation and re-use of atmosphere must be determined for each airlock configuration for the particular vehicle design constraints and missions. The break-even point above which the expendable atmosphere system is not competitive is usually between three and six uses if the weight of the airlock is not included. A major problem for a pump-down system design is the development of a flight-type, flight-weight, pump and motor combination.

## ATMOSPHERE SUPPLY SYSTEM

The information required to size the atmospheric supply and storage system is derived from Sections 2 through 4. The number of crewmen and their metabolic requirements, the make-up atmosphere for leakage, and for repressurization must be added to determine the atmospheric supply weight penalty from the data in Section 5 for different methods of storage. No new tests were conducted because adequate data were available from the documents referenced in Section 5.

An example problem is given in Section 7 and summarized in Figure 1-2 for a 3-man, 90-day mission. This indicates a major weight savings can be obtained in the atmospheric storage and pressurization system by using helium diluent. For example, at 5 psia, a system using supercritical storage weighs 1046 lb for helium-oxygen, 1052 lb for oxygen, and 1083 lb for nitrogen-oxygen. The one-gas oxygen system will be heavier than the helium-oxygen system because helium is lighter than the make-up oxygen for leakage. For 7 psia, supercritically stored helium-oxygen can save 119 lb as compared to using nitrogen-oxygen, as shown in Figure 1-2.

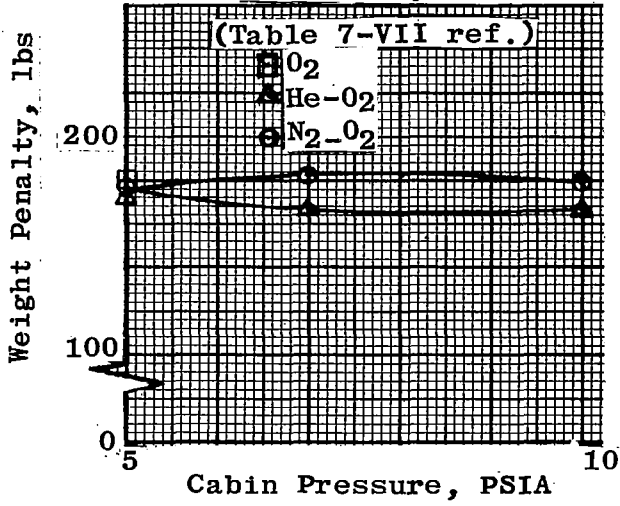
Supercritical storage of oxygen and nitrogen provides minimum weight penalty using the present state of the art. Supercritical storage of helium is not as well developed as nitrogen or oxygen. The future development of subcritical storage for gas delivery will produce additional weight savings. The two major subcritical storage development problems which require flight qualification are fluid transfer and quantity measurement. Subcritical storage, as indicated by the weight penalty curves, represents a potential 18% weight saving over supercritical storage.

## THE EFFECT OF ATMOSPHERE SELECTION ON COMPONENT HEAT AND MASS TRANSFER

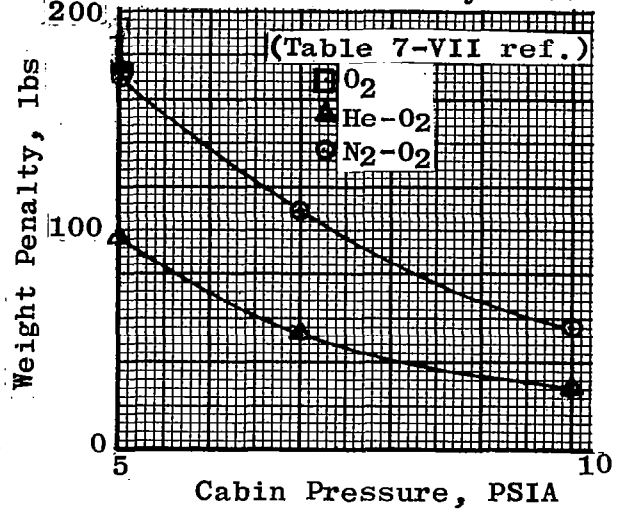
In most instances, the influence of atmosphere selection on heat exchanger weight is small compared with the effect on fan power requirements and the associated power-weight penalty. The weight ratio, pressure drop ratio, and power ratio from heat exchanger test data are presented in Table 1-III.

Test data were obtained for silica gel and molecular sieve beds for adiabatic conditions for helium-oxygen and nitrogen-oxygen at 5 psia and for air at 14.7 psia to determine the effect of atmosphere on CO<sub>2</sub> removal system design. The data are presented in a form that can be used to size an adiabatic design. An isothermal method is also presented to size internally cooled molecular sieve and silica gel configurations as noted in Section 6.

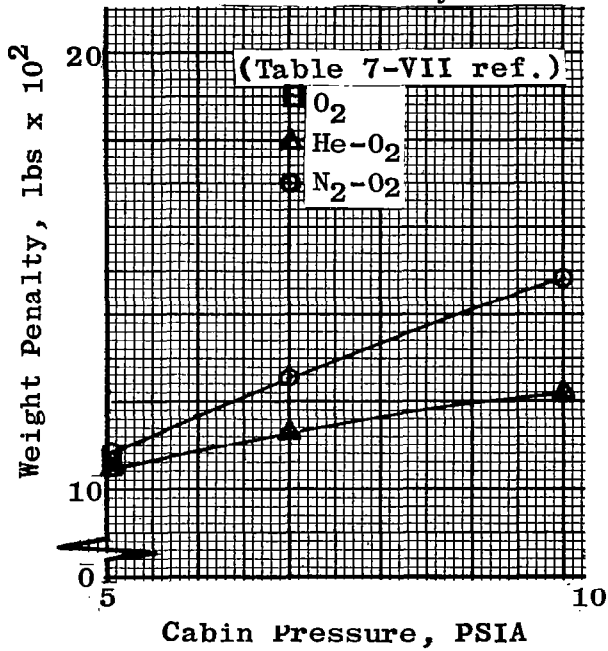
### Atmospheric Purification & Control System



### Thermal Control System



### Atmospheric Supply and Pressurization System



### Total Environmental Control System

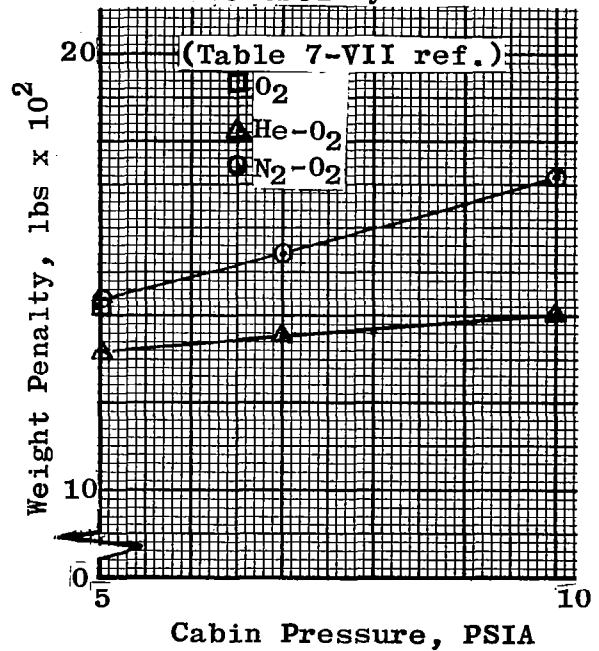


Figure 1-2 Life Support System Weight Trend

TABLE 1-III  
HEAT EXCHANGER DATA--WEIGHT, PRESSURE DROP,  
AND POWER RATIOS

Pressure <sup>a</sup> (psia)	Wt. N <sub>2</sub> -O <sub>2</sub> / Wt He-O <sub>2</sub>	$\Delta P$ N <sub>2</sub> -O <sub>2</sub> / $\Delta P$ He-O <sub>2</sub>	Power N <sub>2</sub> -O <sub>2</sub> / Power He-O <sub>2</sub>
5	0.802	1.77	1.63
7	0.925	1.67	1.43
10	0.960	1.69	1.38
<sup>a</sup> 3.5 psia O <sub>2</sub>			

The initial bed concentration for the molecular sieve and silica gel beds to be regenerated has a greater influence on bed size and power required to regenerate than the choice of the diluent added to the cabin atmosphere or the cabin pressure level. An internally cooled bed also enables considerable reduction in molecular sieve or silica gel bed size.

The savings in heat exchanger or adsorption bed weight obtained through the difference in mass and heat transfer resulting from the selection of cabin atmosphere diluent is usually small when compared to the total system weight as shown in Table 7-VII in Section 7. The thermal control system is the major system that is influenced by the cabin atmospheric temperature and pressure. The major penalty differences are obtained from the allowable cabin temperature level and cabin pressure which directly influence the gas weight flow rate and therefore the blower power penalty.

#### THE EFFECT OF ATMOSPHERE SELECTION ON LIFE SUPPORT SYSTEM PENALTY

The experimental tests and analysis completed and applied to an example problem for a three-man orbital laboratory in Section 7 indicate that a weight and power savings can be obtained in life support system design by using helium as a diluent as shown in Figure 1-2. The major difference in weight penalty savings is obtained primarily in the atmospheric storage and thermal control systems. This results, principally because (1) helium is lighter than oxygen or nitrogen and (2) a higher allowable cabin temperature level for comfort can be used when helium is the diluent. This reduces the required rate of atmosphere to be pumped through the thermal control system which saves fan power.

The airlock and atmospheric purification and control system is not affected significantly by choice of atmosphere composition and pressure.

As shown in the example problem summarized in Figure 1-2, helium-oxygen appears attractive from a weight penalty over nitrogen-oxygen. A favorable pressure level from a penalty standpoint is in the 5 to 8 psia range.

#### COMPARISON OF ATMOSPHERES FOR FIRE PREVENTION

Logic indicates that even using the utmost care, the materials, the power source, and the ventilation rate exist on-board a manned spacecraft that could cause some material to ignite and fire to propagate in any atmosphere. Therefore, common materials were selected to determine the effect of cabin atmosphere on the burning phenomena. Test data for cotton cloth, insulated wire, and other materials in the literature were reviewed. Most of the published procedures and tests were not specifically directed toward null gravity "burning rate tests." Therefore, specimen and test methods were established to obtain 1-g baseline data and also to be compatible for subsequent null gravity flights. The baseline materials selected for determining the effect of atmosphere composition on ignition and burning rate in null gravity and at 1 g were cotton cloth, a single insulated wire, and a wire bundle. Free and forced convection tests, oxygen starvation tests, and a limited number of null gravity burning tests were performed to gain a better understanding of the ignition and combustion phenomenon. A review of completed tests is given in the following paragraphs.

More input energy is required to start a fire in helium-oxygen than in either pure oxygen or in nitrogen-oxygen. For example, at a constant power of 57.1 W, the higher conductivity of helium reduced a wire igniter temperature to 880°C for the cotton cloth tests compared to 1035°C in nitrogen-oxygen. The time required to reach the measured 650°C minimum ignition temperature for the cloth sample increased for the helium mixture, as noted in Section 8, Table 8-IV.

The ignition temperature is essentially independent of the amount and nature of atmosphere diluent but is dependent on oxygen partial pressure as shown in Figure 1-3. The ignition temperature of cotton cloth decreased as the oxygen partial pressure in the atmosphere was increased. For example, the ignition temperature was lowered from 630°C at 3.5 psia oxygen partial pressure to 550°C at 5 psia pure oxygen for the cloth sample tested. From a fire prevention standpoint it would be advisable to increase ignition temperature by lowering the oxygen partial pressure to a minimum. The power required to reach the ignition temperature is not significantly higher in ambient sea level air than in pure oxygen atmospheres at 3.5 and 5 psia. The power input required to reach the same operating temperature is considerably greater using helium as a diluent than when nitrogen is used. For example, for the tests reported in Section 8, 50% more power is required in a 7 psia total pressure atmosphere containing equal concentrations of helium-oxygen than in nitrogen-oxygen mixtures to ignite the cotton cloth sample.

The presence of an inert diluent, once ignition occurs, reduced the flame propagation rate for most of the cotton cloth samples tested. Nitrogen diluent had a greater effect on the reduction of flame propagation rate in 1-g than helium with and without forced convection. As shown in Figure 1-4, the

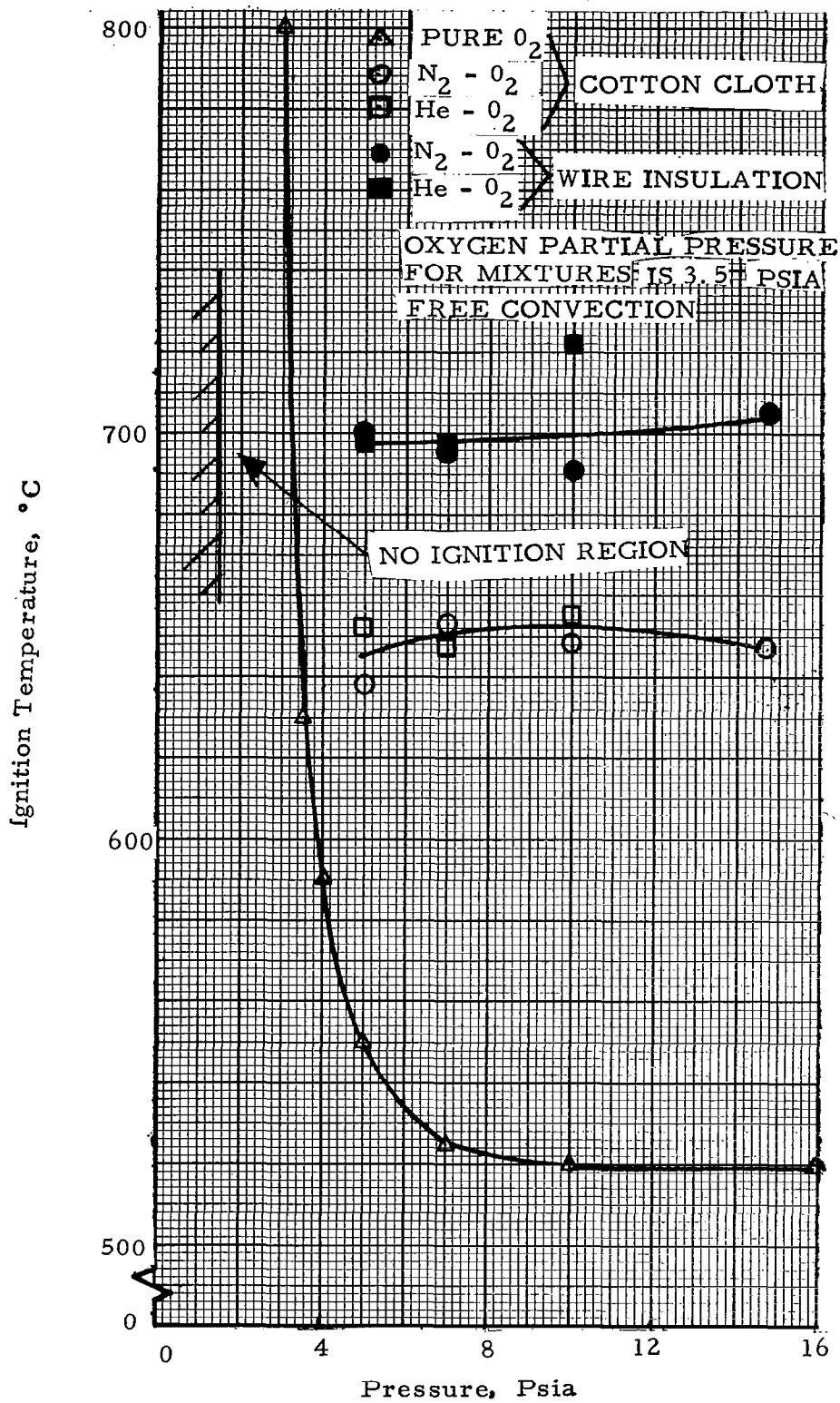


Figure 1-3 Ignition Temperature for Cotton Cloth and Wire Insulation

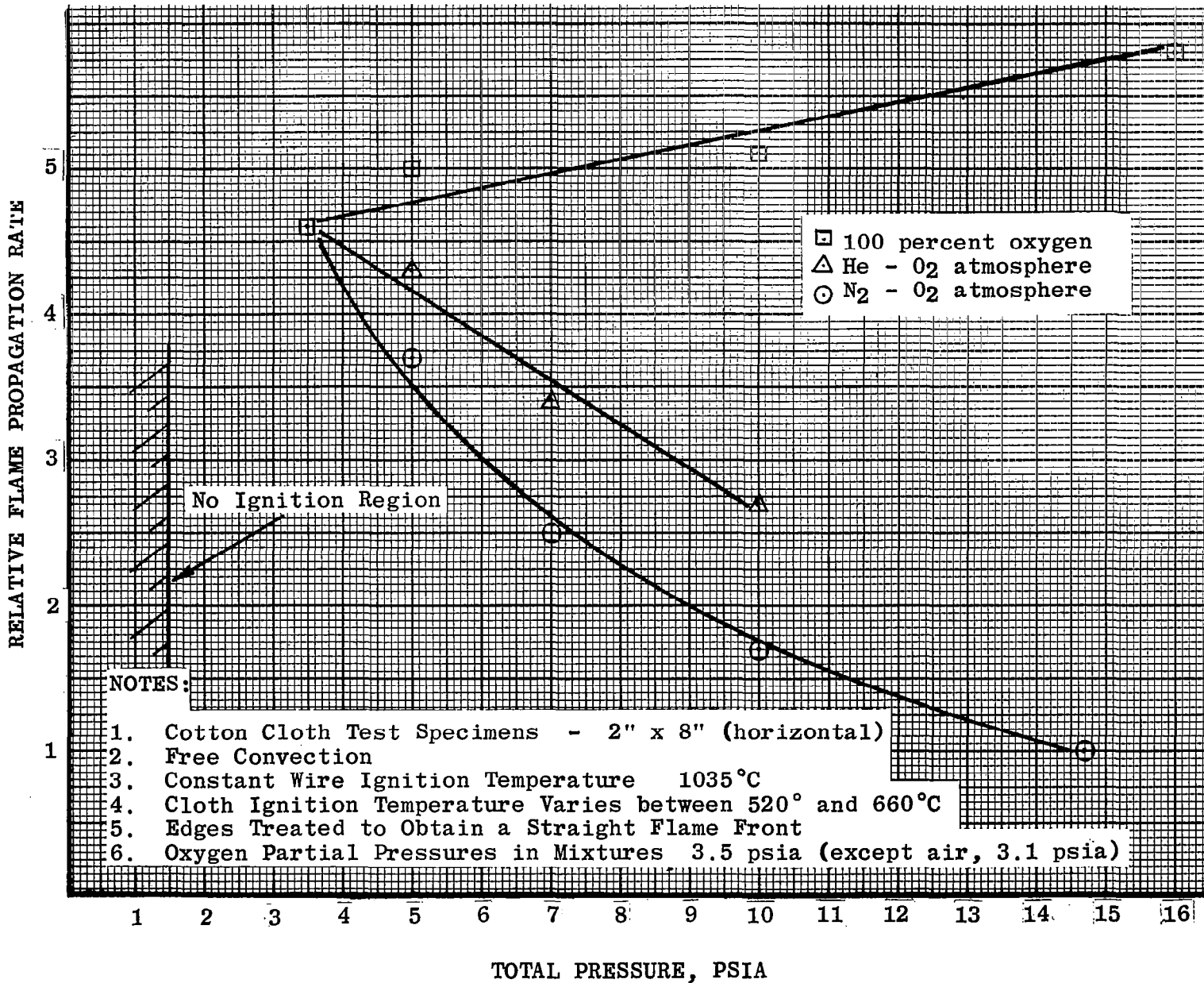


FIGURE 1-4 Flame Propagation Rates Relative to Rate in Air at 14.7 PSIA

burning rate of the horizontal cotton cloth with treated edges in oxygen at 5 psia is nearly five times that in air at 14.7 psia. At the same total pressure, the ratio is reduced to 4.25 for helium-oxygen and 3.7 for nitrogen-oxygen with 3.5 psia partial pressure of oxygen. Nitrogen-oxygen at 7 psia produced a significant reduction in burning rate to a ratio of 2.5 to 1.

Tests indicated that minimum ignition temperature is dependent on the type of material. The minimum ignition temperature is affected very little by gravity and forced ventilation. For cotton cloth, the ignition temperature was  $650^{\circ}\text{C} \pm 10^{\circ}\text{C}$  and for the insulated wire  $700^{\circ}\text{C} \pm 20^{\circ}\text{C}$  for all total pressures from 5 psia to 14.7 psia with a 3.5 psia oxygen partial pressure in both nitrogen-oxygen and helium-oxygen mixtures. The establishment of ignition temperature establishes one important parameter for future null gravity tests.

Tests at 1 g and 2 g indicated that the flame was always larger for the nitrogen-oxygen mixture than for helium-oxygen. In null gravity only a char front existed for the cotton cloth in helium-oxygen at 7 psia, and a small flame was evident in the nitrogen-oxygen mixture as shown in Figure 1-5. Analysis and tests indicate that a fire could extinguish itself in null gravity without forced convection. High ventilation rates would probably propagate the fire in either diluent. Helium is more attractive from a fire retardant standpoint than nitrogen, because more energy and/or time-energy is necessary for ignition. Consideration should be given to the various gravity levels encountered by the spacecraft in selecting an atmosphere composition, pressure, and operating procedures, from a fire-retarding standpoint. For example, for an entry or launch condition under high-gravity conditions, the percentage of inert diluent in the atmosphere can be increased with the crewmen wearing space suits. Null gravity tests are planned with varying ventilation rates to determine the effect of forced convection on the burning phenomenon. These data can be used to verify an analytical correlation of the effects of gravity. The effects on the burning phenomenon with different materials should also be tested in null gravity and compared to the 1-g baseline tests.

Flash ignition of the combustible gases built up during null gravity resulted for both helium-oxygen and nitrogen-oxygen mixtures. Comparison of these tests at 7 psia showed a smaller, more confined flash for the nitrogen-oxygen mixture. In null gravity, the formation of a smoke cloud could be a problem for any atmosphere. It can be speculated that, because of the tendency of helium to suppress the ignition of the material, more smoke and contaminants may form and a larger ignition flash will result unless adequate ventilation is provided to remove the generated combustible gases. More null gravity tests are planned to evaluate the ignition flash in pure oxygen, helium-oxygen, and nitrogen-oxygen mixtures.

Inspection of Figure 1-6 reveals that the choice of diluent has a significant effect on smoke production and on the burn-through of an overloaded electrical wire. The time required for a test wire insulation to begin to smoke and burn-through in a helium-oxygen atmosphere is considerably greater than in a nitrogen-oxygen atmosphere because of helium's high conductivity as shown in Figure 1-6. This difference increases as the amount of diluent is increased with a constant partial pressure of oxygen. In the presence of

Run No. 4 Atmosphere: Nitrogen and Oxygen  
Pressure: 7 Psia Total (3.5 Psia N<sub>2</sub> & 3.5 Psia O<sub>2</sub>)  
Power Input: 2.4 Volts, 8.4 Amps  
Wire Temperature: 870°C



Time: 8.98 sec, Null Gravity Burning

Run No. 12 Atmosphere: Helium and Oxygen  
Pressure: 7 Psia Total (3.5 Psia He & 3.5 Psia O<sub>2</sub>)  
Power Input: 2.4 Volts, 8.4 Amps  
Wire Temperature: 750°C



Time: 15.28 sec, Char Front Propagation in  
Null Gravity

Figure 1-5 Representative Null Gravity Test of Cotton Cloth

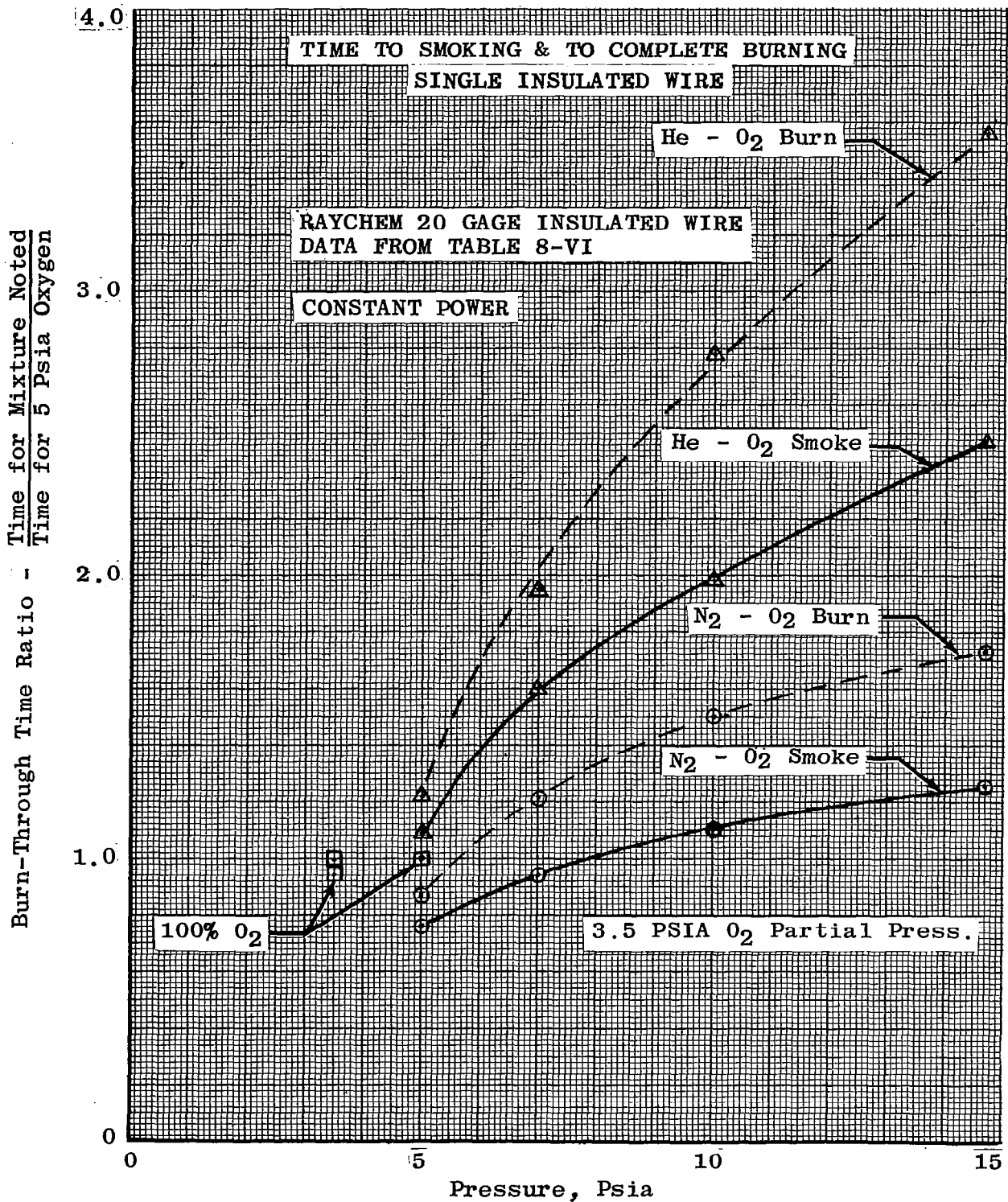


Figure 1-6 Relative Time to Smoking and Burn Through, Single Insulated Wire

3.5 psia of pure oxygen, an overloaded electrical wire begins smoking and burning almost simultaneously. As the total pressure of the atmospheric mixture increases by adding nitrogen, the time interval between smoking and burn-through of the wire increased. The time intervals between smoking and burn-through are even more pronounced in helium-oxygen atmospheres. When wires are in bundles, the time to smoke and burn-through was greater under all conditions tested as compared to single wires, as shown in Figure 1-7. The possibility of smoke creating an explosive or toxic mixture before ignition in null gravity must be evaluated.

#### REPORT USAGE AND GENERAL RECOMMENDATIONS

The above summary provides generalized information for atmosphere selection based on the limited examples constructed for the specific design conditions, and constraints given in each of the sections. The particular vehicle design and its associated constraints must be individually evaluated to determine the applicable penalty associated with atmosphere selection. The information presented in Sections 2 through 8 can be used to help evaluate the effect of atmosphere selection on vehicle weight penalty. Selection criteria of importance, besides weight penalty, are the availability of flight-qualified hardware, development lead time, cost of new or modified hardware, number of launches, reliability, and system simplicity.

Recommended key development items and study areas include: (1) the obtaining of additional controlled comfort zone tests with more subjects for clothing equivalent (CLO) values of 0.5 to 1.0 and for a broader range of work load and cabin wall temperature, (2) leakage tests for various cabin hatch seals for different cabin atmospheres and pressure levels, (3) the development of a leak locator, (4) tests to define the problem of helium leakage into electronic components and lights and development of a design to eliminate the problem, (5) the development of a flight-weight, low-power airlock motor/pump combination for pumpdown, (6) the development of sub-critical storage of cryogenic fluids, supercritical storage of helium, and an integrated two-gas sensor and control system, and (7) long-duration fire tests at null g and launch and entry g levels conducted to evaluate the ignition flash problem and burning rate phenomena with, and without, forced ventilation.

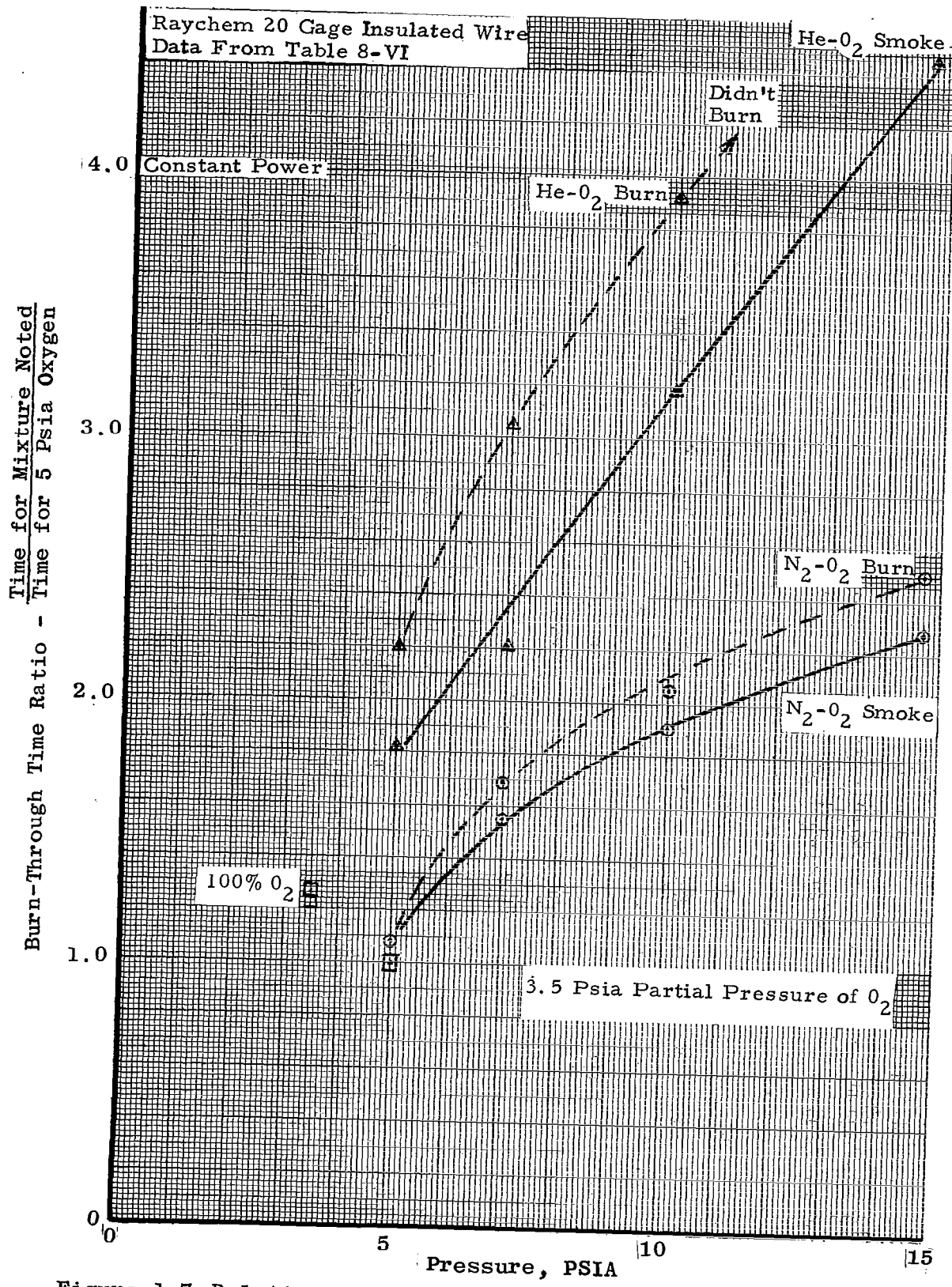


Figure 1-7 Relative Time to Smoking and to Burn-Through,  
One Wire in Bundle of Insulated Wires

## Section 2

### COMFORT ZONE

The comfort zone has a major effect on vehicle design and must be determined, because the design of many components is influenced by cabin atmospheric conditions. Comfort zone refers to the combination of pressure, atmosphere, wall temperature, gas ventilation, and humidity that creates a comfortable environment for a crew. Because of the high thermal conductivity of helium gas mixtures, the comfort zones for helium and nitrogen atmospheres are expected to differ appreciably. Although comfort tests were not run with mixtures of argon-oxygen and neon-oxygen, analytical methods presented in this report are valid for predicting comfort zones for these gases. In general, the comfort zones for argon-oxygen and neon-oxygen are not expected to differ greatly from that of nitrogen-oxygen.

Very little published comfort zone data are available for atmospheres containing helium diluent and nitrogen diluent with a variation of pressure level and clothing weight. Apollo and Gemini vehicles were designed for crewmen who will be wearing pressure suit undergarments of medium weight while working in shirt sleeve conditions. The first step has been taken in a test program to obtain comfort data on crewmen wearing medium-weight clothing in helium-oxygen and nitrogen-oxygen atmospheres at different cabin-pressure levels.

This section presents correlated parameters that describe the results of the comfort test program. The analytical theory to perform the correlations is also given, and procedures are presented for applying these data to any atmosphere, metabolic rate, and gravity level. The following atmospheres were tested:

5 and 7 psia nitrogen-oxygen (3.5 psia oxygen)

5, 7, and 10 psia helium-oxygen (3.5 psia oxygen)

Test data indicate that only minor temperature differences exist in different atmospheric mixtures for unclothed subjects. This may explain why statements have been made to the effect that the difference in temperature for comfort in helium-oxygen mixtures, as compared to nitrogen-oxygen mixtures is psychological, since past tests have been conducted with subjects wearing little or no clothing. However, test results for medium or heavy clothing show an appreciable difference in comfort temperatures between atmospheric mixtures. For the 5 psia tests run in the comfort simulator, the comfort temperature level was 5°F higher for helium-oxygen than for nitrogen-oxygen. At 7 psia, a 7°F higher comfort temperature was selected by the subjects for the helium-oxygen atmosphere. Comfort tests were supplemented by

full-scale space cabin simulator tests which simulated the random velocities, temperatures, and metabolic rates that would exist in an actual vehicle. Results of these tests show that the comfort temperature for subjects in medium-weight clothing and under 1-g conditions range from 75° to 78°F for a 7 psia nitrogen-oxygen atmosphere, and from 80° to 85°F for 5 and 7 psia helium-oxygen atmospheres. These results are in general agreement with comfort simulator tests in which comfort temperatures were from 5° to 7°F higher for a helium-oxygen mixture. To better define the comfort zone, additional tests which will use more subjects and which will use atmospheres of helium-oxygen and nitrogen-oxygen, as well as other diluents, are recommended.

A number of assumptions were made in the establishment of the comfort zone, and are summarized as follows:

- (1) The heat-transfer model for free and forced convection was assumed to be 1-ft-diam cylinder with a surface area of 19.5 sq ft (ref. 2-1).
- (2) Comfort is a state of minimum physiological strain wherein
  - (a) mean skin temperature is in the range of 91° to 94°F,
  - (b) deep body temperature is in the normal range of 98.6° ±0.5°F,
  - (c) there is no active sweating, and
  - (d) there is no body storage of heat (ref. 2-2).
- (3) All metabolic energy shows up as thermal energy.
- (4) Heat removed by conduction is negligible.
- (5) Insensible heat loss is given as
 
$$\dot{q}_{\text{ins}} = (242 + 0.112 \dot{q}_m)(0.7295 - P_{\text{H}_2\text{O}})$$
- (6) Radiation view factor is 0.8 and emissivity factor is 0.94 (refs. 2-1, 2-3, and 2-4).
- (7) Thermal conductivity of the clothing is directly proportional to thermal conductivity of the entrapped gas.
- (8) Crewman is assumed to be in shirtsleeve condition. Comfort for pressure-suited operation cannot be predicted with the information presented in this section.

Test data could be obtained for only a limited number of conditions such as clothing weight, metabolic rate, gas velocities, cabin wall temperature, and gravity level. To use these data for conditions other than those tested, analytical means must be employed to predict the comfort zone for untested conditions. In the following paragraphs, required analytical procedures are presented for the accomplishment of this task.

## COMFORT ZONE ANALYTICAL CONSIDERATION

A crewman in a space vehicle may be considered a heat machine which is producing work and heat. At the low metabolic levels anticipated for space cabin activity, metabolic energy will eventually all appear as heat energy. Generated heat must be removed to maintain the deep body temperature at a nearly constant level of 98.6°F.

The body has a number of thermoregulatory mechanisms which maintain a constant deep body temperature. Of primary concern, when operating within the comfort zone, is the vasomotor mechanism which regulates circulation at the skin. Innumerable branches of the circulatory system are located near the skin surface and one function of these branches is to circulate blood near the skin surface for heat rejection. The blood circulation rate, which is thus the rate of heat rejection, is controlled by constriction of cuffs around the branches. An above-normal rise in body core temperature produces a response (through the nervous system) which dilates the circulatory branches, which thereby delivers more blood for more heat rejection. As the body core temperature falls below normal, the branches will be constricted to reduce blood flow. Comfort is considered to be related to the amount of constriction of the circulatory branches (ref. 2-2). It has been shown in ref. 2-2 and verified at Douglas that comfort is a state of minimum physiological strain, that is (a) mean skin temperature is in the range of 91° to 94°F, (b) deep body temperature is in normal range of 98.6° ± 0.5°F, (c) there is no active sweating, and (d) there is no body storage of heat. This definition of comfort permits Earth (1-g) comfort data to be extended to the zero-g space environment, or to other sets of conditions.

Crew comfort is obtained by providing adequate cooling to maintain mean skin temperatures within the comfort range. A heat balance shows that crew-generated heat is carried by the circulatory system to the body surface, where it is rejected to the environment. Heat is rejected in several ways and those applicable to shirtsleeve operation are as follows:

- (1) Conduction.
- (2) Radiation.
- (3) Convection.
- (4) Evaporation of body water.

Conduction cooling is difficult to predict because the contact areas and properties of contacting materials are not known. For most space vehicle applications, conducted heat transfer can be neglected.

A heat balance may be written for the crewmen as follows:

$$\dot{q}_m - \dot{q}_r - \dot{q}_{ins} - \dot{q}_{sw} - \dot{q}_C = mC_b \frac{dT_b}{dt} - \dot{q}_w \quad (2-1)$$

This equation expresses the difference, between metabolic rate and cooling provided, as an increase in body temperature. Because the body does not store heat with comfortable conditions, and work output is negligible for the low metabolic rates assumed, the right side of the equation vanishes. In addition, active sweating cannot be allowed for comfort and the equation reduces to

$$\dot{q}_m - \dot{q}_r - \dot{q}_{ins} - \dot{q}_C = 0 \quad (2-2)$$

Therefore, conditions for comfort require that the amount of cooling necessary is identical to the metabolic rate. To a large extent, the insensible loss is a function primarily of cabin-water vapor pressure and metabolic rate. The expression for insensible loss shown below includes the effects of diffusion through the skin and respiration loss. No effects could be discerned for total pressure in the space simulator test data.

$$\dot{q}_{ins} = \left( 242 + 0.112 \dot{q}_m \right) \left( 0.7295 - P_{H_2O} \right) \quad (2-3)$$

where  $P_{H_2O}$  is the water vapor pressure corresponding to saturation at skin temperature in psia. Equation (2-3) is plotted in fig. 2-1.

In general, heat transferred by forced convection can be expressed as

$$\dot{q}_C = hA(T_S - T_g) \quad (2-4)$$

the film coefficient,  $h$ , can be expressed in terms of dimensionless quantities as

$$Nu_D = \frac{hD}{k} = 0.60 (Re_D)^{0.5} (Pr)^{0.31} \quad (2-5)$$

This equation is valid for a theoretical cylindrically shaped man (ref. 2-5) functioning normally in a gaseous atmosphere. The film coefficient given by equation (2-5) will be about midway between the many proposed models for forced convection from a crewman, i. e., flat-plate, multicylinder man, and the many empirically obtained relationships (refs. 2-1, 2-2, and 2-6).

Equation (2-5) is valid for either forced convection in a zero-g field or in a gravity field where the forced convection coefficient is greater than the free convection heat transfer coefficient. For free convection at 1 g or reduced g, the following equation may be used:

$$Nu_D = C_1 (Gr_D Pr)^{C_2} \quad (2-6)$$

where the constants  $C_1$  and  $C_2$  are functions of the product of Grashof and Prandtl numbers and may be obtained from ref. 2-7.

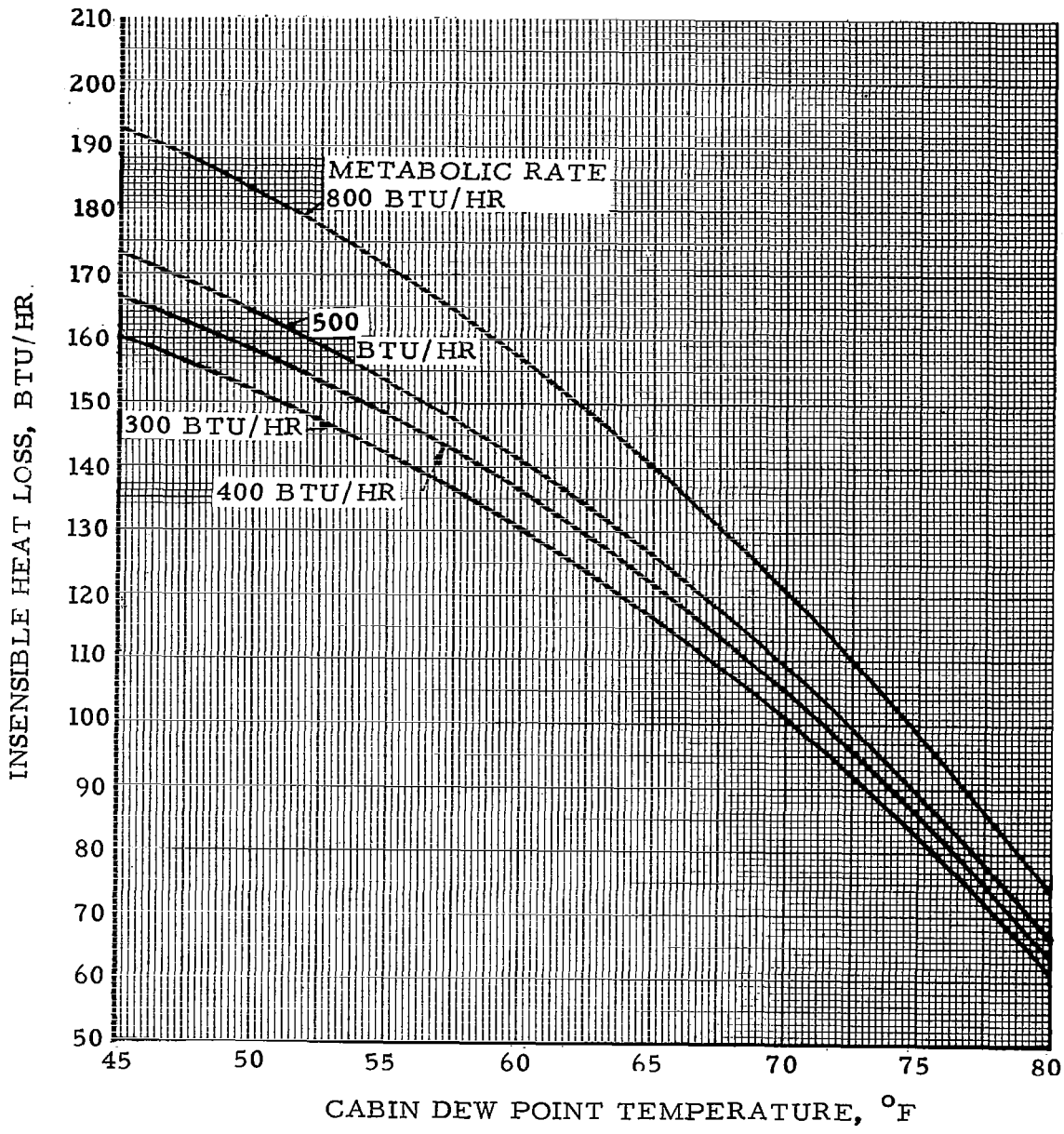


FIGURE 2-1 INSENSIBLE HEAT LOSS

Lower and upper limits may be placed on gas velocity. It is felt that at least 20 ft/min of atmospheric movement is essential to carry the metabolic products (carbon dioxide, water vapor, etc.) away from each crewman. On the other hand, too high a velocity will cause discomfort, eye irritation, and impairment of performance. A value of 100 ft/min appears to be an absolute upper comfort limit of atmospheric movement.

The skin of each crewman should be at a temperature somewhat higher than the surrounding equipment and walls in most designs, so that heat is lost to the surroundings by thermal radiation. The general equation for heat lost by this mechanism may be written as follows:

$$\dot{q}_r = \sigma A_b F_E F_A (T_S^4 - T_{mr}^4) \quad (2-7)$$

In current space vehicle designs, crewmen are almost completely surrounded by equipment. Some of this equipment, such as hot coolant lines, electronic, and electrical gear, will be above atmospheric temperature. Other gear, which will be below atmospheric temperature, will include cold coolant lines, cooling heat exchangers, and cold walls. Space cabin walls and equipment for the test conditions were  $\leq 2^\circ\text{F}$  from atmospheric gas temperatures. Most hot and cold equipment is expected to be well insulated to improve performance; therefore, a good initial approximation is that the mean radiation temperature will be near cabin gas temperature.

Published data show that the surface area of the average man is 19.5 sq ft (ref. 2-1). The view factor has been determined to be 0.8 (ref. 2-3). This agrees reasonably well with the Bioastronautics Data Handbook (ref. 2-4). For a crewman completely enclosed by cabin walls, the emissivity factor approaches the emissivity of the crewman (taken as 0.94 in reference 2-1). With these values for the constants, equation (2-7) becomes:

$$\dot{q}_r = 2.52 \times 10^{-8} (T_S^4 - T_g^4) \quad (2-8)$$

Equation (2-8) is plotted in fig. 2-2. For unclothed crewmen, body surface temperature will be the mean skin temperature. Clothing temperature will be lower than mean skin temperature of the suited crewman, and the amount is given as:

$$T_{sk} - T_S = \frac{(\dot{q}_r + \dot{q}_C) \text{CLO}}{A_b} \quad (2-9)$$

As previously mentioned, comfort tests have shown that the clothing (CLO) value is dependent upon the thermal conductivity of the atmospheric gas. Therefore, a correction must be made for an air CLO value in order to be valid for helium mixtures. Figure 2-3 gives the necessary correction. Equations 2-2 through 2-6, 2-8, and 2-9 will be used to determine the operating atmospheric envelope in the paragraphs to follow.

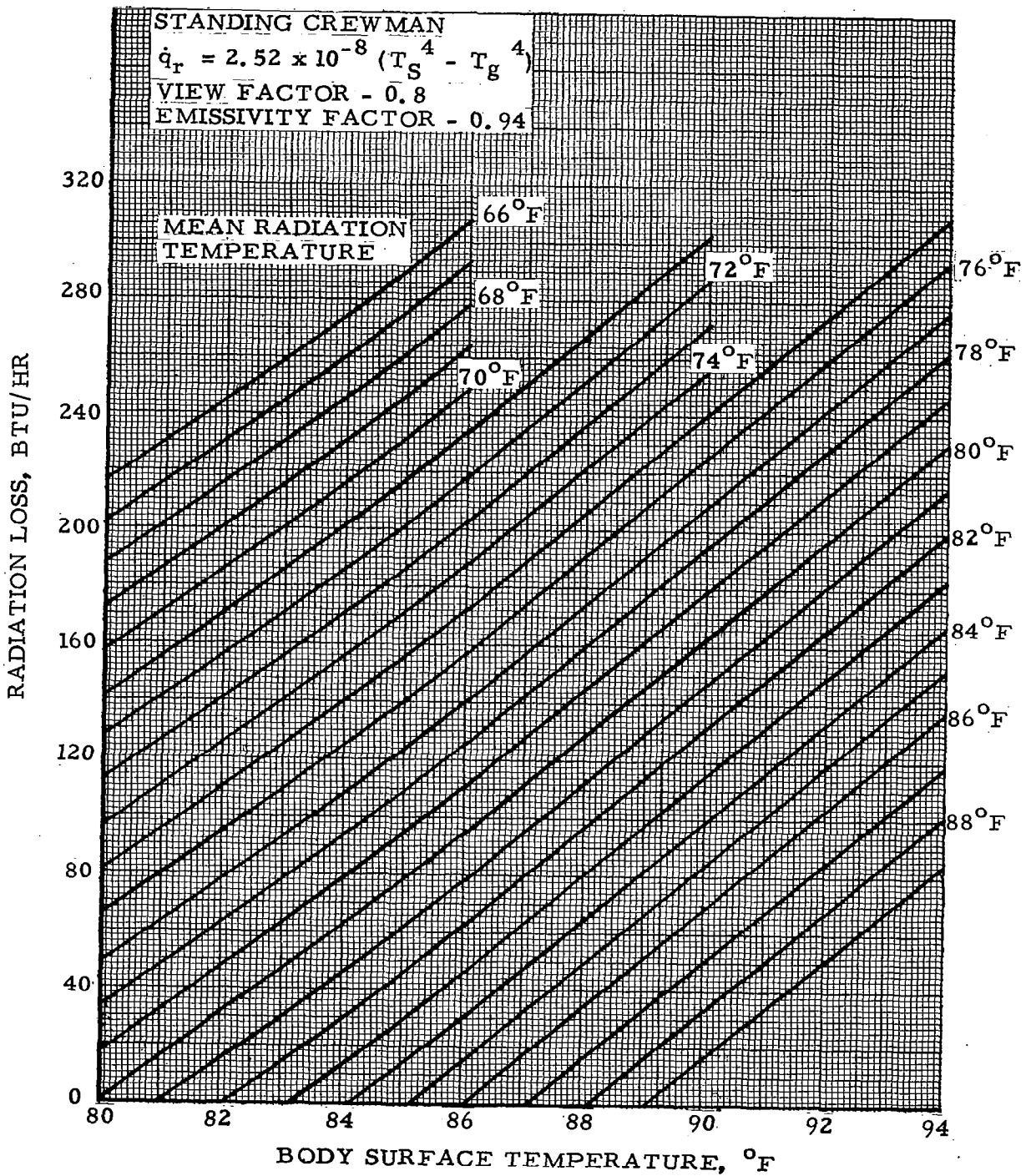


FIGURE 2-2 RADIATION HEAT LOSS

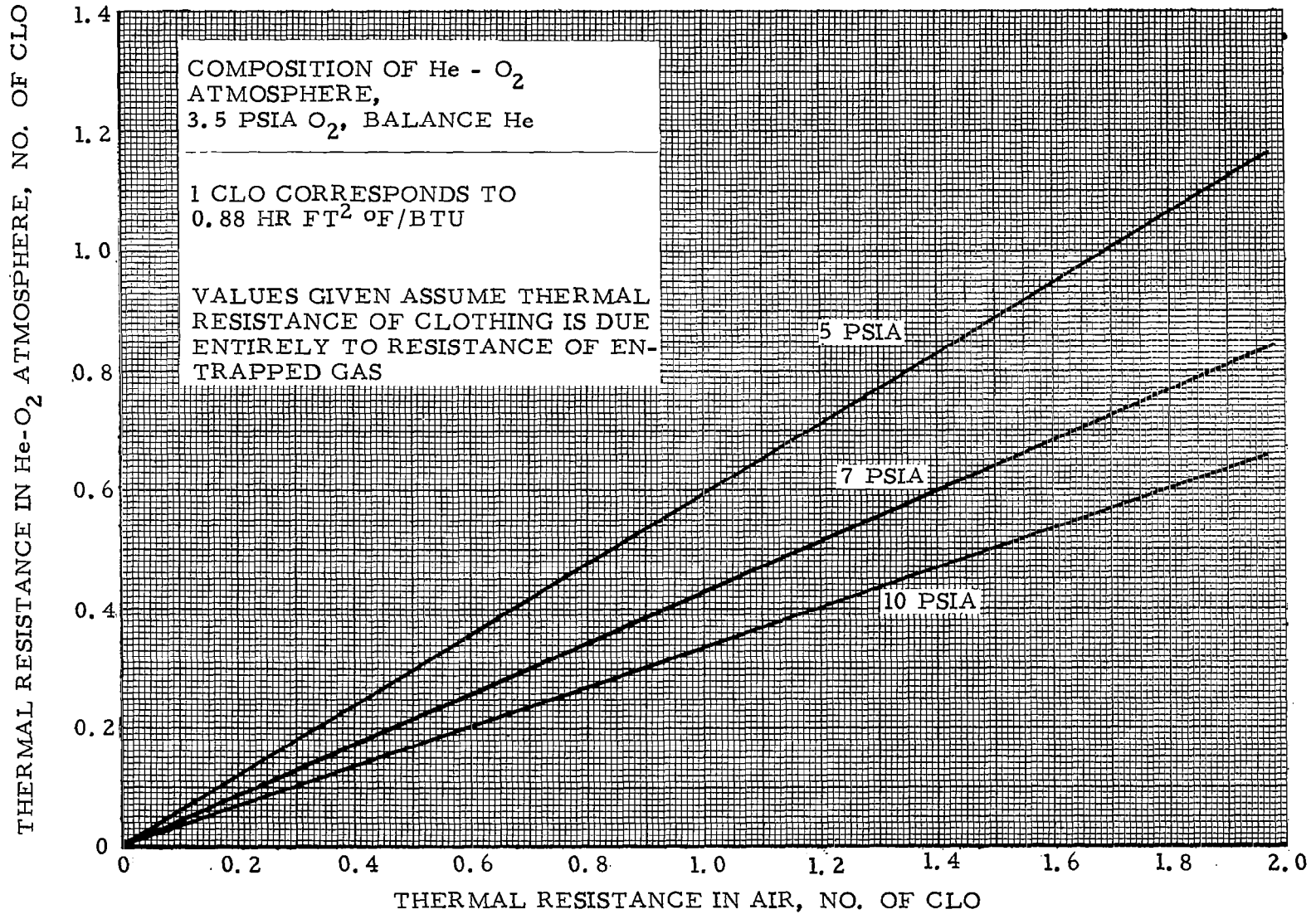


FIGURE 2-3 EFFECT OF GAS COMPOSITION ON CLOTHING THERMAL RESISTANCE

## COMFORT ZONE TEST PROCEDURE

The test apparatus consisted of the comfort simulator located in the space cabin simulator (fig. 2-4). The double walls of the six-sided chamber are constructed of insulating board and aluminized mylar. Atmospheric gas was introduced into the chamber through diffusers, flowed parallel to the test subjects, and then passed between the double walls to the exterior. This pattern of flow resulted in the inner wall being surrounded on both sides by gas at nearly a uniform temperature. The wall temperature followed within 2°F of atmosphere gas temperature. The test simulator was designed so that the atmospheric temperature equaled the wall temperature because this is the normal design condition for most space vehicles. High-performance wall insulation is necessary to prevent undesirable fluctuations in wall temperature with vehicle orientation and to prevent moisture from condensing on a cold wall. A well-insulated vehicle design will result in the wall temperature approximating the atmospheric temperature. In the event a vehicle is designed where the wall temperature is not equal to the atmospheric temperature, the equations from the preceding paragraphs can be used to extrapolate from test conditions. The chamber volume was 120 cu ft to approximate the volume of the operational portion of a small orbital laboratory. Figures 2-5 and 2-6 show the comfort simulator in the command area of the space cabin simulator. This simulator was, therefore, at the same atmospheric pressure, humidity, and composition as the cabin. Four different test subjects were used during the 18 days of testing in 79 test runs. Test atmospheres included 5- and 7-psia nitrogen-oxygen and 5-, 7-, and 10-psia helium-oxygen. The partial pressure of oxygen for these atmospheres was 3.5-psia. The pressure profile in the space cabin simulator for the 18-day test is shown in fig. 2-7.

A blower, located in the diffusion plenum of the comfort simulator, provided nominal gas velocities of 20, 50, and 80 fpm on the downstream side of the diffusers. Gas velocity rate was controlled by the subject inside the cabin by damping inlet flow to the blower. Water vapor partial pressure was maintained at approximately 10 to 12 mm Hg from within the cabin by the humidity control system. Dry bulb temperature was controlled by the test subject in the chamber. The temperature control system was designed to allow a temperature variation from 70° to 120°F about the set point at a rate of approximately 2°F/min. The response button used by the subject operated valves which controlled the increase or decrease in temperature of a circulating fluid passing through the heat exchanger. Comfort judgments made by the subject during an experimental session were recorded outside the cabin.

During the test, a subjective random-walk technique, was used in which the subject was told to allow the temperature to increase until he felt warm before pushing the response button and then to allow the temperature to decrease until he felt cool before pushing the button again. In this way, gas temperature was made to oscillate and the amplitude of these oscillations at the time the response button was pushed indicated upper and lower temperature limits. Each experimental session lasted 3 to 4 hr during which period approximately 10 upper and 10 lower determinations were obtained. A typical temperature history for a test is shown in fig. 2-8. A more detailed description of the test procedure can be found in ref. 2-9.

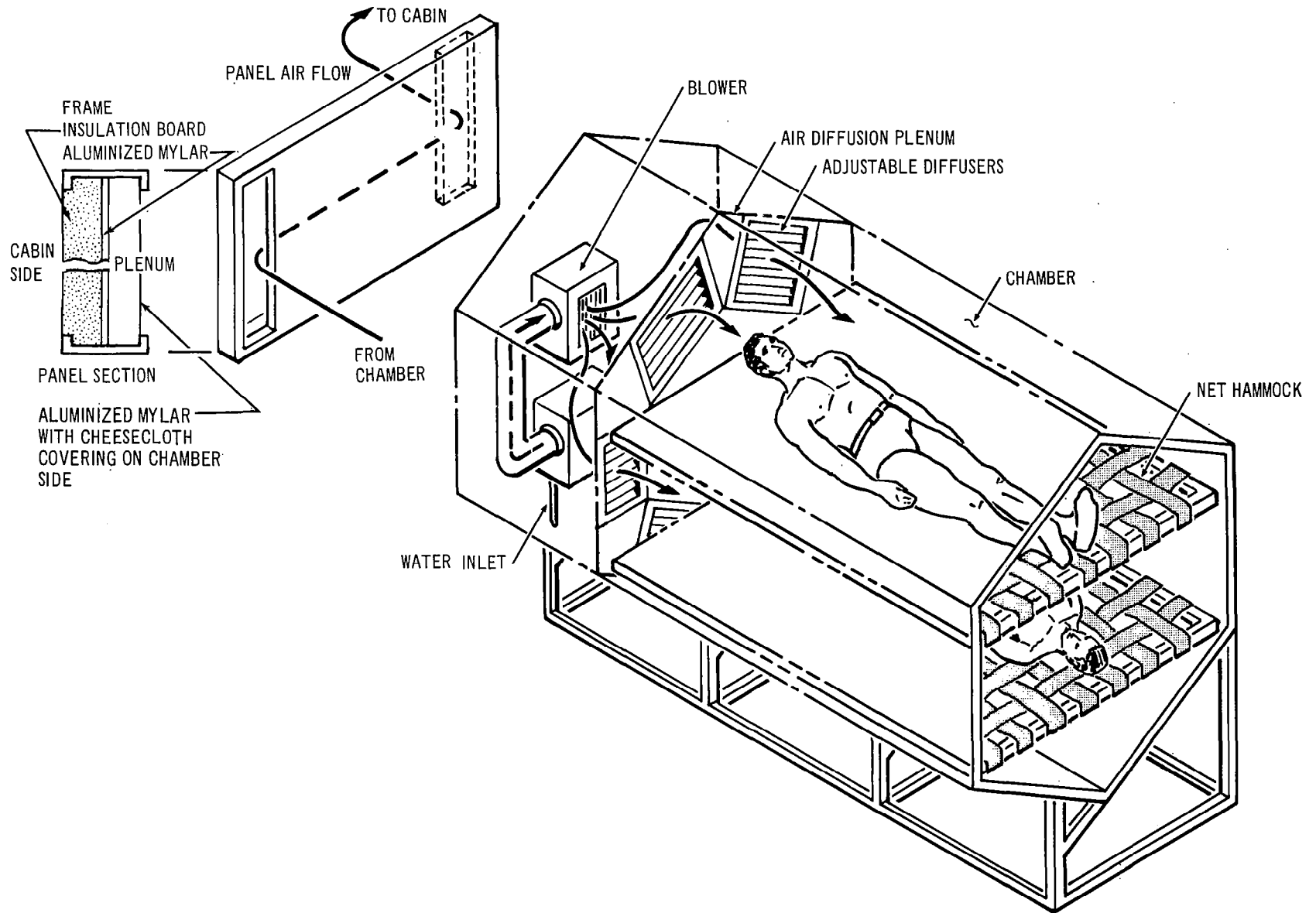


FIGURE 2-4. COMFORT SIMULATOR CONFIGURATION

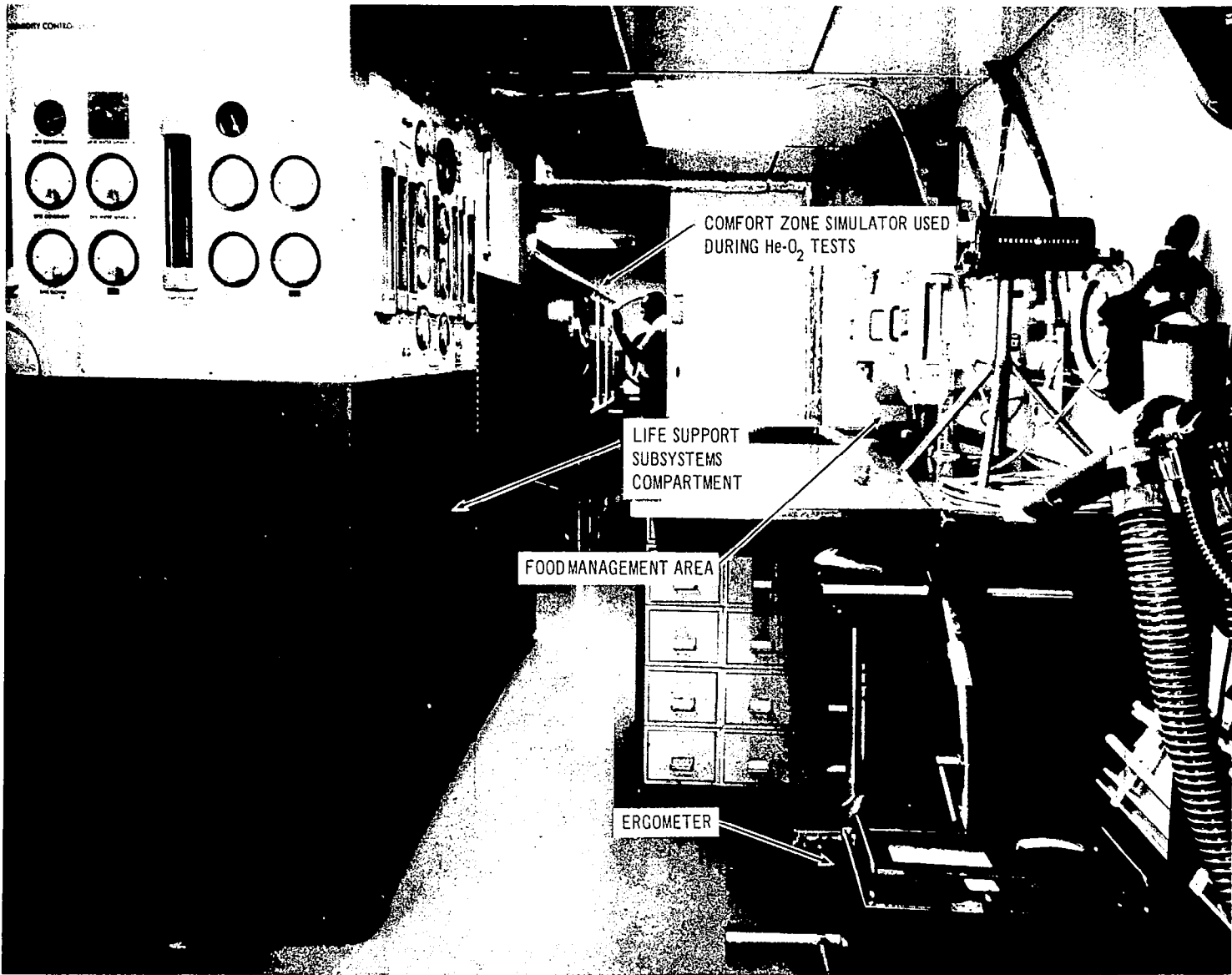


FIGURE 2-5. SPACE CABIN SIMULATOR LOOKING TOWARD COMMAND CENTER

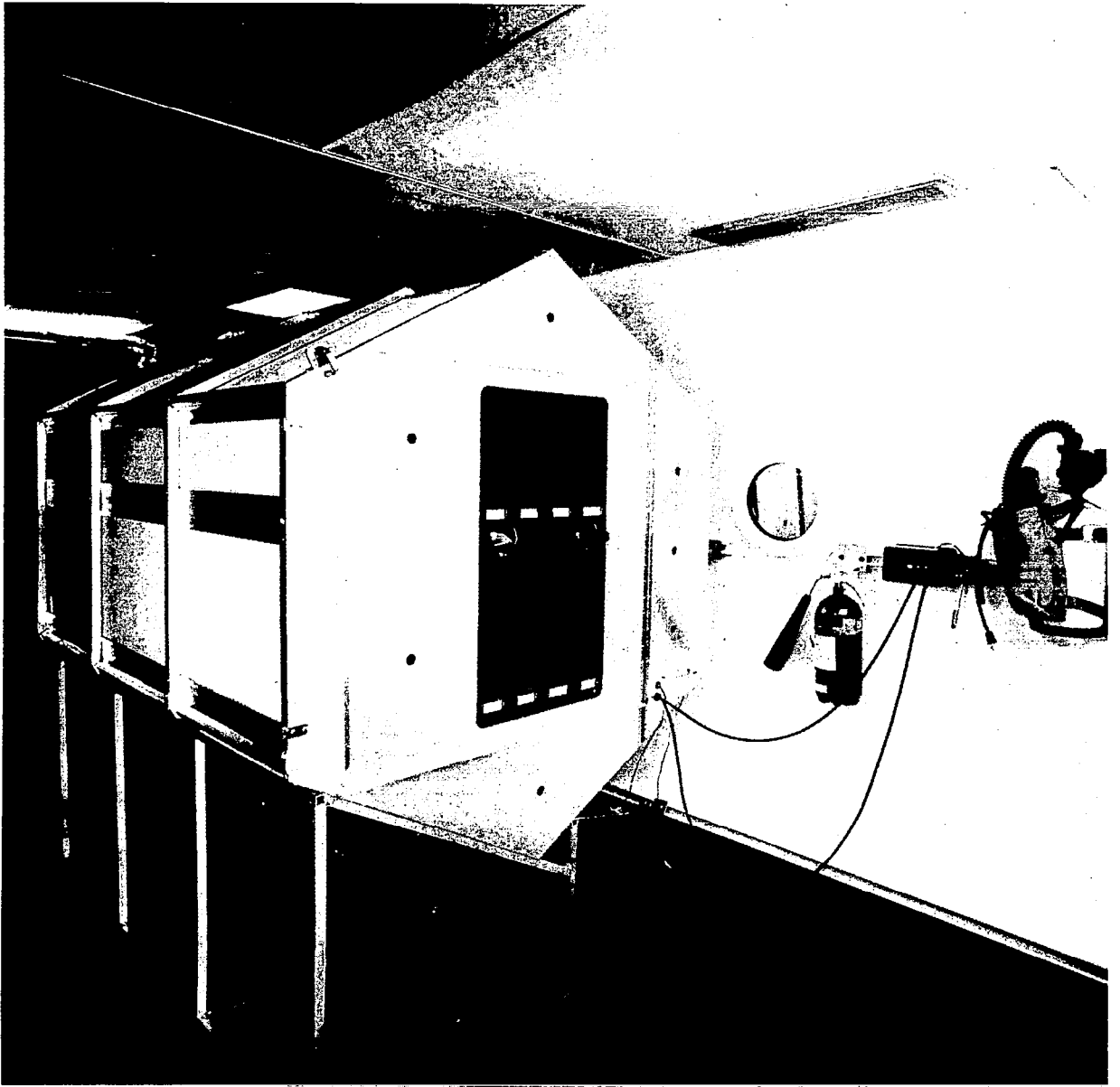


FIGURE 2-6 COMFORT SIMULATOR IN THE SPACE CABIN

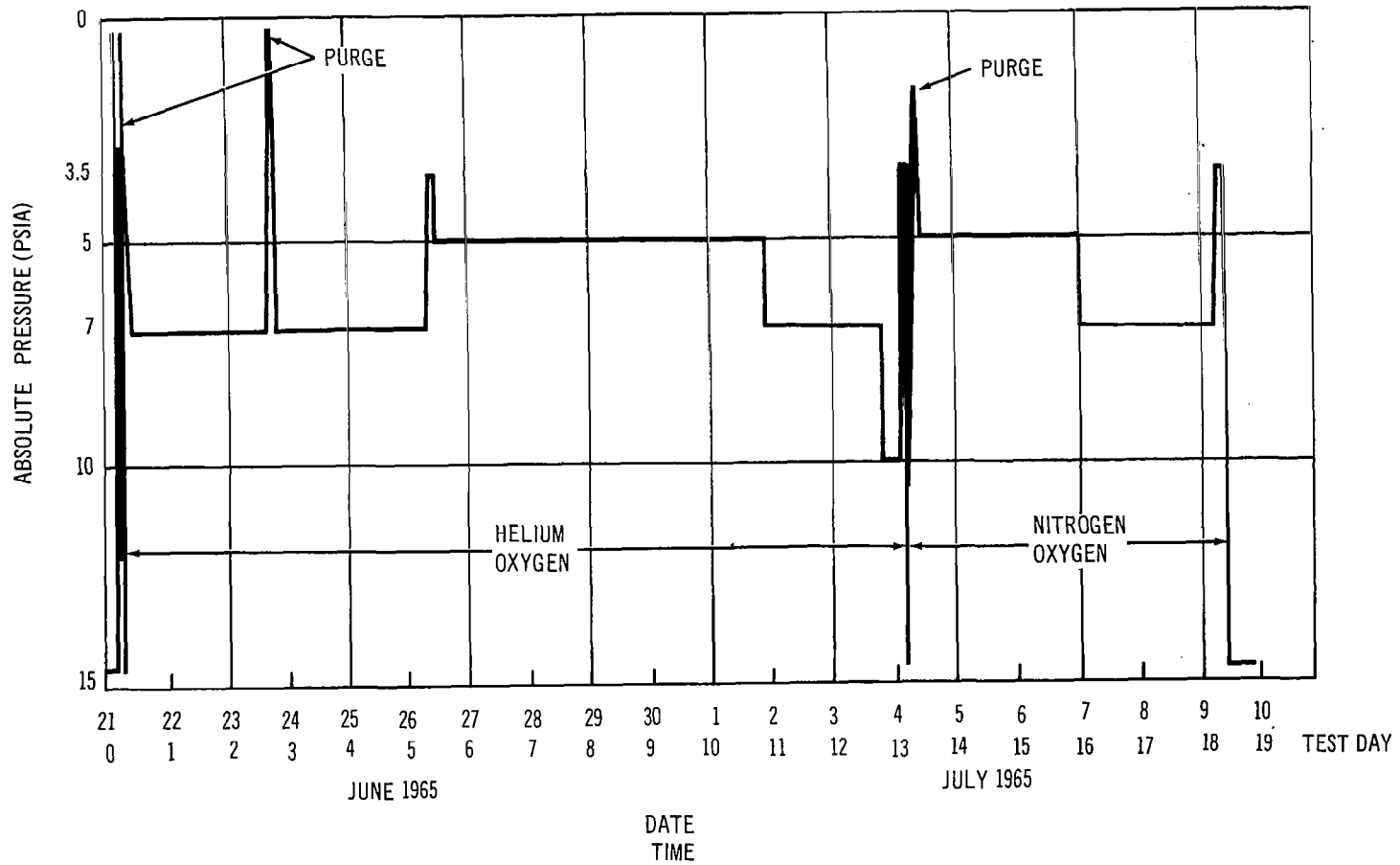


FIGURE 2-7. SPACE CABIN SIMULATOR PRESSURE PROFILE

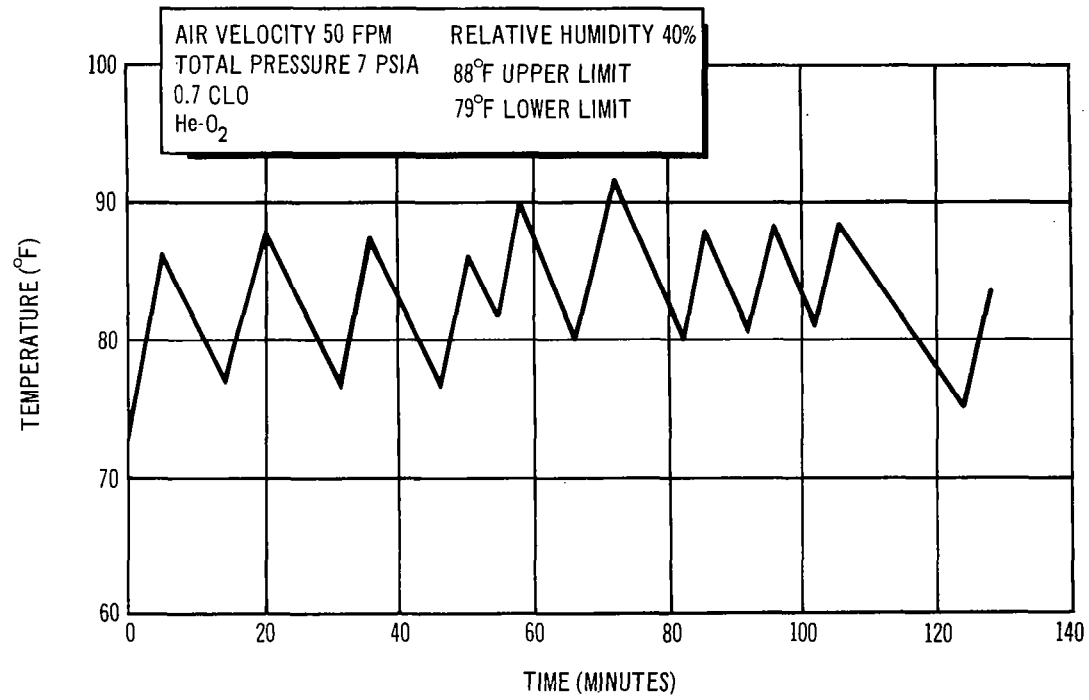


FIGURE 2-8. THERMAL COMFORT ZONE REPRESENTATIVE TEST RUN

In addition to the 18 days of tests with the comfort simulator, additional full-scale testing was performed under random space-vehicle conditions. During this time, actual space-cabin conditions were simulated in which the metabolic rates, gas velocities, and duty cycles were typical of a space mission. These tests included 30 days at 7 psia nitrogen-oxygen and 5 days at 5 psia helium-oxygen. Crewmen were allowed to select the most comfortable temperature during each test run.

## DATA CORRELATION

Test data obtained from the comfort tests were in the form of minimum and maximum gas temperatures for a given velocity, gas composition, and pressure. During the testing, the average time for temperature to go from maximum temperature to the coldest temperature was 10 minutes. Subsequent tests showed that this is not sufficient time for the body thermoregulatory mechanisms to react fully. Although the upper and lower limits were on the verge of comfort for short transient conditions, the subjects might become uncomfortable during long-term exposure to these conditions. However, the mean of the upper and lower limits should represent comfort for long-term exposure. This conclusion assumes that thermoregulatory devices react approximately linearly over the transient temperature range used in the testing. A comfort zone may then be established, based on the mean of upper and lower temperatures, for the different subjects.

Table 2-I presents test data from the 18-day comfort simulator tests for each of the test subjects. Note that the temperatures are averaged for all velocities. This table shows the variation of comfortable temperature between subjects. Table 2-II presents the data averaged for all subjects, but at each velocity so that velocity effects can be seen. The heat balance theory previously developed was used to calculate mean skin temperature for the conditions listed in table 2-II. Clothing values shown in table 2-II are corrected for increased thermal conductivity of the helium mixtures. Results show that mean skin temperatures vary from about 89.3° to 92.6°F. To avoid misleading results, data which varied excessively from the mean were not used.

Comfort skin temperatures did not vary appreciably between gas compositions and pressures. This verifies that the effects of gas composition and total pressures were properly taken into account in the analytical equations. General trends of the test data are shown along with the estimated zero-g comfort temperatures in figs. 2-9 and 2-10. Estimated comfort temperatures for varying velocities, clothing weights, and pressures are shown for zero g in figs. 2-11, 2-12, and 2-13. Test results from the comfort simulator are in good agreement with data from the full-scale space cabin simulator tests which used a work-rest cycle of MORL where the metabolic load was varied from that of full exercise to sleep.

TABLE 2-1

REPRESENTATIVE DATA FOR UPPER AND LOWER LIMITS OF COMFORT ZONE FOR EACH SUBJECT AS A FUNCTION OF ATMOSPHERIC COMPOSITION, PRESSURE AND CLO VALUE\*

Gas mixture**		He-O <sub>2</sub>					N <sub>2</sub> -O <sub>2</sub>			
Pressure		5 psia		7 psia		10 psia	5 psia		7 psia	
CLO value		0	0.7	0	0.7	0	0	0.7	0	0.7
<u>Subjects</u>	<u>Limit</u>									
CB	UL**	85	83	85	88	-	89	84	86	83
	LL**	76	73	77	77	-	76	72	77	73
JC	UL	100	101	102	100	100	104	-	104	-
	LL	77	71	77	74	77	72	-	79	-
BZ	UL	86	87	85	86	89	87	81	86	84
	LL	75	75	78	78	79	77	70	77	73
FD	UL	99	97	103	101	-	98	-	98	-
	LL	77	72	77	75	-	77	-	77	-
Means	UL	93	92	94	94	95	95	83	94	84
	MP***	84	82	86	85	86	86	77	86	78
	LL	76	73	77	76	78	76	71	78	73
<p>*Entries in degrees F  **Gas velocity--20 fpm to 80 fpm  ***UL - Upper Limit  MP - Mean Point  LL - Lower Limit</p>										

TABLE 2-II  
COMFORT ZONE TEST CONDITIONS AND RESULTS

Gas composition	Pressure (psia)	CLO value	Nominal velocity (ft/min)	Gas temperature (°F)	Calculated skin temperatures (°F)
He-O <sub>2</sub>	10	0	20	88.5	94.6
He-O <sub>2</sub>	10	0	80	84	89.4
He-O <sub>2</sub>	7	0	80	84	90.5
He-O <sub>2</sub>	7	0	50	84.5	90.7
He-O <sub>2</sub>	7	0.3	50	85	93.6
He-O <sub>2</sub>	7	0	20	88	94.5
He-O <sub>2</sub>	7	0.3	20	85	93.3
He-O <sub>2</sub>	5	0	80	85	91.9
He-O <sub>2</sub>	5	0	50	82.5	89.3
He-O <sub>2</sub>	5	0.41	50	83.5	93.6
He-O <sub>2</sub>	5	0	20	85	91.9
He-O <sub>2</sub>	5	0.41	20	80.5	89.7
N <sub>2</sub> -O <sub>2</sub>	5	0	20	84.5	91.7
N <sub>2</sub> -O <sub>2</sub>	5	0.7	20	79	91.1
N <sub>2</sub> -O <sub>2</sub>	5	0	50	85.5	91.4
N <sub>2</sub> -O <sub>2</sub>	5	0.7	50	75.5	86.2
N <sub>2</sub> -O <sub>2</sub>	7	0	20	85.5	92.6
N <sub>2</sub> -O <sub>2</sub>	7	0.7	20	77	88.5
N <sub>2</sub> -O <sub>2</sub>	7	0	50	85.5	92.6
N <sub>2</sub> -O <sub>2</sub>	7	0.7	50	79.5	90.9

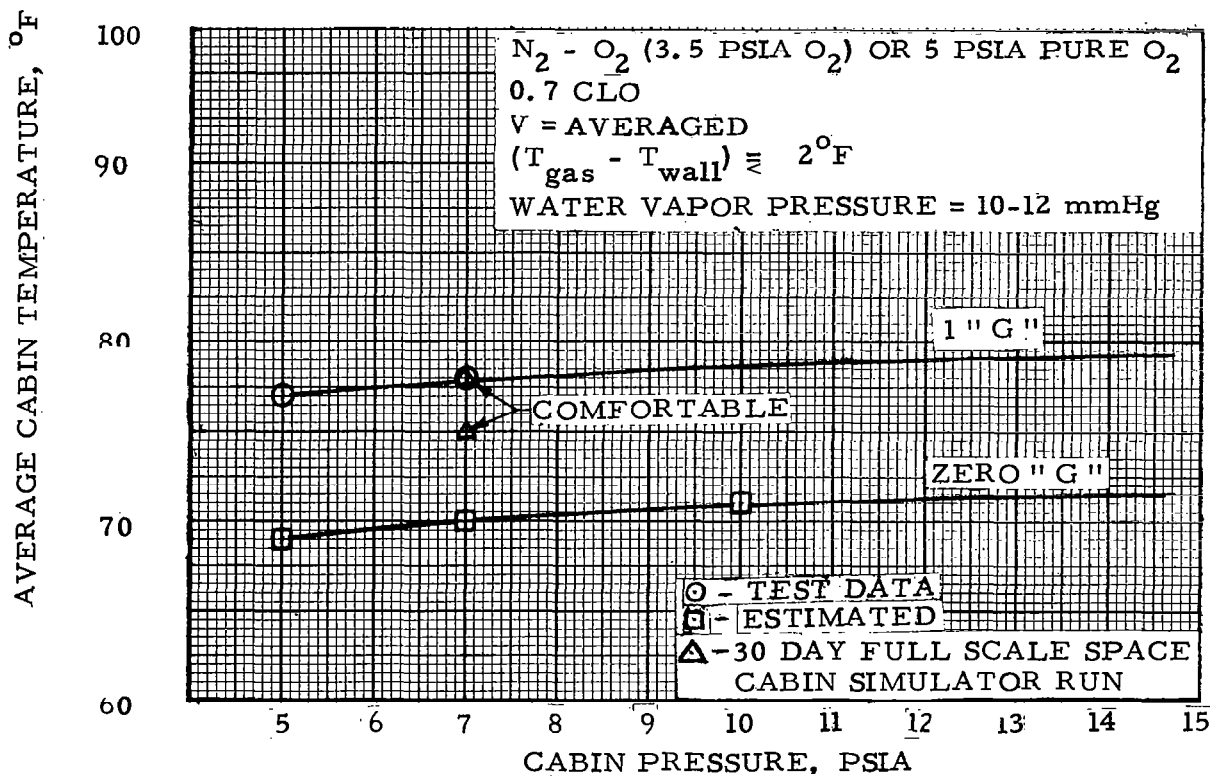
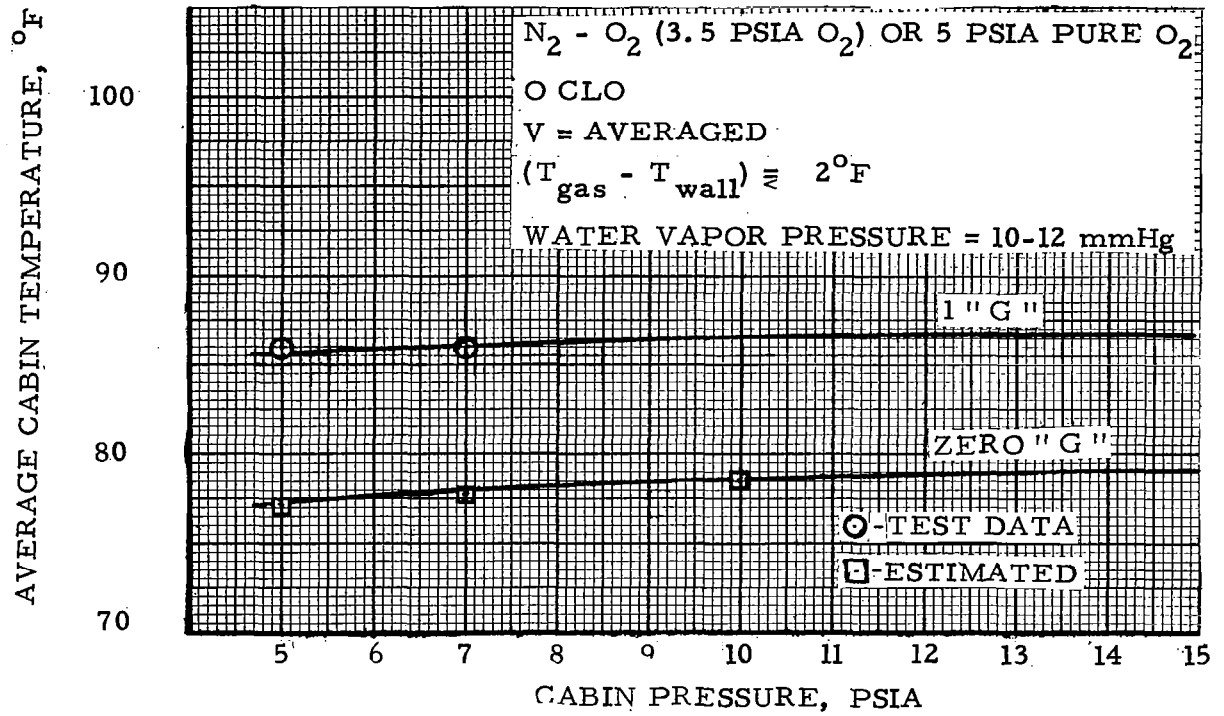


FIGURE 2-9 COMFORT TEMPERATURE DATA FOR NITROGEN-OXYGEN ATMOSPHERES

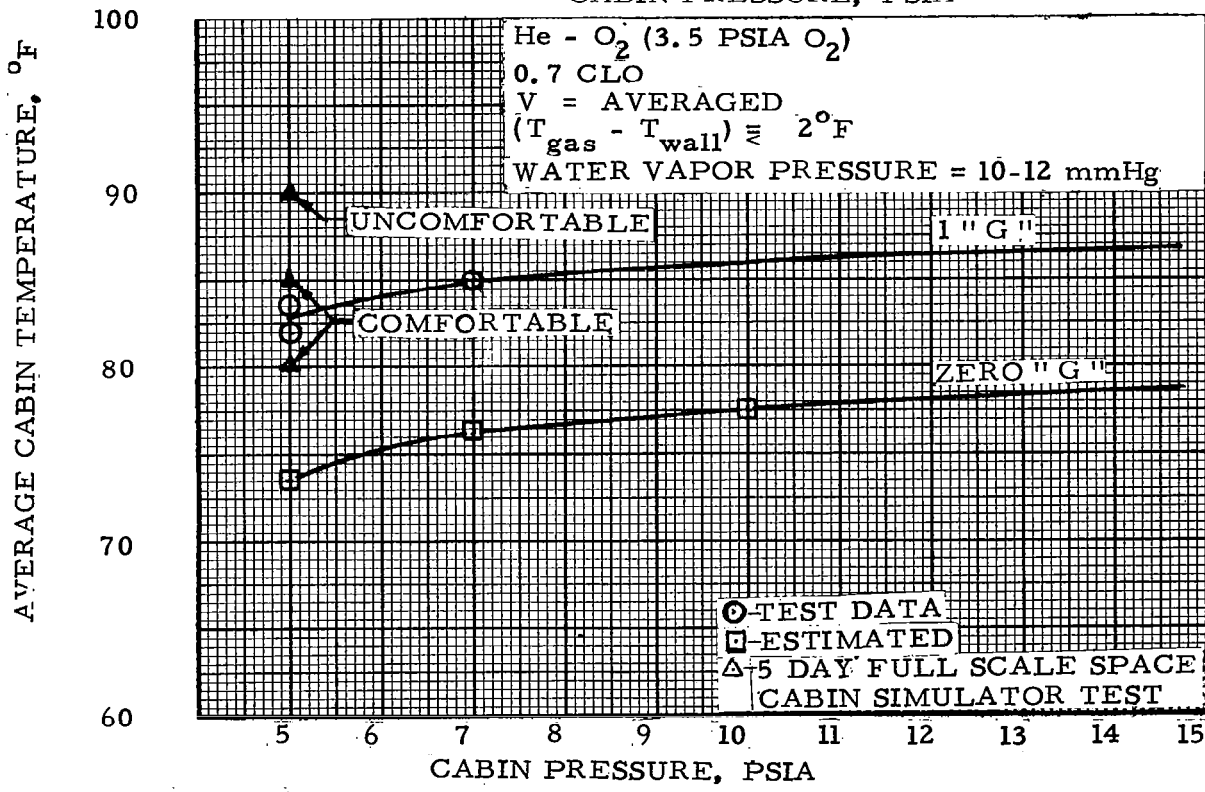
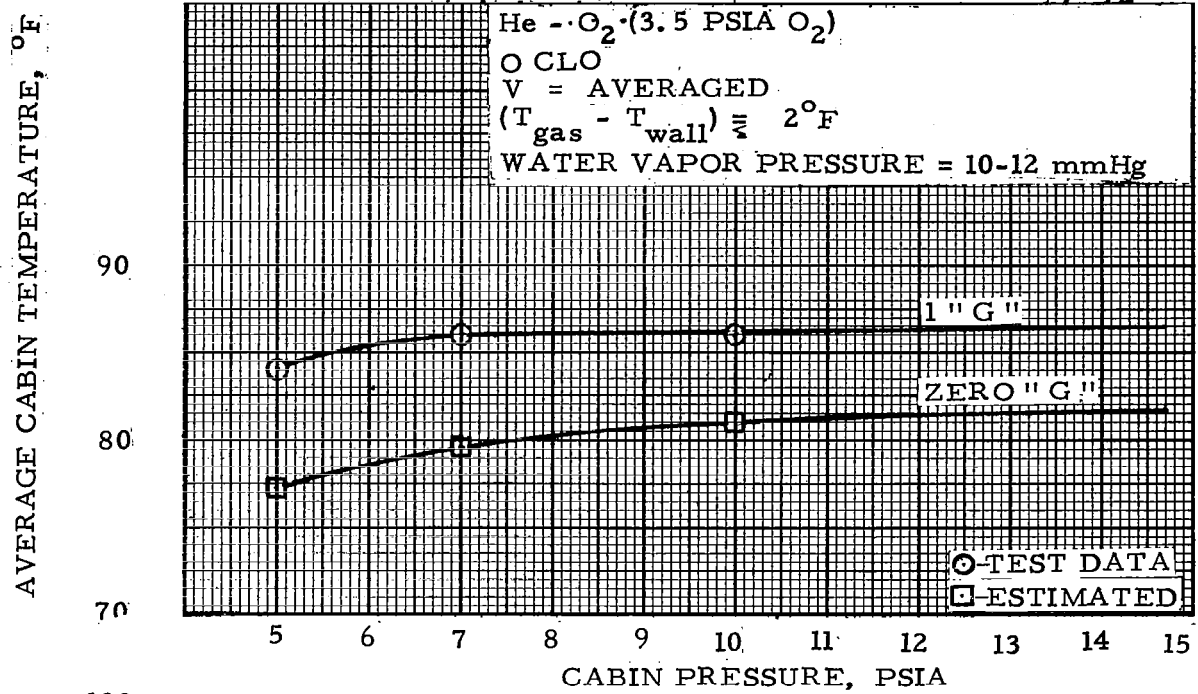


FIGURE 2-10 COMFORT TEMPERATURE DATA FOR HELIUM-OXYGEN ATMOSPHERE

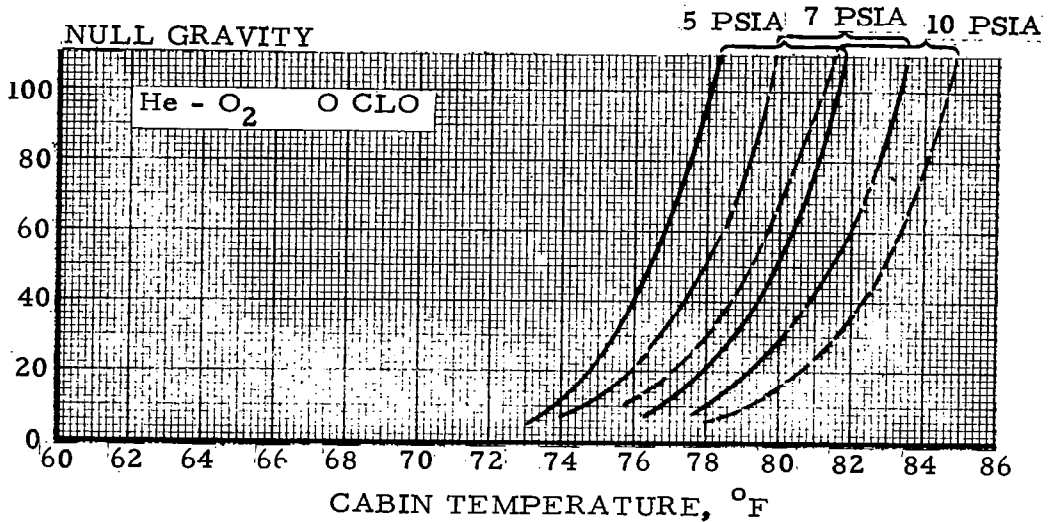
MEAN RADIATION TEMPERATURE  
EQUALS GAS TEMPERATURE

METABOLIC RATE = 460 BTU/HR

INSENSIBLE LOSS PER EQUATION (2-3)

RADIATION LOSS PER EQUATION (2-8)

VENTILATING VELOCITY, FT/MIN



MEAN RADIATION TEMPERATURE  
EQUALS GAS TEMPERATURE

METABOLIC RATE = 460 BTU/HR

INSENSIBLE LOSS PER EQUATION (2-3)

RADIATION LOSS PER EQUATION (2-8)

VENTILATING VELOCITY, FT/MIN

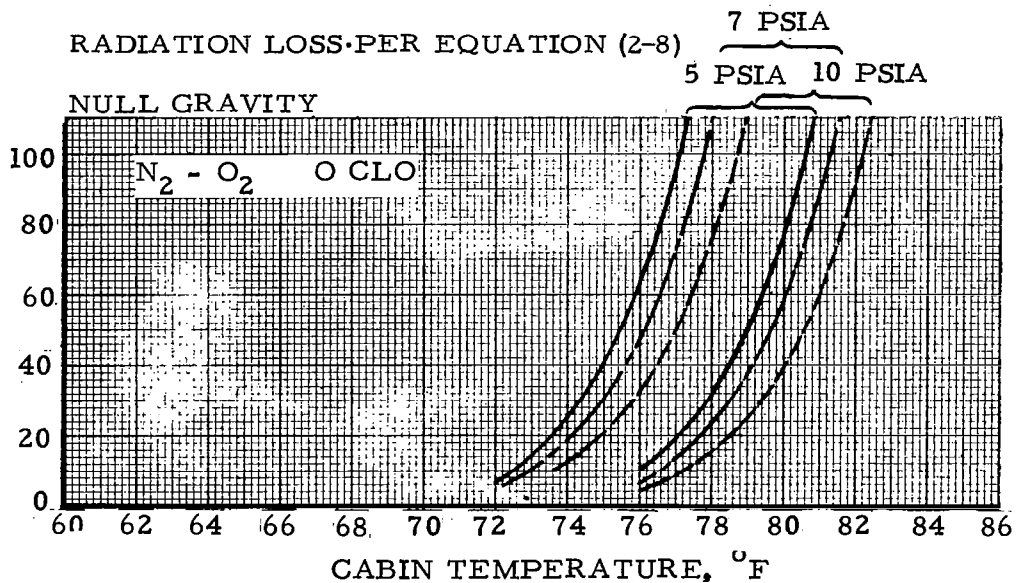


FIGURE 2-11 COMFORT ZONE

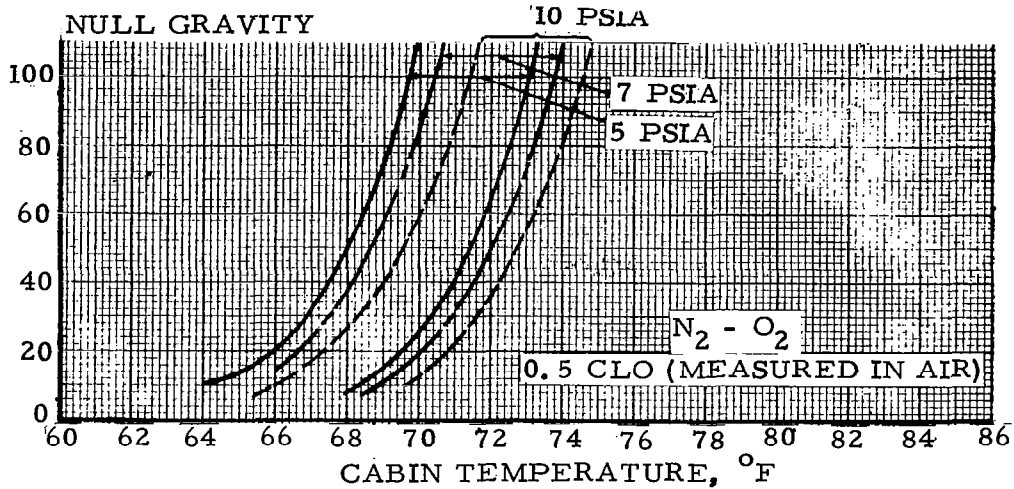
MEAN RADIATION TEMPERATURE  
EQUALS GAS TEMPERATURE

METABOLIC RATE = 460 BTU/HR

INSENSIBLE LOSS PER EQUATION (2-3)

RADIATION LOSS PER EQUATION (2-8)

VENTILATING VELOCITY, FT/MIN



MEAN RADIATION TEMPERATURE  
EQUALS GAS TEMPERATURE

METABOLIC RATE = 460 BTU/HR

INSENSIBLE LOSS PER EQUATION (2-3)

RADIATION LOSS PER EQUATION (2-8)

VENTILATING VELOCITY, FT/MIN

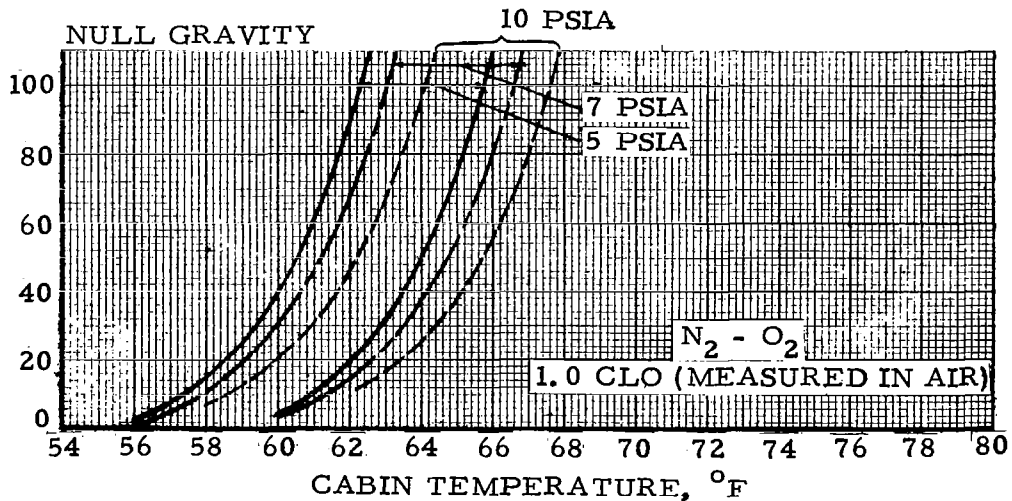


FIGURE 2-12 COMFORT ZONE

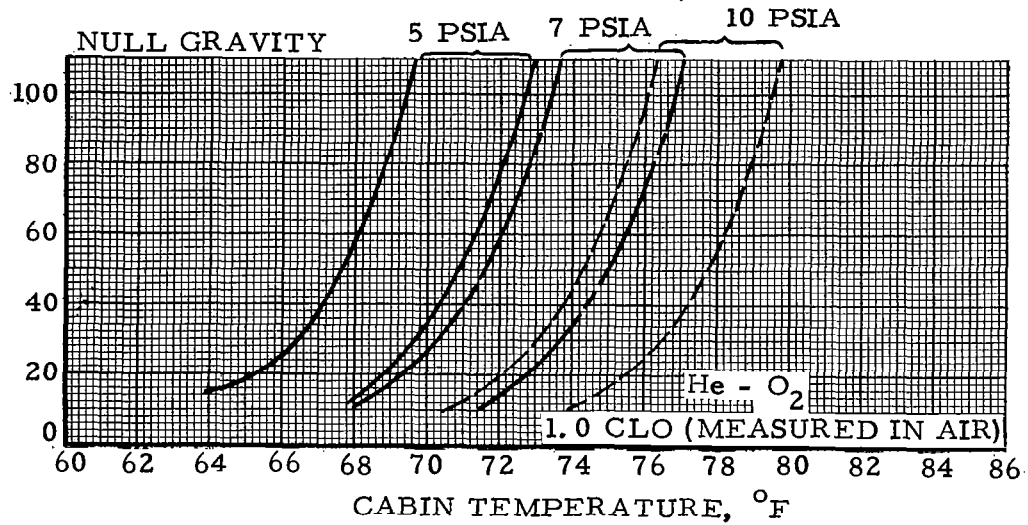
MEAN RADIATION TEMPERATURE  
EQUALS GAS TEMPERATURE

METABOLIC RATE = 460 BTU/HR

INSENSIBLE LOSS PER EQUATION (2-3)

RADIATION LOSS PER EQUATION (2-8)

VENTILATING VELOCITY, FT/MIN



MEAN RADIATION TEMPERATURE  
EQUALS GAS TEMPERATURE

METABOLIC RATE = 460 BTU/HR

INSENSIBLE LOSS PER EQUATION(2-3)

RADIATION LOSS PER EQUATION (2-8)

VENTILATING VELOCITY, FT/MIN

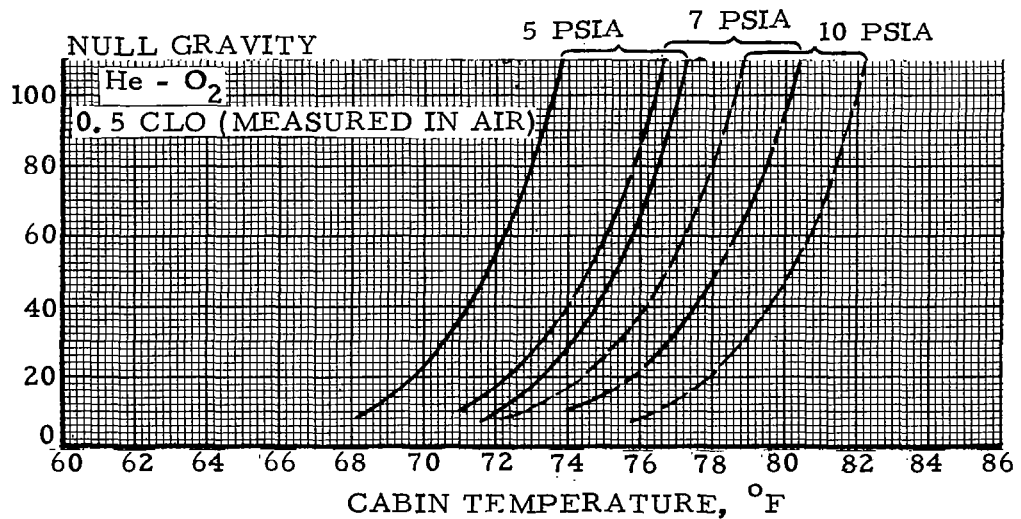


FIGURE 2-13 COMFORT ZONE

In general, comfort temperatures were considerably higher for helium mixtures for Earth conditions, medium clothing (0.7 CLO), and normal 20 ft/min to 80 ft/min gas velocities as can be seen from the following summary.

	5 psia*	7 psia*
He-O <sub>2</sub>	92°F upper limit 82°F average 73°F lower limit	94°F upper limit 85°F average 76°F lower limit
N <sub>2</sub> -O <sub>2</sub>	83°F upper limit 77°F average 71°F lower limit	84°F upper limit 78°F average 73°F lower limit
*3.5 psia O <sub>2</sub>		

From these data, the conclusion can be made that with helium diluent, approximately a 5°F to 7°F higher temperature can be used and still permit crew comfort.

The analysis, along with the range of comfortable mean skin temperatures, may be used to determine comfort conditions for the combinations of gas velocity, temperature, composition, pressure, wall temperature, gravity level, clothing value, and humidity which will produce a comfortable environment. Figures 2-11, 2-12, and 2-13 present some of these conditions in the form of comfort regions for null gravity.

Most future spacecraft will use high-performance super-insulation to minimize heat lost or gained by the spacecraft. This is also done to prevent moisture condensation on the walls and to prevent large fluctuations in wall temperature. Therefore, inside wall temperatures in many advanced vehicles will approach atmospheric cabin gas temperature. In addition, the many items of equipment in a spacecraft cabin act to block radiation. It can be assumed that equipment will be well insulated and that temperatures of equipment surfaces will be approximately the same as cabin temperature. Therefore, the assumption of mean radiation being near cabin temperature is reasonable until vehicle design details are known. If the surrounding walls and equipment are at a higher temperature than the cabin gas, then helium atmospheres are still more attractive than nitrogen for comfort. An example may be considered where the wall temperature is 80°F, the gas velocity is 50 ft/min, cabin pressure is 7 psia and the metabolic rate is 460 Btu/hr. Comfort temperatures evaluated from equation (2-2) to (2-9) are 70°F for helium-oxygen and 50°F for nitrogen-oxygen. Therefore, the comfort temperature difference is greater between the candidate diluents when radiation temperatures are greater. The lower atmospheric temperature for the nitrogen-oxygen will require a greater penalty for heat rejection due to the close approach of the cabin atmospheric temperature and the heat rejection temperature.

## CONCLUSIONS AND RECOMMENDATIONS

The comfort data presented provides information that can be used to guide penalty-tradeoff engineering. Comfort zones presented in figs. 2-11, 2-12, and 2-13 cover most anticipated space vehicles conditions. Comfort levels are applicable for a shirt-sleeve condition where minimal or no sweating occurs. The metabolic rate appears not to depend on the gas composition. The metabolic rate of 460 Btu/hr and cabin dew point of 60°F is considered to be a representative design condition based on 24-hr space-laboratory operation. Full-scale, long-duration tests at varying work loads tend to verify this assumption. Comfort temperature for other conditions may be approximated with the analytical equations given.

The following are representative data which have been modified to approximate null gravity conditions. The temperature range is for He-O<sub>2</sub> and N<sub>2</sub>-O<sub>2</sub> atmospheres with a gas velocity of 50 ft/min and a metabolic rate of 460 Btu/hr. Oxygen, argon, and neon comfort temperature level should approximate N<sub>2</sub>-O<sub>2</sub> data. Wall temperature is assumed to be within ±1°F of average cabin temperature.

	5 psia	7 psia	10 psia
He-O <sub>2</sub>			
0 CLO	76° - 80°F	78° - 81°F	79° - 83°F
0.5 CLO	72° - 75°F	75° - 78°F	77° - 80°F
1.0 CLO	68° - 71°F	72° - 75°F	74° - 78°F
N <sub>2</sub> -O <sub>2</sub>			
0 CLO	75° - 79°F	76° - 80°F	77° - 81°F
0.5 CLO	68° - 71°F	69° - 72°F	70° - 73°F
1.0 CLO	61° - 64°F	61° - 65°F	62° - 66°F

It has been indicated in the literature that not more than 2°F increase should be allowed for the helium-oxygen mixture when it is used instead of oxygen or nitrogen-oxygen (refs. 2-10 and 2-11). Low metabolic rates, the lack of accurate skin temperature data, and the small number of subjects tested throughout the nation has produced conjecture regarding large increases in temperature difference between He-O<sub>2</sub> and N<sub>2</sub>-O<sub>2</sub> mixtures. Full-scale space-cabin tests with a crew of four were conducted continuously for 30 days in a 4 000 cu ft chamber in N<sub>2</sub>-O<sub>2</sub> at 7 psia with clothing values between 0.5 and 0.7 and a wall temperature within 2°F of gas temperature. Crewmen had a work/rest cycle comparable to MORL varying from rest to full exercise. The average cabin-temperature level selected by the crew varied from a low of 75°F to a high of 78°F. A 5-day helium-oxygen test

at 5 psia under the same conditions was conducted by the same crewman. Crewmen were tested at 80°F for 24 hr and 85°F for 72 hr and stated that they were comfortable under both conditions. A 90°F cabin temperature created an uncomfortable situation. The cabin temperature difference between the N<sub>2</sub>-O<sub>2</sub> and He-O<sub>2</sub> atmospheres for these test conditions was about 7°F higher for the helium diluent. These tests, although subjective, tend to validate the magnitude of the temperature levels from the 18-day comfort data test as well as the selection of a metabolic rate of 400-500 Btu/hr for the full scale tests. A similar metabolic rate assumption for cabin average temperature selection can be considered valid for an engineering spacecraft design.

The most significant result with regard to predicted comfort zone from 1-g data concerns the higher comfort temperature for helium mixtures where the crewmen wear clothing. There were only minor temperature differences in tests for different atmospheric mixtures for zero or very little clothing conditions. This may explain why statements have been made that the comfort zone difference between He-O<sub>2</sub> and N<sub>2</sub>-O<sub>2</sub> is negligible. Average comfort temperature differences during the tests was 5° to 7°F for normal clothing values of 0.5 to 0.7. It is evident that the difference in heat transfer effect between nitrogen-oxygen and helium oxygen is small for light clothing weights, but becomes quite large for heavier clothing. Two effects are present: one is due to the larger convection heat transfer coefficient with helium mixtures caused by higher gas conductivity, the second results from the influence of gas conductivity on the resistance to heat flow in the clothing. Thermal resistance of clothing appears to be dependent on the thermal resistance of the atmospheric gas entrapped in the clothing.

Tests for accurately determining clothing resistance in various atmospheres are needed to further substantiate this observation for heavier clothing. In addition, comfort tests are recommended using more test subjects with varying clothing weight in atmospheres containing diluents of nitrogen, helium, argon and neon at varying pressures. The effect of insensible loss and skin temperatures must be measured accurately during the tests. The effect of increased cabin wall temperature on allowable cabin atmosphere temperature should be tested and the equations presented in this section substantiated for extrapolation to conditions where the wall temperature greatly differs from the cabin gas temperature. This will refine the comfort zones and will allow the effects of atmospheric composition to be investigated more fully. Tests are also needed to determine thermal conductivity of clothing samples in various gas mixtures to establish the effect of entrapped gas on effective thermal conductivity.

## REFERENCES

- 2-1. Jansen, J. E.: Thermal Comfort in Space Vehicles, ASME paper 59-A-207, 1959.
- 2-2. Biotechnology 130AB Syllabus, UCLA Department of Engineering, 1957.
- 2-3. Dubois, E. F.: Mechanism of Heat Loss and Temperature Regulations, Trans. of the Assn. of Am. Physicians, vol. 51, 1936, p. 252.
- 2-4. Webb, Paul, editor: Bioastronautics Data Handbook, NASA Scientific and Technical Information Division, 1964.
- 2-5. Ulsamer, J., Forschung a.d. Geb. d. Ingenieurwes. 3, 94; 1932.
- 2-6. Berenson, P. J.: General Analysis of Human Thermal Comfort, NASA Report CR 216, 1965.
- 2-7. Chapman, A. J.: Heat Transfer, Macmillan Company, New York, 1960.
- 2-8. Winslow, C.; Gagge, A. P.; and Herrington, L. P.: The Influence of Air Movement Upon Heat Losses from the Clothed Human Body, Amer. J. Physiol., 127: 1939, pp 505-518.
- 2-9. Space Cabin Life Support Systems, Douglas Report SM-49256, vo. 3, Jan. 1966.
- 2-10. Epperson, W. L.; et al: Observations on Man in an Oxygen-Helium Environment at 380 mm Hg Total Pressure. III Heat Exchange, Aerospace Medicine, May 1966.
- 2-11. Roth, E. M.: Space Cabin Atmospheres, Part IV, Engineering Trade-offs of One Versus Two Gas Systems, Lovelace Foundation for Medical Education and Research NASA, 15 Mar. 1966.

### Section 3

#### LEAKAGE

One of the prime considerations in spacecraft-atmosphere supply-system design is cabin leakage. This includes the penalty for provision of make-up for continuous leakage, the design restraints imposed by requirements for safe-time during transient leakage, such as that caused by meteoroid puncture, and the provisions for repressurization following loss of atmosphere.

Data have been obtained and are presented in the following section which covers transient and steady-state leakage for helium-oxygen and nitrogen-oxygen atmospheres. Cabin pressures considered were 5, 7, and 10 psia with an oxygen partial pressure of 3.5 psia in all cases. In addition, normal air was tested at 14.7 psia. The correlation of these data with various theoretical models is discussed. In general, test data are reasonably close to that predicted by theory.

Besides the leakage of atmosphere from the space cabin, a secondary leakage problem is introduced by the leakage of helium into vacuum tubes and other evacuated containers if this gas is a constituent of the chosen atmosphere. Data on this leakage are also presented.

Two basic types of vehicle atmospheric leakage were considered in the test program: (1) slow leakage through minute cracks, penetrations, and seals; and (2) emergency leakage, such as that which could be caused by meteoroid penetration, structural failure, or malfunction of overboard valves. Most of the designers engaged in future spacecraft studies have used normal leakage rates that range from 1 to 5 lb/day, depending on vehicle size and design. Major leakage, in most instances, has been through hatch and/or hanger seals. Total vehicle leakage has been accounted for by carrying sufficient supply gas to compensate for normal steady-state leakage and to provide for at least one complete compartment or vehicle repressurization for emergency conditions.

Test results for steady-state leakage indicated that, in all cases, leakage flow by weight was greater for nitrogen-oxygen than for helium-oxygen at the same total pressure primarily because of the low density of helium mixtures. However, the quantity of oxygen lost with helium diluent is greater than with nitrogen. This additional loss results from the higher sonic velocity of the helium-oxygen mixtures. At constant oxygen partial pressure, the density of oxygen in the mixture is constant. Because the velocity of helium-oxygen flow is higher than an equivalent nitrogen-oxygen mixture, the volumetric flow rate increases with increasing helium concentration. The result is an increasing oxygen loss even though the density is constant. This agrees with the results of the tests with the

Douglas space cabin simulator in which higher oxygen leakage rates were noted during long-duration helium-atmosphere tests.

The difference in leakage between the two mixtures depended on atmospheric pressure and hole size. The leakage rate for nitrogen-oxygen was from 20% to 159% higher by weight than for helium atmospheres. Test results on cabin pressure decay followed adiabatic decompression theory reasonably closely. Flow coefficients calculated from the data were approximately 0.6. These values agree well with the values given in ref. 3-1 and 3-2. In all tests, cabin decompression times were less for helium-oxygen mixtures. Crew members in helium-oxygen cabins would have from 12% less time at 5 psia to 40% less at 10 psia to take emergency action during decompression.

For a typical spacecraft application, the difference in leakage rate can be translated into launch weight penalty, with the consideration of the storage penalty and gas weight. A 1-year-in-orbit space station with a 90-day resupply period and a design leakage of 2 lb per day for nitrogen-oxygen at 7 psia is an example. The leakage rate for helium-oxygen for the equivalent hole size and cabin pressure is 1.21 lb/day. When considering leakage only, the use of helium-oxygen will save approximately 55 lb at 7 psia and 92 lb at 10 psia for each 90-day resupply period. No appreciable savings are noted at 5 psia, because the weight of gas saved is offset by the high helium-storage penalty.

The penalty for leakage from meteoroid puncture or other emergency conditions can be accounted for by assuming complete loss of gas from one compartment. The weight savings for a MORL volume of 5360 cu ft for helium-oxygen as compared to nitrogen-oxygen is 5 lb at 5 psia, 57 lb at 7 psia, and 155 lb at 10 psia. These penalties are based on the gases being stored as supercritical cryogenic fluid. Storage penalties are based on data presented in the Section 5 on gas storage penalties.

Another potential problem area noted during simulator runs with helium atmospheres was premature failure of vacuum tubes. An analytical study indicated that helium leakage rates through some types of electronic tube glass may be great enough to adversely effect component life. Leakage into tubes was verified by measuring helium concentration after exposure to helium atmospheres. It is not known with certainty if the leakage occurred through the glass or through the metal-to-glass seals. Additional testing is needed to determine the nature of helium leakage and the design modifications needed to avoid contamination. Based on current knowledge of the problem, it is believed that the electron tube contamination problem can be solved by modifying equipment design.

The following sections describe leakage tests performed, analytical theory from which correlations are made, and recommended applicable equations for leakage predictions based on the correlated test results.

## ORIFICE FLOW, CAPILLARY FLOW, AND LAMINAR PIPE FLOW THEORY

The relative leakage rates of candidate atmospheres depend largely upon the assumed leakage geometry. The two types of leakage considered are low, normal-rate leakage and emergency high-rate leakage. The two types of leakage differ in flow geometry and with upstream pressure variation. The small normal-leak rate occurs during the entire mission and therefore cabin pressure must remain constant. On the other hand, an emergency leakage occurs when the leak rate is larger than the make-up gas flow rate and pressure decay occurs in the cabin.

Orifice Flow Theory. Orifice flow occurs when the diameter of the hole is large compared to the length. Because the flow through the orifice is assumed to be discharging to space, sonic flow occurs at the vena contracta. The equation for this type of flow is

$$\dot{w} = P C_D A \left[ \frac{g}{RT} \right]^{1/2} \left[ \gamma \left( \frac{2}{\gamma+1} \right)^{\frac{\gamma+1}{\gamma-1}} \right]^{1/2} \quad (3-1)$$

This equation applies to both steady-state and transient cases. Steady-state conditions occur during normal spacecraft operation when the leakage rate is small. For this case, relative leak rates for the candidate atmospheres can be calculated.

Table 3-I gives the ratio of leak rate by weight for nitrogen-oxygen and helium-oxygen at the pressures under consideration. Constant upstream pressure is assumed.

TABLE 3-I

RATIO OF NITROGEN-OXYGEN TO HELIUM-OXYGEN  
LEAK RATES BY WEIGHT FOR SONIC FLOW

5 psia	7 psia	10 psia
1.113	1.250	1.393

The values assume that the discharge coefficient does not vary appreciably with the gas mixtures considered, and this was verified by test results. The table shows that the nitrogen-oxygen leak rate, by weight, is from 11.3 to 39.3% higher than for helium-oxygen.

A differential equation may be obtained describing cabin pressure decay as a function of time for the case of variable upstream pressure and temperature. This is done by differentiating the equation of state [eq. (3-2)], then combining the result with [eq. (3-1)] and the relationship between pressure and temperature [eq. (3-3)]. The result may then be integrated with appropriate boundary conditions (ref. 3-3). For an isothermal process, the specific heat ratio  $\gamma$  becomes unity, and the integrated form is [eq. (3-4)]. If the process is adiabatic, the integrated result is [eq. (3-5)]. Polytropic processes can occur where the value of gamma,  $\gamma$ , is between unity and the specific heat ratio. Equation (3-5) is also valid for polytropic processes.

$$Pv = RT \quad (3-2)$$

$$P \frac{1-\gamma}{\gamma} T = \text{constant} \quad (3-3)$$

$$P = P_o e^{-\alpha t} \quad (3-4)$$

$$P = P_o \left[ \alpha \left( \frac{\gamma-1}{2} \right) t + 1 \right]^{\frac{2\gamma}{1-\gamma}} \quad (3-5)$$

where

$$\alpha = \frac{C_{DA}}{V} \left( \frac{gR_u T_o}{M} \right)^{1/2} \left[ \gamma \left( \frac{2}{\gamma+1} \right)^{\frac{\gamma+1}{\gamma-1}} \right]^{1/2}$$

A typical plot of pressure decay characteristics is shown in fig. 3-1. The figure shows that an adiabatic process will result in a more rapid pressure decay. The isothermal case decays at the slowest rate with the polytropic case decaying at a rate between adiabatic and isothermal.

Capillary Flow. The leakage path in capillary flow is assumed, analytically, to be a long straight tube. Gas enters the tube at cabin pressure and the flow at this point is laminar continuum flow. As gas flows down the tube, the gas expands sufficiently to cause a transition to free molecular flow before exiting the tube to space vacuum.

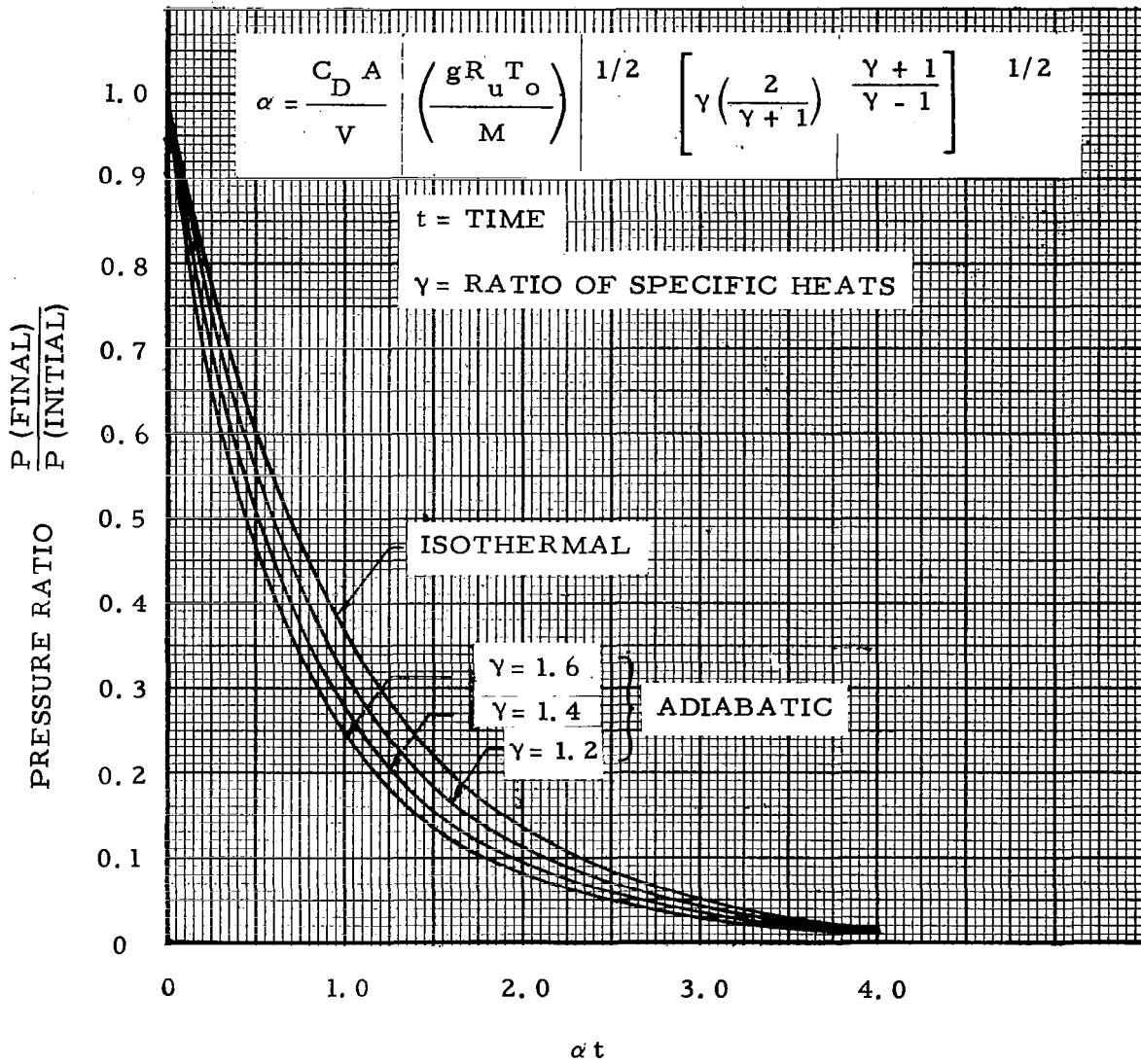


FIGURE 3-1 PRESSURE DECAY CHARACTERISTICS

Mason (ref. 3-5) has proposed the following equation for capillary flow

$$Q = \frac{5.22 D^4 P'^2}{10^6 \mu' L_C} + \frac{7.42 D^3 P'}{10^6 L_C} \sqrt{\frac{T'}{M'}} + \left[ \frac{7.44 D^2 \mu' T'}{10^8 M' L_C} \right] \left[ \ln \left( 1 + \frac{23.9 D P'}{\mu'} \sqrt{\frac{M'}{T'}} \right) \right] \quad (3-6)$$

Table 3-II shows the ratio, by weight, of the leakage rates for nitrogen-oxygen atmosphere to helium-oxygen atmosphere, as calculated by equation 3-6. These data are calculated for oxygen partial pressure of 3.5 psia and diluent partial pressures of 1.5, 3.5, and 6.5 psia. This table shows that the leakage rate is higher when nitrogen is the diluent than when helium is used, and this difference is increased as the pressure is increased (corresponding to an increase in diluent fraction). Also, the weight of nitrogen-oxygen leakage increases relative to helium-oxygen leakage as hole size is increased.

TABLE 3-II  
RATIO OF NITROGEN-OXYGEN TO HELIUM-OXYGEN  
LEAK RATES BY WEIGHT FOR CAPILLARY FLOW

Hole diameter ( $\mu$ )	Total pressures		
	5 psia	7 psia	10 psia
1.0	1.170	1.354	1.633
3.0	1.219	1.473	1.850
10.0	1.281	1.540	2.095
30.0	1.320	1.716	2.220

In reference 3-5, Mason also calculates the number of leakage paths required to produce 1 lb/day leakage and concludes that this number is prohibitively large for holes smaller than  $1\mu$ . According to his data,  $9.7 \times 10^7$  capillaries of 1 mm length and  $1\mu$  diameter would be required for 1 lb/day leakage; only 590 are required if the diameter is increased to  $30\mu$ .

As shown in the following derivation and subsequent test data, there is a fault in Mason's theory and the resulting equation (3-6). He assumes the entering pressure to the tube is at cabin pressure, and the discharge pressure is at free space pressure, with the pressure loss distributed along the length of the tube and a gradual transition from laminar continuum flow to free molecular flow within the tube. Actually, as shown by several investigators, the pressure loss in the tube causes a gradual decrease in fluid density and a corresponding acceleration. The limiting velocity in the tube is the acoustic velocity, which can only be reached at the outlet end of the tube. If this velocity is reached, the pressure at the outlet of the tube is determined by upstream conditions and further reduction in downstream (external) pressure cannot influence the flow. Calculations of pressure drop along real capillaries show that this is generally the case except when they are very small or very long. The pressure at the outlet of the tube is very much higher than in free space, the remaining pressure loss is in the supersonic expansion external to the tube, and pressures are sufficiently high so that continuum flow is maintained within the tube.

If the flow within the tube can be assumed to be laminar, continuum flow, at constant temperature the pressure drop is given by the following equation (equation (168), page 186, of reference 3-15)

$$\frac{P_1^2 - P_2^2}{P_1^2} = \frac{fL v_1^2}{d g P_1 v_1} \quad (3-7)$$

in which the subscript 1 refers to tube inlet conditions and 2 to the outlet. By the perfect gas law,

$$P_v = \frac{P}{\rho} = RT \quad (3-8)$$

or

$$\rho = \frac{P}{RT}$$

According to the Hagen-Poiseuille law for laminar flow, (page 154, Ref. 3-6),

$$f = \frac{64}{Re_D} \quad (3-9)$$

where

$$Re_D = \frac{\rho DU}{\mu}$$

Substituting into equation (3-7) results in:

$$\frac{P_1^2 - P_2^2}{P_1^2} = \frac{64\mu L U_1}{g d^2 P_1} \quad (3-10)$$

By the continuity equation,

$$\frac{\dot{W}}{A} = \rho U = \rho_1 U_1 = \rho_2 U_2 \quad (3-11)$$

or

$$U_1 = \frac{\dot{W}}{A \rho_1} \quad (3-11)$$

Substituting equations (3-8) and (3-11) in equation (3-10),

$$P_1^2 - P_2^2 = \frac{64 \mu L}{g d^2} RT \frac{\dot{W}}{A} \quad (3-12)$$

By definition of Mach number,

$$Ma = \frac{U}{\sqrt{\gamma g RT}} \quad (3-13)$$

At the outlet of the tube,

$$U_2 = Ma_2 \sqrt{\gamma g RT} \quad (3-14)$$

Substituting equations (3-8) and (3-14) in equation (3-11),

$$\frac{\dot{W}}{A} = \rho_2 U_2 = \frac{P_2}{RT} Ma_2 \sqrt{\gamma g RT}$$

$$\frac{\dot{W}}{A} = P_2 Ma_2 \sqrt{\frac{\gamma g}{RT}} \quad (3-15)$$

Substituting equations (3-15) into (3-12) and dividing by  $P_1^2$ ,

$$1 - \left(\frac{P_2}{P_1}\right)^2 = \left[\frac{64 L}{d^2}\right] \left[\frac{Ma_2}{P_1} \sqrt{\frac{T}{g}}\right] \left[\mu \sqrt{\gamma R}\right] \frac{P_2}{P_1} \quad (3-16)$$

Defining  $C_L$ :

$$C_L = \frac{1}{2} \left[\frac{64 L}{d^2}\right] \left[\frac{Ma_2}{P_1} \sqrt{\frac{T}{g}}\right] \left[\mu \sqrt{\gamma R}\right] \quad (3-17)$$

and substituting in equation (3-16) results in

$$\left(\frac{P_2}{P_1}\right)^2 + 2 C_L \frac{P_2}{P_1} - 1 = 0 \quad (3-18)$$

Equation (3-18) may be solved by the quadratic equation:

$$\frac{P_2}{P_1} = -C_L + \sqrt{1 + C_L^2} \quad (3-19)$$

Note that the positive sign is used because only positive solutions for pressure ratio are desired. Also, the expression for  $C_L$  (equation 3-17) includes three groups of symbols. The first depends on tube geometry; the second upon flow conditions, and the third upon the gas composition.

Direct solution of equation (3-19) depends upon knowledge of the tube inlet pressure  $P_1$ . If the inlet velocity head is negligible, this pressure is equal to the cabin pressure. However, if there is appreciable velocity at the inlet this reduces  $P_1$ , and an iterative solution is required.

Because velocity is inversely proportional to pressure for the isothermal flow,

$$M_{a1} = M_{a2} \frac{P_2}{P_1} \quad (3-20)$$

The inlet pressure of the capillary can then be found from the following equation.

$$P_1 = \frac{P_o}{\left(1 + \frac{\gamma - 1}{2} M_{a1}^2\right)^{\gamma / \gamma - 1}} \quad (3-21)$$

For the typical flow condition in which a significant excess pressure remains at the outlet of the capillary, the flow solution can be found as follows:

- (1) Evaluate  $C_L$  from equation (3-17) for  $M_{a2} = 1.0$  and assuming  $P_1 = P_o$  (cabin pressure).
- (2) Solve equation (3-19) for  $P_2 / P_1$ .
- (3) Evaluate equation (3-21). If  $P_1$  is sufficiently different from that assumed previously, in evaluating  $C_L$ , re-evaluate and return to step 2.
- (4) Find  $P_2$ .
- (5) The flow through the capillary is given by equation (3-15):

$$\frac{W}{A} = P_2 \sqrt{\frac{\gamma g}{RT}}$$

The above procedure has been followed for capillaries having diameters from 1 to 300  $\mu$  at cabin pressures of 5, 7, and 10 psia, with helium-oxygen or nitrogen-oxygen atmospheres. In all cases, the partial pressure of oxygen is 3.5 psia. Figure 3-2 shows the capillary outlet pressure  $P_2$  as a function of these variables and figure 3-3 shows  $W/A$ . Figure 3-4 shows the ratio of nitrogen-oxygen flow to helium-oxygen flow rates, by weight, from the above solution.

For the case in which  $C_L$  is large (capillary diameter is small or length is large), an approximate solution of equation 3-19 is possible. First, factor  $-C_L$ :

$$\frac{P_2}{P_1} = -C_L \left[ 1 - \sqrt{\frac{1}{C_L^2} + 1} \right]$$

Representing the square root by the first term of the series expansion,

$$\frac{P_2}{P_1} = -C_L \left[ 1 - \frac{1}{2 C_L^2} - 1 \right]$$

Therefore,

$$\frac{P_2}{P_1} = \frac{1}{2 C_L} \quad (3-22)$$

Because  $C_L$  is large,  $Ma_1$  is small and

$$P_1 = P_o$$

Therefore,

$$P_2 = \frac{P_o}{2 C_L}$$

The weight flow rate is

$$\frac{\dot{W}}{A} = P_2 \sqrt{\frac{Yg}{RT}} = \frac{P_o}{2 C_L} \sqrt{\frac{Yg}{RT}} \quad (3-23)$$

For two-gas mixtures, denoted by the subscripts A and B, with other parameters equal, the ratio of weight flow rates is given by

$$\frac{\dot{W}_A}{\dot{W}_B} = \frac{C_{LB}}{C_{LA}} \sqrt{\frac{Y_A}{Y_B} \frac{R_B}{R_A}} \quad (3-24)$$

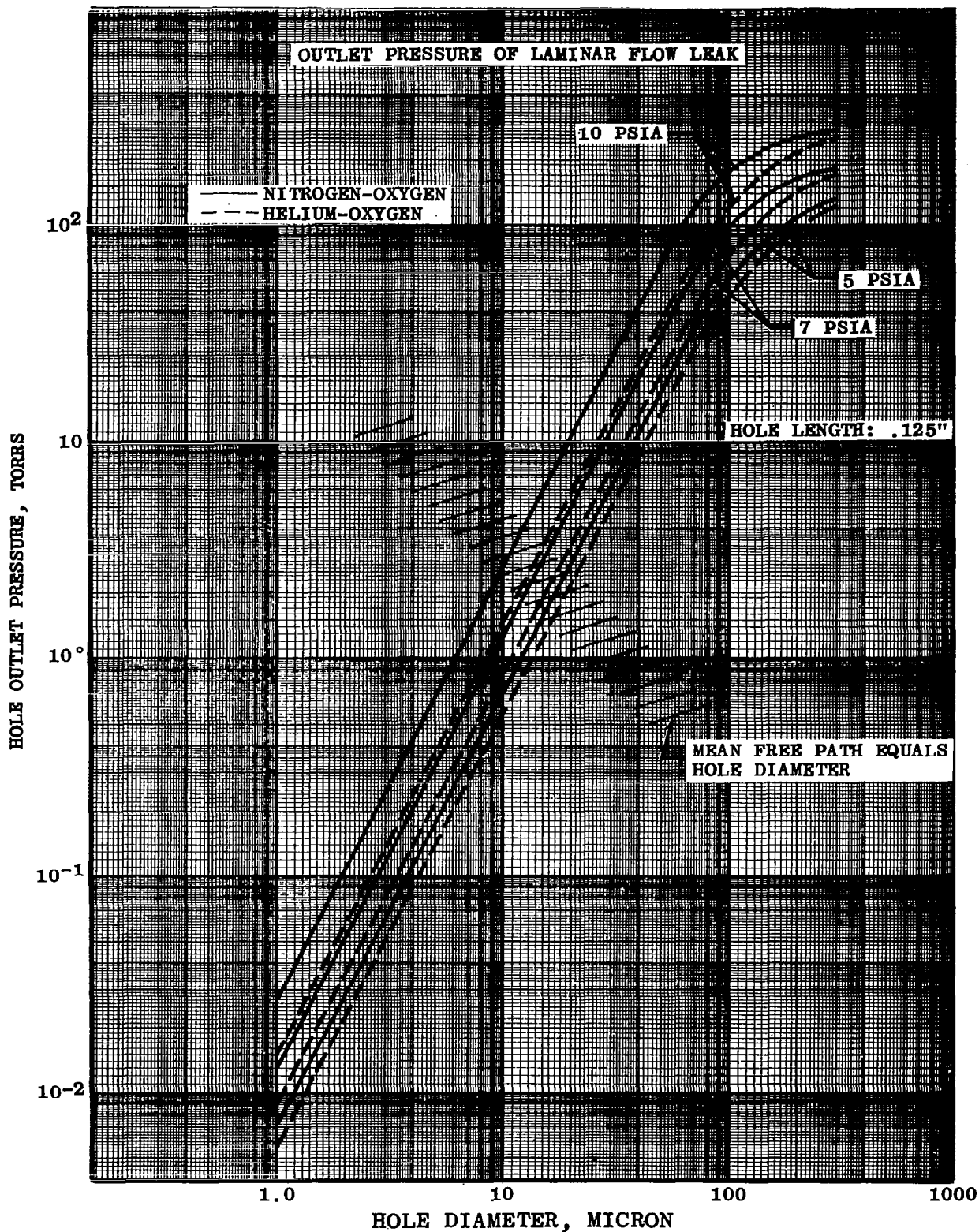


FIGURE 3-2 OUTLET PRESSURE OF LAMINAR FLOW LEAK

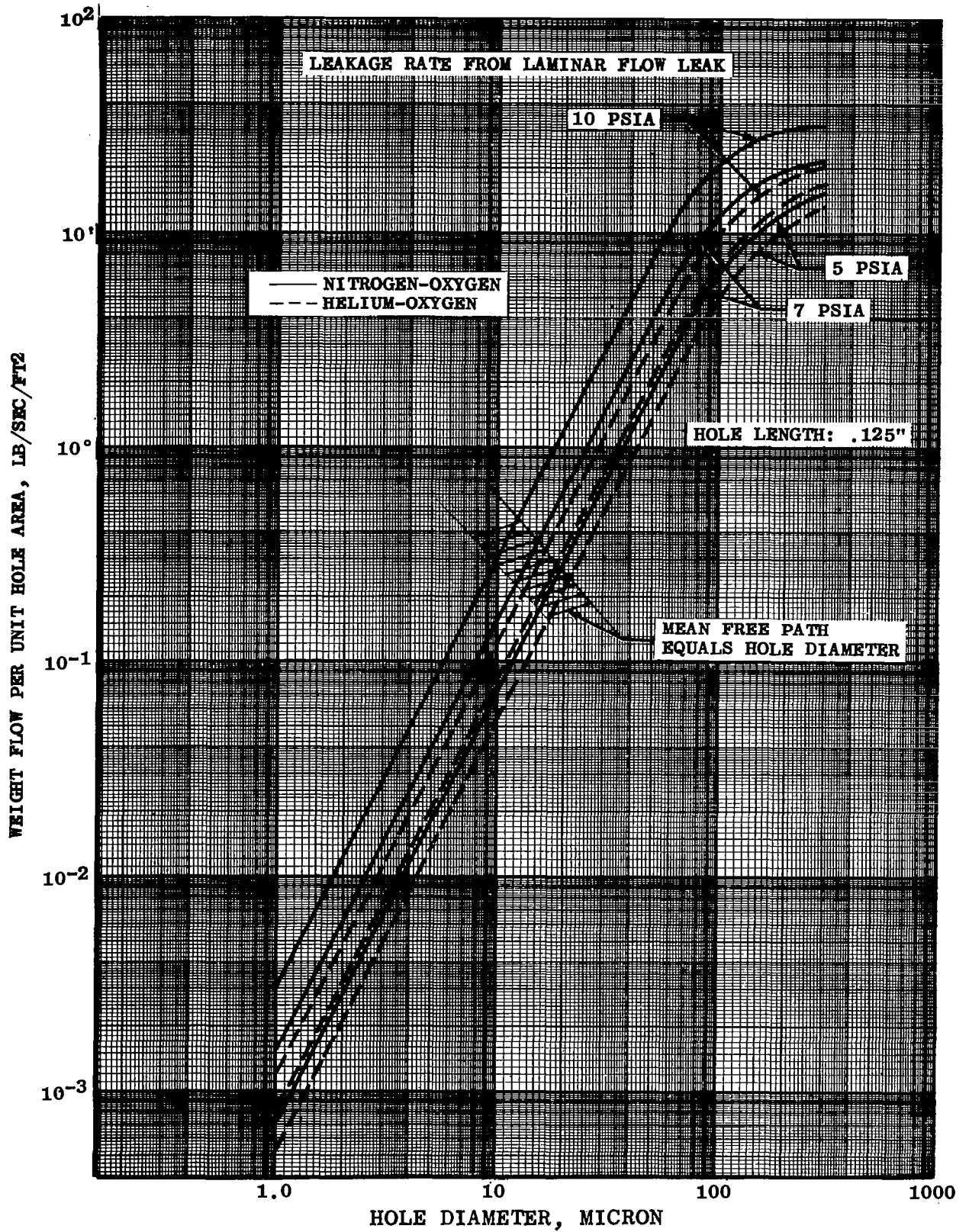


FIGURE 3-3 LEAKAGE RATE FROM LAMINAR FLOW LEAK

RATIO OF NITROGEN-OXYGEN FLOW TO HELIUM-OXYGEN FLOW

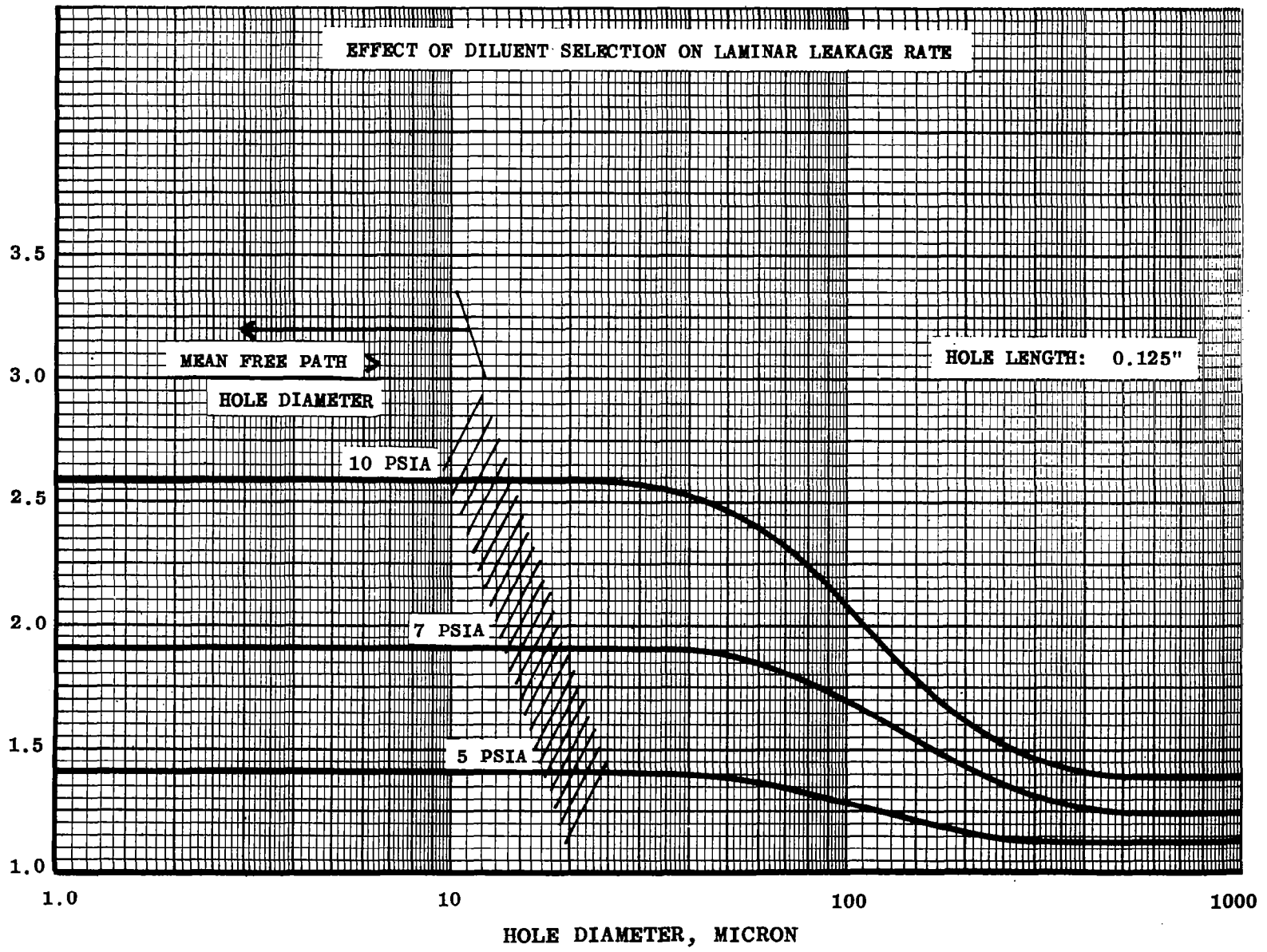


FIGURE 3-4 EFFECT OF DILUENT SELECTION ON LAMINAR LEAKAGE RATE

and

$$\frac{C_{LA}}{C_{LB}} = \frac{\mu_A}{\mu_B} \sqrt{\frac{\gamma_A}{\gamma_B} \frac{R_A}{R_B}} \quad (3-25)$$

Therefore,

$$\frac{\dot{W}_A}{\dot{W}_B} = \frac{\mu_B}{\mu_A} \sqrt{\left(\frac{\gamma_B}{\gamma_A} \frac{R_B}{R_A}\right) \left(\frac{\gamma_A}{\gamma_B} \times \frac{R_B}{R_A}\right)}$$

$$\frac{\dot{W}_A}{\dot{W}_B} = \frac{\mu_B}{\mu_A} \frac{R_B}{R_A} \quad (3-26)$$

Equation (3-26) is an expression for the asymptote approached by the weight flow ratio of two gases as hole diameter is reduced. The other asymptote, as hole size is increased, is given by the orifice flow, (eq. 3-1 or table 3-I). Table 3-III shows the weight ratio calculated by equation 3-26 for nitrogen-oxygen and helium-oxygen mixtures. Note that the ratios tabulated for the mixed flow theory of Mason, from table 3-II, approach the values from table 3-III as hole diameter increases.

TABLE 3-III

RATIO OF NITROGEN-OXYGEN TO HELIUM-OXYGEN LEAK RATES,  
BY WEIGHT, FOR LAMINAR FLOW IN SMALL CAPILLARIES

5 psia	7 psia	10 psia
1.395	1.890	2.59

The validity of the assumption of laminar flow must be tested. On the upper end of the range, the Reynold's number, based on hole diameter, for the 300  $\mu$  orifice is predicted to be about 2350 for 10 psia, O<sub>2</sub> - N<sub>2</sub> mixtures and 1370 for 10 psia, O<sub>2</sub> - He mixtures. This appears to indicate that transition from laminar flow is near.

At the lower end of the range, the boundary will be the transition to molecular flow. This will undoubtedly cause flow rates less than theoretical but the effect on flow rate ratio is not clear. The curve of mean free molecular path for nitrogen-oxygen equal to the capillary diameter, is indicated on figures 3-2, 3-3 and 3-4. As this indicates, the accuracy of the laminar continuum flow theory becomes questionable for hole diameters below 30  $\mu$  at the length and inlet pressures considered.

## STEADY-STATE AND TRANSIENT LEAKAGE TEST PROCEDURE

The test set-up for steady-state leakage is shown in figure 3-5. The test gas was mixed before the test and was contained in a high-pressure cylinder. During the leakage test, gas left the cylinder and passed through a regulator where gas pressure was reduced. Only sufficient gas was passed through the metering valve to maintain total pressure upstream of the test specimen at the test pressure; pressure was monitored on a mercury manometer. Flow was measured with a precision wet-test meter. A vacuum pump maintained downstream pressure at a low value, and this pressure was monitored with a mercury manometer.

Three test specimens were used for the steady-state testing. These simulated very small diameter leakage paths similar to those which might be found in spacecraft. A brief description of these follows:

- (1) Sintered metal plug--0.0002 in. ( $5.04 \mu$ ) mean pore opening (3/8 diam x 1/8 in. thick).
- (2) Sintered metal plug--0.0013 in. ( $32.7 \mu$ ) mean pore opening (3/8 diam x 1/8 in. thick).
- (3) Plate drilled with five 0.0135 in. ( $340 \mu$ ) diameter holes.

Pressure decay tests were run with the Douglas space cabin simulator air lock (156.5 cu ft) to simulate a space cabin. The air lock was charged by metering in the test gas to the partial pressures corresponding to the test atmospheres. The test hole, which simulated a large leakage path, was drilled in a 1/4-in. thick plate and mounted at the entrance of the vacuum duct leading from the air lock. The air lock atmosphere was dumped through a quick-opening valve to a large-capacity vacuum system. The vacuum source was of sufficient capacity to maintain a critical pressure ratio across the hole. Temperatures and pressures of the atmosphere just upstream and downstream of the orifice were recorded.

### Transient And Steady-State Leakage Data

Data taken from steady-state leakage tests are presented in Table 3-IV. The weight ratio of nitrogen-oxygen flow to helium-oxygen flow from these data is plotted on figure 3-6. In addition, the theoretical values for weight ratio, from figure 3-4, are repeated for comparison. The agreement between theory and test is good at 5 and 7 psia cabin pressure. Even at 10 psia the trend is indicated. Of course, the theory was developed for a smooth, constant area capillary while the test data were for porous plugs and for drilled holes having a relatively small length to diameter ratio (less than 10).

Pressure decay tests were run on the airlock as explained above, with hole sizes of 0.5 and 1.0 in. and initial pressures of 5, 7, and 10 psia. Data were obtained using helium and nitrogen as diluents with the oxygen partial pressure held at 3.5 psia. In addition, pure oxygen was tested at 5 psia.

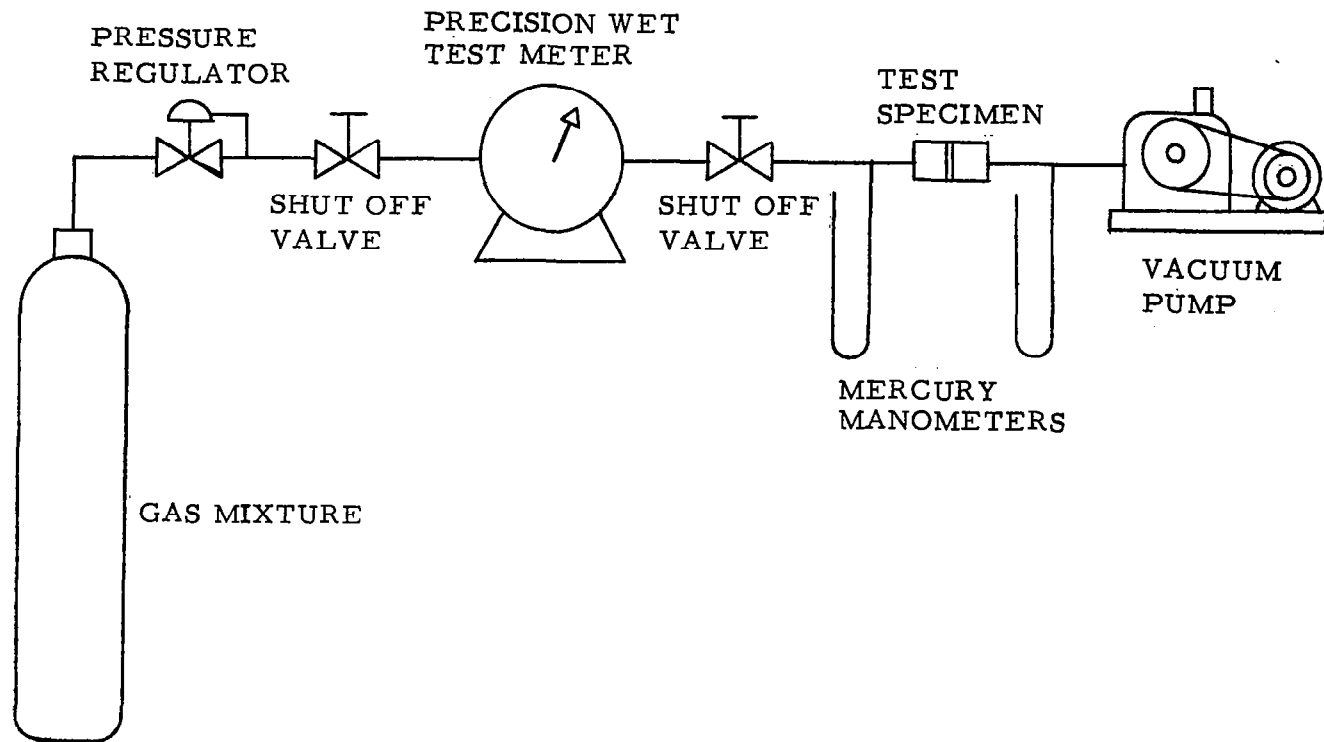


FIGURE 3-5 TEST ARRANGEMENT FOR STEADY STATE LEAKAGE

TABLE 3-IV

## RESULTS OF STEADY-STATE LEAKAGE TESTS

Press. psia	Gas mixture	Leakage lb/day	Weight Ratio	Hole size in.	
10	N <sub>2</sub> - O <sub>2</sub>	1.08	2.46	0.0002	
	He - O <sub>2</sub>	0.44			
7	N <sub>2</sub> - O <sub>2</sub>	0.57	1.96		
	He - O <sub>2</sub>	0.29			
5	N <sub>2</sub> - O <sub>2</sub>	0.28	1.22		
	He - O <sub>2</sub>	0.23			
	O <sub>2</sub>	0.25			
10	N <sub>2</sub> - O <sub>2</sub>	7.13	1.67		0.0013
	He - O <sub>2</sub>	4.26			
7	N <sub>2</sub> - O <sub>2</sub>	4.87	1.73		
	He - O <sub>2</sub>	2.81			
5	N <sub>2</sub> - O <sub>2</sub>	2.65	1.29		
	He - O <sub>2</sub>	2.05			
	O <sub>2</sub>	2.78			
10	N <sub>2</sub> - O <sub>2</sub>	12.35	1.27	0.0135	
	He - O <sub>2</sub>	9.76			
7	N <sub>2</sub> - O <sub>2</sub>	9.78	1.28		
	He - O <sub>2</sub>	7.60			
5	N <sub>2</sub> - O <sub>2</sub>	7.28	1.16		
	He - O <sub>2</sub>	6.15			
	O <sub>2</sub>	7.45			

RATIO OF NITROGEN-OXYGEN FLOW TO HELIUM-OXYGEN FLOW

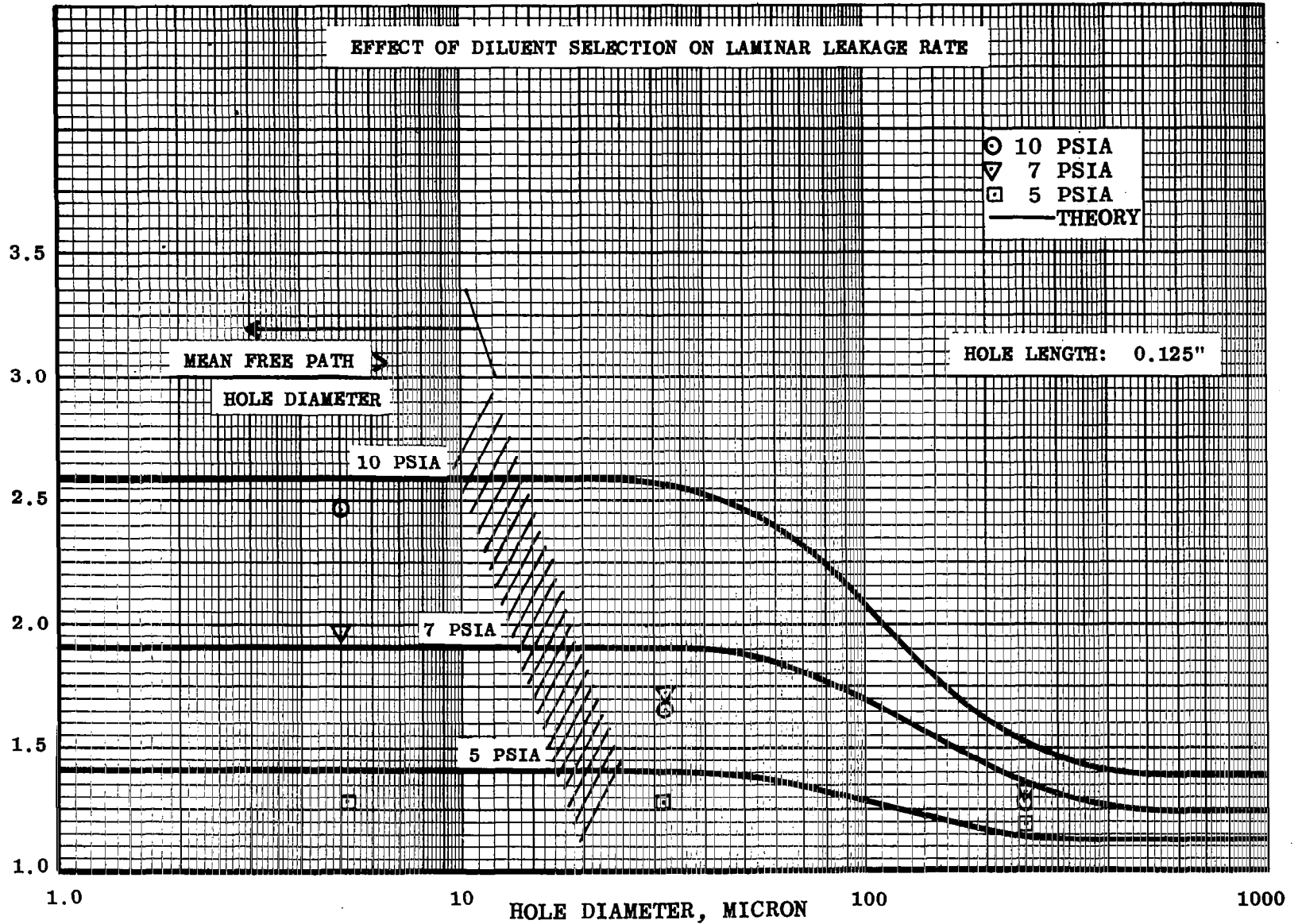


FIGURE 3-6 STEADY STATE LEAKAGE DATA

Data from these tests are shown in figures 3-7 through 3-13. During the test runs, the temperature drop of the gas was from 7° to 23°F. If the pressure decay were adiabatic, a temperature drop of 100° to 220°F would be predicted from theory. Therefore, the temperature decay indicates a nearly isothermal process. On the other hand, pressure decay rates follow the theory for an adiabatic process more closely than for an isothermal process. A check of the temperature instrumentation yielded no explanation for the nearly isothermal temperature behavior. A plot of a typical temperature history is shown in figure 3-14. It can be seen that temperature drops rapidly at the start of the test but then becomes nearly stable near the end of the test. This general behavior suggests heat transfer between the gas and the chamber walls. A calculation of free convection heat-transfer shows that the heat transfer calculated between the wall and atmosphere is sufficient to maintain the atmosphere at a nearly constant temperature. Therefore, results of the pressure decay tests indicate a nearly constant temperature behavior with pressure decay following a nearly adiabatic process. The theoretical adiabatic process is shown with the test data in figures 3-7 through 3-13. The flow coefficients for these calculations were based on final pressure and time. These are shown as a function of Reynolds number in figure 3-15. The flow coefficients vary only slightly from 0.6 for all tests and gas mixtures. This is very near the value determined by other investigators (refs. 3-1 and 3-2).

#### HELIUM LEAKAGE INTO ELECTRONIC COMPONENTS

Permeation of helium for different glasses has been investigated. A rather extensive literature survey was made and the most pertinent references are listed at the end of the section (refs. 3-7 through 3-10). It was found that gas permeation through solids is a process of adsorption, solution, diffusion, and desorption. Permeation through a plane section of material may be expressed by the relation:

$$Q_G = \frac{K'A (P - P_{in}) t}{t_w} \quad (3-27)$$

This equation was used to predict internal helium pressure for different glasses and times. It was found that, depending on the type of glass envelope, the life of a vacuum electronic component will range from seconds to years. The most commonly used glass, Pyrex Brand No. 7052, is not satisfactory for extended use in helium-rich environment because of its high permeation constant. Glasses such as those of lead borate composition are expected to greatly increase tube life in the helium atmosphere. This example has not treated factors such as metal-to-glass seals, tube warmup, or outgassing, which may accelerate permeation rates.

During the Phase I testing in the space cabin simulator, premature failure of some types of electronic equipment was noted. One pertinent finding was that seven vidicon television monitoring tubes failed in the helium-oxygen space cabin atmosphere. During 13 days of testing with three tubes inside the simulator, the average tube life was about 60 hr. It appears that helium diffused either through the glass or through the tube seal between the electrode and the glass portion of the tube. Helium gas entered the tube and raised its

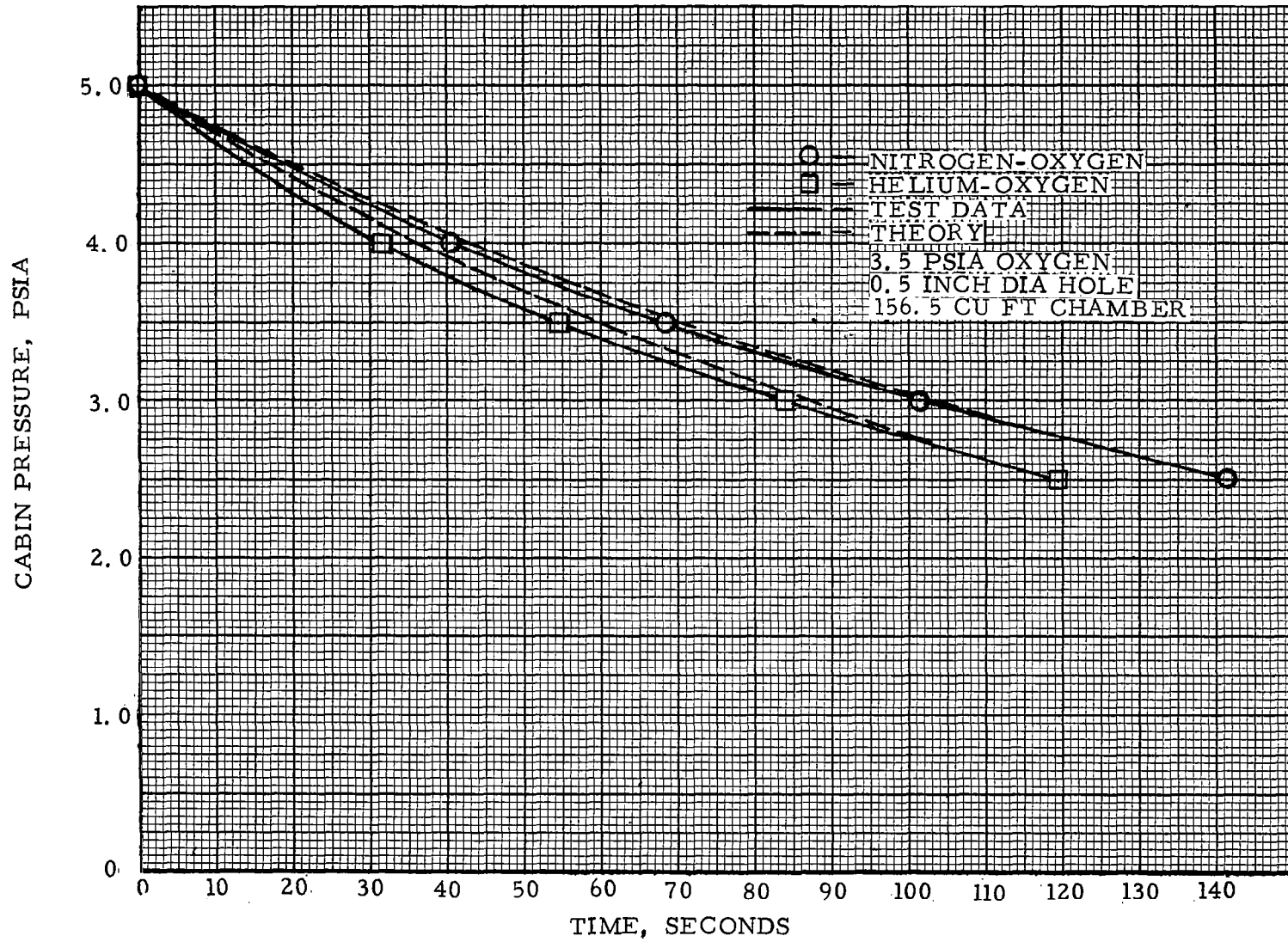


FIGURE 3-7 PRESSURE DECAY TEST FOR 5 PSIA AND 0.5 INCH HOLE

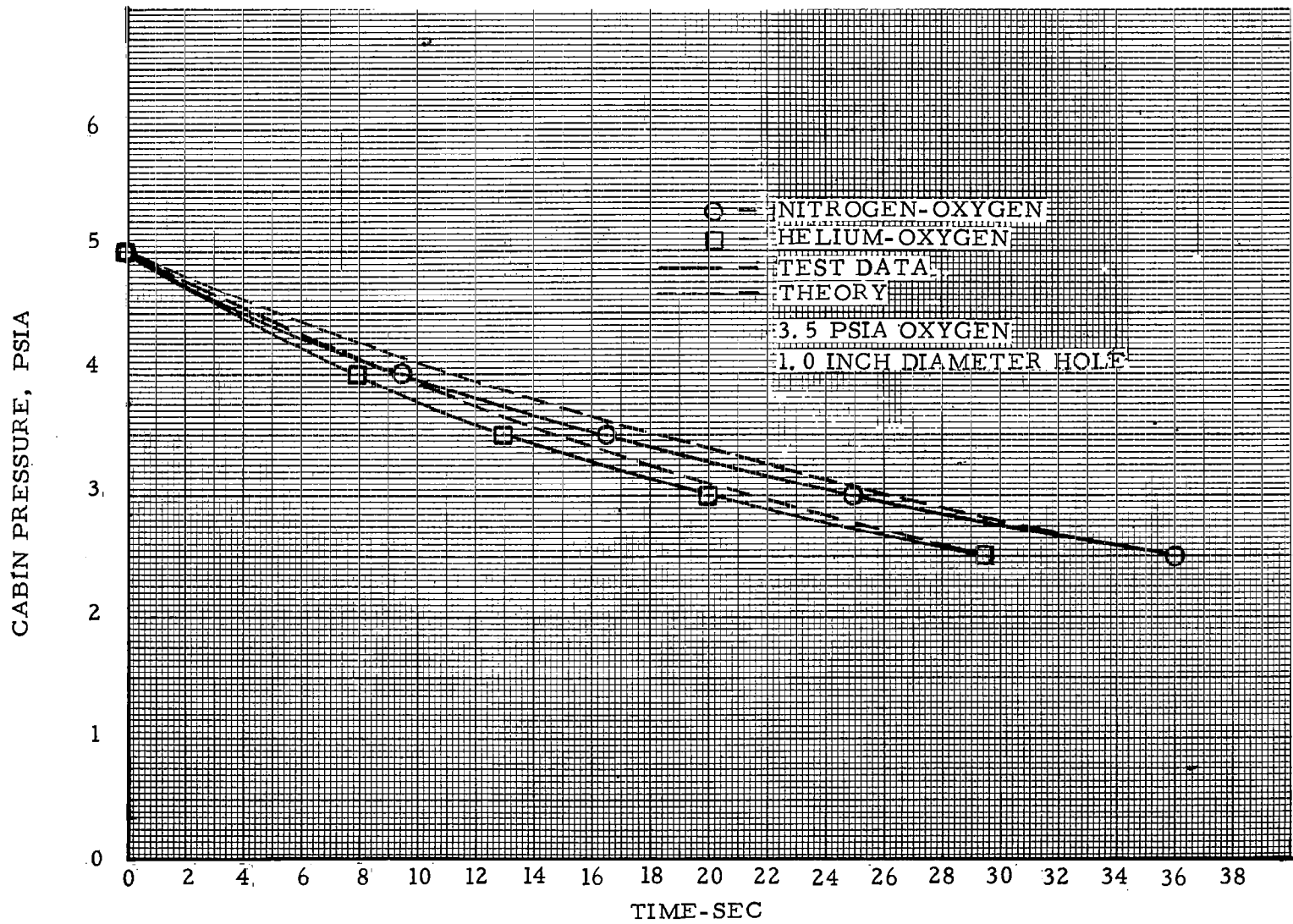


FIGURE 3-8 PRESSURE DECAY DATA FOR 5 PSIA AND 1.0 INCH DIAMETER HOLE

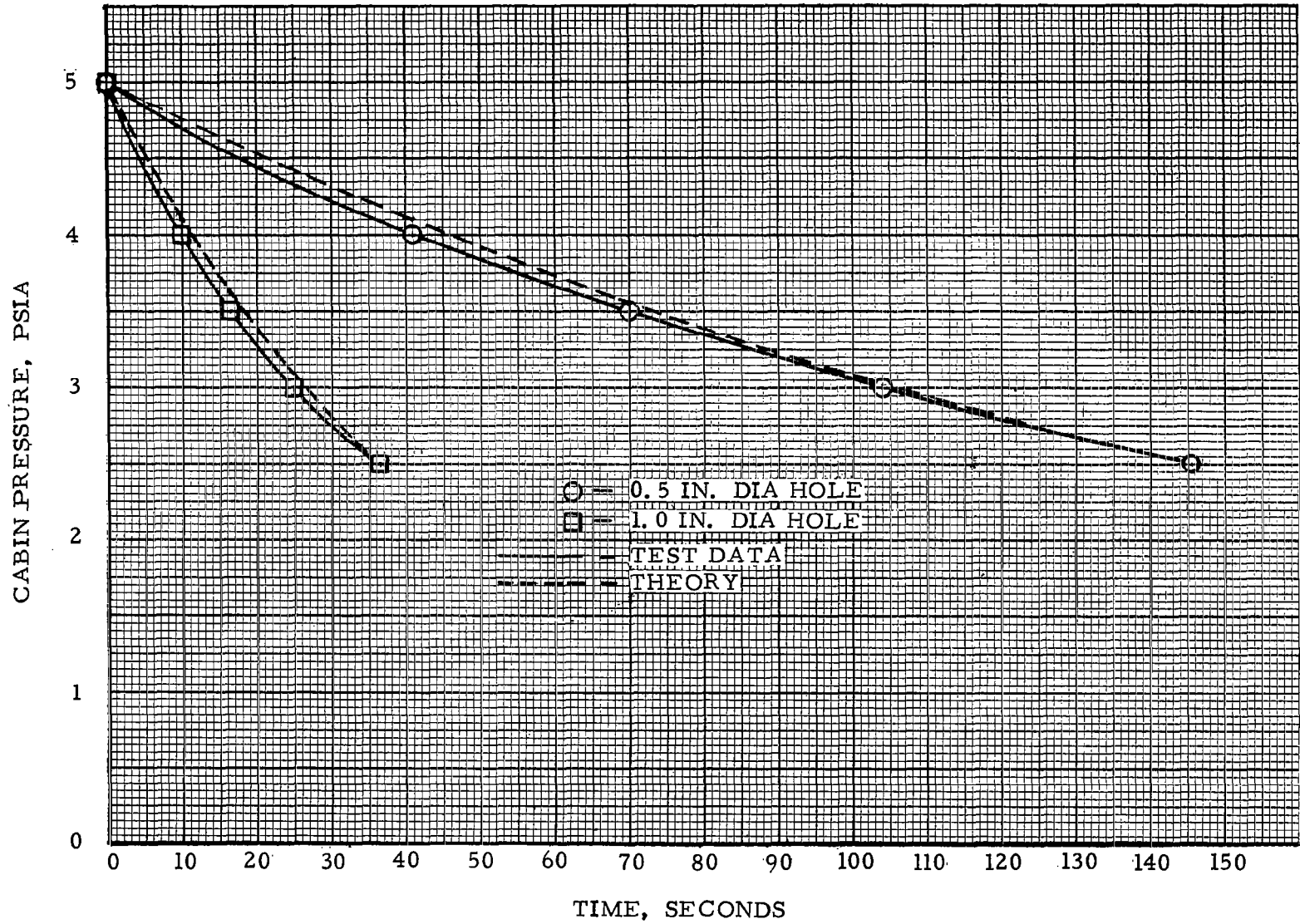


FIGURE 3-9 PRESSURE DECAY DATA FOR 5 PSIA PURE OXYGEN

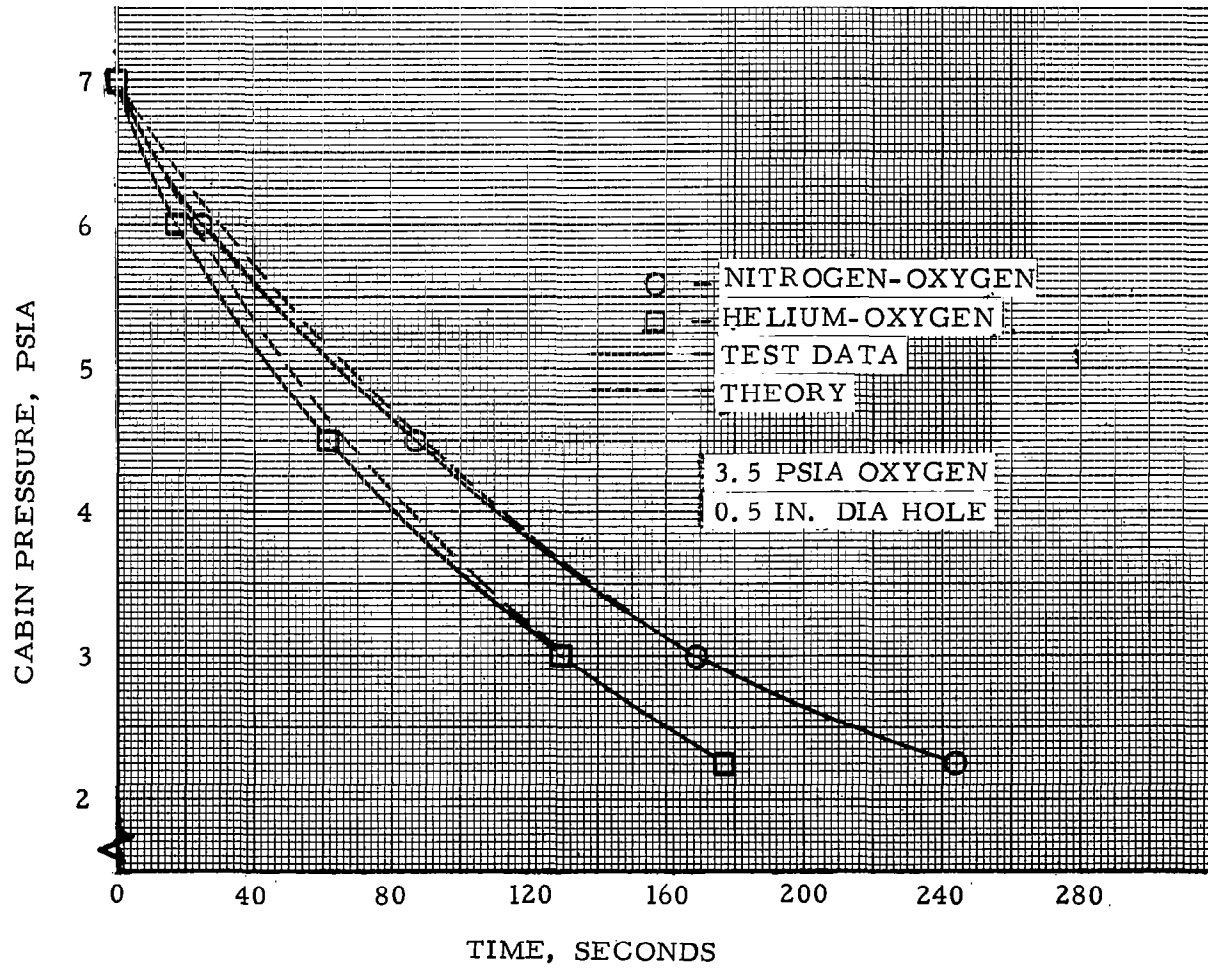


FIGURE 3-10 PRESSURE DECAY DATA FOR 7 PSIA AND 0.5 IN. DIAMETER HOLE

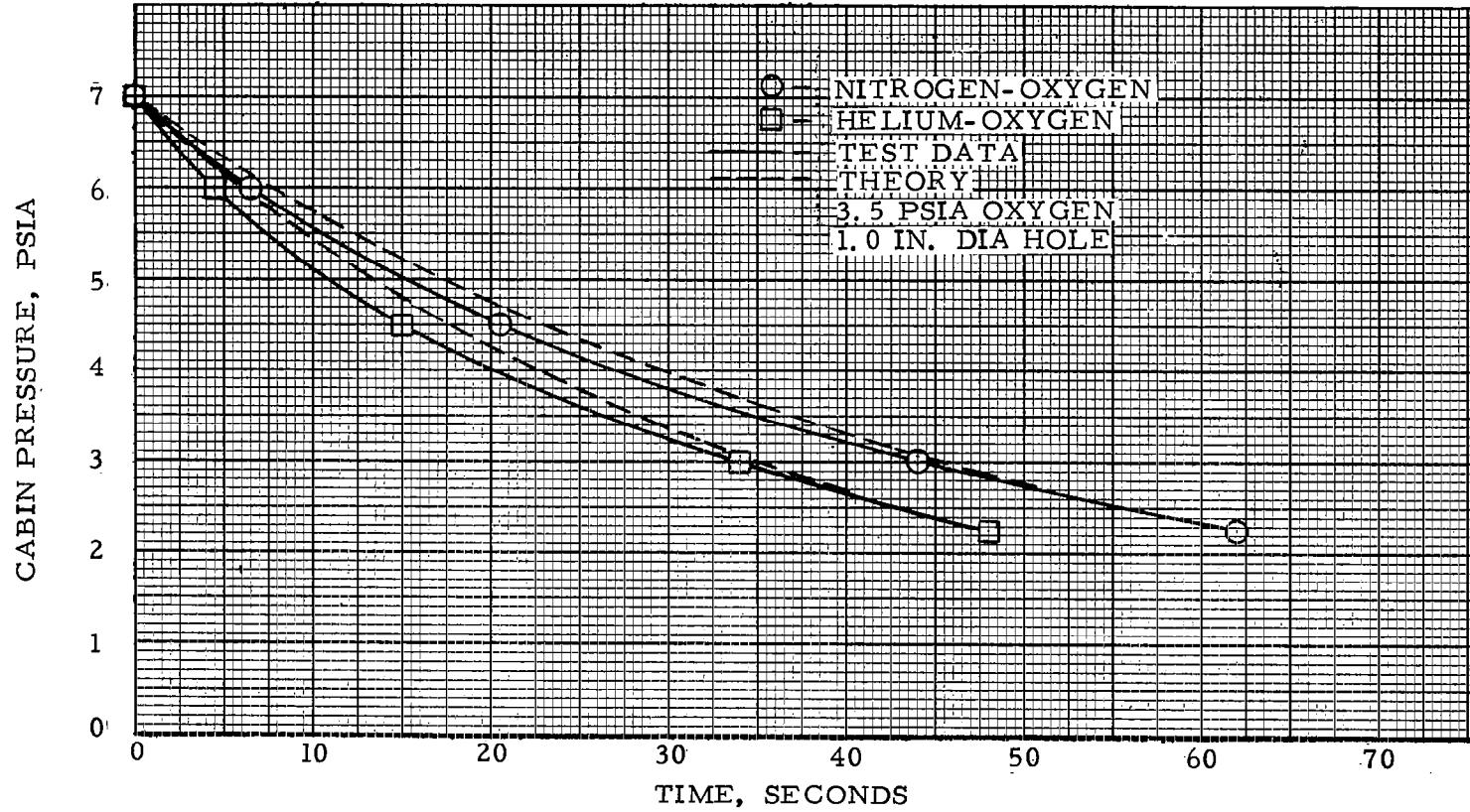


FIGURE 3-11 PRESSURE DECAY DATA FOR 7 PSIA AND 1.0 INCH DIAMETER HOLE.

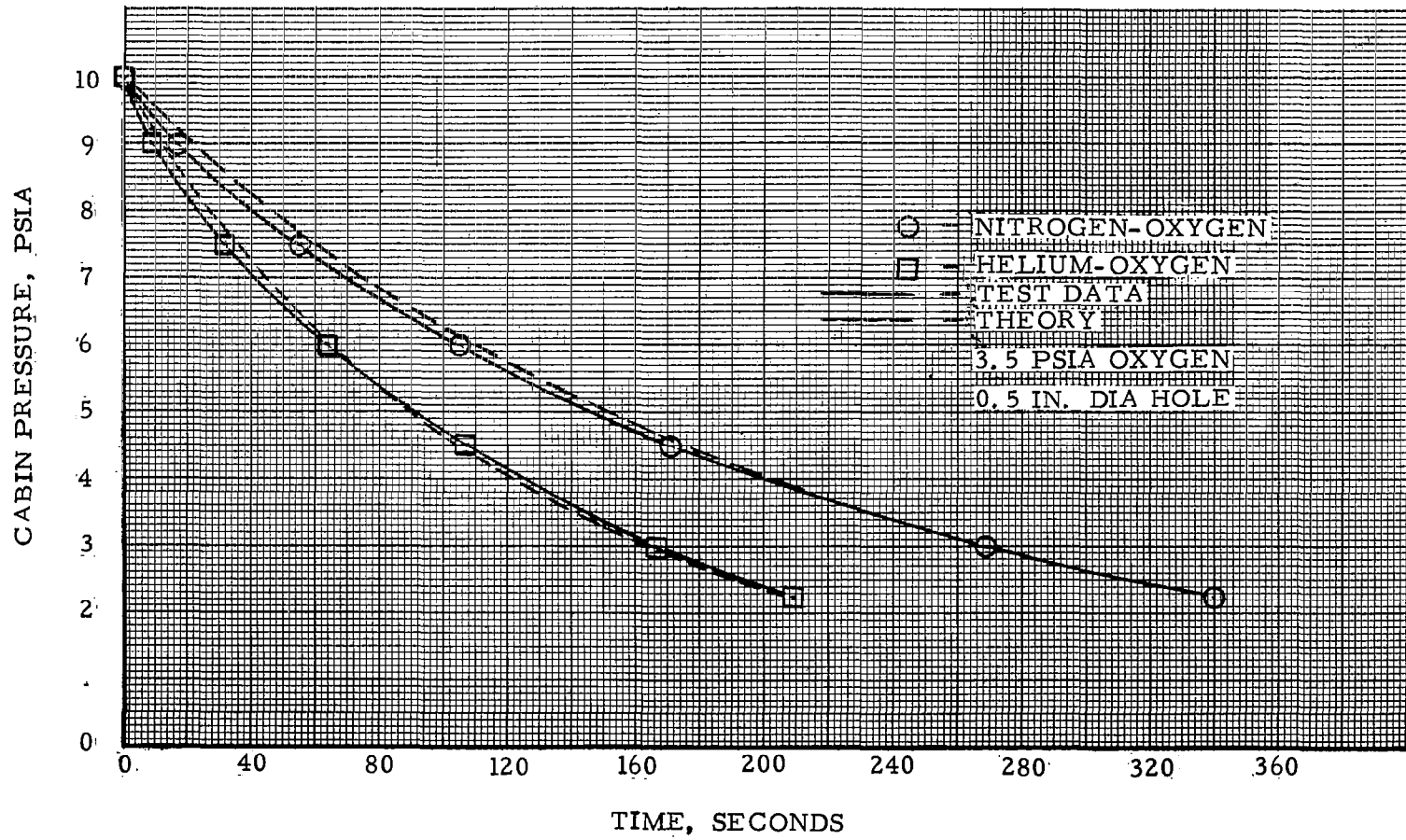


FIGURE 3-12 PRESSURE DECAY TEST FOR 10 PSIA AND 0.5 INCH DIAMETER HOLE

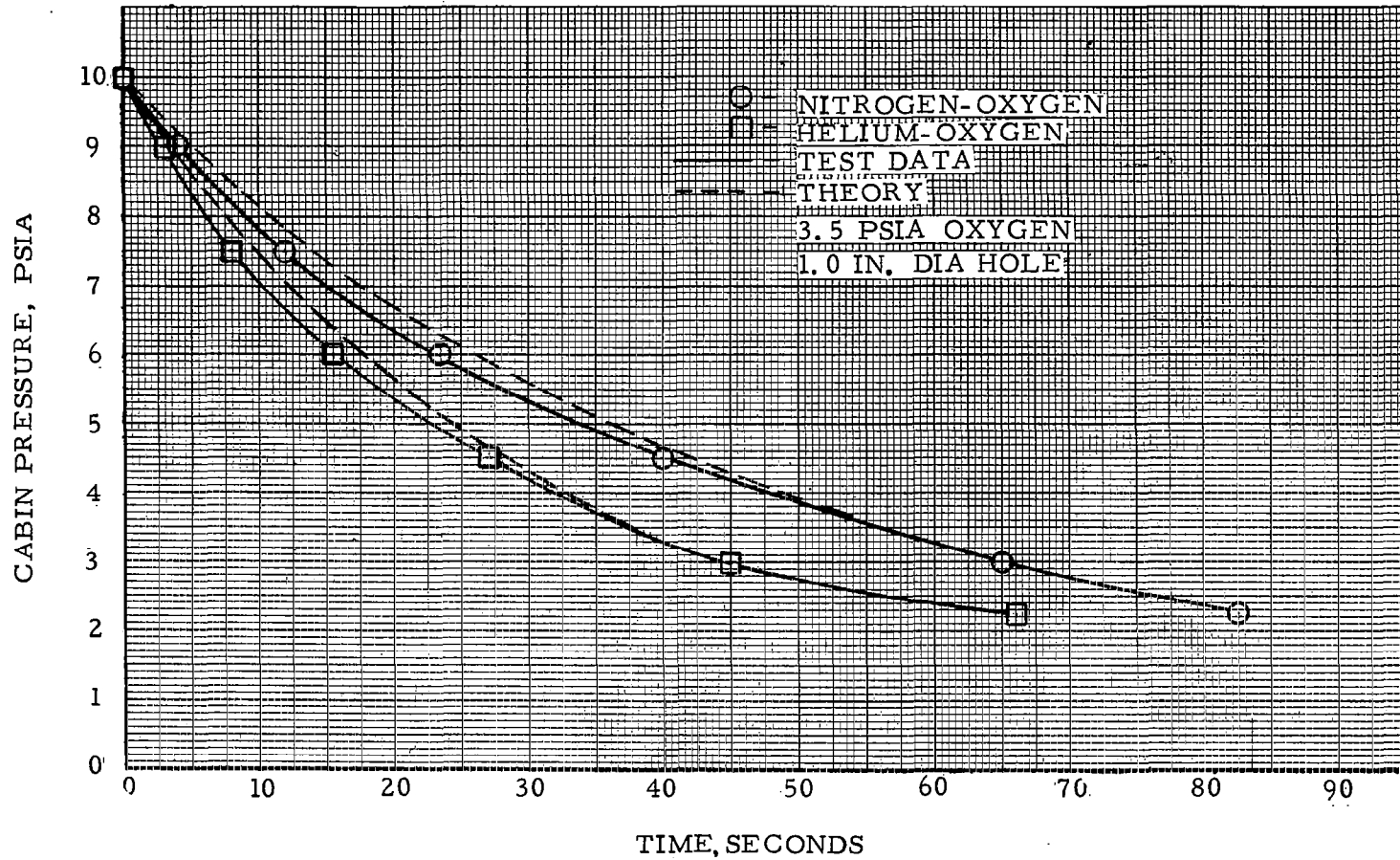


FIGURE 3-13 PRESSURE DECAY DATA FOR 10 PSIA AND 1.0 IN. DIAMETER HOLE

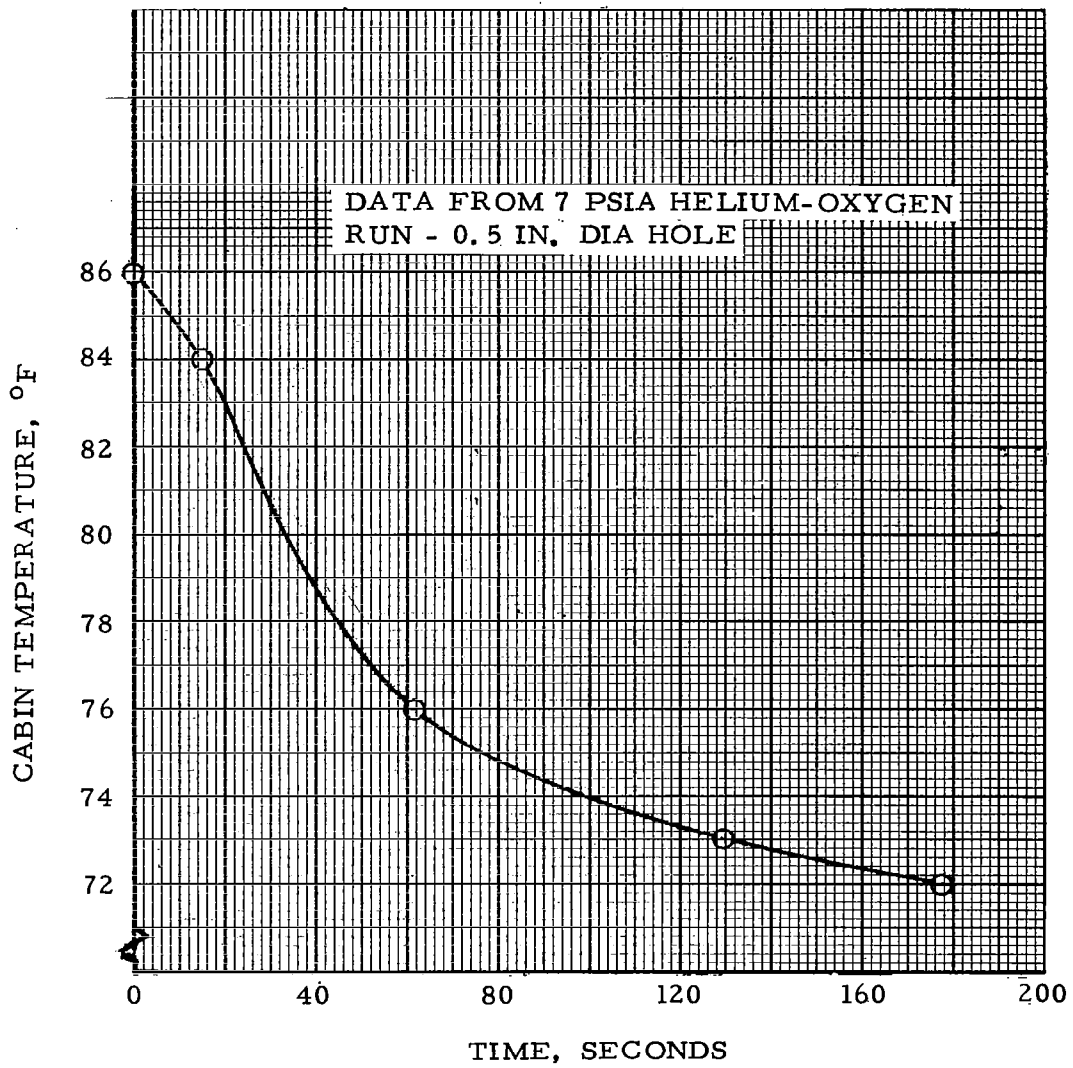


FIGURE 3-14 TYPICAL TEMPERATURE DECAY DURING PRESSURE DECAY TEST

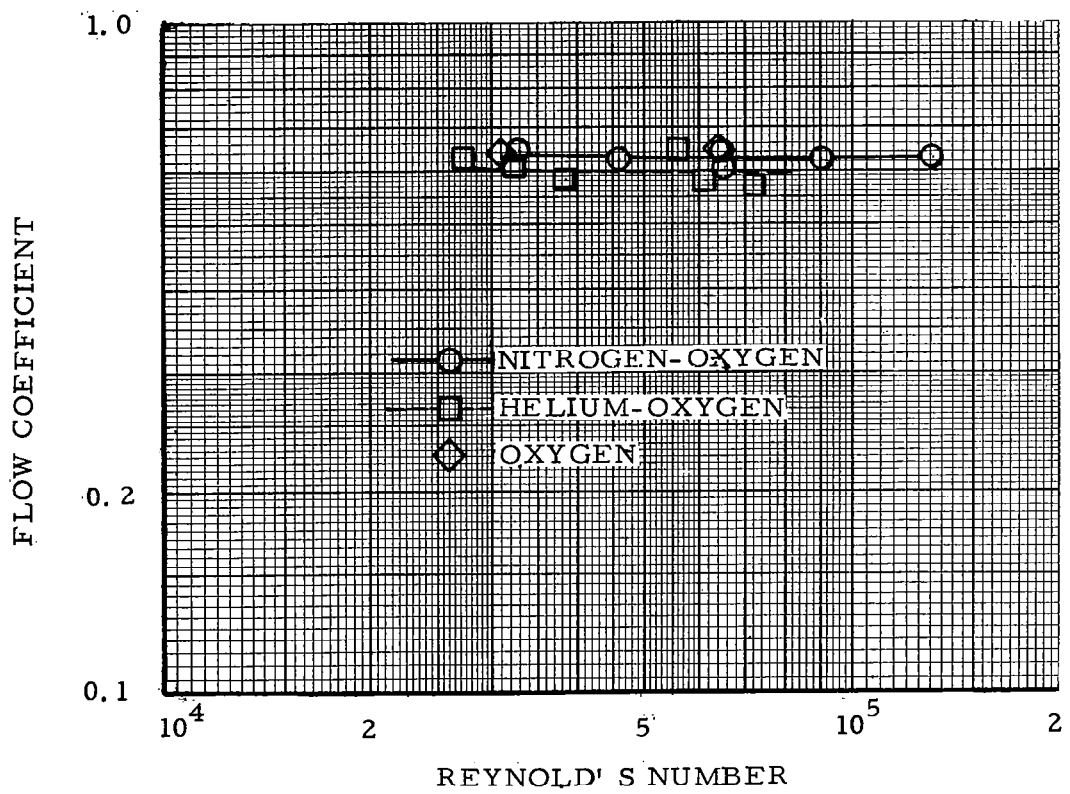


FIGURE 3-15 FLOW COEFFICIENTS FOR PRESSURE DECAY TESTS

internal pressure causing a gaseous tube condition. No failures occurred during any of the 42 days of tests with nitrogen diluent, or during a 2-day checkout test with helium-oxygen.

In addition, a 5-day Phase II test was performed with a helium-oxygen atmosphere at 5 psia. Electronic equipment installed in the cabin consisted of three television monitor cameras and a standard 17 in. RCA television monitor set. Lights in the cabin consisted of 40 W fluorescent overhead lights, a 100 W incandescent bulb, and 1/25 W miniature neon bulbs. New vidicon tubes and one new light in each area were installed before the test. The television monitor was turned on after 36 hr of exposure and turned off immediately when the crew noticed hissing and crackling noises. Unit operation was satisfactory before and after the test at sea-level conditions. A 5-in. DuMont oscilloscope was sent into the chamber on the 4th day and operated normally for the remainder of the test (approximately 8 hr). No vidicon tube failures occurred during the 5-day test as had occurred during the previous 18-day test. Quality of the pictures did not seem to deteriorate, except for some bright spots on one monitor screen. Previous failures occurred after operation at total pressures of 5, 7, and 10 psia, and a constant 3.5 psia O<sub>2</sub> partial pressure. The higher partial pressure of helium may account for the difference. No failure or decrease in brightness occurred with the fluorescent, incandescent, or neon lights.

Helium concentration for several components was measured with a mass spectrometer after a 5-day space cabin simulator test. The incandescent bulb had over 763 mg/m<sup>3</sup> helium and the fluorescent light had 5.9 mg/m<sup>3</sup> helium. The vendor stated that essentially no helium should be present in new bulbs. This was substantiated when no helium was measured in the new bulbs tested.

Helium contamination of electronic gear appears to be a definite problem. At the present, it is not known whether the leakage occurs through the glass or through the metal-to-glass seals. Additional testing is necessary to determine the nature of the leakage and to define satisfactory solutions to the problem. However, based on present knowledge, the problem of contamination of electronic components can be solved by the use of special design techniques or nonpermeable materials.

#### LEAKAGE PENALTY

A review of previously conducted studies was made to determine the predicted leakage rates for spacecraft of varying design requirements and the experimentally determined leakage data for the various components that may contribute to leakage. From this information, typical leakage rates may be determined. The data previously presented in this section then allow an estimate of the comparative leakage levels based upon pressure level and diluent selection. The associated weight penalties can then be estimated by using the storage vessel weights from Section 5 in addition to the gas leakage rates.

A MORL-type space station for a 4- to 9-man crew was designed to 2 lb/day leakage, and a 24 to 36 man LORL lost 4.75 lb/day (refs. 3-11 and 3-12). The major normal leakage occurred through hangar and hatch seals. Sources and orders of magnitude of leakage used for these vehicles for a 7 psia nitrogen-oxygen atmosphere are shown in table 3-V.

TABLE 3-V  
LEAKAGE SOURCES AND ORDERS OF MAGNITUDE

Leakage source	Order of magnitude
Hatches and hangar door seals	$2.85 \times 10^{-5}$ to $7 \times 10^{-3}$ lb/day/in.
Electrical leads	$10^{-7}$ lb/day/in. (negligible)
O-ring seals (replaceable)	$10^{-9}$ lb/day/in. (negligible)
Valves	$10^{-3}$ lb/day/valve (negligible)
Seams and joints (welded)	$10^{-4}$ lb/day (negligible)
Diffusion through vehicle skin	$10^{-14}$ lb/day (negligible)

The major leakage source should occur through hatches or hangar seals, except for the emergency situation of a meteoroid penetration, seal failure, or other type of inherent failure. The assumed seal leakage ( $7 \times 10^{-3}$  lb/day/in.) is based on MIL Standard S8484 for gaskets and is comparable to the lowest recorded value for Mercury capsule missions ( $12.1 \times 10^{-3}$  lb/day/in., if all leakage was through the hatch). This value is also of the same order of magnitude as Gemini and Apollo design goals. Approximately 12 ft of seal will result in a leakage of 1 lb/day, based on the values above; therefore the value of  $7 \times 10^{-3}$  lb/day/in. appears to agree with present vehicle design goals.

Actual seal leakage test data were obtained for a flight-type airlock by Douglas under NASA Contract NASL-3893. A number of different hatch seals was used. Internal pressure of 14.7 psia was simulated with external pressure on the order of  $10^{-6}$  mm Hg. Maximum leakage for an inflatable seal after 50 hatch operations was 17.3 cc per 24 hr, which amounts to  $2.85 \times 10^{-5}$  lb/day/in. The usage of  $7 \times 10^{-3}$  lb/day/in. for seals appears to be a conservative value for design use for  $N_2-O_2$  and pure  $O_2$  at 7 psia. The equivalent leak rate for helium-oxygen would be  $4.21 \times 10^{-3}$  lb/day/in.

The foregoing data appear to indicate that most spacecraft atmosphere loss will occur from hatch and seal leakage. A relatively large range of hole sizes is probably present. So that the effects of leakage on atmosphere selection can be evaluated, the arithmetic mean of test data presented in figure 3-6 will be used to predict loss rates. The mean values of weight ratios used for steady-state leakage calculations are given in table 3-VI.

TABLE 3-VI  
MEAN VALUES OF STEADY-STATE LEAKAGE DATA

Total pressure (psia)	Ratio of N <sub>2</sub> - O <sub>2</sub> to He - O <sub>2</sub>
5	1.23
7	1.66
10	1.80

Basic leakage rates of 1 and 2 lb per day with 50% N<sub>2</sub>-50% O<sub>2</sub> mixture at 7 psia were chosen for analysis. The weight ratios presented in table 3-VI were used to predict equivalent losses with helium diluent. For a given mixture, leakage was assumed proportional to cabin pressure. Weight penalties include the weight of supercritical cryogenic storage vessels from data in Section 5. Figures 3-16 and 3-17 present the results of the weight penalty evaluation for the basic 1- and 2-lb/day leakage rates respectively.

The weight penalty associated with leakage is basically not affected by diluent selection for a 5 psia cabin pressure because the additional storage vessel weight counteracts the lower weight rate of leakage. The selection of the helium diluent will result in savings of about 21% at 7 psia and 36% at 10 psia compared with nitrogen. This increasing advantage basically results from the reduced weight rate of leakage, as shown in table 3-VI.

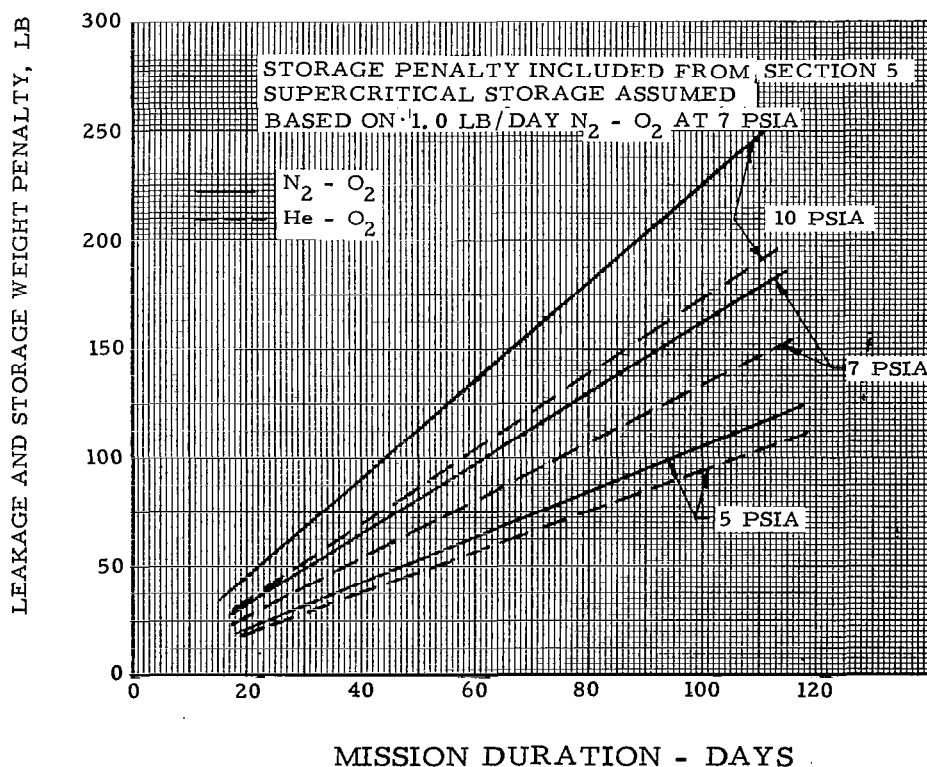


FIGURE 3-16 REPRESENTATIVE LEAKAGE WEIGHT PENALTY  
1.0 LB/DAY N<sub>2</sub>-O<sub>2</sub>

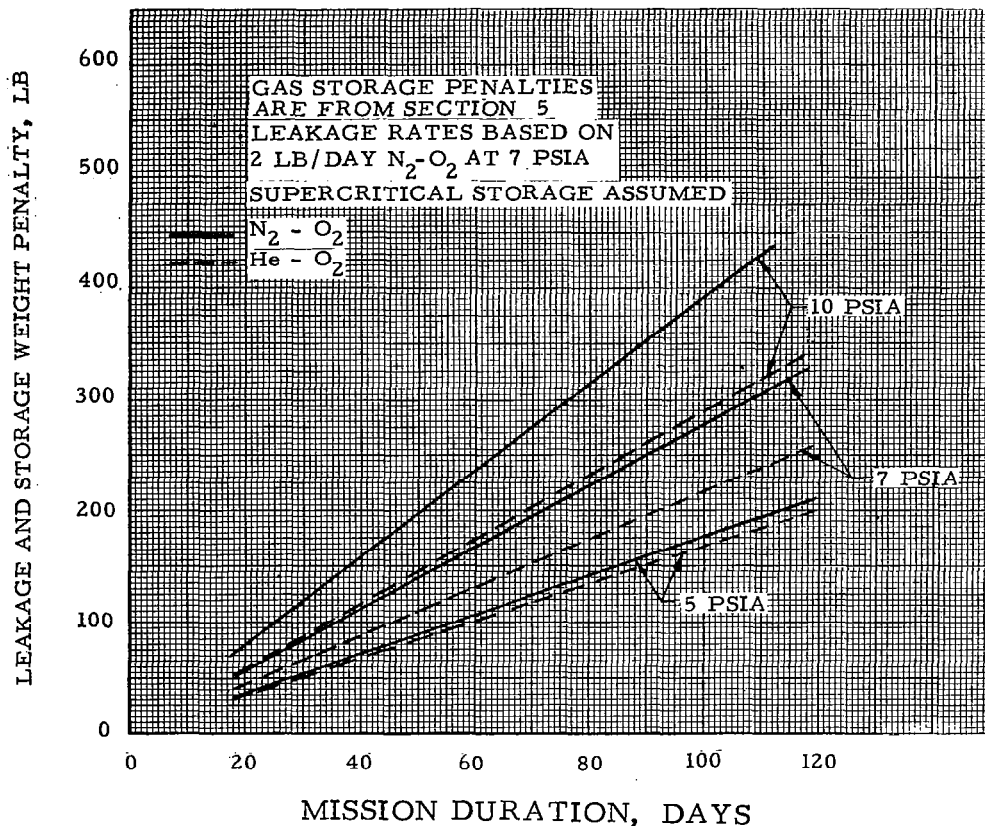


FIGURE 3-17 REPRESENTATIVE LEAKAGE WEIGHT PENALTY--  
2 LB/DAY N<sub>2</sub>-O<sub>2</sub>

The previous discussion evaluates penalties only for those leaks causing continuous gradual loss of atmosphere. Provisions must also be made for sudden transient leaks such as those caused by meteoroid penetration, and seal or valve failure. Make-up gas must be provided for maintenance of atmosphere until the crew is safe following such a puncture and for repressurizing the compartment following repairs. The time for leak detection, location, and repair can be evaluated for estimated hole sizes and the corresponding amount of gas loss can be calculated.

Besides the weight penalty associated with a sudden puncture, the relative time available for crew protection during the pressure decay depends upon selection of atmospheric pressure, diluent, and oxygen partial pressure. Pressure decay rates can be estimated for specific cabin volume and hole sizes from previously presented data. This indicates that pressure loss rates initially are faster than predicted by theory but analytical models are followed relatively closely at lower pressures. Use of a flow-coefficient of 0.6 with sonic orifice flow and adiabatic decompression yields accurate pressure transients although the temperature decay is considerably less than that predicted by adiabatic expansion theory.

The safe time available to the crew in the event of puncture may be defined as the time for the cabin to decompress to an oxygen partial pressure of 70 mm Hg. Figure 3-18 shows the safe time for a cabin of 400 cu ft and a hole diameter of 0.5 sq in. This curve indicates that safe times are less using helium as a diluent than using nitrogen. The difference varies from 12% at 5 psia to 40% at 10 psia.

## CONCLUSIONS AND RECOMMENDATIONS

Analysis of the effects of leakage can be made with the information presented. In general, representative normal leakage rates obtained from past studies have been 1 lb/day for a small (2 to 3 man), tightly-sealed vehicle; 2 lb/day for a 4- to 9-man, well-sealed orbiting laboratory (MORL); and as high as 5 lb/day for a larger 24- to 36-man vehicle such as LORL. Leakage rates for these vehicles were based on 7 psia nitrogen-oxygen atmospheres.

Corresponding leakage rates for 7 psia helium-oxygen atmospheres would be 60% of the values given above based on the mean leakage data given in table 3-VI. If the laboratory design details are known, particularly the length of the hatch and the hangar door seal, then a more direct number can be obtained by using as values a minimum of  $2.85 \times 10^{-5}$  lb/day/in. and a maximum of  $7 \times 10^{-3}$  lb/day/in. for 7 psia nitrogen-oxygen. Test data indicate that the greater part of space cabin leakage is around hatches, doors, and seals. The comparable leakage rate for 7 psia helium-oxygen is from  $1.72 \times 10^{-5}$  to  $4.22 \times 10^{-3}$  lb/day/in.

Cabin gas-loss penalty for emergency conditions such as that produced by a meteoroid penetration can be accounted for by assuming partial or total loss of gas in at least one compartment. The safe time to take corrective action such as repairing a leak, donning a space suit, or leaving the compartment can be approximated for different hole sizes. The difference in weight penalty incurred between the different atmospheres can be obtained by using the information presented. For example, the difference in relative penalty between using helium-oxygen and nitrogen-oxygen mixture for a four- to nine-man vehicle is shown in table 3-VII for the following conditions.

- (1) Duration of system usage without resupply = 90 days.
- (2) Cabin pressure = 7 psia.
- (3) Cabin volume = 5,360 cu ft.
- (4) Oxygen partial pressure = 3.5 psia.
- (5) Leakage rate for 7 psia  $N_2 - O_2$  = 2 lb/day.
- (6) Leakage rate of 7 psia  $He - O_2$  = 1.2 lb/day (factor of 1.66 lb.  $N_2 - O_2$ /lb  $He - O_2$  is from table 3-VI).

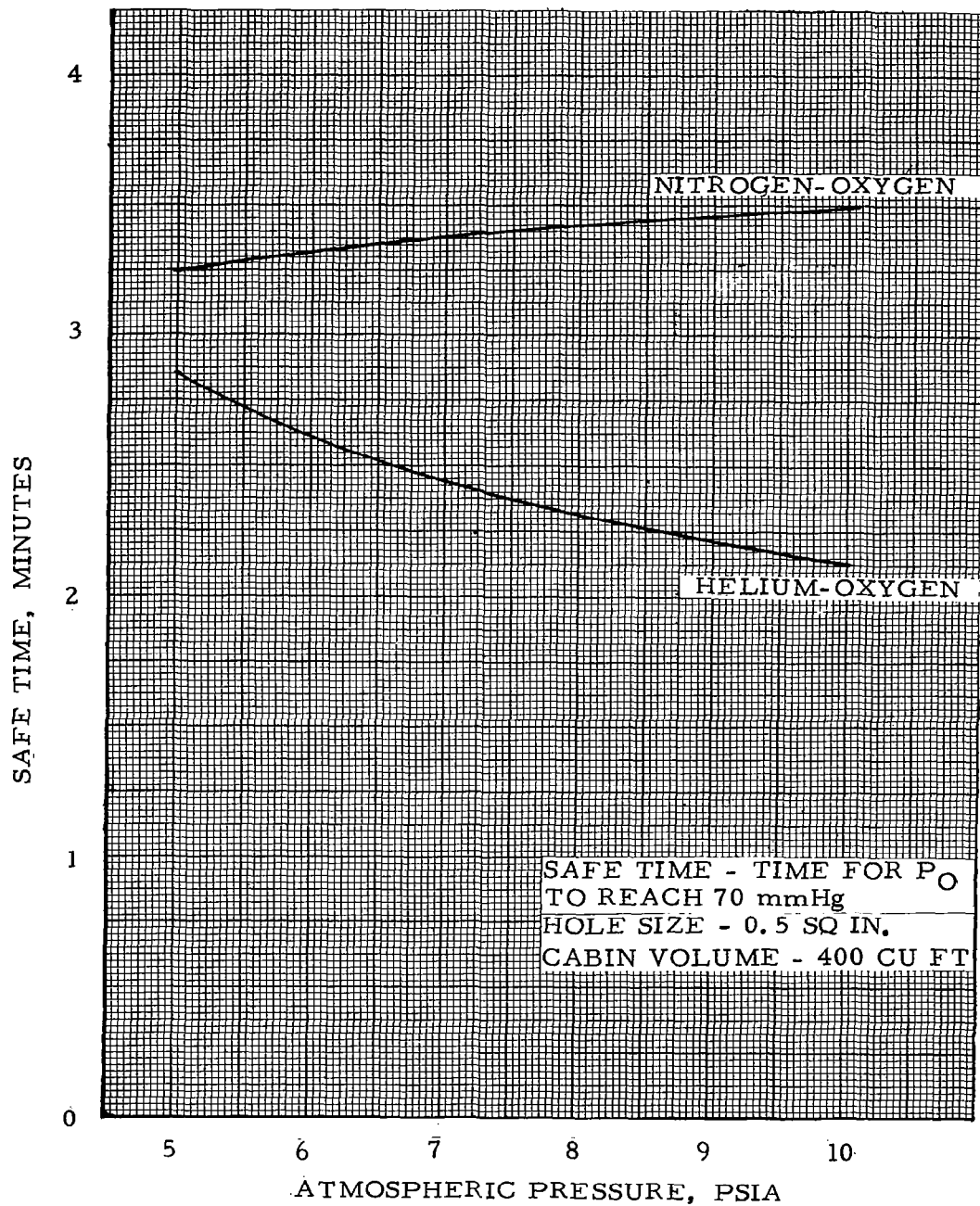


FIGURE 3-18 SAFE TIMES FOR CABIN PRESSURE DECAY

TABLE 3-VII  
RELATIVE PENALTY DIFFERENCE

Item	Penalty weight (lb)	
	N <sub>2</sub> -O <sub>2</sub>	He-O <sub>2</sub>
Normal leakage		
Oxygen gas leaked	96.0	96.3
Oxygen tank weight	27.8 (0.29 lb tank/ lb gas)	27.9 (0.29 lb tank/lb gas)
Diluent gas leaked	84.0	12.0
Diluent tank weight	42.0 (0.5 lb tank/ lb gas)	60.0 (5 lb tank/ lb gas)
Repressurization of cabin		
Weight of oxygen	106.0 (0.29 lb tank/ lb gas)	106.0 (0.29 lb tank/lb gas)
Oxygen tank weight	30.8	30.8
Diluent weight	92.0	13.0
Diluent tank weight	46.0 (0.5 lb tank/ lb gas)	65.0 (5 lb tank/ lb gas)
Total Weight	524.6	411.0

(7) Cabin repressurization = 1 repressurization.

(8) Gas storage penalty from Section 5 based on supercritical storage.

(9) Oxygen consumption rate is 2.06 lb/man day.

The cabin decompression time should be sufficiently long to allow the crew to take corrective actions. For example, a 2 sq in. hole would allow a decompression time of 11.3 min from a 7 psia total pressure to 70 mm Hg of oxygen partial pressure with nitrogen as diluent and 8.2 min for He-O<sub>2</sub>.

A more precise leakage calculation may be made if the detailed vehicle design is known. The theoretical equations (3-1, 3-6, or 3-15) may be used to calculate steady-state leakage directly for the majority of anticipated hole

geometries. Adiabatic pressure decay theory is recommended (eq. (3-5) or fig. 3-1) for cabin decompression calculations with flow coefficients from figure 3-15. Although actual pressure may decay slightly faster than equation (3-5) predicts, the times for pressure to decay to dangerous levels will be accurately predicted with the recommended theory. Storage penalties may be calculated with data on storage vessel design given in Section 5.

These recommended equations may also be used for argon and neon mixtures. Because the properties of these mixtures fall generally within the range covered by He-O<sub>2</sub> and N<sub>2</sub>-O<sub>2</sub>, the leakage penalties will not be greatly different from the mixtures considered. The results of steady-state leakage show that the total weight flow of nitrogen-oxygen will be greater than for helium-oxygen. Leakage loss of oxygen may be greater for helium-oxygen than for nitrogen-oxygen.

Leakage of helium into electronic equipment has been shown to be a problem. Further effort is recommended to determine the nature of this helium contamination. When the source of leakage is established design modifications can be made to rectify the problem. Additionally, more complete testing is needed on various hatch seal configurations with a variation of pressure levels and potential cabin gas atmospheres, particularly He-O<sub>2</sub>.

## REFERENCES

- 3-1. Vennard, J. K. : Elementary Fluid Mechanics, 3rd Edition, John Wiley and Sons, 1954.
- 3-2. Cambel, A. B. : Gas Dynamics, McGraw-Hill Book Company, 1958.
- 3-3. Analytical Methods for Space Vehicle Atmospheric Control Processes, Part II, ASD Technical Report 61-162 Part II, July 1962.
- 3-4. Mason, J. L. : et al. : The Two Gas Spacecraft Cabin Atmosphere Engineering Considerations, Paper to be published.
- 3-5. Binder, R. C. , Ph.D. ; Fluid Mechanics, Prentice Hall Inc. , 1943.
- 3-6. Eckert, E. R. G. , and Drake, R. M. , Jr. , Heat and Mass Transfer, McGraw Hill Book Company, 1959, p. 154.
- 3-7. Williams, E. L. : Diffusion Studies in Glass, Glass Industry, 43, 1962, pp 113, 186, 257, 394, 437.
- 3-8. Altemose, U.O. : Helium Diffusion Through Glass, Journal of Applied Physics, 28, 1957, p 34.
- 3-9. Norton, F. J. : Permeation of Gases Through Solids, Journal of Applied Physics, 28, 1957, p 34.
- 3-10. Collins, R. H. ; and Turnball, J. C. : Degassing and Permeation of Gases in Tube Materials, Advances in Electron Tube Techniques, 1960, p 186.
- 3-11. Manned Orbital Research Laboratory System Improvement Study, Task Area IV, Book 2, SM-48816, Dec. 1965.
- 3-12. Manned Orbital Laboratory, SM-45561, Volume II, Mar. 1964.



## Section 4 AIRLOCK SYSTEM

Space vehicles and laboratories may have an airlock for extravehicular activities. The airlock permits entering and exiting of the vehicle without subjecting the entire crew and equipment to vacuum and also, for most laboratories, reduces the total weight penalty. The penalty resulting from the airlock depends on the pump-down and repressurization system design, and the type of atmosphere used. If airlock usage is minimal and/or the vehicle is small, the cabin may be used as the airlock. This situation exists for Gemini and Apollo. Analysis is presented to evaluate the penalty of atmospheric selection on various potential airlock pressurization systems proposed for space laboratories. The space laboratory and vehicle size range and airlock types considered include those that have been considered in many vehicle studies, including 3-man AAP, 4- to 9-man MORL and 24- to 36-man LORL.

The simplest airlock pressurization system is an expendable gas system. All or a portion of the airlock atmosphere is expended overboard for each airlock use. An alternate method saves most of the airlock atmosphere by pumping most of it from the airlock into the cabin or a separate receiver for re-use. The major penalties associated with an expendable system are simply the weight of the gas expended, valving, and storage system. The penalty associated with a pump-down system is the weight of residual gas expended after each pump-down, the pump-down system, reservoirs, power penalty, and the gas supply tankage penalty.

Representative airlock expendable gas systems for one and two airlock configurations are shown in figure 4-1. If the vehicle under consideration incorporates a second airlock for other operational requirements, a 30% saving of expended gas penalty can be realized by utilizing the secondary airlock as a receiver. A dual airlock with a pump-down system can be evaluated by applying the one airlock pump-down system analysis.

Airlock "pump-down systems," using an adjacent compartment or a separate tank as a reservoir, are shown in figure 4-2. The pump-down to receiver system was considered for high airlock usage rates where the ratio of cabin to airlock volume is small and pumping directly into the cabin would increase cabin pressure beyond an acceptable limit. If, for a particular vehicle and mission, the airlock is to be used only a few times, the expended-gas system appears more attractive than the pump-down system, since pumping penalties may be greater than the weight of gas discarded. However, for a much larger number of airlock uses per mission, the expendable-gas system may discard an amount of gas greater than the total pump-down system weight and gas penalty. The pump-down system will result in less weight penalty if the airlock usages exceed three to five per mission.

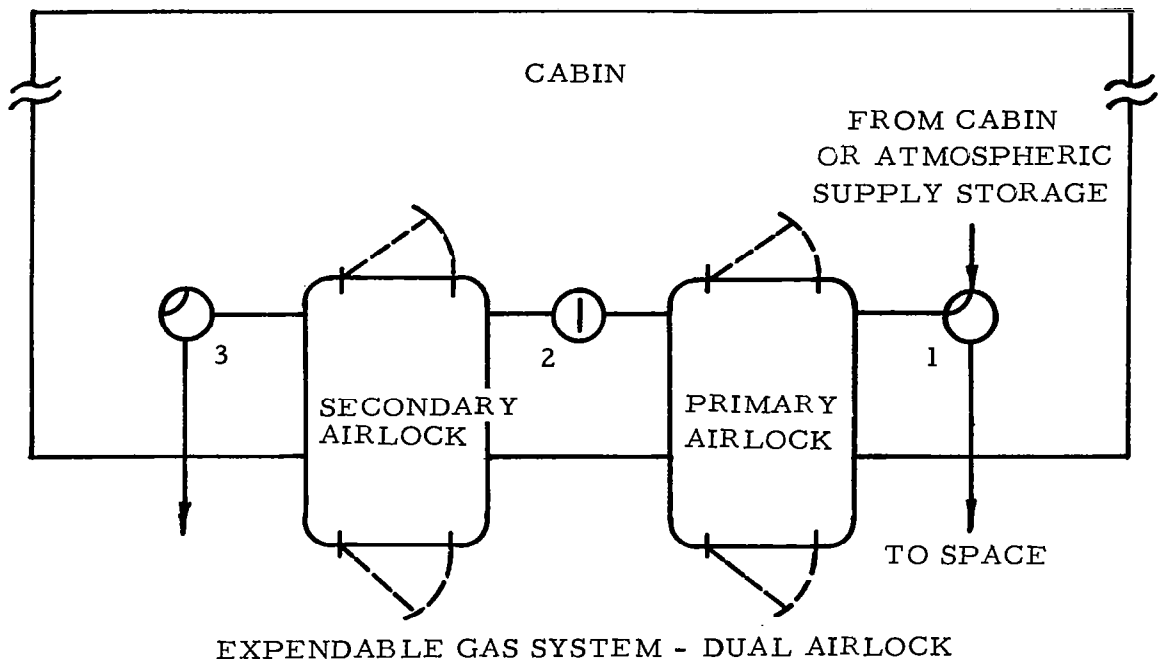
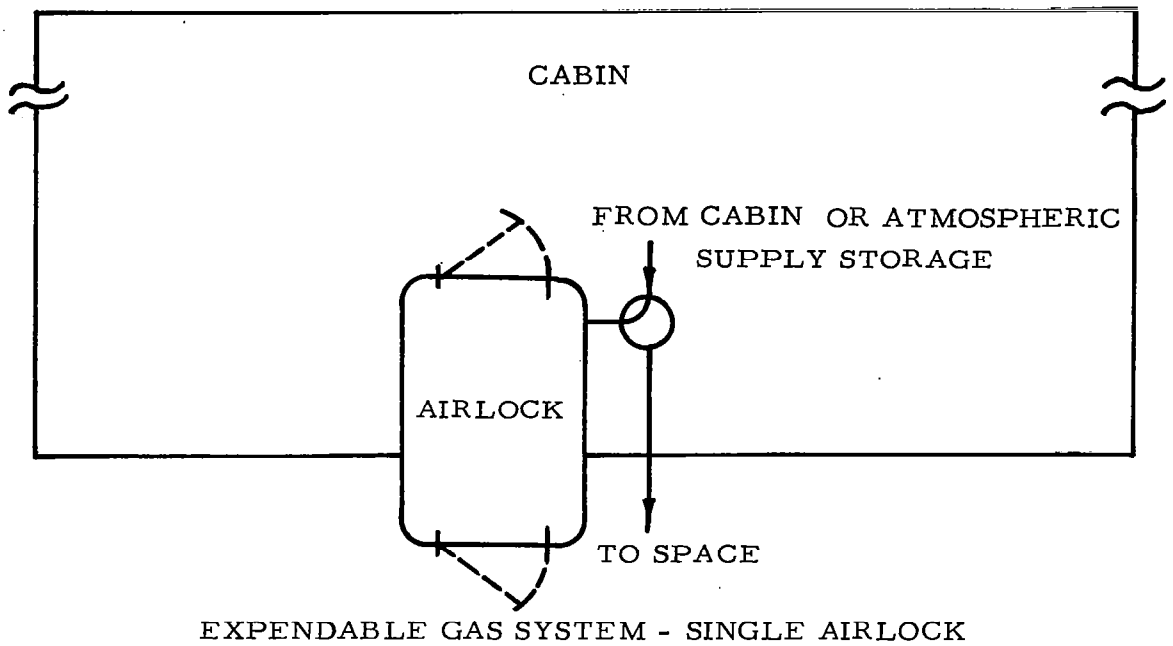
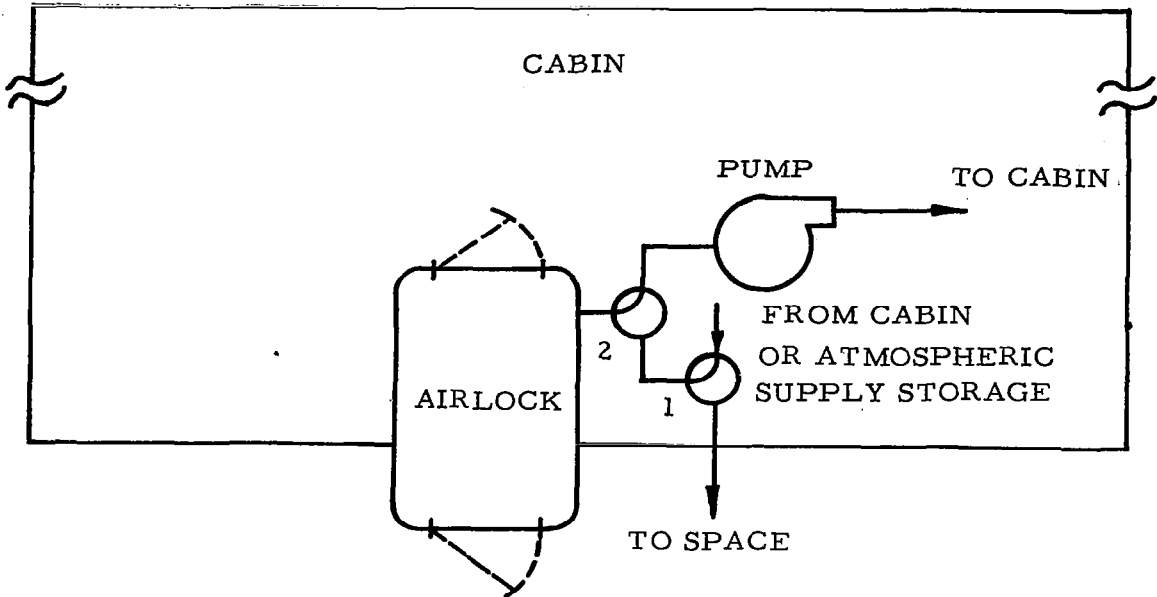
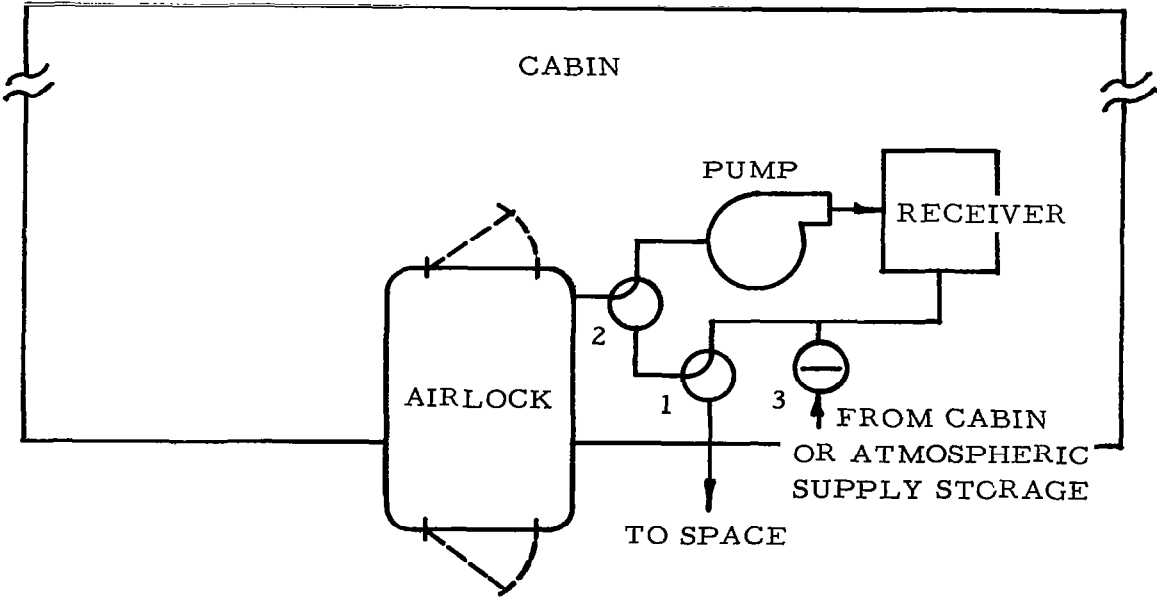


FIGURE 4-1 REPRESENTATIVE AIRLOCK EXPENDABLE GAS SYSTEMS



PUMP-DOWN FROM AIRLOCK TO CABIN



PUMP-DOWN FROM AIRLOCK TO RECEIVER

FIGURE 4-2 REPRESENTATIVE AIRLOCK PUMP-DOWN SYSTEMS

The total penalty for both the pump-down and expendable-gas systems were determined for the following atmospheres:

- (1) Pure oxygen at 5 psia
- (2) Nitrogen-oxygen at 5.0, 7.0, and 10 psia total pressure, with oxygen partial pressure of 3.5 psia
- (3) Helium-oxygen at 5.0, 7.0, and 10 psia total pressure, with oxygen partial pressure of 3.5 psia
- (4) Atmospheric air at 14.7 psia

The presented information may be utilized for vehicle airlock optimization studies. However, no attempt was made to optimize for the example problems. The candidate atmospheres were compared under identical conditions.

In this study, the following assumptions were made:

- (1) Isotope-Brayton power penalty = 503 lb/kW
- (2) Solar cell/battery power penalty:
  - Panel Array = 140 lb/kW
  - Nickel-cadmium Batteries = 50 lb/kWh
- (3) Fuel cell power penalty:
  - Equipment = 86 lb/kW
  - Oxidizer and fuel = 1.28 lb/kWh
- (4) Initial cabin and airlock gas temperature was set at 70°F
- (5) Final airlock pressure after pump-down was set at 0.1 psia
- (6) Pumping system efficiency was set at 40%
- (7) An ideal gas adiabatic process was assumed during pump-down
- (8) The pump volumetric flowrate was assumed constant during pump-down
- (9) Weight of airlock not included in the analysis

Analyses are included which show the total expendable-gas system weight penalty and the pump-down system total penalty including power penalty. Penalty factors associated with the pump-down system are included to permit calculation of total pump-down system weight penalties for most vehicle configurations and missions. Analysis indicated that penalties associated with the candidate atmospheres are ranked primarily in the order of initial density, with the most dense atmosphere having the greatest penalty for both the expendable-gas and pump-down systems. Table 4-I shows the results for representative vehicle systems analyzed.

TABLE 4-1  
COMPARISON OF AIRLOCK SYSTEM CONFIGURATIONS

Vehicle	Time between resupply or total mission (days)	$U_t$ (uses)	Vehicle power system	Airlock system	Atmosphere <sup>a</sup>	Total system penalty (lb)
3-man space station of 200 ft <sup>3</sup> with the cabin used as an airlock	30	30	Fuel cell	Expendable single airlock	5.0 psia O <sub>2</sub>	217
					5.0 psia H <sub>e</sub> -O <sub>2</sub>	188
					5.0 psia N <sub>2</sub> -O <sub>2</sub>	223
				Pump-down to receiver	5.0 psia O <sub>2</sub>	71.2
					5.0 psia H <sub>e</sub> -O <sub>2</sub>	72.5
					5.0 psia N <sub>2</sub> -O <sub>2</sub>	71.4
4 to 9 man space station of 10 000 ft <sup>3</sup> with a 100 cu ft airlock	100	100	Isotope-Brayton cycle	Expendable dual airlock	7.0 psia H <sub>e</sub> -O <sub>2</sub>	273
					7.0 psia N <sub>2</sub> -O <sub>2</sub>	342
				Pump-down to cabin	7.0 psia H <sub>e</sub> -O <sub>2</sub>	38.1
					7.0 psia N <sub>2</sub> -O <sub>2</sub>	40.3

<sup>a</sup>3.5 psia oxygen partial pressure for all mixtures

## AIRLOCK SYSTEM OPERATION, USAGE, AND THEORY

An airlock is required to provide vehicle egress and ingress for EVA and maintenance in space. The airlock can also be used to transfer men and supplies from one vehicle to another and for emergency conditions. Airlock atmospheric pressure must be equalized to that of cabin pressure before a suited crewman may enter the airlock from the cabin. After entering the airlock and before exiting into space, the crewman must reduce airlock pressure to nearly that of space. This process must be reversed to permit the crewman to re-enter the cabin. The analysis will consider various methods of performing this operation and the associated penalty for different cabin atmospheres.

A typical operational sequence of an expendable-gas system with a single airlock, shown in figure 4-1, is as follows. The airlock is pressurized by opening the valve from the cabin or atmospheric supply system. The airlock is depressurized by venting the valve to space.

For vehicles using the expendable-gas airlock system, a portion of the gas normally expended overboard may be saved by bleeding the gas to a secondary airlock or receiver as shown in figure 4-1. The operation is as follows:

- (1) At the start of airlock operation, the secondary airlock is at a pressure somewhat below the primary airlock pressure which is equalized at cabin pressure by opening valve 1 from the cabin or atmospheric supply source while valves 2 and 3 are closed.
- (2) Valve 2 is now opened and the pressure equalizes between the primary and secondary airlock at a pressure somewhat below that of the cabin.
- (3) Valve 2 is then closed and valve 1 is vented to space to bleed the remaining airlock gas overboard.
- (4) For re-entry, the airlock is repressurized by first closing valve 1 and opening valve 2 to equalize the pressure again between the primary and secondary airlocks.
- (5) After the pressure stabilizes, valve 2 is closed and valve 1 is vented to the cabin to equalize pressures.

Operation of the pump-down from airlock to cabin system, shown in figure 4-2, is as follows:

- (1) At the start of airlock operation, valves 1 and 2 are vented to cabin to equalize pressures.
- (2) Valve 2 is then vented to the pump and the airlock is pumped down to a predetermined final pressure, while the cabin is slightly pressurized.

- (3) The airlock residual gas is now dumped overboard, thereby equalizing airlock pressure with space by venting valves 1 and 2 to space.
- (4) For re-entry to the cabin, the airlock is repressurized by venting valves 1 and 2 to the cabin and/or the atmospheric supply tankage.

Operation of the pump-down from airlock to receiver system, shown in figure 4-2, is as follows:

- (1) At the start of airlock operation, valves 1, 2, and 3 are vented to cabin to equalize pressures.
- (2) Valve 3 is then closed and valve 2 is vented to the pump. The airlock is now pumped down while the receiver is pressurized.
- (3) Airlock residual gas is now dumped overboard by venting valves 1 and 2 to space.
- (4) For re-entry to the cabin, the airlock is repressurized by first venting valves 1 and 2 to the receiver, then opening valve 3 to equalize airlock and cabin pressure.

#### Equations for Airlock Expendable-Gas System

The penalty for an expendable-gas system is the total weight of atmospheric gas dumped overboard during a mission plus the cryogenic tankage weight for storage of this gas. Total weight of gas expended is found by the following:

$$m_{a,i} = V_a \rho_{a,i} U_t$$

Cryogenic storage factors are expressed as total poundage, gas, and tankage per pound of gas. For a one-gas atmosphere, the total system penalty is:

$$PEN_{sys} = m_{a,i} F$$

$$PEN_{sys} = V_a \rho_{a,i} U_t F \quad (4-1)$$

However, if a two-gas system, consisting of oxygen and a diluent (He or N<sub>2</sub>), is considered, the cryogenic storage factor must be expressed as a percentage (by weight) of the two gases. For a two-gas system, the total system penalty is:

$$PEN_{sys} = V_a \rho_{a,i} \left( \frac{M_d p'_{d,i} F_d + M_o p'_{o,i} F_o}{M_G P_{a,i}} \right) U_t \quad (4-1a)$$

If a dual airlock system is considered, weight of the gas normally expended overboard may be reduced by utilizing the second airlock as a receiver. Gas is saved by an amount equal to that which is bled to the receiver (secondary airlock) during the pressure equalization process when the crewman is leaving the cabin via the airlock.

An isothermal process is assumed since this pressure equalization process must be slow to prevent the bends. Therefore, expressions may be written for the receiver at the end of the various operational steps. At the start of each airlock operation, initial weight of gas in the receiver is:

$$m_{R,i} = 144 \frac{M_p P_{k,i} V_R}{R T}$$

Initial weight of gas in the airlock, after equalizing with the cabin, is:

$$m_{a,i} = 144 \frac{P_{k,i} K_v V_R}{R T}$$

After equalizing airlock and receiver pressure in the first operation, receiver pressure is:

$$P_{R,1} = \frac{(m_{a,i} + m_{R,i}) R T}{144 (V_a + V_R)}$$

By substitution:

$$P_{a,1} = \frac{P_{k,i} (K_v + M_p)}{1 + K_v}$$

Gas dumped in this first operation is:

$$m_{a,1} = 144 \frac{P_{k,i} (K_v + M_p) K_v V_R}{(1 + K_v) R T} \quad (4-2)$$

Gas saved and remaining in the receiver is:

$$m_{R,1} = 144 \frac{P_{k,i} (K_v + M_p) V_R}{(1 + K_v) R T}$$

After re-entry and repressurizing, the airlock with receiver gas:

$$P_{R,2} = \frac{P_{k,i} (K_v + M_p)}{(1 + K_v)^2}$$

At the start of the mission, receiver pressure may be at nearly any pressure and will probably be at cabin pressure. However, analysis has shown that after six airlock operations, receiver pressure at the start of the airlock operation will reach a steady-state value. Therefore:

$$P_{R,6} = P_{R,i}$$

and

$$M_p = \frac{1}{2 + k_v} \quad (4-3)$$

By substituting equation (4-3) into equation (4-2), gas lost per operation is:

$$m_a = 144 \frac{P_{k,i} V_R K_v (1 + K_v)}{R T (2 + K_v)} \quad (4-4)$$

Gas loss will be reduced as receiver volume increases over airlock volume, thereby reducing  $K_v$ .

However, due to receiver weight penalty, receiver volume is limited to a reasonably small size. An optimum receiver may be found considering weight of expended gas and receiver weight. Calculations were made based on receivers sized for a variable volume ratio ( $K_v$ ). It was found that due to the low pressures involved, tank thickness was extremely thin for tanks sized from stress considerations. If the receiver wall thickness was made great enough to withstand handling, vibration, and mounting loads, no minimum occurred. This was due to the very slight increase in gas saved while the tank weight decreased rapidly as volume ratio increased. Therefore, for most practical applications, it would not be advantageous to use a receiver to save expended airlock gas.

However, the occasion may arise where two airlocks are needed for safety or operational requirements and these may be operated in the manner discussed previously to reduce expended gas. In this case, no penalty can be assigned to the second airlock.

Assuming identical airlocks ( $K_v = 1$ ), equation (4-4) becomes:

$$m_a = \frac{2}{3} V_a \rho_{a,i}$$

which is merely 2/3 of the single airlock system gas loss, and equations (4-1) and (4-1a) become:

$$PEN_{sys} = \frac{2}{3} V_a \rho_{a,i} U_t F \quad (4-5)$$

$$PEN_{sys} = \frac{2}{3} V_a \rho_{a,i} \left( \frac{M_d p'_{d,i} F_d + M_o p'_{o,i} F_o}{M_G P_{a,i}} \right) U_t \quad (4-5a)$$

### Penalty Evaluation For The Expendable-Gas System

Expendable-gas system penalties, for both the single and dual airlock system, were calculated for the eight candidate atmospheres using equations (4-1), (4-1a), (4-5), and (4-5a). The following variables were fixed at representative values:

- (1) Airlock volume ( $V_a$ ) = 100 ft<sup>3</sup>
- (2) Initial airlock temperature ( $T_{a, i}$ ) = 70°F
- (3) Number of airlock usages ( $U_t$ ) = 1.0

Results of these calculations are shown on fig. 4-3. Total system penalty for any other airlock volume and usage may be obtained from the following relationship:

$$PEN_{sys} = \frac{V_a U_t}{100} (PEN_{sys}, \text{fig. 4-3}) \quad (4-6)$$

### Equations For The Airlock Pump-Down System

In this analysis the pumping process is assumed to be adiabatic. However, the actual process will be polytropic (between isothermal and adiabatic). The actual process will depend on the amount of heat rejected to the vehicle structure and environmental control system. The higher the heat loss from the gas, the closer the process will approach a true isothermal process. This heat loss is dependent on vehicle detail design and must be considered in the design of an actual system. However, since the purpose of this section is not the detail design of a pump-down system but a comparison of atmospheres, the adiabatic process was assumed as being the more conservative approach.

The analytical procedure used was to combine the conservation equations for mass and energy. The resultant differential equation is then solved to determine parameters, namely; final pressures, final temperatures, pumping work, and gas flow rate, at a certain time or to find the time at which these parameters reach certain values. In this instance, the end value of two of the parameters, final airlock pressure ( $P_{a, f}$ ) and the time ( $\theta_P$ ) to reach that value of the parameter, have been assumed to be fixed. For this reason, the technique used here was to take successive finite increments of mass from the airlock until final pressure was reached. When this has been accomplished, the sum of all volume increments, divided by the total time, determines the volume flow rate which was assumed to be constant. In this study, the equations were solved using a Fortran computer program.

During pump-down, the airlock was considered to be adiabatic. With the assumption of an ideal gas, airlock conditions (a) after removing an increment of gas ( $\Delta m$ ) are as follows:

$$m_a = m_{a, i} - \Delta m$$

$$v_a = v_{a, i} m_{a, i} / m_a$$

$$P_a = (v_{a, i} / v_a)^{\gamma} P_{a, i} \quad (4-7)$$

$$T_a = 144 P_a V_a M_G / m_a R_u \quad (4-8)$$

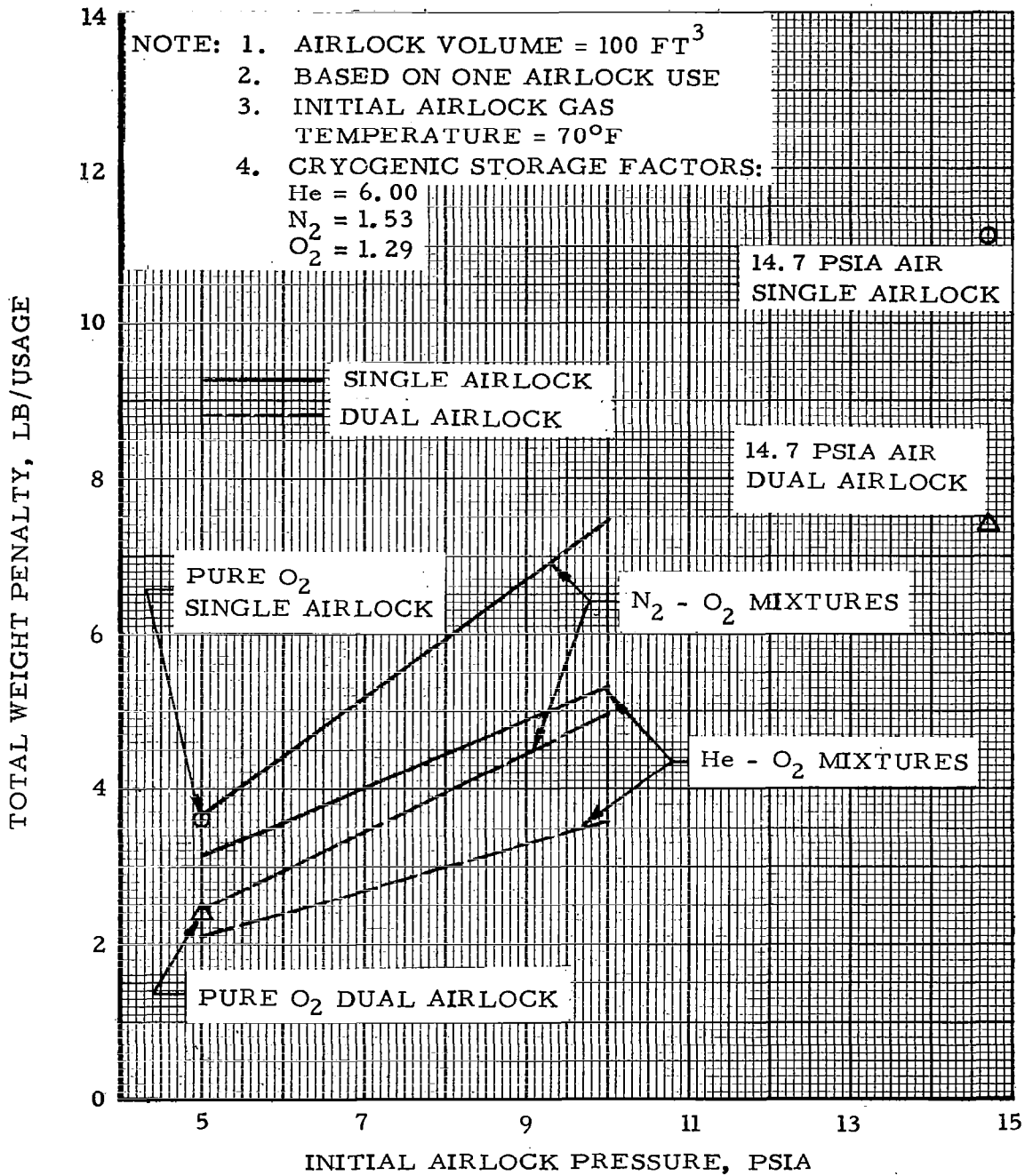


FIGURE 4-3 EXPENDABLE GAS AIRLOCK SYSTEM PENALTY INCLUDING CRYOGENIC STORAGE PENALTY

The enthalpy removed from the airlock is:

$$\Delta H_a = m_{a,i} h_{a,i} - m_a h_a$$

Assuming constant pressures over the increment, the ideal incremental amount of work required to pump  $\Delta m$  pounds is:

$$\Delta W' = \frac{\Delta m R_u T_{a,i} \gamma}{778 M_G (\gamma - 1)} \left[ \left( \frac{P_{k,i}}{P_{a,i}} \right)^{\frac{\gamma - 1}{\gamma}} - 1 \right]$$

Assuming an overall (motor and pump) efficiency of  $\eta_P$ , the actual incremental work requirement is:

$$\Delta W_A = \Delta W' / \eta_P$$

The cabin or receiver specific enthalpy ( $h_k$ ) is now:

$$h_k = \frac{m_{k,i} h_{k,i} + \Delta H_a + \Delta W_A}{m_k}$$

where:

$$m_k = m_{k,i} + \Delta m$$

Assuming a thermally perfect cabin atmosphere (constant  $C_p$ ) yields the results:

$$T_k = (h_k + h_{k,i}) / C_p + T_{k,i} \quad (4-9)$$

$$v_k = v_{k,i} \left( m_{k,i} / m_k \right)$$

and:

$$P_k = m_k R_u T_k / M_G V_k \times 144 \quad (4-10)$$

The volume of air pumped during this increment of  $\Delta m$  is:

$$\Delta V = v_{a,i} \Delta m$$

The power required would be:

$$PWR = 0.01765 \Delta W_A / \Delta \theta_P$$

However, the time increment ( $\Delta\theta_P$ ) will not be known until the end of the pump-down when the total volume pumped becomes available. Therefore, the parameter of specific energy (SE) is chosen as:

$$SE = \Delta W_A / \Delta V$$

In the same manner, successive increments of cabin atmosphere may be taken until  $P_a = P_{a,f}$  by replacing all initial values, i. e., sub-i values, in the above equations with the most recent values. As this is done, successive volume increments ( $\Delta V$ ) are summed until the process is complete. Volume flowrate is then:

$$Q_G = \Sigma \Delta V / \theta_P$$

as the volume flowrate has been assumed constant. In the same manner, work increments ( $\Delta W_A$ ) are summed and the total work is:

$$W_A = \Sigma \Delta W_A$$

The average power is:

$$PWR_{avg} = 0.01765 W_A / \theta_P \quad (4-11)$$

During pump-down, specific energy (SE) values are surveyed and the maximum ( $SE_{max}$ ) is selected. Thus, maximum power is:

$$PWR_{max} = 0.01765 (SE_{max}) Q_G \quad (4-12)$$

Total pump-down system penalty consists of the pump power penalty, pump equipment weight penalty, expended residual gas penalty, and receiver weight penalty (if a receiver is required). The exact determination of these penalties is dependent upon vehicle configuration and mission.

The pump power penalty is normally determined from a weight to power factor relating kilowatts to pounds and is dependent upon the type of power system used in the vehicle, i. e., isotope Brayton cycle, fuel cell, solar cell, batteries, etc. This factor is expressed in units of lb/kW ( $\phi$ ) or in units of lb/kWh ( $\phi'$ ), if the power system is time sensitive. This power penalty for continuous usage is:

$$PEN_{po} = \phi (PWR_{avg}) (\text{fraction of use/day})$$

or

$$PEN_{po} = \phi' (PWR_{avg}) (\text{use time})$$

However, the pump is used only for a fraction of time per day. Therefore, the penalty is:

$$PEN_{po} = \phi (PWR_{avg}) \frac{\theta_P U_t}{1,440 t_m} \quad (4-13)$$

or,

$$PEN_{po} = \phi' (PWR_{avg}) \frac{\theta_P U_t}{60} \quad (4-13a)$$

The pump equipment weight penalty can be expressed as a function of volumetric flow ( $Q_G$ ). In a recent study an airlock pump was sized (ref. 4-1). For this study, flow will be assumed to be 25 cu ft/min with a 15-lb equipment weight. A basic weight of 5 lb will be assumed for the pump motor. Therefore, the pump equipment weight penalty is as follows:

$$PEN_P = 0.4 Q_G + 5 \quad (4-14)$$

The expended residual gas penalty represents the amount of gas left in the airlock after pump-down and includes the cryogenic storage penalty, which is discussed in the storage vessel penalty section of this report. For a one-gas system (i. e., 5-psia pure oxygen), this penalty is:

$$PEN_{ex} = V_a \rho_{a,f} F U_t \quad (4-15)$$

However, if a two-gas system is considered, the cryogenic storage factor must be expressed as a percentage (by weight) for the two gases. Assuming that the percentages remain constant during pump-down, this penalty is:

$$PEN_{ex} = V_a \rho_{a,f} \left( \frac{M_d p'_{d,i} F_d + M_o p'_{o,i} F_o}{M_G P_{a,i}} \right) U_t \quad (4-15a)$$

The receiver weight penalty (if required) is simply the material weight of the receiver structure. Assuming a sphere, the weight was calculated using the following equations (ref 4-2):

$$t_w = \frac{P_R d_i (SF)}{4 F_{ty}} \quad (d_i \text{ in inches})$$

$$PEN_R = \pi (d_i)^2 \rho_{RM} \left( \frac{t_w}{d_i} \right) = 4 \pi (r_i)^2 \rho_{RM} t_w$$

Combining the equations:

$$PEN_R = \frac{2\pi(r_i)^3 \rho_{RM} P_R (SF)}{F_{ty}}$$

The volume of the spherical receiver is:

$$V_R = \frac{4}{3} \frac{\pi(r_i)^3}{1,728} ; r_i^3 = \frac{3}{4} \frac{V_R}{\pi} \times 1,728$$

by substitution:

$$PEN_R = \frac{3}{2} \frac{V_R \rho_{RM} P_R (SF) 1,728}{F_{ty}}$$

let:

$$(SF) = 2$$

$$PEN_R = \frac{5,184 P_R V_R}{\left( \frac{F_{ty}}{\rho_{RM}} \right)} \quad (4-16)$$

The total pump-down system penalty is:

$$PEN_{sys} = PEN_{po} + PEN_P + PEN_{ex} \quad (4-17)$$

If a separate receiver is required

$$PEN_{sys} = PEN_{po} + PEN_P + PEN_{ex} + PEN_R \quad (4-17a)$$

#### Evaluation For The Airlock Pump-Down System Penalty

Aside from the eight candidate atmospheres, determination of the pump-down system penalty was dependent upon several other independent variables, namely, pump-down time, pump efficiency, number of airlock usages, initial temperature, airlock volume, cabin volume (or volume of separate receiver, if used), and final airlock pressure. Of these, the following were fixed at representative values:

- (1) Pump efficiency ( $\eta_P$ ) = 40%
- (2) Airlock volume ( $V_a$ ) = 100 ft<sup>3</sup>
- (3) Initial temperature ( $T_{a,i}$ ) = 70°F

- (4) Pump-down time ( $\theta_P$ ) = 15 min
- (5) Final airlock pressure ( $P_{a,f}$ ) = 0.1 psia
- (6) Number of airlock usages ( $U_t$ ) = 1.0

The remaining variable, cabin or receiver volume was treated as a parameter. This parameter was given values from 10 to 10,000 ft<sup>3</sup>.

Using these fixed values, pumping equations were solved using a Fortran computer program. These results are shown on figs. 4-4 through 4-7 and table 4-II.

The pump average power (fig. 4-4) is in terms of average power (kilowatts) as a function of cabin (or receiver) to airlock volume ratio for the eight candidate atmospheres. Average power for other airlock volumes and/or pump-down times may be calculated by selecting the proper factor from fig. 4-4 for the desired volume ratio and atmosphere, and computing actual power from the following relationship:

$$PWR_{avg} = 0.15 \frac{V_a}{\theta_P} (PWR_{avg}, \text{fig. 4-4}) \quad (4-18)$$

The pump power penalty is calculated by substituting equation (4-18) into either equation (4-13) or (4-13 a), depending upon the type of vehicle power system. The pump power penalty is now:

$$PEN_{po} = \frac{\phi U_t V_a}{9600 t_m} (PWR_{avg}, \text{fig. 4-4}) \quad (4-19)$$

or

$$PEN_{po} = \frac{\phi' U_t V_a}{400} (PWR_{avg}, \text{fig. 4-4}) \quad (4-19a)$$

Although not used in the penalty calculation, maximum power is important, since if peak power during pump-down exceeds the vehicle available power, the pump-down system is impractical. This power is shown in fig. 4-5. The use of this curve is identical to the average power curve. Actual maximum power for any airlock volume and/or pump-down time is:

$$PWR_{max} = 0.15 \frac{V_a}{\theta_P} (PWR_{max}, \text{fig. 4-5}) \quad (4-20)$$

The pump equipment weight penalty, expended residual gas penalty, and pump volumetric flow are shown in table 4-II for each candidate atmosphere.

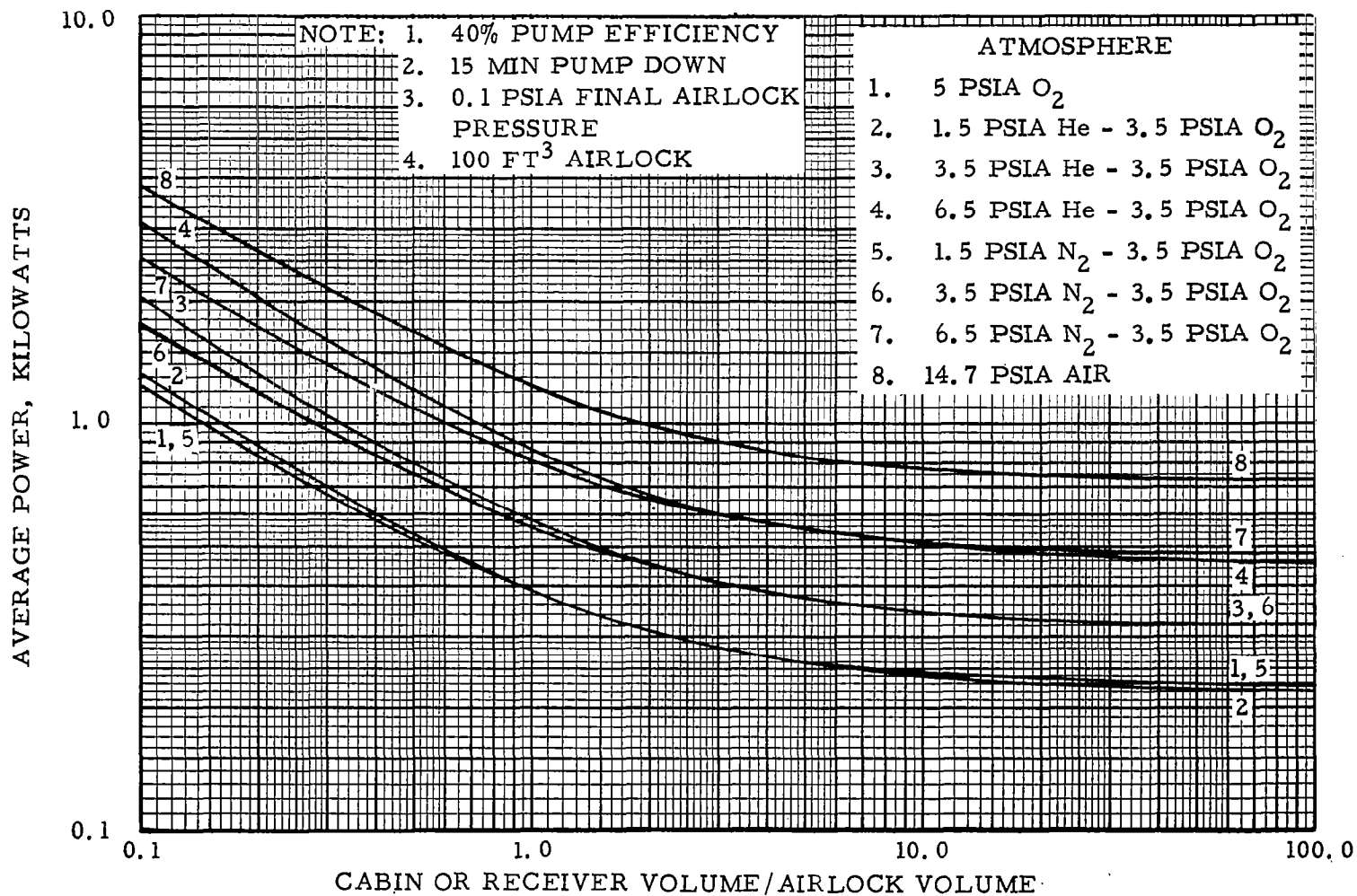


FIGURE 4-4 AVERAGE AIRLOCK PUMP POWER REQUIRED

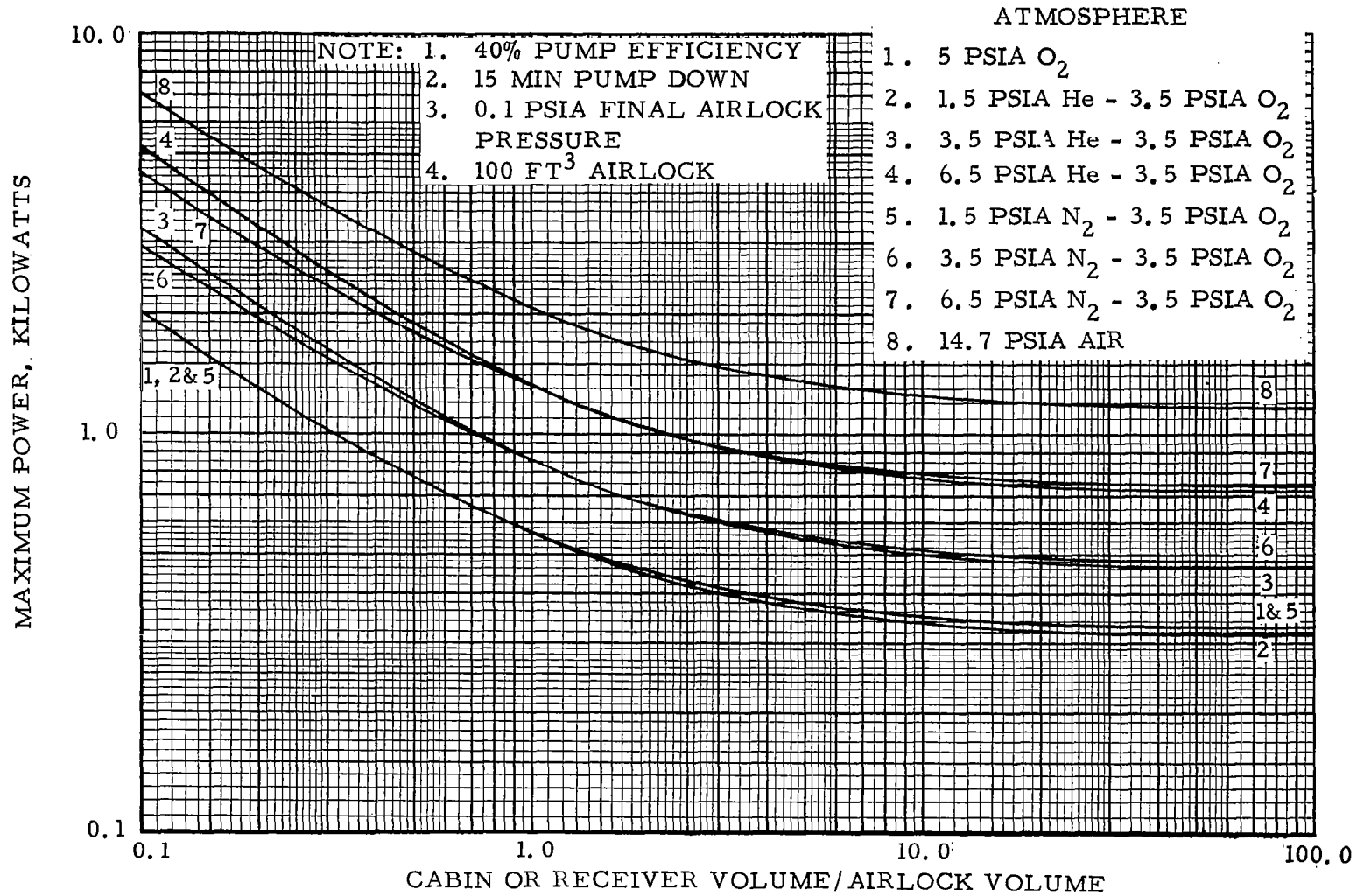


FIGURE 4-5 MAXIMUM AIRLOCK PUMP POWER REQUIRED

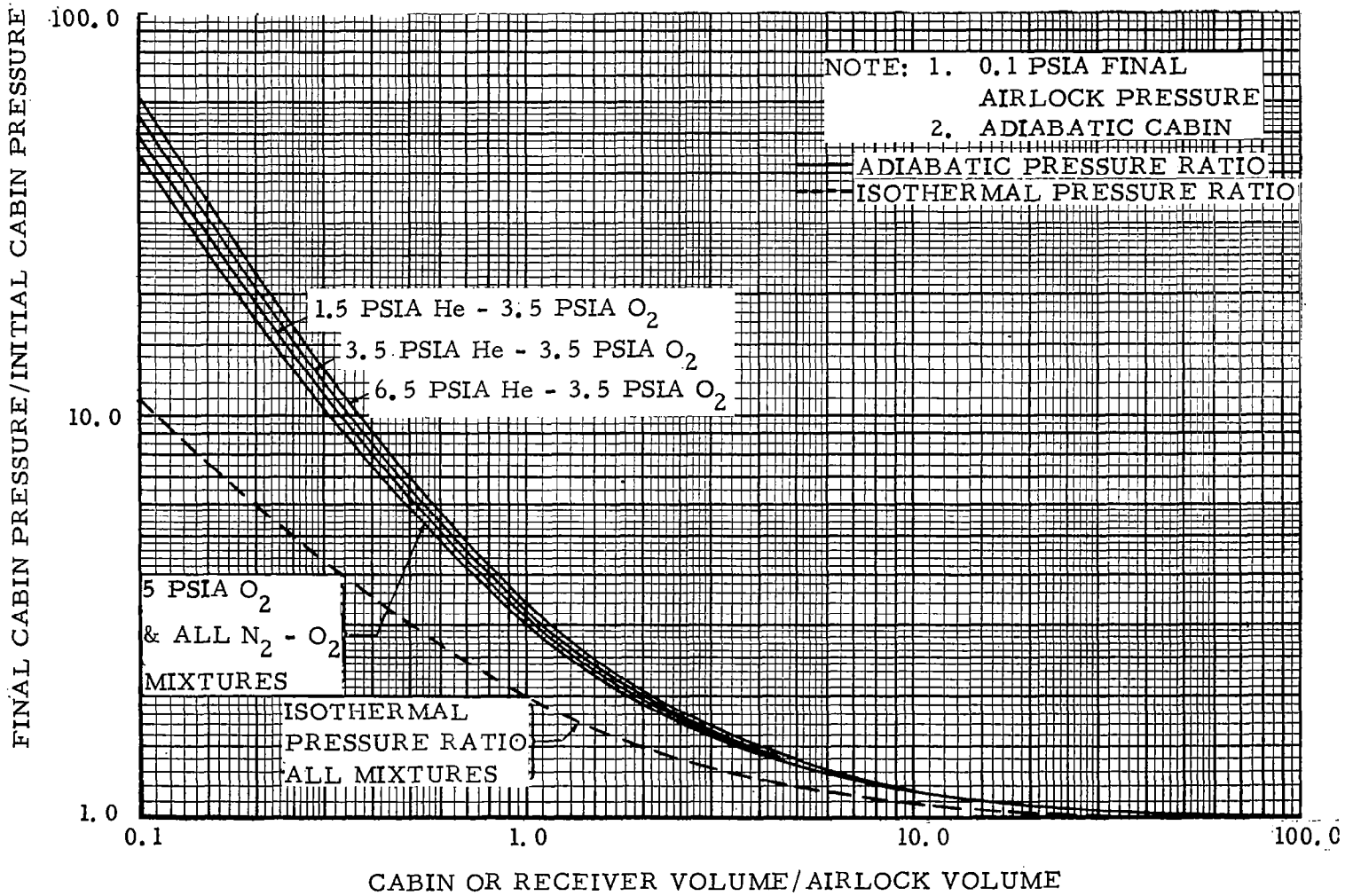


FIGURE 4-6 RATIO OF FINAL CABIN PRESSURE TO INITIAL CABIN PRESSURE

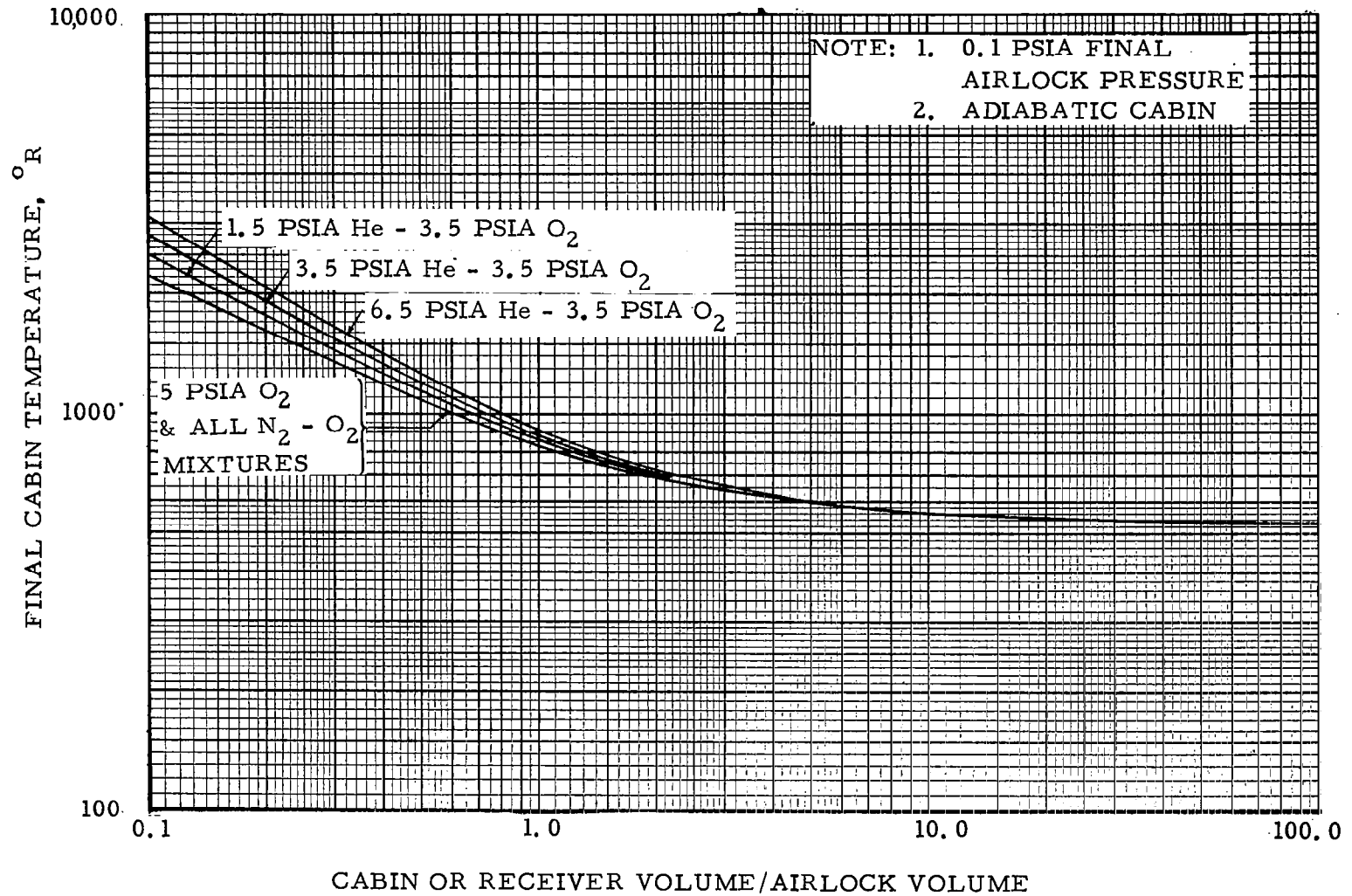


FIGURE 4-7 FINAL CABIN TEMPERATURE

TABLE 4-II  
AIRLOCK PUMP-DOWN PENALTY

Atmosphere	Pump Weight (lb)	Expendable Weight (lb/use)	Pump out rate (cu ft/min)
5 psia O <sub>2</sub>	12.3	0.218	18.25
5 psia He - O <sub>2</sub>	11.9	0.221	17.30
7 psia He - O <sub>2</sub>	12.3	0.241	18.25
10 psia He - O <sub>2</sub>	12.7	0.264	19.36
5 psia N <sub>2</sub> - O <sub>2</sub>	12.3	0.221	18.25
7 psia N <sub>2</sub> - O <sub>2</sub>	12.7	0.259	19.36
10 psia N <sub>2</sub> - O <sub>2</sub>	13.3	0.298	20.69
14.7 psia air	13.9	0.331	22.36

- Note: (1) Both penalties: 100 ft<sup>3</sup> airlock  
 (2) 0.1 psia final airlock pressure  
 (3) Pump penalty for 15-min. pump-down  
 (4) 3.5 psia oxygen partial pressure for all mixtures

Actual values for any airlock volume and/or pump-down time are:

$$PEN_P = 0.15 \frac{V_a}{\theta_P} \left[ (PEN_P, \text{ table 4-II}) - 5 \right] + 5 \quad (4-21)$$

$$PEN_{ex} = \frac{V_a}{100} U_t (PEN_{ex}, \text{ table 4-II}) \quad (4-22)$$

$$Q_G = 0.15 \frac{V_a}{\theta_P} (Q_G, \text{ table 4-II}) \quad (4-23)$$

Final cabin (or receiver) pressure and temperature, expressed as the ratio of final to initial condition, are shown on figs. 4-6 and 4-7 respectively. This analysis considered the pumping process to be adiabatic. However, since the actual process will be somewhere between adiabatic and isothermal, the isothermal pressure ratio is also shown on fig. 4-6 for comparison.

The actual pressure and temperature ratios will depend on the amount of heat rejected to structure and the vehicle environmental control system. This factor must be considered in the design of an actual system but cannot be considered in this study due to the many unknowns. Therefore, the adiabatic pressure and temperature ratios will be used to compare the candidate atmospheres.

For cases in which the cabin pressure, temperature and/or the heat load from pump-down is excessive for the vehicle under consideration, the airlock atmosphere must be pumped into a separate receiver. The weight penalty for this receiver must be added to the total system penalty.

Since the receiver may normally be located in an area of high heat loss, the receiver was evaluated at a temperature less than the maximum computed (adiabatic) receiver gas temperature. In addition, the receiver was stressed at a pressure less than the maximum computed (adiabatic) gas pressure. The temperature selected was 600°F and the pressure selected was 137 psia. The material selected was a titanium alloy (4Al-3Mo-1V, ST and AGED) which has a strength-to-density ratio of 820,000 at 600°F (ref. 4-3). Using these values, equation (4-16) now becomes:

$$PEN_R = 0.865 V_R \quad (4-24)$$

The total pump-down system penalty is now obtained from either equation (4-17) or (4-17a).

#### COMPARISON OF AIRLOCK PENALTY FOR DIFFERENT ATMOSPHERIC CONDITIONS AND AIRLOCK DESIGNS

Airlock configurations previously discussed include those from a completely expendable system to those that provide gas conservation by adding a

pump-down system. Gases in the pump-down system are either stored in the vehicle compartments or in a reservoir. Reservoir storage is attractive where increased cabin pressure would not be attractive from a sudden decompression standpoint or the airlock gas and/or increased cabin pressure could interfere with a controlled experiment. In this section, the use of the parametric data, tabular data, and equations will be illustrated by example calculations. Two representative vehicle configurations and missions are considered and evaluated for various atmosphere compositions and pressure levels.

### Airlock Penalty Evaluation for a Representative Small Laboratory

A 3-man spacecraft was assumed to be the equivalent size of the combined Apollo Command Module and the LEM and have a fuel cell power system. The problem specifications for this example are as follows:

- (1) Mission time ( $t_m$ ) = 30 days
- (2) Total airlock uses ( $U_t$ ) = 30
- (3) Cabin volume ( $V_k$ ) = 200 ft<sup>3</sup>
- (4) Airlock volume ( $V_a$ ) = 200 ft<sup>3</sup>
- (5) Fuel cell power system
- (6) Initial cabin temperature ( $T_{k,i}$ ) = 70° F

The three-man space laboratory example problem will be presented for expendable and pump-down systems for atmospheric conditions of 5 psia pure O<sub>2</sub>, 5 psia N<sub>2</sub>O<sub>2</sub>, and 5 psia He-O<sub>2</sub>.

Fuel Cell Penalty. - - Two fuel cell units are assumed (ref. 4-4)

$$\phi_{sys} = 2 \left( 86 \frac{\text{lb}}{\text{kWh}} \right) = 172 \frac{\text{lb}}{\text{kWh}}$$

The weight penalty for fuel and oxidizer (H<sub>2</sub> and O<sub>2</sub>), without the cryogenic penalty, without redundancy, is as follows (ref. 4-4)

$$\phi' = 0.93 \frac{\text{lb}}{\text{kWh}}$$

However, the cryogenic storage penalty must be included. Assuming a fuel flow of 5 lb/day for hydrogen (ref. 4-2):

$$F_h = 2.1$$

The oxygen cryogenic factor is obtained from the storage vessel penalty section of this report:

$$F_o = 1.29$$

Approximately 8 lb of oxygen are used per lb of hydrogen and 1 lb of fuel is required per kWh. Therefore:

$$F_{sys} = \frac{8 \times 1.29 + 2.1}{9} = 1.38$$

$$\phi'_{sys} = 1.38 \times 0.93 = 1.28 \frac{\text{lb}}{\text{kWh}}$$

The actual power penalty is the sum of equations (4-19) and (4-19a) and becomes:

$$PEN_{po} = U_t V_a \left( \frac{\phi}{9,600 t_m} + \frac{\phi'}{400} \right) (PWR_{avg}, \text{ fig. 4-4})$$

$$PEN_{po} = 22.7 (PWR_{avg}, \text{ fig. 4-4}) \quad (4-25)$$

#### Case No. 1: 5 Psia O<sub>2</sub> Atmosphere

1. Assume: Pump-down to cabin

$$\theta_P = 15 \text{ min}$$

The pump weight is obtained from equation (4-21):

$$PEN_P = \frac{0.15 \times 200}{15} \left[ (PEN_P, \text{ table 4-II}) - 5 \right] + 5$$

$$PEN_P = 2(12.3 - 5) + 5$$

$$PEN_P = 19.6 \text{ lb}$$

The expended gas penalty is obtained from equation (4-22):

$$PEN_{ex} = \frac{200 \times 30}{100} (PEN_{ex}, \text{ table 4-II})$$

$$PEN_{ex} = 60(0.218) = 13.1 \text{ lb}$$

Since  $V_k/V_a = 1.0$ , the average power from equation (4-18) is:

$$PWR_{avg} = \frac{0.15 \times 200}{15} \text{ (PWR}_{avg}, \text{ fig. 4-4)}$$

$$PWR_{avg} = 2(0.390) = 0.780 \text{ kW}$$

The power penalty is obtained from equation (4-25):

$$PEN_{po} = 22.7(0.390) = 8.85 \text{ lb}$$

Total system penalty is obtained from equation (4-17):

$$PEN_{sys} = 19.6 + 13.1 + 8.85 = 41.55 \text{ lb}$$

Final cabin pressure and temperature is obtained from figs. 4-6 and 4-7 with  $V_k/V_a = 1.0$ :

$$P_{k,f} = 15 \text{ psia (adiabatic)}$$

$$P_{k,f} = 10 \text{ psia (isothermal)}$$

$$T_{k,f} = 370^\circ\text{F}$$

Even if the isothermal pressure is considered, the pressure rise is excessive. In addition, the heat added to the cabin might be excessive. Therefore, a receiver should be considered.

2. Assume: Pump-down to receiver

$$\theta_P = 15 \text{ min}$$

$$V_R = 20 \text{ ft}^3$$

The pump and expended gas penalties are the same as in 1 above:

$$PEN_P = 19.6 \text{ lb}$$

$$PEN_{ex} = 13.1 \text{ lb}$$

Since  $V_R/V_a = 0.1$ , the average power is:

$$PWR_{avg} = 2(1.25) = 2.5 \text{ kW}$$

$$PEN_{po} = 22.7(1.25) = 28.5 \text{ lb}$$

Receiver penalty is obtained from equation (4-24):

$$PEN_R = 0.865 (20) = 17.3 \text{ lb}$$

Total system penalty is obtained from equation (4-17a):

$$PEN_{\text{sys}} = 19.6 + 13.1 + 28.5 + 17.3 = 78.5 \text{ lb}$$

However, average power is excessive. Maximum power is obtained from equation (4-20):

$$PWR_{\text{max}} = \frac{0.15 \times 200}{15} \text{ (PWR}_{\text{max}}, \text{ fig. 4-5)}$$

$$PWR_{\text{max}} = 2 (2) = 4 \text{ kW}$$

Since the maximum power available per fuel cell on the Apollo module is 2.5 kW, this system is impractical and a longer pump time must be considered.

3. Assume: Pump-down to receiver

$$\theta_P = 30 \text{ min}$$

$$V_R = 20 \text{ ft}^3$$

The expended gas, power, and receiver penalties are the same as in 2 above:

$$PEN_{\text{ex}} = 13.1 \text{ lb}$$

$$PEN_{\text{po}} = 28.5 \text{ lb}$$

$$PEN_R = 17.3 \text{ lb}$$

Since  $\theta_P$  is larger, the volumetric flow of the pump decreases and the pump penalty becomes:

$$PEN_P = \frac{0.15 \times 200}{30} (12.3-5) + 5$$

$$PEN_P = 1.0 (7.3) + 5 = 12.3 \text{ lb}$$

Total system penalty is:

$$PEN_{\text{sys}} = 12.3 + 13.1 + 28.5 + 17.3 = 71.2 \text{ lb}$$

Although the power penalty is the same as 2 above, actual powers are:

$$PWR_{avg} = \frac{0.15 \times 200}{30} (1.25) = 1.25 \text{ kW}$$

$$PWR_{max} = \frac{0.15 \times 200}{30} (2) = 2.0 \text{ kW}$$

Therefore, with the longer pumping time, the system becomes feasible.

4. Assume: Expendable gas system

For this analysis, only one airlock is available and the penalty is obtained from equation (4-6):

$$PEN_{sys} = \frac{200 \times 30}{100} (PEN_{sys}, \text{ fig. 4-3})$$

$$PEN_{sys} = 60 (3.63) = 217 \text{ lb}$$

Case No. 2: 3.5 Psia O<sub>2</sub> - 1.5 Psia He Atmosphere

1. Assume: Pump-down to cabin

$$\theta_p = 15 \text{ min}$$

The same procedure is followed as in Case No. 1. However, the proper atmosphere curves and tabular data must be utilized.

$$PEN_p = 2(11.9-5) + 5 = 18.8 \text{ lb}$$

$$PEN_{ex} = 60 (0.221) = 13.3 \text{ lb}$$

$$PWR_{avg} = 2(0.390) = 0.780 \text{ kW}$$

$$PEN_{po} = 22.7 (0.390) = 8.85 \text{ lb}$$

$$PEN_{sys} = 18.8 + 13.3 + 8.85 = 40.95 \text{ lb}$$

$$P_{k,f} = 15 \text{ Psia (Adiabatic)}$$

$$P_{k,f} = 10 \text{ Psia (Isothermal)}$$

$$T_{k,f} = 370^\circ \text{F}$$

Again, the pressure and temperature rise is excessive and a receiver is required.

2. Assume: Pump-down to receiver

$$\theta_P = 15 \text{ min}$$

$$V_R = 20 \text{ ft}^3$$

The pump and expended gas penalties are the same as in 1 above:

$$\text{PEN}_P = 18.8 \text{ lb}$$

$$\text{PEN}_{\text{ex}} = 13.3 \text{ lb}$$

Receiver penalty is identical to Case No. 1:

$$\text{PEN}_R = 17.3 \text{ lb}$$

Since  $V_R/V_a = 0.1$ :

$$\text{PEN}_{\text{po}} = 22.7 (1.32) = 30 \text{ lb}$$

$$\text{PEN}_{\text{sys}} = 18.8 + 13.3 + 17.3 + 30 = 79.4 \text{ lb}$$

However, power is again excessive:

$$\text{PWR}_{\text{avg}} = 2 (1.32) = 2.64 \text{ kW}$$

3. Assume: Pump-down to receiver

$$\theta_P = 30 \text{ min}$$

$$V_R = 20 \text{ ft}^3$$

The expended gas, power, and receiver penalties are the same as in 2 above:

$$\text{PEN}_{\text{ex}} = 13.3 \text{ lb}$$

$$\text{PEN}_{\text{po}} = 30 \text{ lb}$$

$$\text{PEN}_R = 17.3 \text{ lb}$$

Pump penalty is:

$$\text{PEN}_P = 1.0 (11.9 - 5) + 5 = 11.9 \text{ lb}$$

Total penalty is:

$$PEN_{sys} = 11.9 + 13.3 + 30 + 17.3 = 72.5 \text{ lb}$$

The actual powers are:

$$PWR_{avg} = 1.32 \text{ KW}$$

$$PWR_{max} = 1.0 (2) = 2 \text{ KW}$$

Therefore, this system is feasible.

4. Assume: Expendable gas system

From Figure 4-3 and equation (4-6):

$$PEN_{sys} = \frac{200 \times 30}{100} (3.14) = 188 \text{ lb}$$

Case No. 3: 3.5 Psia O<sub>2</sub> - 1.5 Psia N<sub>2</sub> Atmosphere

1. Assume: Pump-down to cabin

$$\theta_P = 15 \text{ min}$$

$$PEN_P = 2 (12.3-5) + 5 = 19.6 \text{ lb}$$

$$PEN_{ex} = 60 (0.221) = 13.3 \text{ lb}$$

$$PWR_{avg} = 2 (0.390) = 0.780 \text{ kW}$$

$$PEN_{po} = 22.7 (0.390) = 8.85 \text{ lb}$$

$$PEN_{sys} = 19.6 + 13.3 + 8.85 = 41.75 \text{ lb}$$

From figures 4-6 and 4-7:

$$P_{k,f} = 15 \text{ Psia (Adiabatic)}$$

$$P_{k,f} = 10 \text{ Psia (Isothermal)}$$

$$T_{k,f} = 370^\circ \text{ F}$$

Therefore, a receiver must be considered.

2. Assume: pump-down to receiver

$$\theta_P = 15 \text{ min}$$

$$V_R = 20 \text{ ft}^3$$

$$PEN_P = 19.6 \text{ lb}$$

$$PEN_{ex} = 13.3 \text{ lb}$$

$$PEN_R = 17.3 \text{ lb}$$

Since  $V_R/V_a = 0.1$ , from figure 4-4:

$$PWR_{avg} = 2 (1.25) = 2.5 \text{ KW}$$

From equation (4-25):

$$PEN_{po} = 22.7 (1.25) = 28.5 \text{ lb}$$

Therefore:

$$PEN_{sys} = 19.6 + 13.3 + 17.3 + 28.5 = 78.7 \text{ lb}$$

However, since power is excessive, a longer pumping time must be considered.

3. Assume: pump-down to receiver

$$\theta_P = 30 \text{ min}$$

$$V_R = 20 \text{ ft}^3$$

The expended gas, power and receiver penalties are the same as in 2 above:

$$PEN_{ex} = 13.3 \text{ lb}$$

$$PEN_{po} = 28.5 \text{ lb}$$

$$PEN_R = 17.3 \text{ lb}$$

Pump penalty is:

$$PEN_P = 1.0 (12.3-5) + 5 = 12.3 \text{ lb}$$

Total penalty is:

$$PEN_{sys} = 12.3 + 13.3 + 28.5 + 17.3 = 71.4 \text{ lb}$$

The actual powers are:

$$PWR_{avg} = 1.25 \text{ KW}$$

$$PWR_{max} = 2.0 \text{ KW}$$

Therefore, this system is feasible.

4. Assume: Expendable-gas system

From figure 4-3 and equation (4-6):

$$PEN_{sys} = \frac{200 \times 30}{100} (3.72) = 223 \text{ lb}$$

These results are shown in table 4-III.

#### Airlock Penalty Evaluation for a Representative Large Space Laboratory

A 4 to 9 man space laboratory was assumed to be the equivalent size of the Manned Orbital Research Laboratory. The on-board power system is a Isotope Brayton unit.

The problem specifications for this example are:

- (1) Mission duration ( $t_m$ ) = 100 days
- (2) Total airlock uses ( $U_t$ ) = 100
- (3) Cabin volume ( $V_k$ ) = 10,000 ft<sup>3</sup>
- (4) Airlock volume ( $V_a$ ) = 100 ft<sup>3</sup>
- (5) Isotope Brayton power system
- (6) Initial cabin temperature ( $T_{k,i}$ ) = 70°F

The 4 to 9 man space laboratory example problem will be presented for both expendable-gas and pump-down systems for atmospheres of 7 psia N<sub>2</sub>-O<sub>2</sub> and He-O<sub>2</sub> with 3.5 psia oxygen partial pressure.

Isotope Brayton Power System Penalty. - - The isotope Brayton cycle power penalty factor given below was obtained from reference 4-5.

$$\phi_{sys} = \frac{5,281 \text{ lb (System Weight)}}{10.5 \text{ KW (System Power)}} = 503 \text{ lb/kW}$$

TABLE 4-III  
AIRLOCK SYSTEM ATMOSPHERE PENALTY COMPARISONS  
(SUMMARY FOR EXAMPLE PROBLEMS)

Total Penalty (lb)

Vehicle	Mission Time	Atmosphere <sup>a</sup>	Vehicle Power System	Expendable-Gas System <sup>b</sup>		Pump-Down System <sup>b</sup>			Remarks
				Single Airlock (lb)	Dual Airlock (lb)	$\theta_P$ (Min)	To Receiver (lb)	To Cabin (lb)	
3-man space station with two, 200 cu ft cabins	30 days	5 psia O <sub>2</sub>	Fuel cell	217	—	15 30	78.5 71.2	41.6 —	A receiver is recommended to prevent excessive cabin pressure rise. A 30-min pump time was required to eliminate excessive power consumption.
		5 psia He - O <sub>2</sub>		188	—	15 30	79.4 72.5	41.0 —	
		5 psia N <sub>2</sub> - O <sub>2</sub>		223	—	15 30	78.7 71.4	41.8 —	
4 to 9 man space station with a 100 cu ft airlock	100 days	7 psia He - O <sub>2</sub>	Isotope Brayton cycle	406	273	15	—	38.1	A receiver was not shown due to the large cabin to airlock volume ratio.
		7 psia N <sub>2</sub> - O <sub>2</sub>		512	342	15	—	40.3	

<sup>a</sup>3.5 psia oxygen partial pressure for all mixtures.

<sup>b</sup>Weight of an airlock not included.

Power penalty for the isotope Brayton cycle is obtained from equation (4-19):

$$\begin{aligned} \text{PEN}_{\text{po}} &= \frac{\phi U_t V_a}{9,600 t_m} (\text{PWR}_{\text{avg}}, \text{ fig. 4-4}) \\ \text{PEN}_{\text{po}} &= 5.24 (\text{PWR}_{\text{avg}}, \text{ fig 4-4}) \end{aligned} \quad (4-26)$$

Case No. 1: 3.5 Psia O<sub>2</sub> - 3.5 Psia He Atmosphere

1. Assume: pump-down to cabin

$$\theta_p = 15 \text{ min}$$

The pump weight penalty is obtained from equation (4-21):

$$\begin{aligned} \text{PEN}_P &= \frac{0.15 \times 100}{15} \left[ (\text{PEN}_P, \text{ table 4-II}) - 5 \right] + 5 \\ \text{PEN}_P &= 1.0 (12.3 - 5) + 5 = 12.3 \text{ lb} \end{aligned}$$

The expended-gas penalty is obtained from equation (4-22):

$$\begin{aligned} \text{PEN}_{\text{ex}} &= \frac{100 \times 100}{100} (\text{PEN}_{\text{ex}}, \text{ table 4-II}) \\ \text{PEN}_{\text{ex}} &= 100 (0.241) = 24.1 \end{aligned}$$

Since  $V_k/V_a = 100$ , the average power from equation (4-18) is:

$$\begin{aligned} \text{PWR}_{\text{avg}} &= \frac{0.15 \times 100}{15} (\text{PWR}_{\text{avg}}, \text{ fig 4-4}) \\ \text{PWR}_{\text{avg}} &= 1.0 (0.320) = 0.320 \text{ kW} \end{aligned}$$

The power penalty is obtained from equation (4-26):

$$\text{PEN}_{\text{po}} = 5.24 (0.320) = 1.68 \text{ lb}$$

Total system penalty is obtained from equation (4-17).

$$\text{PEN}_{\text{sys}} = 12.3 + 24.1 + 1.68 = 38.08 \text{ lb}$$

Final cabin pressure and temperature is obtained from figures 4-6 and 4-7 with  $V_k/V_a = 100$ :

$$P_{k,f} = 7.0 \text{ Psia}$$

$$T_{k,f} = 70^\circ\text{F}$$

Since there is no change in cabin temperature or pressure, a receiver is not required.

2. Assume: expendable-gas system utilizing one airlock only.

The total penalty is obtained from equation (4-6):

$$PEN_{sys} = \frac{100 \times 100}{100} (PEN_{sys}, \text{ fig 4-3})$$

$$PEN_{sys} = 100(4.06) = 406 \text{ lb}$$

3. Assume: expendable-gas system utilizing two airlocks

$$PEN_{sys} = 100 (2.73) = 273 \text{ lb}$$

Case No. 2: 3.5 Psia O<sub>2</sub> - 3.5 Psia N<sub>2</sub> atmosphere

1. Assume: pump-down to cabin

$$\theta_P = 15 \text{ min}$$

The same procedure is followed as was done in Case No. 1. However, the proper atmosphere curves and tabular data must be utilized.

$$PEN_P = 1.0 (12.7-5) + 5 = 12.7 \text{ lb}$$

$$PEN_{ex} = 100 (0.259) = 25.9 \text{ lb}$$

$$PWR_{avg} = 1.0 (0.320) = 0.320 \text{ kW}$$

$$PEN_{po} = 5.24 (0.320) = 1.68 \text{ lb}$$

$$PEN_{sys} = 12.7 + 25.9 + 1.68 = 40.28 \text{ lb}$$

$$P_{k,f} = 7.0 \text{ Psia}$$

$$T_{k,f} = 70^\circ\text{F}$$

Again the pressure and temperature remains unchanged and a receiver is not required.

2. Assume: expendable gas system utilizing one airlock only.

From figure 4-3 and equation (4-6):

$$PEN_{sys} = 100 (5.12) = 512 \text{ lb}$$

3. Assume: expendable gas system utilizing two airlocks

$$PEN_{sys} = 100 (3.42) = 342 \text{ lb}$$

Table 4-III presents a tabulation of the penalty results for both the small and large space laboratories.

### CONCLUSIONS AND RECOMMENDATIONS

The penalty of airlock usage for a wide range of vehicle sizes and configurations can be evaluated from an atmospheric selection standpoint from the presented analysis. Table 4-III presents penalty data for a representative small 3-man space laboratory and a larger 4 to 9 man space laboratory. In general, for both types of airlock systems, expendable-gas and gas conservation by pump-down, the atmosphere with the lowest density provides the lightest system. In most instances, gas conservation by pump-down and gas storage is much lower in total penalty than an expendable-gas system where the airlock must be used frequently and/or the cabin volume is large. A tradeoff analysis of the four- to nine-man space laboratory showed that pump-down resulted in a weight savings after three airlock operations with 7 psia  $N_2-O_2$  in comparison with expending the atmosphere at each usage.

The major development problem for a pump-down system design is the development of a flight-type, flight-weight, pump, and motor combination. Since actual flight-type airlock pump-down hardware has not been developed, the pump weight penalty calculations, contained in this analysis, were based on the limited information available. For this analysis basic assumptions were made for the airlock pump design:

- Pumping efficiency = 40%
- Final airlock pressure = 0.1 psia
- Volumetric flow constant
- Equipment weight based on best vendor information available and engineering judgment

For a final optimization study more information must be available to evaluate the design of an actual system. However, since this study is concerned with the comparison of atmospheres, the basic conclusion, that the minimum penalty occurs with least-dense atmosphere for any airlock system, is valid.

## REFERENCES

- 4-1. Report on a System Comparison and Selection Study of a Manned Orbital Research Laboratory, Douglas Report SM-44607, Volume I, September 1963.
- 4-2. Analytical Methods for Space Vehicle Atmosphere Control Process, ASD Technical Report 61-162, Part II, November 1962.
- 4-3. Compilation of Advanced Material Data for Aerospace and Hypersonic Vehicles, Douglas Engineering Technical Report 32155, April 1965.
- 4-4. Power Subsystems State of the Art and Projection Report, Douglas Report SM 52024, July 1966.
- 4-5. MORL Isotope Power System Briefing, Douglas Report SM-48156, February 1965.

## Section 5

### ATMOSPHERIC SUPPLY SYSTEM

Information required to determine system volume and weight penalties incurred for the storage of atmospheric gas constituents is presented in this section. No attempt has been made to generate new data for storage vessel design because an abundance of data that can be used to evaluate storage vessel penalty is available.

Atmospheric gas supplies will be needed for crew breathing, leakage makeup, airlock usage makeup, and cabin repressurization. If an oxygen recovery subsystem is used in the spacecraft, the gas storage requirements are primarily limited to those needed for makeup gases.

The penalty charged to the atmosphere supply system depends primarily on the method of storage used. The storage methods for constituent atmospheric gases discussed in this section have been divided into the following classes:

- (1) High pressure gaseous storage at ambient temperature
- (2) Supercritical storage at cryogenic temperature
- (3) Subcritical storage at cryogenic temperatures.

High pressure gaseous storage is the heaviest supply system for most applications; subcritical storage has the smallest penalty. During subcritical storage, the two phases of saturated liquid and saturated vapor exist simultaneously in the vessel. For an atmosphere supply system, it is preferable to draw off the vapor rather than the liquid. This allows for a greater design heat leak, which reduces the requirement for insulation. Techniques to selectively draw off vapor are currently under development but have not been flight qualified. Supercritical storage circumvents the two-phase problem and has been used in Gemini vehicles. Saturated liquid, thermally pressurized at constant density, is heated above the critical pressure and maintained at constant pressure during withdrawal until critical temperature is exceeded. The pressure is allowed to decrease after passing the critical temperature, until the tank contents are exhausted. The penalty for supercritical storage is somewhat higher than that of subcritical storage primarily because the higher operating pressure of supercritical storage, as compared to subcritical storage, requires a heavier vessel wall. Gaseous storage at ambient temperature requires high pressure and large tank volumes for most applications. The high pressures require vessels which are relatively heavy. Therefore, for nominal use rates, high-pressure storage penalties are much greater than those for supercritical storage.

However, in instances of very low use rates or long standby times, high-pressure storage may be advantageous. The data collected and the information for evaluating penalty for high pressure storage and supercritical and subcritical storage are presented.

A computer program was used to evaluate the weight penalties of cryogenic storage tanks. The computer program incorporated the latest vendor and current technology and data, particularly for helium storage vessels. The interacting effects of storage volume, pressure, heat leak, standby time, usage rates, insulation effectiveness, and storage time on the weights of systems used for the cryogenic storage of helium, nitrogen, and oxygen were considered. Data concerning high-pressure gaseous storage tanks were collected from the large amount of information in the literature which describes the current systems.

### HIGH-PRESSURE GASEOUS STORAGE

Figure 5-1 shows the representative hardware and controls needed for a typical high pressure gas storage system (ref. 5-1). High-pressure tanks for both oxygen and nitrogen are near minimum weight at a fill pressure of 3,000 to 3,500 psi and near a minimum volume at a pressure of 20,000 to 30,000 psi. High gas pressure tankage weight and volume penalties for oxygen and nitrogen are shown in figures 5-2 and 5-3, for a nominal fill pressure of 7,500 psi. Spherical vessels are assumed to be made of SAE 4340 steel in the case of oxygen and titanium TiC-120 Av in the case of nitrogen. The weight and volume of spherical titanium helium tanks are shown as a function of nominal fill pressure in figure 5-4 where the data were limited to pressures below 6,000 psi.

### SUPERCRITICAL STORAGE

Supercritical storage of atmospheric constituent gases at cryogenic temperatures provides for storing fluids at relatively high density and lower operating pressures. In turn, this leads to lower specific weight and volume of the cryogenic tankage. Weight and volume criteria used for supercritical storage are based on the properties of cryogenic fluids and storage vessel design data listed in table 5-I, as well as references 5-2, 5-3, and 5-4 for oxygen, nitrogen, and helium, respectively.

Supercritical storage tanks are first filled at a low pressure level with saturated liquid and a small amount of entrapped vapor. The vessel is then capped and heated at constant density to a pressure higher than critical. This mixture acts in the supercritical pressure state as a homogeneous one-phase fluid. Fluid can then be withdrawn from the tank at a constant pressure if the pressure level is maintained by the addition of heat to the storage space. Heat input,  $q$ , to the fluid at constant pressure,  $p$ , is given by the following relationship (ref. 5-1).

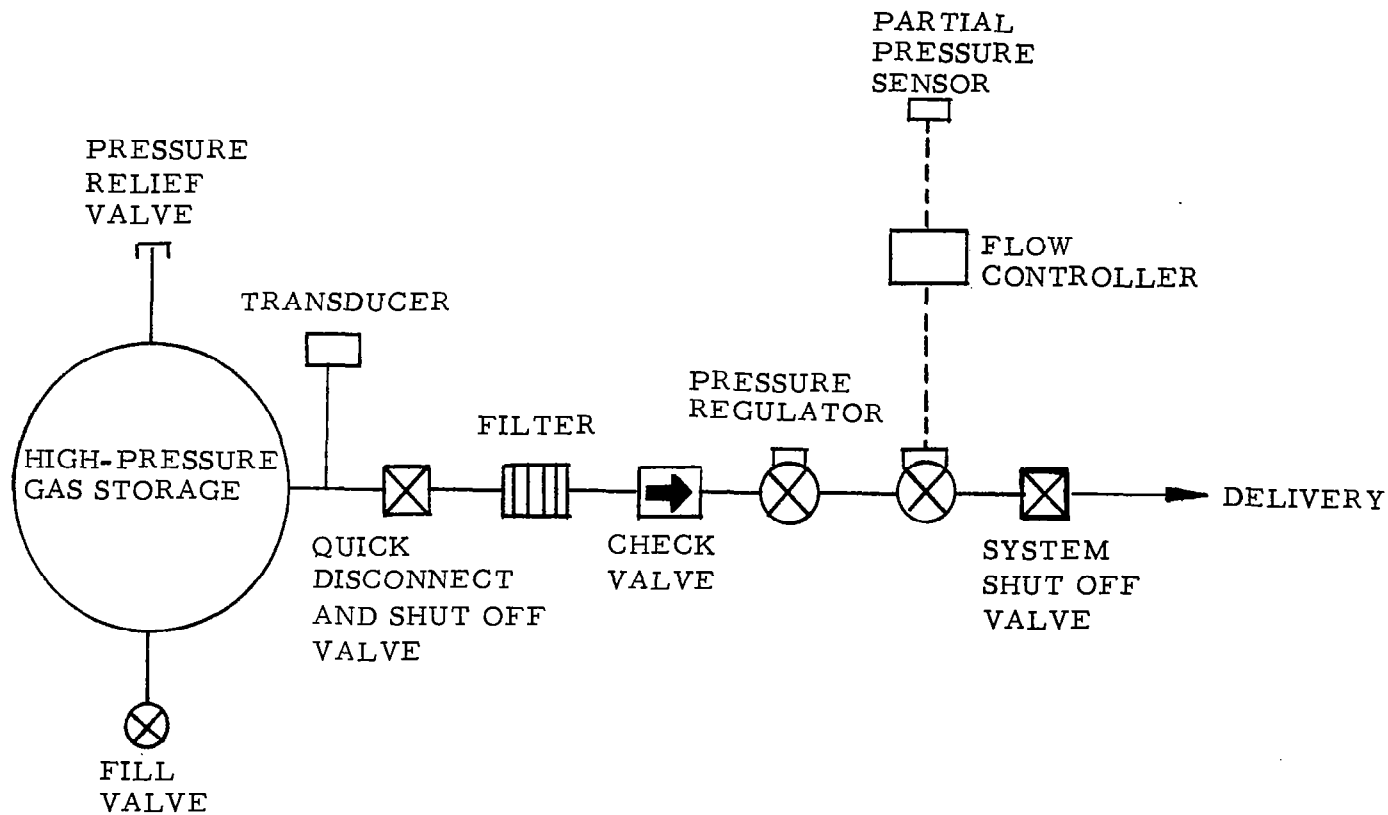


FIGURE 5-1 HIGH-PRESSURE GAS STORAGE - GAS SUPPLY SUBSYSTEM DIAGRAM

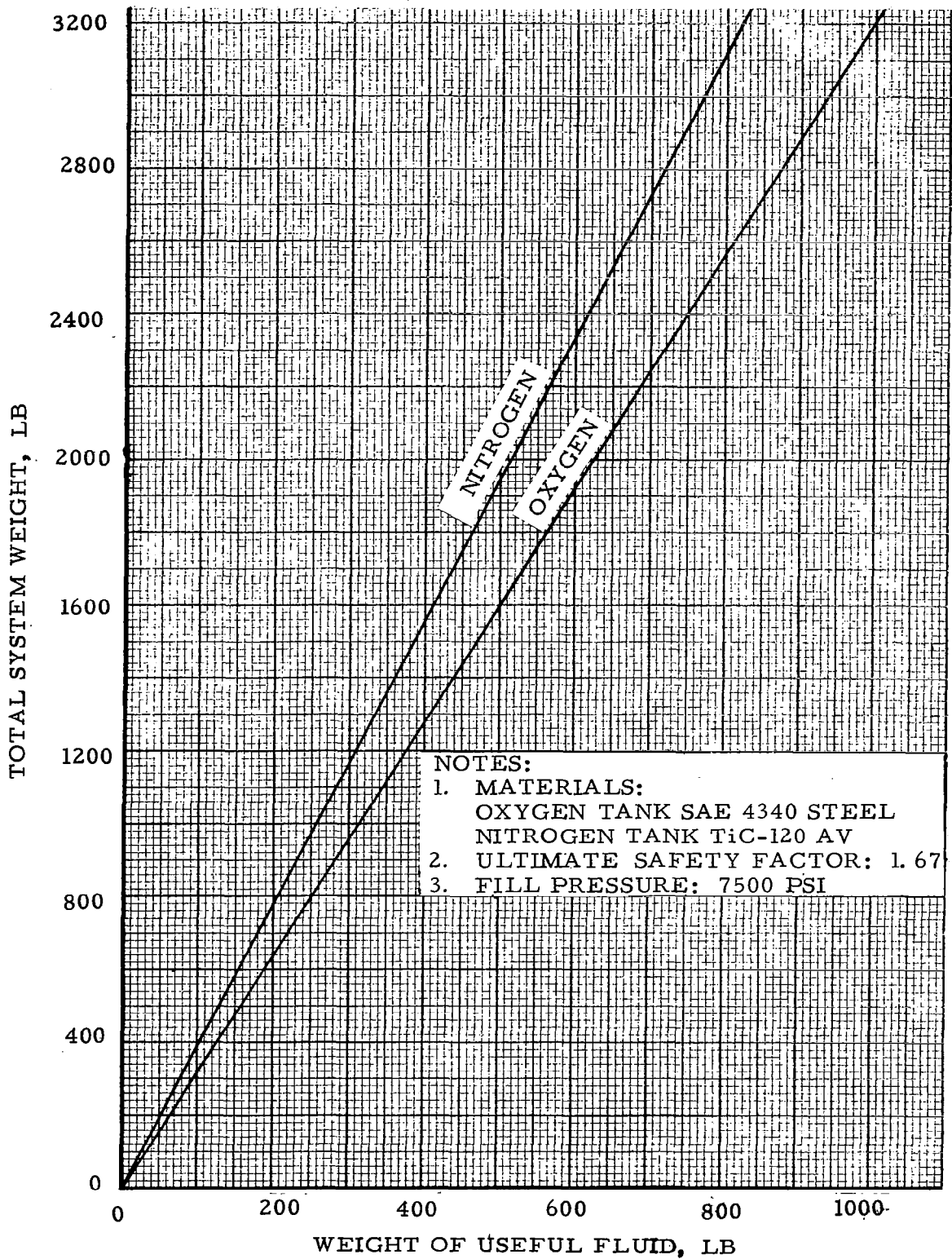


FIGURE 5-2 WEIGHT PENALTIES OF SPHERICAL HIGH-PRESSURE OXYGEN AND NITROGEN STORAGE SYSTEM

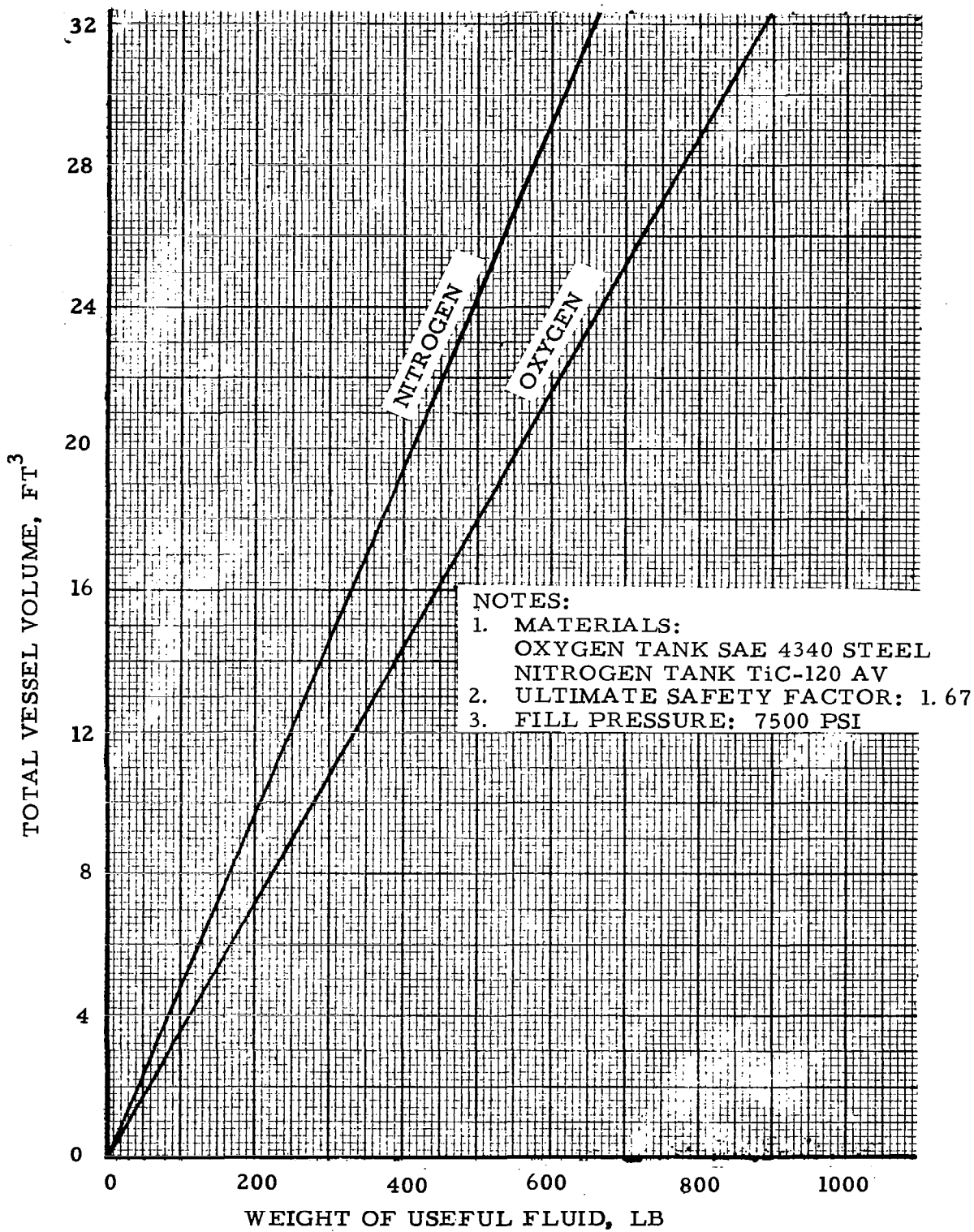


FIGURE 5-3 VOLUME PENALTIES OF SPHERICAL HIGH-PRESSURE OXYGEN AND NITROGEN TANKS

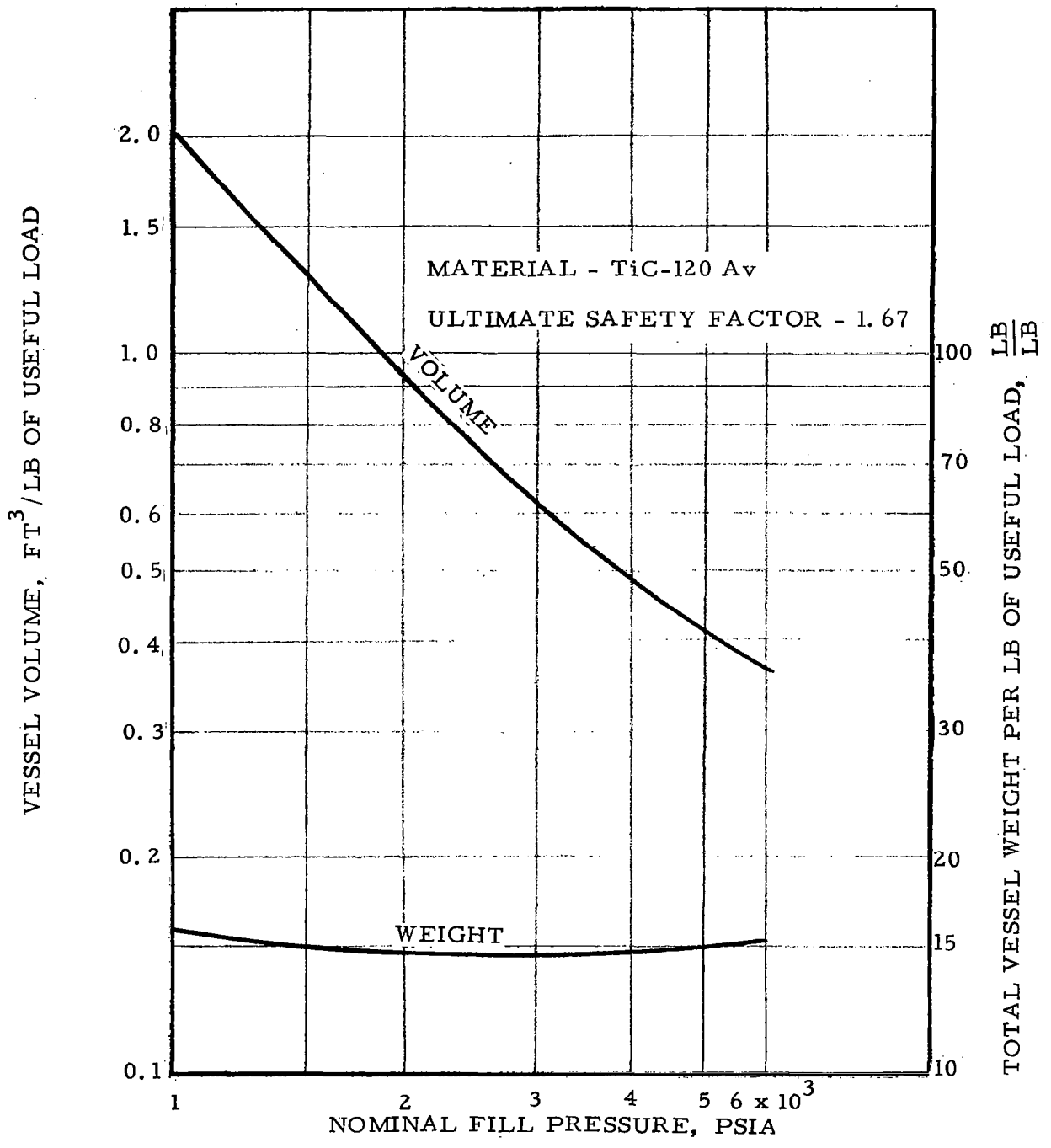


FIGURE 5-4 VOLUME AND WEIGHT PENALTIES OF SPHERICAL HIGH-PRESSURE HELIUM TANKS

TABLE 5-1  
 PROPERTIES OF CRYOGENIC FLUIDS AND SUPERCRITICAL  
 STORAGE VESSEL DESIGN DATA

	Oxygen	Nitrogen	Helium
Critical Pressure, psia	739	492	40.6
Critical Temperature, °R	278	227	9.36
Normal Boiling Point, °R	162.3	139.2	7.6
Heat of Vaporization, Btu/lb	91.6	85.2	8.84
Liquid Density, lb/cu ft	71.2	50.4	7.8
Design Pressure, psia	800	800	2 300
Maximum Pressure, psia	880	880	3 000
Inner Shell Material	Inconel 718	Ti-5Al-2.5 SnELI	Ti-5Al-2.5 SnELI
Type of Insulation	Super insulation	Super insulation	Super insulation plus vapor- cooled shields
Outer Shell Material	Al 6061- T6	Al 6061- T6	Al 6061-T6
Liquid Fraction at Fill	0.95	0.95	0.95
Vessel Shape	Spherical	Spherical	Spherical

$$q = w \left[ \rho \left( \frac{\partial h}{\partial \rho} \right)_p \right]$$

where  $w$  is fluid weight,  $\rho$  is density, and  $h$  is enthalpy, in consistent units. The vessel heat leak is selected to match a minimum heat input at minimum delivery rate. Tank insulation design is based on the minimum allowable vessel heat leak. Storage fluid acts as a compressed gas when the vessel is almost empty. In this state of operation, pressure may thus be allowed to fall, without incurring liquid separation. Heating requirements are usually relaxed during this last phase of delivery until a design cutoff temperature is reached. Delivery of fluid from the tank may be continued after the cutoff temperature is attained by the addition of more heating to the fluid. Both heating and temperature requirements increase rapidly when the vessel is almost empty.

Typical supercritical tanks are double-walled spherical vessels with layers of aluminized Mylar super insulation in the annular space between the two spheres. The annular space is also evacuated to a high vacuum, and compressed fiber glass pads separate the two spheres. Inconel 718 steel is used for oxygen tank inner shells, and a titanium alloy, such as Ti-5Al-2.5 SnELI, is used for nitrogen and helium tank inner shells (ref. 5-5). The titanium alloy is not compatible with oxygen under pressure. A number of one or more vapor-cooled shields, in which the fluid leaving the tank intercepts heat being transferred through the insulation, may also be used in addition to the super insulation. A typical supercritical cryogenic fluid storage system is shown schematically in figure 5-5 (ref. 5-6). The accessories shown in figure 5-5 have a total weight of approximately 14 lb. The weight and size of accessories is, in most instances, independent of the size of the storage vessel. However, this conclusion does not apply to such items as heat exchangers, the sizes of which are directly proportional to the amount of required heat transfer, and therefore, the required expulsion rate. Design data from computer runs and a brief description of each of the storage systems are given for oxygen, nitrogen, and helium supercritical storage.

Supercritical oxygen storage tanks are usually designed for a maximum pressure of approximately 880 psi, which is sufficiently above the oxygen critical pressure of 739 psi to ensure single-phase operation. A near-ambient design cutoff temperature of 500° to 510°R is usually used. Total system weight penalties per pound of useful fluid are given in figure 5-6 for representative oxygen use rates. Supercritical nitrogen tanks are considered to be designed for the same maximum pressure as oxygen tanks, although nitrogen has a much lower critical pressure. The high pressure of 880 psi permits an increased rate of delivery for emergency repressurization or fire extinguishing. A near ambient design cutoff temperature of 500° to 510°R is also used for nitrogen. Figure 5-7 shows the total weight penalties per pound of useful fluid for representative nitrogen use rates.

The major factor affecting the design of helium supercritical storage tanks is that a very low mass flow of fluid is normally required. The helium tankage weight penalty is principally determined on the basis of heat leakage to the tanks. Figure 5-8 shows representative tank heat leaks for O<sub>2</sub>, N<sub>2</sub> and helium (ref. 5-5). Helium supercritical tanks are operated at relatively high pressures due to heat leakage into the unit. There are two methods of fluid withdrawal from supercritical helium tanks: (1) fluid is discharged at constant pressure, and (2) operating pressure is allowed to rise during low flow periods and dropped to a minimum when a high mass flow is required. Figure 5-9 presents the weight penalty incurred by supercritical helium tanks for a number of typical flow rates. It should be noted that the weights given are only for the basic tank and fluid, and do not include accessory structures, heater power, and instrumentation. Tank insulation included the use of a number of vapor-cooled shields.

## SUBCRITICAL STORAGE

Subcritical storage of atmospheric constituents at cryogenic temperatures offers all of the advantages cited above for supercritical storage. In addition, subcritical storage offers further weight savings due to low-pressure

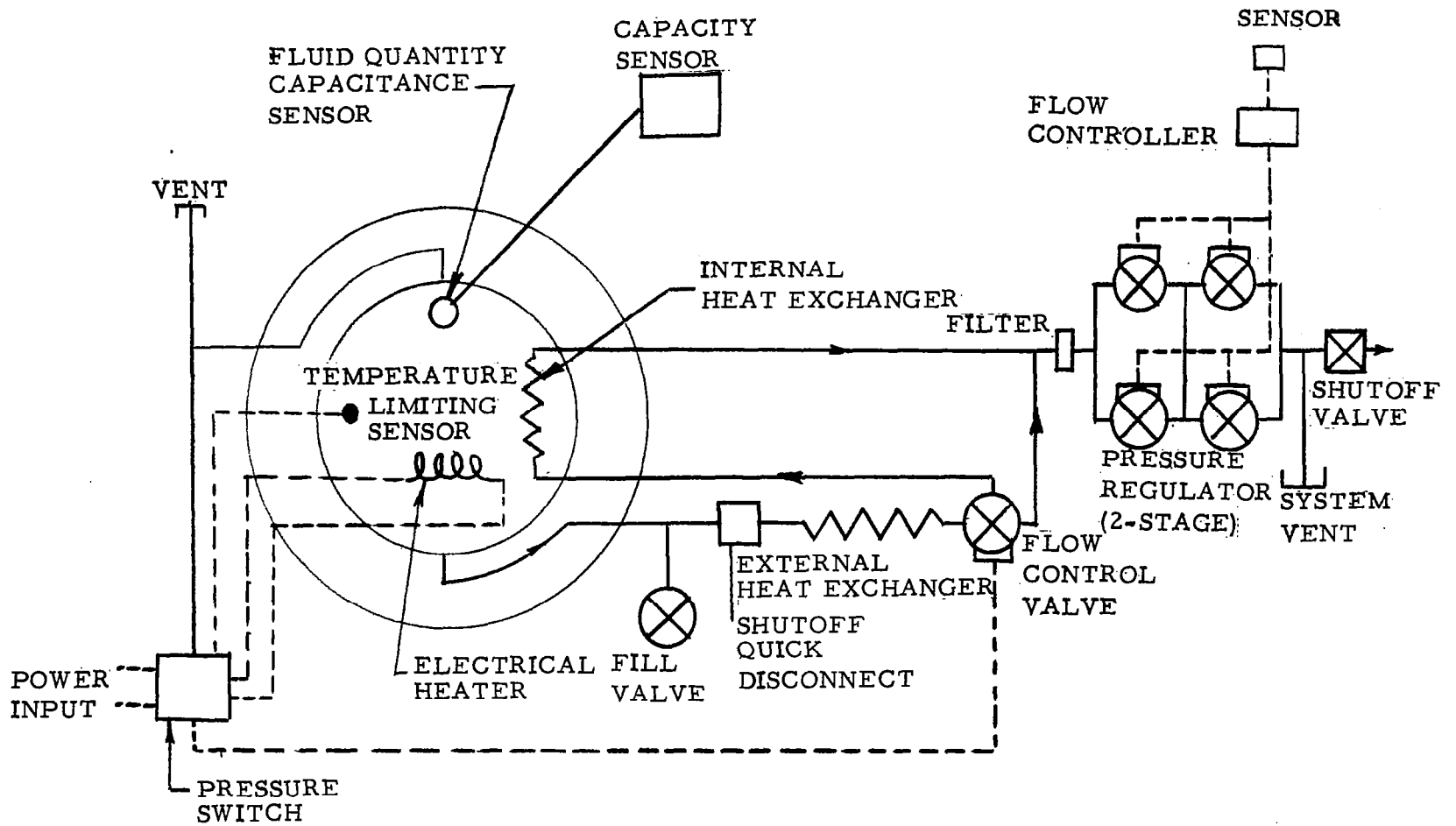


FIGURE 5-5 SUPERCRITICAL CRYOGENIC FLUID STORAGE

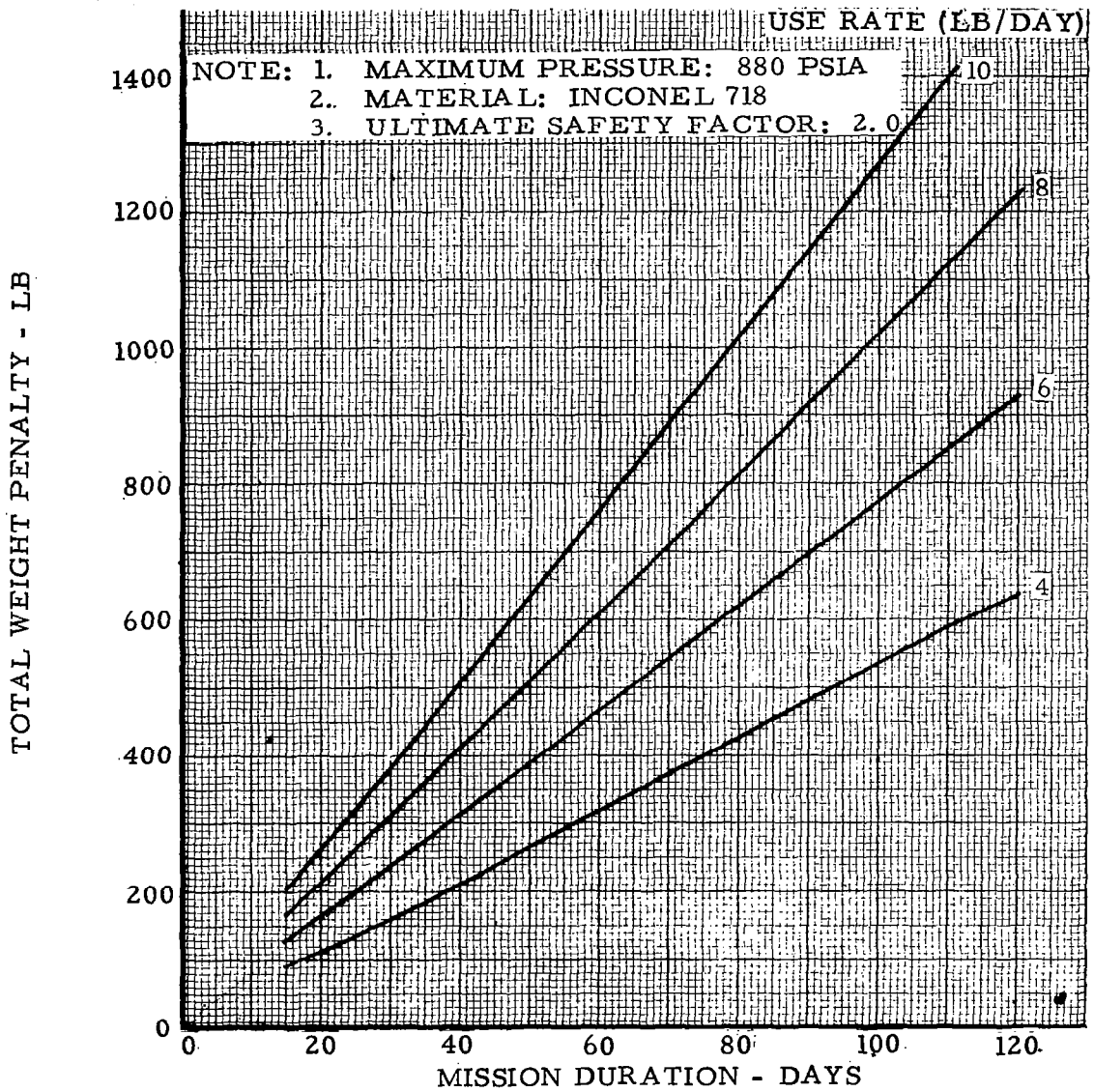


FIGURE 5-6 SUPERCritical OXYGEN STORAGE PENALTY

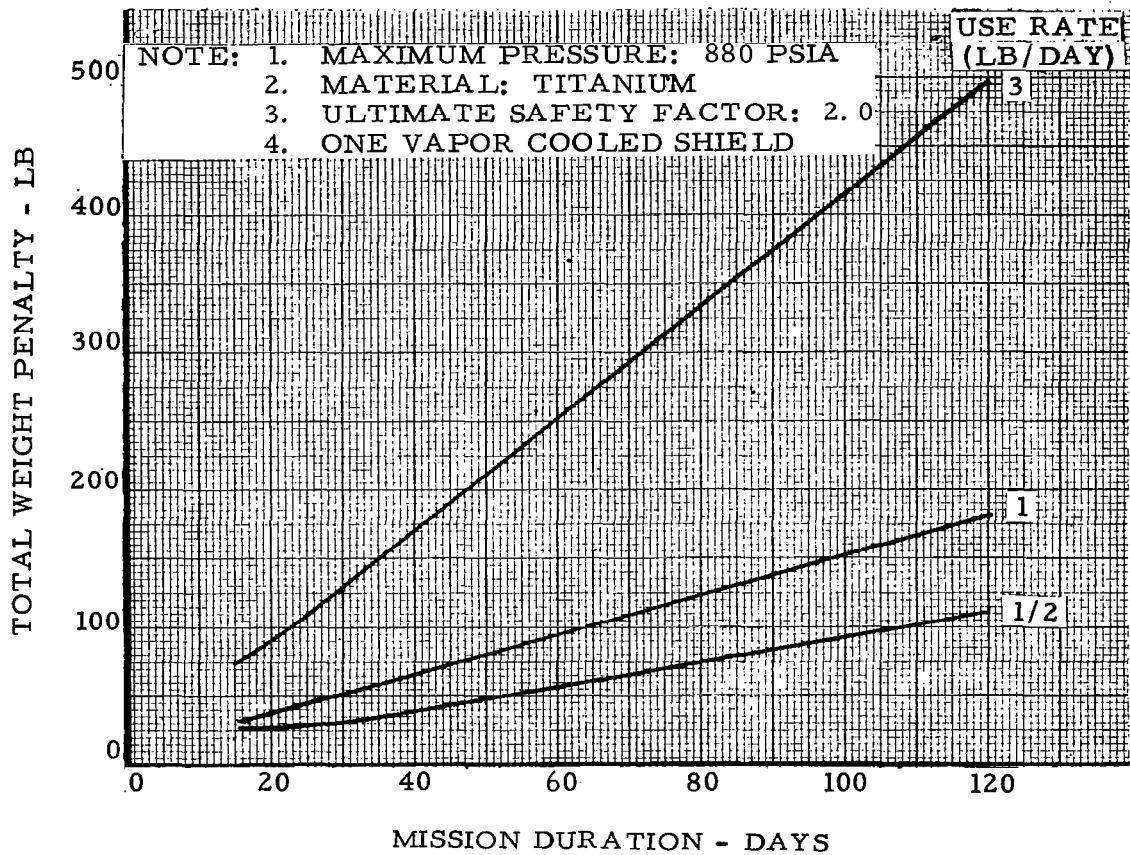


FIGURE 5-7 SUPERCRITICAL NITROGEN STORAGE PENALTY

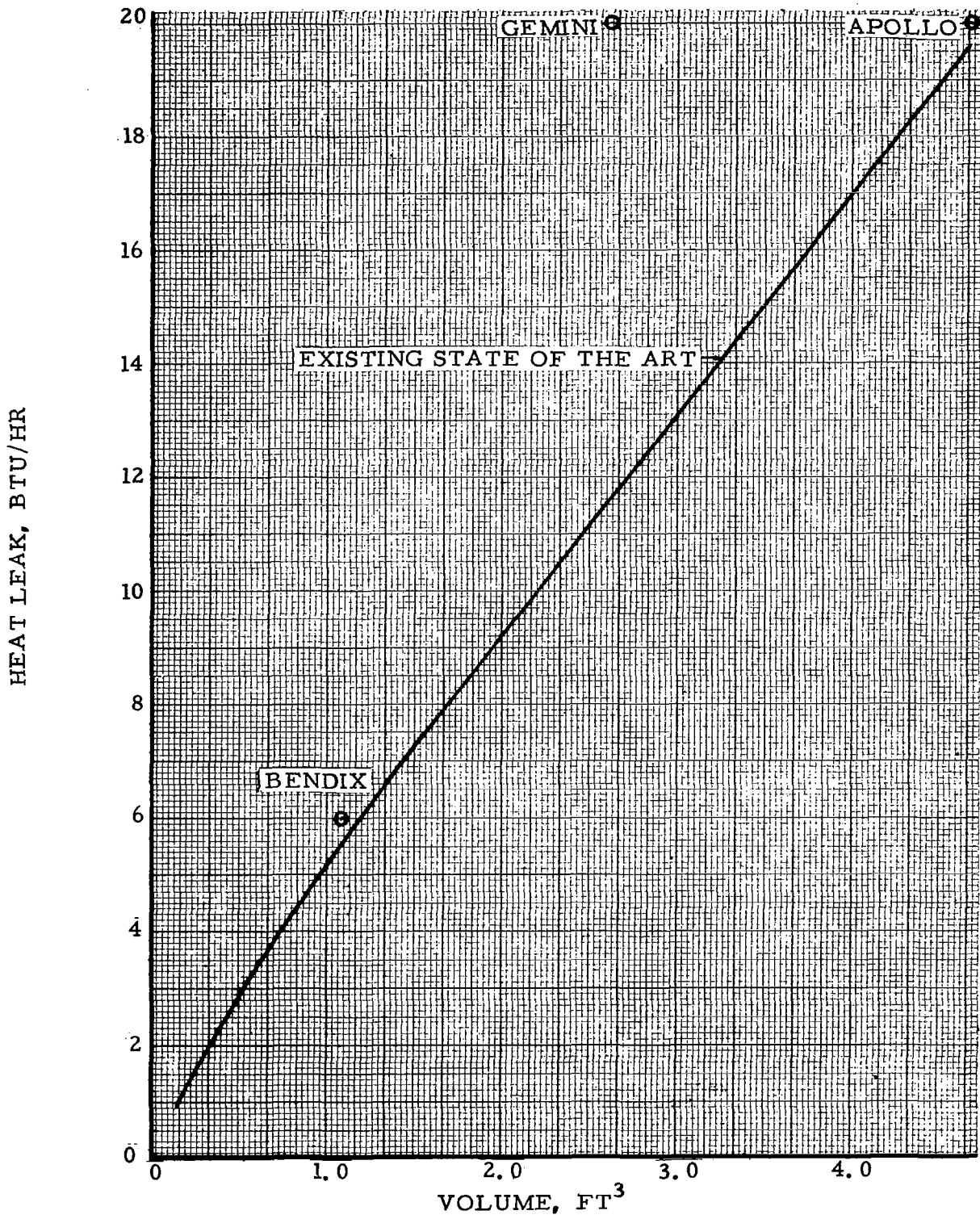


FIGURE 5-8 ESTIMATED HEAT LEAKS FOR SUPERCRITICAL TANKS

USE RATE	3	1	1/2	1/10	1/20
NUMBER OF VAPOR COOLED SHIELDS	0	1	1	1	2

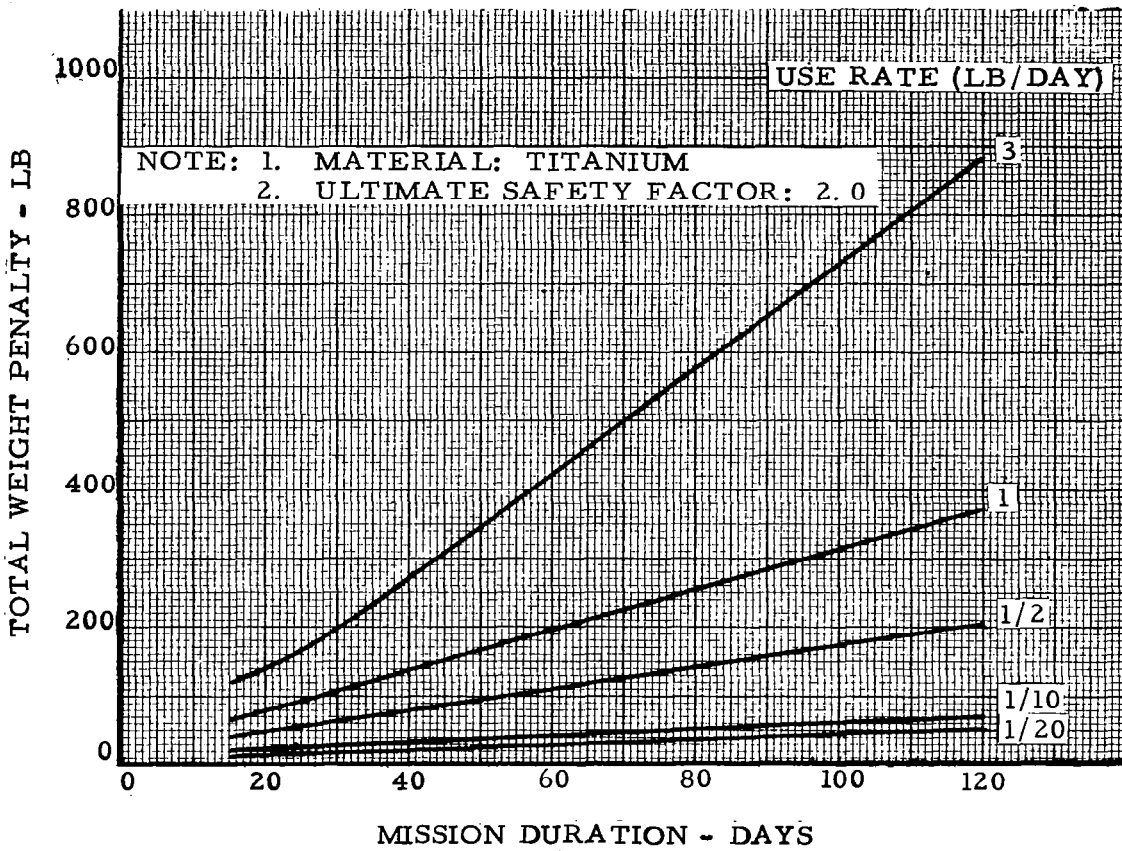


FIGURE 5-9 SUPERCRITICAL HELIUM STORAGE PENALTY

operation. Two methods of fluid expulsion from subcritical cryogenic tanks have been considered. Early prototypes were built in which the fluid was contained in a bladder and expelled by pressurizing with a gas. This approach has been discarded because of the low reliability of the bladders at cryogenic temperatures. The second method of expulsion used in current designs, uses thermally pressurized vessels, as in the supercritical design.

Delivery of a single-phase fluid under zero-g conditions is the major problem encountered in subcritical storage. Successful tests have been conducted with a configuration that uses an internal heat exchanger located within the inner shell of the tank. Fluid is circulated through the heat exchanger after throttling and is heated by the mass of the stored fluid to ensure vapor delivery. Figure 5-10 illustrates the fluid withdrawal process used on a pressure-enthalpy diagram for one promising method of tank-heat addition. Pre-use pressurization is similar to the process described for supercritical storage. In the absence of gravity, the mass sampled at any point in the tank may consist of liquid and vapor in any proportion. Sampling state may thus range from point 2 to point 2' on figure 5-10. Fluid to be delivered is first passed through a valve and throttled to a pressure lower than the tank pressure. However, during the throttling process, the fluid temperature falls below the storage temperature. Passage of the vent fluid through a heat exchanger, within the storage tank, transfers energy along paths 3 to 4 of 3' to 4 at nearly constant pressures. The fluid is evaporated and superheated slightly before being discharged at a temperature close to that of the stored fluid, but at a lower pressure. Tank heat addition for pressurization is similar to that for supercritical storage. The delivered fluid is heated to ambient temperature. Fluid quantity measurement is possible by use of several techniques including a matrix-type capacitance gage. The described design can provide automatic phase separation during venting for gas delivery under zero-g conditions. Tankage must be designed to minimize heat leaks into the cryogenic fluid during storage, and to be compatible with the design gas use rate.

Weight penalty of subcritical oxygen and nitrogen storage tanks are presented in figures 5-11 and 5-12, for a number of typical use rates. An aluminum tank inner shell was used for oxygen and a titanium inner shell was used for nitrogen. A maximum design pressure of 150 psi was considered for both fluids.

## CONCLUSIONS AND RECOMMENDATIONS

High-pressure gas storage systems are in the most advanced state of development and are most reliable. However, high-pressure gas storage has a prohibitive weight and volume penalty for most spacecraft applications. High-pressure gas storage has major applications in backup, short-time, emergency usage and for providing relatively low total quantities of gas. A two-gas atmospheric supply system which uses helium as a diluent, may use high pressure storage of the helium because of the high penalty for supercritical storage of helium. The potential weight increase of high pressure

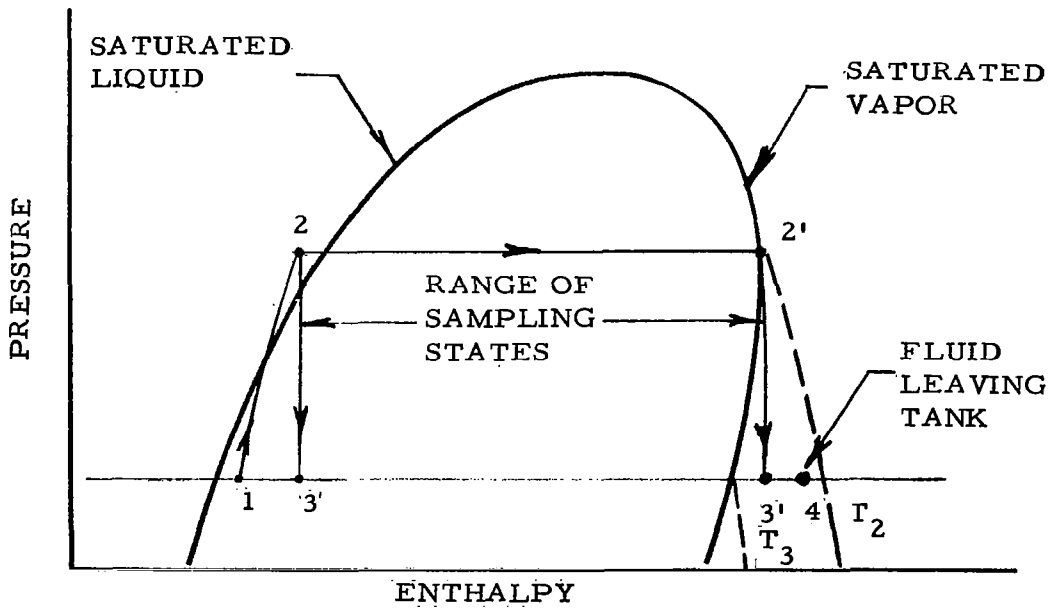
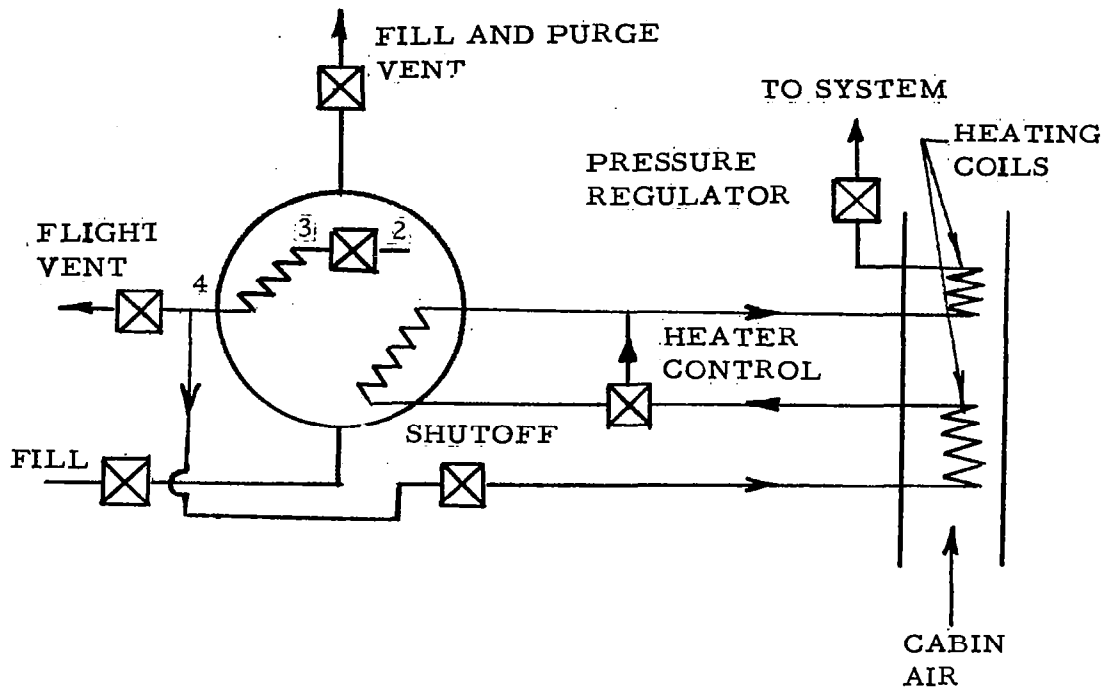


FIGURE 5-10 TWO-PHASE STORAGE WITH VAPOR DELIVERY

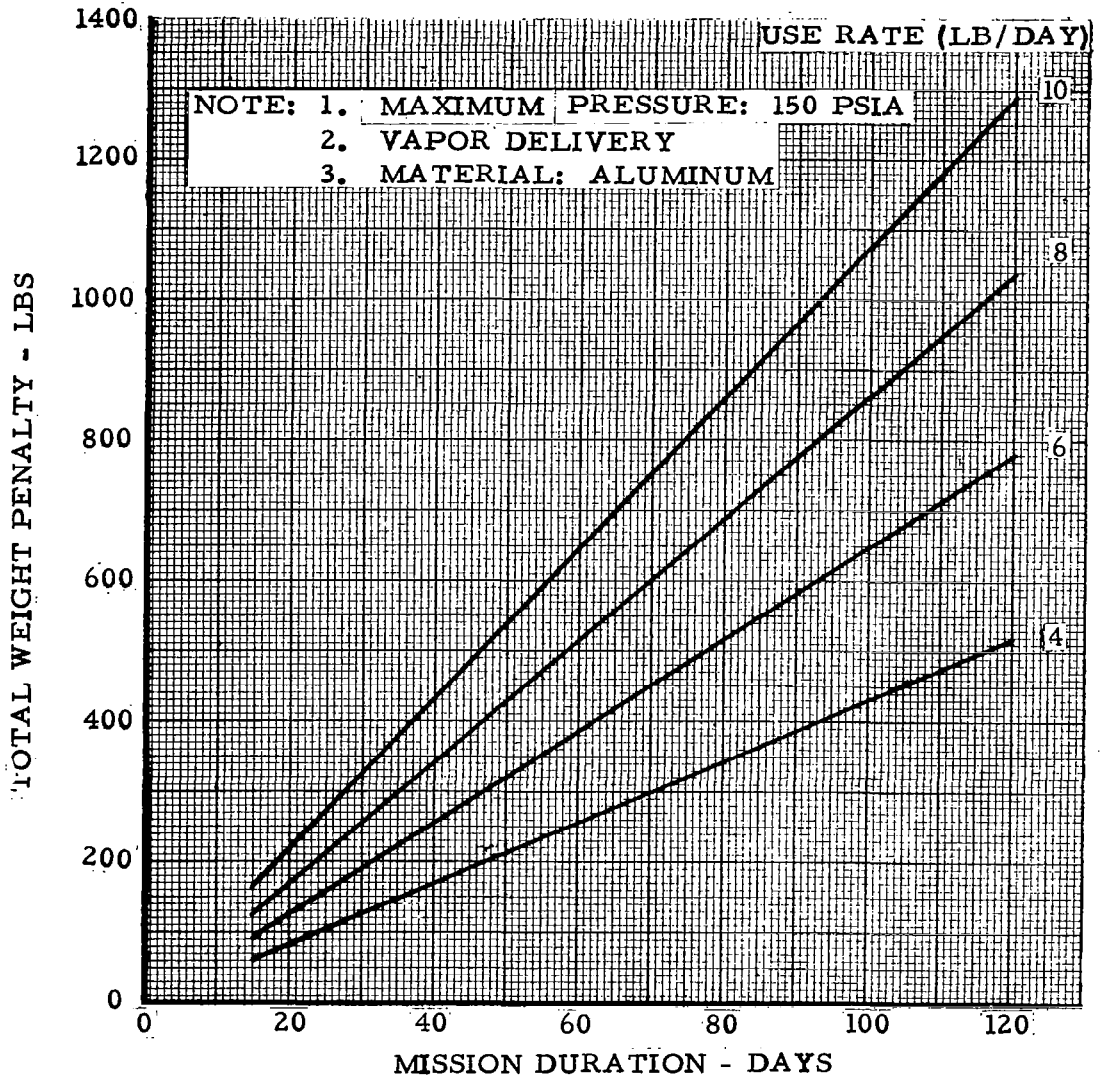


FIGURE 5-II SUBCRITICAL OXYGEN STORAGE PENALTY

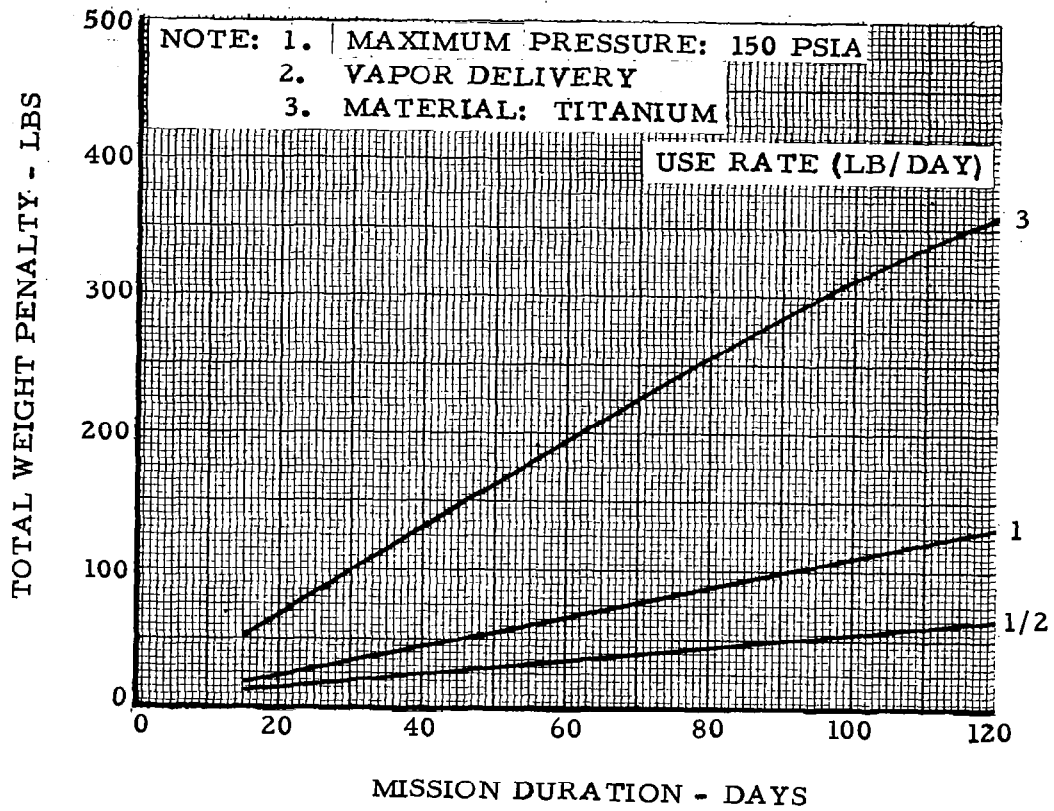


FIGURE 5-12 SUBCRITICAL NITROGEN STORAGE PENALTY



The gas and tankage weights for a 90 day period are given below. Storage penalties are obtained from the figures in this section with minimum use rates based on metabolic and leakage requirements. The breakdown of the constituent atmospheric gas requirements for the 90-day mission is as follows:

	Gas Weight (lb)	
	N <sub>2</sub> -O <sub>2</sub>	He-O <sub>2</sub>
Metabolic oxygen	556.0	556.0
Oxygen leakage loss	96.0	96.3
Diluent leakage loss	84.0	12.0
Oxygen for cabin repressurization	106.0	106.0
Diluent for cabin repressurization	92.0	13.3
Oxygen lost in airlock operation	8.87	10.6
Diluent lost in airlock operation	7.74	1.34

The breakdown of the stored gas and tankage weight requirements for the above conditions is as follows.

	Storage and Gas Weights (lb)
Total oxygen requirements for N <sub>2</sub> -O <sub>2</sub> atmosphere	766.8
Oxygen tank--supercritical storage	200.0 (figure 5-6 with 7.25 lb/day use rate)
Oxygen tank--subcritical storage	61.3 (figure 5-11 with 7.25 lb/day use rate)
Total oxygen requirements for He-O <sub>2</sub> atmosphere	768.9
Oxygen tank--supercritical storage	200.0 (figure 5-6 with 7.25 lb/day use rate)
Oxygen tank--subcritical storage	61.4 (figure 5-11 with 7.25 lb/day use rate)

Total nitrogen requirement	183.7
Nitrogen tank--supercritical storage	96.4 (figure 5-7 with 0.94 lb/day use rate)
Nitrogen tank--subcritical storage	18.4 (figure 5-12 with 0.94 lb/day use rate)
Total helium requirement	26.64
Helium tank--supercritical	132.00 (figure 5-9 with 0.13 lb/day use rate)
Helium tank--high pressure gas	400.00 (figure 5-4 at 5000 psia)

The above data have been used to compare weights of the helium-oxygen and nitrogen-oxygen atmospheres with different combinations of storage techniques. The resulting system weight penalties are as follows.

	System Weight (lb)
Supercritical nitrogen/supercritical oxygen system	1247
High pressure helium/supercritical oxygen system	1396
Supercritical helium/supercritical oxygen system	1128
Supercritical He/subcritical O <sub>2</sub> system (still in development)	989
Subcritical N <sub>2</sub> /subcritical O <sub>2</sub> system (still in development)	1030

The above comparisons show the relative system weight savings with the more advanced concepts such as subcritical oxygen and supercritical helium storage methods. Supercritical storage is currently the most probable choice for long duration missions because additional development is required for subcritical storage. Supercritical storage for both helium and oxygen represents a saving of 290 lb, or approximately 20%, over a comparable system with high-pressure helium and supercritical oxygen for the typical spacecraft example. The supercritical helium-oxygen system is 119 lb lighter than the corresponding nitrogen-oxygen system.

## REFERENCES

- 5-1. Analytical Methods for Space Vehicle Atmospheric Control Processes, Report No. ASD-TR-61-162 - Part II, November 1962.
- 5-2. Stewart, R. B.; Hart, I. G.; and McCarty, R. D., Interim Thermodynamic Properties for Gaseous and Liquid Oxygen at Temperatures from 55°K to 300°K and Pressures to 300 Atmosphere, N.B.S. Report 7922, October 1, 1963.
- 5-3. Strobridge, T.R.; The Thermodynamic Properties of Nitrogen from 114 to 540°R, Between 1 and 3000 psia; N.B.S. Technical Note 129, Feb., 1963.
- 5-4. Mann, D. B.; The Thermodynamic Properties of Helium from 6 to 540°R, Between 10 and 1500 psia, N.B.S. Technical Note 154A, Jan. 1962.
- 5-5. Roth, E. M.: Space Cabin Atmospheres, Part IV, Engineering Trade-Offs of One versus Two Gas Systems, Lovelace Foundation for Medical Education and Research, NASA Contract NASr-115, 15 March 1966.
- 5-6. Atmospheric Control Systems for Space Vehicles, ASD-TDR-62-527, March 1963.



## Section 6

### THE EFFECT OF ATMOSPHERE SELECTION ON COMPONENT HEAT AND MASS TRANSFER

A number of key components in space environmental control systems rely on heat and mass transfer processes for operation. Examples of such components are heat exchangers, gas to liquid condensers, and adsorption beds. Cabin atmospheric gas is used to reject the cabin heat load and, in some cases, a portion of this gas is processed to remove carbon dioxide and small amounts of water vapor. Since heat and mass transfer rates together with pressure drops depend, to some extent, upon the physical properties of the process gas, the performance and size of the Environmental Control System (ECS) components can be affected by atmospheric composition. Therefore, tests were conducted on typical spacecraft components that were considered to be influenced the most by cabin atmosphere. Test atmospheres consisted of helium-oxygen ( $\text{He-O}_2$ ) and nitrogen-oxygen ( $\text{N}_2\text{-O}_2$ ) mixtures at 5, 7, and 10 psia total pressure, pure oxygen at 5 psia, and air at 14.7 psia. The mixed gas atmospheres were composed of 3.5 psia oxygen with the balance consisting of a nitrogen or helium diluent. Transient mass transfer tests were conducted for carbon dioxide adsorption on molecular sieve and water vapor adsorption on silica gel. Adiabatic bed designs were used in both cases. Steady-state heat transfer tests were run on a typical space type heat exchanger and transient heat transfer tests were performed with the molecular sieve and silica gel adsorption beds. Pressure drop data were obtained for both adsorption beds and the heat exchanger.

Results of the tests indicate that the weights of heat exchangers and adsorption beds may be slightly greater for  $\text{He-O}_2$  atmospheres than  $\text{N}_2\text{-O}_2$  atmospheres. However, fan power is generally lower. The total weight penalty, which includes the heat exchanger or adsorption bed weight and a weight penalty for fan power, depends on the particular system design criteria and vehicle power system used. For example, the sample problem chosen assumed that a heat exchanger for a three-man system using a 7 psia  $\text{N}_2\text{-O}_2$  atmosphere weighed 10 lb, required 15W of fan power, and was accessed a power penalty of 0.503 lb/W. As shown in a sample problem, when designed for a  $\text{He-O}_2$  atmosphere at equivalent heat loads and temperatures, a reduction of 1.5 lb in system weight, including power penalty, is obtained. For adsorption beds, based on a three-man system, adiabatic bed designs, and the above power penalty, the total weight penalties generally differed less than 5% between  $\text{He-O}_2$  and  $\text{N}_2\text{-O}_2$  atmospheres. In general, as indicated in section 7, the heat exchanger and adsorption bed weight savings incurred by changing atmospheres are small compared to the total system weight penalty. A more significant penalty decrease is realized, as indicated in section 2, by using a  $\text{He-O}_2$  mixture which permits a higher allowable cabin temperature level than a  $\text{N}_2\text{-O}_2$  mixture at equivalent cabin pressure. Sec. 7 presents tradeoff data considering this point.

In the evaluation of the experimental data, it was found that the application of the standard Colburn moduli for heat and mass transfer did not result in satisfactory data correlation. Additional terms had to be applied to the heat exchanger heat transfer data to account for the low Prandtl numbers of the He-O<sub>2</sub> mixtures. The heat exchanger pressure drop data also required a correction factor which incorporated the Prandtl number. The adsorption bed test data appeared to lie in a transitional flow region and the Colburn moduli did not provide satisfactory correlations. However, the adsorption bed heat transfer data were correlated by plotting Nusselt number/Prandtl number versus Reynolds number and the mass transfer data were correlated by plotting Sherwood number/Schmidt number versus Reynolds number. Also a relationship between heat and mass transfer was obtained for the test data. The adsorption bed pressure drop data were successfully correlated in two different manners, both of which agree well with published data.

In the following discussion, the standard correlation techniques are presented and the anticipated performance differences are noted between atmospheres. Testing procedure is discussed and the test data is shown in correlated form. Finally, typical penalties for applicable ECS equipment are given, based on the correlated test data.

## HEAT EXCHANGER AND CONDENSER EVALUATION

### Heat Exchanger Theory

An atmosphere comparison study must include the effects of atmospheric composition on heat exchanger and condenser performance. Most current vehicles rely on some active thermal control using a heat exchanger. The most practical method of humidity control is by condensing moisture in a condensing-type heat exchanger. In both applications, cabin atmosphere is cooled by a cold liquid in a compact heat exchanger. Efficiency of the cooling process is largely dependent upon the physical properties of the atmosphere, i. e., thermal conductivity, viscosity, and molecular weight. Because the unusually high thermal conductivity and specific heat, as well as low molecular weight of helium gas, He-O<sub>2</sub> mixtures have physical properties considerably different from N<sub>2</sub>-O<sub>2</sub>.

It should be emphasized at this point that a truly rigorous comparison of atmospheres must compare the weights of optimum heat exchangers, which takes into account fluid pumping power as well as heat exchanger weight. This will be done in section 7. In the following paragraphs, the general theory for heat exchangers will be developed and approximate weight comparisons will be made. Weight comparisons are particularly useful to discern the major influencing parameters. The amount of sensible heat that is transferred in the heat exchanger is given by the following equation

$$\dot{q} = UA \Delta T_M \quad (6-1)$$

In turn, UA is related to the heat exchanger area, fin effectiveness, and heat transfer coefficients by the following expression:

$$UA = \frac{(\eta_o hA)_g}{1 + \frac{(\eta_o hA)_g}{(\eta_o hA)_l}} \quad (6-2)$$

For liquid to gas heat exchangers, the liquid side conductance  $(\eta_o hA)_l$ , is large compared to the gas side conductance. Using this result, eq. (6-2) can be simplified as follows:

$$UA \cong (\eta_o hA)_g \cong \frac{\dot{q}}{\Delta T_M} \quad (6-3)$$

Heat transferred in the heat exchanger can be obtained by calculating the change in fluid heat content through the unit:

$$\dot{q} = \dot{w}_l C_{p,l} (T_{l,o} - T_{l,i}) = \dot{w}_g C_{p,g} (T_{g,i} - T_{g,o}) \quad (6-4)$$

Mean temperature can be accounted for by using the NTU method (number of transfer units) described in ref. 6-1. The NTU can be written for either heat exchanger fluid and is written below for the gas:

$$NTU_g = \frac{\Delta T_g}{\Delta T_M} \quad (6-5)$$

Eq. (6-5) can be used with eq. (6-3) to obtain the heat exchanger required UA. The number of transfer units is a function of the thermal capacity ratio of the fluids and temperature effectiveness. These two parameters are written as follows:

$$Z_g = \frac{\dot{w}_g C_{p,g}}{\dot{w}_l C_{p,l}} \quad (6-6)$$

$$E_g = \frac{T_{g,i} - T_{g,o}}{T_{g,i} - T_{l,i}} \quad (6-7)$$

Ref. 6-1 gives NTU as a function of thermal capacity ratio and temperature effectiveness. For multiple-pass exchangers a relationship can be used to

find effectiveness per pass. The NTU is found for each pass and the total NTU is obtained simply by multiplying single-pass NTU by the number of passes. The expression is as follows:

$$\frac{E_g}{\text{pass}} = \frac{\left(\frac{1 - Z_g E_g}{1 - E_g}\right)^{1/n} - 1}{\left(\frac{1 - Z_g E_g}{1 - E_g}\right)^{1/n} - Z_g} \quad (6-8)$$

Once the mean temperature difference and heat transfer rate is known, eq. (6-1) is used to calculate the required UA, which is basically a measure of heat exchanger size. An approximate heat exchanger size can be obtained by assuming that heat exchanger weight is proportional to UA. The proportionality factor depends on the type of heat exchanger, but a good factor for space-type equipment is 25 Btu/hr-°F-lb. After the required UA has been determined, the performance of actual heat exchanger surfaces is used to find a heat exchanger design that yields the required UA. This design, for the most part, is a trial-and-error process, which can be done manually or by using a computer. Basic fin designs are arranged into a core geometry and fin performance curves are used to calculate available UA. Core geometry is established, based on envelope considerations, or the heat exchanger may be optimized, taking fluid pumping power into consideration.

Heat exchanger fin performance is normally correlated in the form of the Colburn modulus or j factor. The j factor [eq. (6-10)] may be obtained by rearranging the basic equation of forced convection heat transfer [eq. (6-9)], as follows:

$$Nu_D = C_3 Re_D^n Pr^{1/3} \quad (6-9)$$

$$j = \frac{Nu_D}{Pr Re_D} Pr^{2/3} = \frac{h}{GC_p} Pr^{2/3} = C_3 Re_D^{n-1} \quad (6-10)$$

The factors  $C_3$  and  $n$  are functions of fin geometry and Reynolds number. The j factor may be conveniently plotted with Reynolds number on logarithmic paper to obtain a nearly linear relationship. Eq. (6-10) may be used along with core geometry, gas properties, and j curves to calculate the average film coefficient (h) for each heat exchanger fluid.

Fin effectiveness is a function of film coefficient and properties of the fin. The equation for fin effectiveness is as follows:

$$\eta_f = \frac{\tanh ml}{ml} \quad (6-11)$$

where

$$m = \sqrt{\frac{2h}{kt_f}}$$

Because of the general form of the equation for UA, it is convenient to establish fin effectiveness in terms of overall fluid passage area, as follows:

$$\eta_o = 1 - \frac{A_f}{A} (1 - \eta_f) \quad (6-12)$$

Eqs. (6-10) and (6-12) are used with heat exchanger area for each fluid side to calculate UA, as given in eq. (6-2). If the calculated UA matches the required UA per eq. (6-3), the heat exchanger has adequate capacity.

#### Heat Exchanger Pressure Drop

Because of the relatively large pumping power penalties, heat exchanger pressure drop characteristics are of prime concern. Pumping power characteristics are a major influencing factor in system tradeoff. The heat exchanger optimization trades off power penalty and heat exchanger weight. Other tradeoff studies involving heat exchanger pressure loss include manifold design and number of passes for the heat exchanger. Pressure drop in the heat exchanger is primarily a function of gas density, flow rate, viscosity, and heat exchanger geometry. A number of pressure losses occur in the heat exchanger because of entrance effects, exit effects, and frictional losses in the core. The basic equation for heat exchanger pressure loss is as follows:

$$\Delta P = \frac{G_s^2}{2g} \left[ \left( 1 - K_i - \delta^2 \right) \frac{1}{\rho_i} + \left( \frac{1}{\rho_o} - \frac{1}{\rho_i} \right) + \frac{4fL}{r} \left( \frac{\rho_i + \rho_o}{2\rho_i \rho_o} \right) - \left( 1 - K_e - \delta^2 \right) \frac{1}{\rho_o} \right] \quad (6-13)$$

The friction factor ( $f$ ) is theoretically a function only of Reynolds number and core geometry. Heat exchanger friction loss is conveniently correlated by plotting friction factor  $f$  as a function of Reynolds number on logarithmic paper. Losses for manifolds are accounted for separately in the same manner as duct losses.

## Heat Exchanger Test Description

Test data were obtained for a space type heat exchanger, using the Douglas Generalized Equipment Performance Test Facility (GEPTF). The heat exchanger tested was a plate-fin unit constructed of aluminum. Flow arrangement was cross counter-flow with one pass on the gas side and four passes on the liquid side. The liquid fin was an offset rectangular fin; a wavy fin was used on the gas side. Water at a high flow rate was circulated on the liquid side so that the gas side conductance was controlling heat exchanger performance. Temperature measurements were taken with thermocouples and recorded. Gas flow rates were measured with standard ASME orifice plates and coolant flow was measured with a rotometer. Liquid side flow was maintained constant for all tests so that differences in gas side conductances would be more discernable. Approximately 10 different flow rates were obtained for each of the eight candidate atmospheres.

## Heat Exchanger Correlation Data

Heat transfer test data were reduced by using equations listed in the foregoing theory and core information supplied from the heat exchanger manufacturer. When the Colburn modulus was plotted as a function of Reynolds number, a good correlation did not result. After attempting a number of corrections for Prandtl number, the correction given by the following equation showed good correlation (the result is shown in fig. 6-1):

$$j' = \frac{Nu}{Pr Re} \left[ 1 - 8.35 Re^{-0.479} (Pr - 1) \right] = C_1 Re^{C_2} \quad (6-14)$$

where  $C_1$  and  $C_2$  are constants to be determined.

This correlation was obtained by first plotting the conventional  $j$  factor on logarithmic paper for He mixtures and for  $N_2$  mixtures. The two curves were rotated and shifted analytically until the two curves coincided. The expression of the result is as follows:

$$j' = 0.079 Re^{-0.345} \quad (6-15)$$

This expression differs somewhat from the theoretical eq. (6-10). The form of eq. (6-15) is similar (in general form) to the equation for turbulent flow (ref. 6-2). This is not too surprising because of the general nature of the gas flow path in the test unit. The wavy flow path would be more likely to produce local separation at certain points and very thin boundary layers would result, as in turbulent flow. Based on the results and analysis of

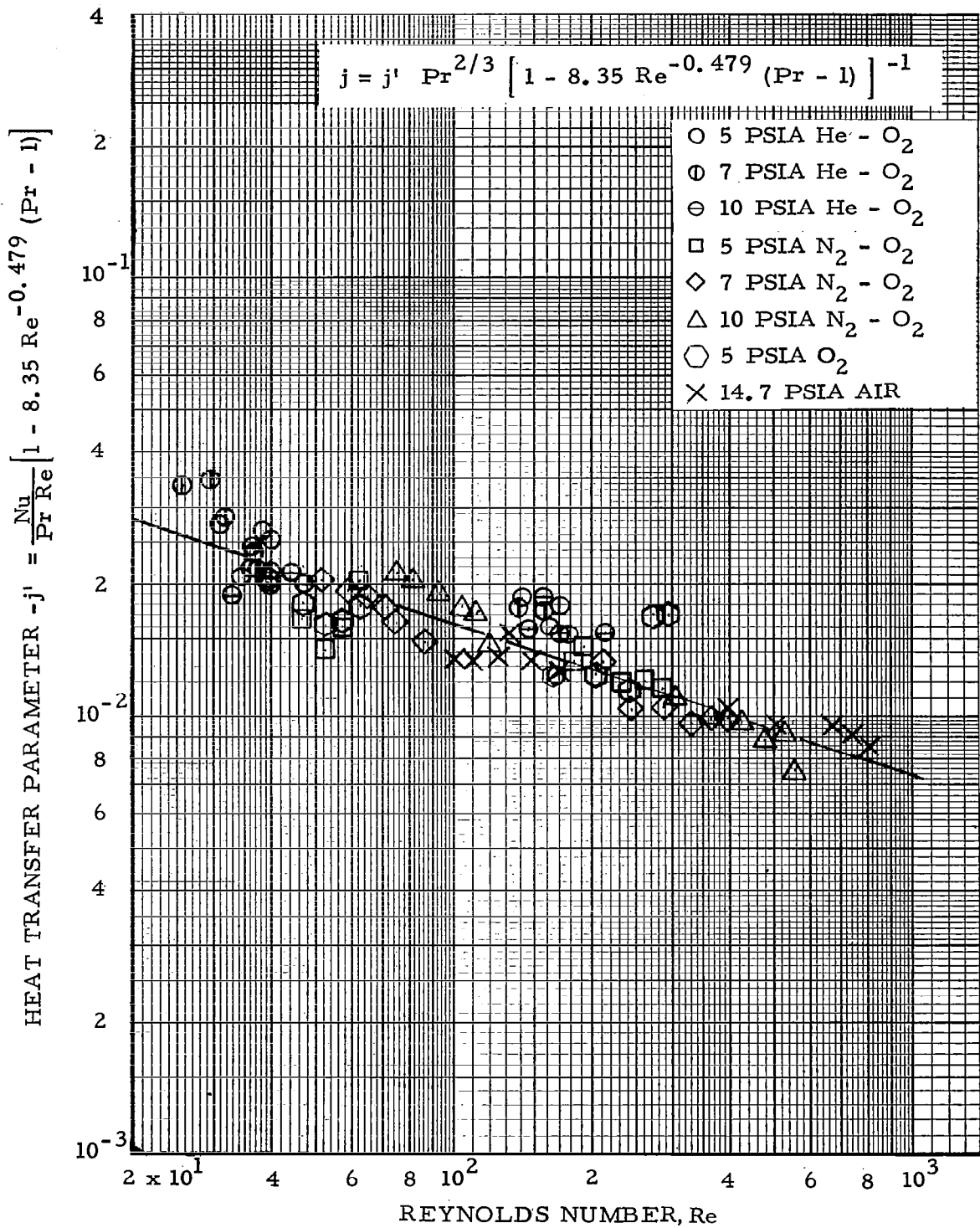


FIGURE 6-1 CORRELATED HEAT TRANSFER DATA FOR HEAT EXCHANGER

heat exchanger data, the following expression gives the Prandtl number correction to the standard Colburn modulus:

$$j' = \frac{j}{Pr^{2/3}} \left[ 1 - 8.35 Re^{-0.479} (Pr - 1) \right] \quad (6-16)$$

Friction factor correlation was not as good as heat transfer data. However, a correction for Prandtl number improved the correlation. The correlated friction factor is given in fig. 6-2. In a manner similar to that used above, the following expression for friction factor resulted:

$$f' = \left[ 13.9 (1 - Pr) - 1 \right] = 115 Re^{-0.745} \quad (6-17)$$

As in the case of heat transfer, a Prandtl number correction was needed to correlate He-O<sub>2</sub> data with the N<sub>2</sub>-O<sub>2</sub> data. Based on the friction loss data, eq. (6-17) may be used to correct conventional friction factor data to account for Prandtl number effects.

#### Heat Exchanger Penalty Comparison

It is of interest to compare the heat exchanger penalty for a typical application to investigate general penalty trends and determine which parameters have a major influence. A number of restrictions may be used for heat exchanger design and the set of restrictions used has a major influence on the resulting weight penalty. From a strict weight tradeoff, heat exchanger weight is traded off with the fluid pumping power penalty. In most cases where this is done, an unrealistic geometry results. Such optimizations, typically result in geometric shapes that could not possibly be packaged effectively in the space vehicle. In general, the heat exchanger must be nearly cubical with no one dimension greater than twice or three times that of any other. Therefore, for the purpose of calculating typical penalties, the heat exchanger will be designed so that the basic shape of the unit is retained.

For comparison of heat exchanger penalties, consider the case where overall fluid temperatures and amount of heat transfer remain constant so that the UA remains fixed. The only fluid property that is allowed to vary is the gas side flow rate and this is varied to result in a constant heat capacity on the gas side.

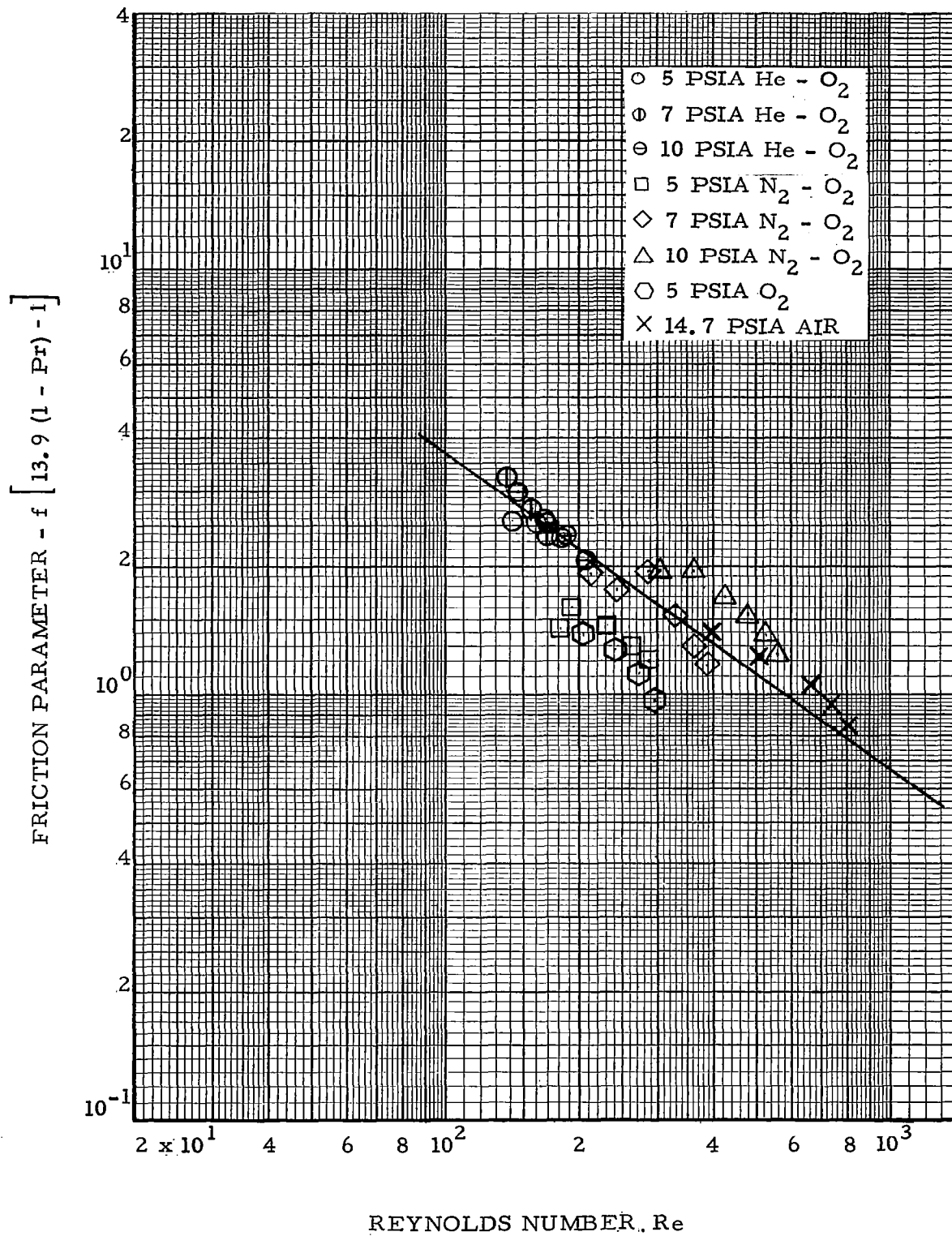


FIGURE 6-2 CORRELATED FRICTION DATA FOR HEAT EXCHANGER

It was shown earlier [eq. (6-3)] that the overall UA is nearly equal to gas side conductance. Based on the assumption that UA is the same for all of the heat exchanger designs made, the ratio of gas side conductances for the He-O<sub>2</sub> and N<sub>2</sub>-O<sub>2</sub> design is given as follows:

$$\frac{(\eta_o hA)_{\text{He}}}{(\eta_o hA)_{\text{N}_2}} = \frac{(UA)_{\text{He}}}{(UA)_{\text{N}_2}} = 1 \quad (6-18)$$

For the designs considered, the fin effectivenesses are nearly independent of gas composition. Additionally, heat exchanger weight may be assumed to be proportional to gas side area and the following relationship results:

$$\frac{WT_{\text{N}_2}}{WT_{\text{He}}} \cong \frac{A_{\text{N}_2}}{A_{\text{He}}} \cong \frac{h_{\text{He}}}{h_{\text{N}_2}} \quad (6-19)$$

Equation (6-15) is now solved for the film coefficient for each candidate atmosphere and substituted into eq. (6-19) as follows:

$$\frac{WT_{\text{N}_2}}{WT_{\text{He}}} = \left( \frac{Re_{\text{N}_2}}{Re_{\text{He}}} \right)^{0.345} \frac{(G_s C_p)_{\text{He}} \left[ 1 - 8.35 Re^{-0.479} (Pr - 1) \right]_{\text{N}_2}}{(G_s C_p)_{\text{N}_2} \left[ 1 - 8.35 Re^{-0.479} (Pr - 1) \right]_{\text{He}}} \quad (6-20)$$

This equation may be reduced further by considering a particular design case in which the gas flow length of the heat exchanger is scaled to meet the performance. The heat exchanger frontal area will remain constant and, as stated previously, heat capacity will remain constant. Based on these assumptions the following equations can be written:

$$\dot{w}_{\text{N}_2} (C_p)_{\text{N}_2} = \dot{w}_{\text{He}} (C_p)_{\text{He}} \quad (6-21)$$

and since flow area is constant

$$(G_s C_p)_{\text{N}_2} = (G_s C_p)_{\text{He}} \quad (6-22)$$

When eqs. (6-22) and (6-20) are combined, the ratio of heat exchanger weights are obtained as follows:

$$\frac{WT_{N_2}}{WT_{He}} = \left( \frac{Re_{N_2}}{Re_{He}} \right)^{0.345} \frac{\left[ 1 - 8.35 Re^{-0.479} (Pr - 1) \right]_{N_2}}{\left[ 1 - 8.35 Re^{-0.479} (Pr - 1) \right]_{He}} \quad (6-23)$$

Where the Reynolds number ratio is obtained from eq. (6-22) and the definition of Reynolds number or,

$$\frac{Re_{N_2}}{Re_{He}} = \frac{(\mu C_p)_{He}}{(\mu C_p)_{N_2}} \quad (6-24)$$

Eqs. (6-23) and (6-24) were used to determine the ratio of heat exchanger weights for a typical Reynolds number of 100 for the  $N_2$ - $O_2$  mixture. The Reynolds number for He- $O_2$  was obtained from eq. (6-24). The results are as follows:

<u>Pressure (psia)</u>	<u><math>\frac{WT_{N_2}}{WT_{He}}</math></u>
5	0.892
7	0.925
10	0.960

Therefore, it can be seen that the  $N_2$  heat exchangers are from 4% to 11% lighter than He- $O_2$  units when the exchangers are compared on the basis of equal frontal areas. A similar analysis may be made for heat exchanger friction pressure drop and fan power. Using eqs. (6-13), (6-17), and (6-22), and the perfect gas law, the following expression is obtained for the assumption of constant heat exchanger frontal area:

$$\frac{\Delta P_{N_2}}{\Delta P_{He}} = \frac{(C_p)_{He}^2}{(C_p)_{N_2}^2} \left( \frac{Re_{He}}{Re_{N_2}} \right)^{0.745} \frac{A_{N_2}}{A_{He}} \frac{\mu_{He}}{\mu_{N_2}} \frac{\left[ 13.9 (1 - Pr) - 1 \right]_{He}}{\left[ 13.9 (1 - Pr) - 1 \right]_{N_2}} \quad (6-25)$$

and the ratio of fan power may be written

$$\frac{PWR_{N_2}}{PWR_{He}} = \frac{\dot{v}_{N_2}}{\dot{v}_{He}} \frac{\Delta P_{N_2}}{\Delta P_{He}} \quad (6-26)$$

Based on the same assumptions as the heat exchanger analysis, the ratio of pressure drops and powers were calculated for the candidate total pressures as follows:

<u>Pressure (psia)</u>	<u><math>\frac{\Delta P_{N_2}}{\Delta P_{He}}</math></u>	<u><math>\frac{PWR_{N_2}}{PWR_{He}}</math></u>
5	1.77	1.63
7	1.67	1.43
10	1.69	1.38

It can be seen that pressure drop and power are higher for the nitrogen-oxygen mixtures although heat exchanger weight is lower. A typical example is calculated for an application where the weight of the nitrogen-oxygen heat exchanger is 10 lb and the fan power is 15 W. The heat exchanger and fan power for the He-O<sub>2</sub> unit may be found as follows:

$$WT_{He} = \frac{10 \text{ lb}}{WT_{N_2} / WT_{He}}$$

$$PWR_{He} = \frac{15 \text{ W}}{PWR_{N_2} / PWR_{He}}$$

The following listing compares the weight penalty of a typical heat exchanger, using the values for comparative weight and power ratios discussed above. The power penalty used is 0.503 lb per W, typical of an isotope Brayton cycle. The operating pressure is assumed to be 7 psia, but consistent results are also obtained at 5 and 10 psia.

Diluent	N <sub>2</sub>	He
Heat exchanger weight, lb	10	10.8
Fan power, W	15	10.5
Power weight penalty, lb	7.6	5.3
Total penalty, lb	17.6	16.1

The above listing shows that the weight savings for He-O<sub>2</sub> mixture amounts to about 1.5 lb at 7 psia.

The information presented above may be used to determine heat exchanger requirements for a particular application. The procedure is to assume a design, then the performance is checked using the theoretical eqs. (6-1) through (6-12) and the fin set performance in a form similar to fig. 6-1. If calculated performance satisfies the requirements, then the heat exchanger design is adequate. If calculated performance is greater or less than that required, then the design is changed until agreement is reached. Because numerous designs may be found that satisfy the performance requirements, an optimization procedure may be used to find the most satisfactory solution. One such procedure is given in ref. 6-3, which trades off the heat exchanger weight and fluid pumping penalty. Envelope limitations must normally be used with this optimization procedure to obtain designs with reasonable dimensions. This procedure is used in the weight comparison study in Sec. 7. A small savings in penalty can be obtained with He-O<sub>2</sub> atmospheres for most heat exchanger applications. The results of a weight comparison depend greatly on the design constraints used and the values of heat exchanger and fluid pumping parameters.

The effect of weight and penalty on heat exchangers when integrated with a life support system is presented in Sec. 7. The significance of increasing allowable cabin temperature level on system power penalty for different atmospheres is given also in Sec. 7. Adsorption heat and mass transfer theory, test data, test data correlation and application of test data to a regenerative CO<sub>2</sub> removal system are presented in the remainder of this section.

## ADSORPTION BED TESTS AND EVALUATION

### Adsorption Bed Heat Transfer Theory

Two major adsorption bed materials proposed for the next generation spacecraft ECS systems are silica gel and zeolites. Zeolites are generally used to remove carbon dioxide and the silica gel is used to remove water vapor. The ECS usually bypasses a small amount of cabin air first through

a silica gel bed, then through the zeolites. This is done because the zeolites adsorb water vapor in preference to carbon dioxide and a small amount of water vapor will "poison" the zeolite's capability to adsorb carbon dioxide.

The adsorption of gas on adsorbent material is an exothermic process. The amount of heat released depends on the bed material's adsorbate concentration and temperature and also on the amount of gas adsorbed. The amount of heat released per unit mass of gas adsorbed is termed the heat of adsorption. This is generally considered to be a constant during the adsorption cycle. This heat of adsorption contributes to a temperature rise in the adsorbent material, which, in turn, reduces its adsorption capability. Convective heat transfer between the carrier gas and the bed material is the major mode of heat rejection. Therefore, it is necessary to determine the convective heat transfer coefficients so that an efficient bed design may be realized. The following discussion will develop the necessary theory for correlation of convective heat transfer coefficients for packed granular beds.

Convective heat transfer coefficients depend on gas properties, bed geometry, and gas flow rates. Dimensional analysis may be applied to the characteristic variables to arrive at a functional relationship between certain dimensionless groupings. For forced convection heat transfer the relationship is as follows:

$$\text{Nu} = C \text{Re}^b \text{Pr}^d \quad (6-27)$$

The values of C, b, and d are constants that are determined from the correlation of experimental data. The dimensionless groupings are familiar; however, definitions of certain variables differ for packed beds. These variables are the superficial mass velocity ( $G_s$ ) and the particle diameter ( $D_p$ ). The superficial mass velocity is used in the Reynolds number and is based on the total bed cross-section, excluding particles. Particle diameter is the characteristic length used in both the Nusselt number and the Reynolds number. Particle diameter is defined by the following equation:

$$D_p = \frac{6(1-p)}{a_v \phi_s} \quad (6-28)$$

$a_v$  = Area of particle surface per unit volume of bed ( $\text{ft}^2/\text{ft}^3$ )

$p$  = Bed porosity  $\left(1.0 - \frac{\rho_B}{\rho_P}\right)$

$\rho_B$  = Density of the packed bed ( $\text{lb}/\text{ft}^3$ )

$\rho_p$  = Density of the individual particles (lb/ft<sup>3</sup>)

$\phi_s$  = Shape factor for non-spherical particles

A more detailed description of these parameters and methods of evaluation will be found in ref. 6-4.

Convective heat transfer data for packed beds have also been correlated in the form of the Colburn heat transfer modulus ( $j_h$ ). Paselk presents  $j_h$  factor data for packed beds in ref. 6-3. Also included in this reference are friction factor data and mass transfer data for packed beds. Paselk suggests that this data be used in the design of ECS adsorption beds; however, the data were determined by the evaporation of water in air for  $Re = 45-5000$  and extrapolated in the lower regions because of agreement with other test data for mass transfer in liquids at lower values of Reynolds number. Typical spacecraft adsorption beds designs, generally, have values of  $Re < 60$  for gas mixtures; therefore, the data presented in ref. 6-3 may not be applicable. This was found to be true for the tests run at Douglas and will be discussed further in the data correlation section. The following section discusses mass transfer theory in adsorption bed, and the analogy between heat and mass transfer for turbulent flow.

#### Adsorption Bed Mass Transfer Theory

The rate of convective mass transfer of adsorbate gas between the carrier gas stream and the exterior surface of the bed material is defined by the following equation:

$$\dot{w}_A = k_G M_A a_v A_F L_B (P_{ag} - P_{ab}) \quad (6-29)$$

The adsorbate gas is generally present as a very dilute mixture in the cabin atmosphere and (because only a small amount of cabin air is passed through the adsorption bed) pressure of the adsorbate gas at the inlet to the bed tends to remain at a relatively constant level during normal operations. Any significant excursions in the adsorbate gas inlet pressure are, of course, functions of the bed size, bed temperature, cycle time, and production rate within the cabin. Pressure of the adsorbate at the surface of the bed material is a function of bed temperature and concentration. The mass transfer coefficient, like the heat transfer coefficient, is a function of the gas properties, bed geometry, and gas flow rates. Dimensional analysis may also be applied to the characteristic variables involved in mass transfer to arrive at functional relationships between certain dimensionless groupings. For forced convection mass transfer the relationship is as follows:

$$Sh = C Re^b Sc^d \quad (6-30)$$

The values of C, b, d are constants which are determined from the correlation of experimental data. As discussed previously, the superficial mass velocity ( $G_s$ ) is used in Reynolds number computations for packed beds, and the characteristic length used for Reynolds number and Sherwood number is the particle diameter ( $D_p$ ).

Convective mass transfer data for packed beds have also been correlated in the form of Colburn mass transfer modulus ( $j_m$ ). Ref. 6-3 presents the correlation of  $j_m$  for a range of Reynolds numbers. These data of ref. 6-3 indicate the heat and mass transfer analogy, which states that  $j_h = j_m = f/2$  for turbulent flow. This relationship was determined for turbulent flow in straight tubes by using Reynolds analogy and empirically correcting the equations for the resistance of the laminar sublayer (ref. 6-5). However, heat, mass, and momentum transfer equations are composed of two components: (1) molecular transport in the laminar sublayer and (2) eddy diffusivity in the buffer zone and turbulent core. In the turbulent flow regime, the eddy diffusivity or turbulent mixing term becomes the most dominant factor and the analogy is valid. However, for flow conditions in the transition or laminar flow regimes, this analogy may not be valid.

The heat and mass transfer analogy for turbulent flow yields the following relationship for mass transfer and heat transfer coefficients:

$$k_G = \frac{h}{C_p P_G M_G} \left( \frac{Pr}{Sc} \right)^{2/3} \quad (6-31)$$

where the gas properties are those pertaining to the carrier gas.

The test data correlation provided a heat and mass transfer coefficient relationship somewhat different from that expressed in eq. (6-31). This is discussed further in the data correlation section.

### Adsorption Bed Pressure Drop Theory

Pressure drop characteristics of adsorption beds are very important because of their effect on the fan power required in the ECS system. The most dominant pressure losses generally occur as frictional losses within the bed, therefore, the theory as applied to this case only is discussed. Entrance and exit loss calculations may be readily determined from any standard text on fluid dynamics.

The frictional pressure drop in packed beds is primarily a function of the gas density, viscosity, and flow rate together with the bed geometry. Many different forms of pressure drop data correlations have been proposed

for packed beds. These generally involve bed porosity ( $p$ ) and particle shape factor ( $\phi_s$ ), however, the most straightforward method appears to be application of the Fanning friction factor equation as follows:

$$\Delta P = 4f \left( \frac{L_B}{D_p} \right) \frac{\rho V_s^2}{2g} = 4f \left( \frac{L_B}{D_p} \right) \frac{G_s^2}{2g\rho} \quad (6-32)$$

Where, again, particle diameter ( $D_p$ ) is used together with superficial velocity ( $V_s$ ) or mass velocity ( $G_s$ ). The Fanning friction factor ( $f$ ) is plotted versus Reynolds number ( $Re$ ) based on  $D_p$  and  $G_s$ . Ref. 6-3 includes  $f$  data plotted in this manner for beds packed with either cylinders or spheres and for  $Re = 60-4000$ . The adsorption bed test data are in excellent agreement with that presented in ref. 6-3.

Another convenient method of presenting pressure drop data is a plot of  $\sigma_g \Delta P/L_B$  vs  $G_s$  for a given bed material and particle size. Ref. 6-6 contains  $\sigma_g \Delta P/L_B$  data for Linde, type 5A, 1/8 in. zeolite pellets, and ref. 6-7 contains the same type of data for Davidson, grade 40, 6-12 mesh silica gel. The test data are also plotted in this manner and are in good agreement with the referenced data. The data correlation section contains the graphical results for the pressure drop correlations.

#### Adsorption Bed Test Description and Procedure

Pressure drop, mass transfer, and heat transfer tests for typical adsorption bed designs were run on the Douglas Generalized Equipment Performance Test Facility (GEPTF). Pressure drop data were easily obtained and required only measurements of flow rate, bed temperature, gas temperature, total pressure, pressure drop across the bed, and composition of the atmosphere. These tests were run at steady-state conditions. The adsorption process is never a steady-state process and, therefore, must be tested under transient conditions. Ref. 6-8 outlines a method for determination of mass transfer coefficients from transient data, providing the following conditions are met.

- (1) The adsorbate concentration is constant throughout the bed at the start of the run.
- (2) A step change in the adsorbate gas concentration at the bed inlet is made at the start of the adsorption test and this inlet concentration is held constant throughout the run.
- (3) Inlet temperature and carrier gas flow rates are held constant throughout the run.
- (4) The adsorption isotherm of the adsorbate on the adsorbent material may be linearized over the range of bed concentrations encountered during the run.

Mass transfer tests require measurement of flow rate, bed temperatures, gas temperatures, adsorbate gas inlet and exit pressures, total pressure, and composition of the atmosphere.

The heat transfer coefficients for adsorption bed materials may be measured under steady-state conditions only if the bed material can be maintained at a constant temperature level different than the atmosphere passing through it. This is difficult to do because of the low thermal conductivity of the adsorbent material. It would require a very efficient heat exchanger surface in direct contact with the bed material (i.e., loading of bed material into a compact heat exchanger core). However, as in the case of mass transfer, the heat transfer coefficients may be determined from transient test data providing certain conditions are met. Ref. 6-8 outlines a method for determining heat transfer coefficients from transient data taken under the following conditions.

- (1) Temperature is constant throughout the bed at the start of the run.
- (2) A step change in the inlet gas temperature is introduced at the start of the heat transfer test and this temperature is held constant throughout the run.
- (3) Inlet gas flow rates are held constant throughout the run.
- (4) Specific heats of the gas and bed are constant over the range of temperatures encountered during the run.

Heat transfer tests require measurement of flow rate, bed temperature, gas temperature, total pressure, and composition of the atmosphere. Temperature measurements were taken with thermocouples and recorded on strip recorders and/or paper punch tape during the tests performed in the GEPTF. Gas flow rates were measured with ASME standard orifice plates, pressure drops with slant tube manometers, and total pressures with Bourdon gages. Carbon dioxide pressures were measured with MSA Lira gas analyzers and water vapor pressures were determined from measuring wet and dry bulb thermocouple temperatures and total system pressure at the bed inlet and exit. An insulated canister for the adsorbent bed material was prepared which would conveniently fit in the GEPTF. Eighteen thermocouples were provided for monitoring bed and gas temperatures in the insulated canister which was 16 in. long and 8 in. wide. Flow through the canister was vertical. Two bed depths were used during the tests: (1) an 8.875-in. depth for adsorption tests and (2) a 2-in. depth for heat transfer tests.

Mass transfer test conditions were selected such that the superficial gas velocity ( $V_g$ ) was approximately 60 ft/min for all atmospheres. This velocity was recommended in refs. 6-6 and 6-7 as a good design. The gas flow into the bed during mass transfer tests was controlled nominally at 50°F and was saturated for the silical gel tests. The molecular sieve mass transfer tests used dry gas with an inlet pressure of carbon dioxide equal to 5 mmHg. These conditions are representative of values used in typical ECS systems. The adsorption beds were purged with predried room air heated to 300°F before each run. Following the purge cycle, the beds were pumped down to vacuum conditions. The proper atmosphere was added to the GEPTF and the bed was cooled to 50°F. Following the cooldown, a step change in the inlet adsorbate

gas concentration was made by metering in either carbon dioxide or steam. This level of inlet adsorbate gas concentration was then held constant until the end of the run. Gas and bed temperatures together with adsorbate pressure levels were monitored throughout the run.

The heat transfer test conditions were also chosen such that  $V_g \approx 60$  ft/min. During the tests, a dry bed was heated up and allowed to soak until the nominal bed temperature was 180°F, at this time the bed was subjected to a cold gas stream at a nominal temperature of 60°F. Gas and bed temperatures were monitored during the cooldown. The pressure drop tests were conducted at ambient temperature for each atmosphere with flow rates varied in incremental steps over the full range capability of the blower in the GEPTF.

### Adsorption Bed Data Correlation

The following geometry characteristics were used in the reduction of test data for the adsorption bed materials:

	$D_p$ (ft)	$a_v$ (ft <sup>2</sup> /ft <sup>3</sup> )
Linde, type 5A, 1/8-in. zeolite pellets	0.0119	309
Davidson, grade 40, 6-12 mesh silica gel	0.0071	396

Adsorption Bed Heat Transfer Data Correlation. -- Heat transfer coefficients for the various atmospheres and bed materials were determined using the methods outlined in ref. 6-8. The dimensionless groups specified in eq. (6-27) were calculated for each test and a correlation in the form of eq. (6-27) was sought. The data are plotted on fig. 6-3 as  $Nu/Pr$  vs  $Re$ . A good correlation of these data appears to be represented by the following equation:

$$Nu = 0.181 Re^{1.22} Pr \quad (6-33)$$

However, ref. 6-1 points out that from theoretical considerations the value of Nusselt number approaches a constant value of two for a Prandtl number of unity. This suggests that perhaps the minimum value of  $Nu/Pr$  approaches two for the data in fig. 6-3. An attempt was made to correlate the data using the Colburn heat transfer modulus,  $j_h$ , and to match the data presented in ref. 6-3. A  $j_h$  versus  $Re$  correlation was very poor for the test data; however, the data did show good agreement with that presented in ref. 6-3 for the higher values of Reynolds Number ( $Re > 50$ ). This suggests that the test data, which represents typical spacecraft bed designs, lie in a transition region, which is governed by a different type of heat transfer correlation. This observation also agrees with the limiting value of Nusselt number mentioned above which generally occurs in fully developed laminar flow. One other point that should be made, is that the mass transfer correlation discussed later is of a similar form with the same exponent for Reynolds number.

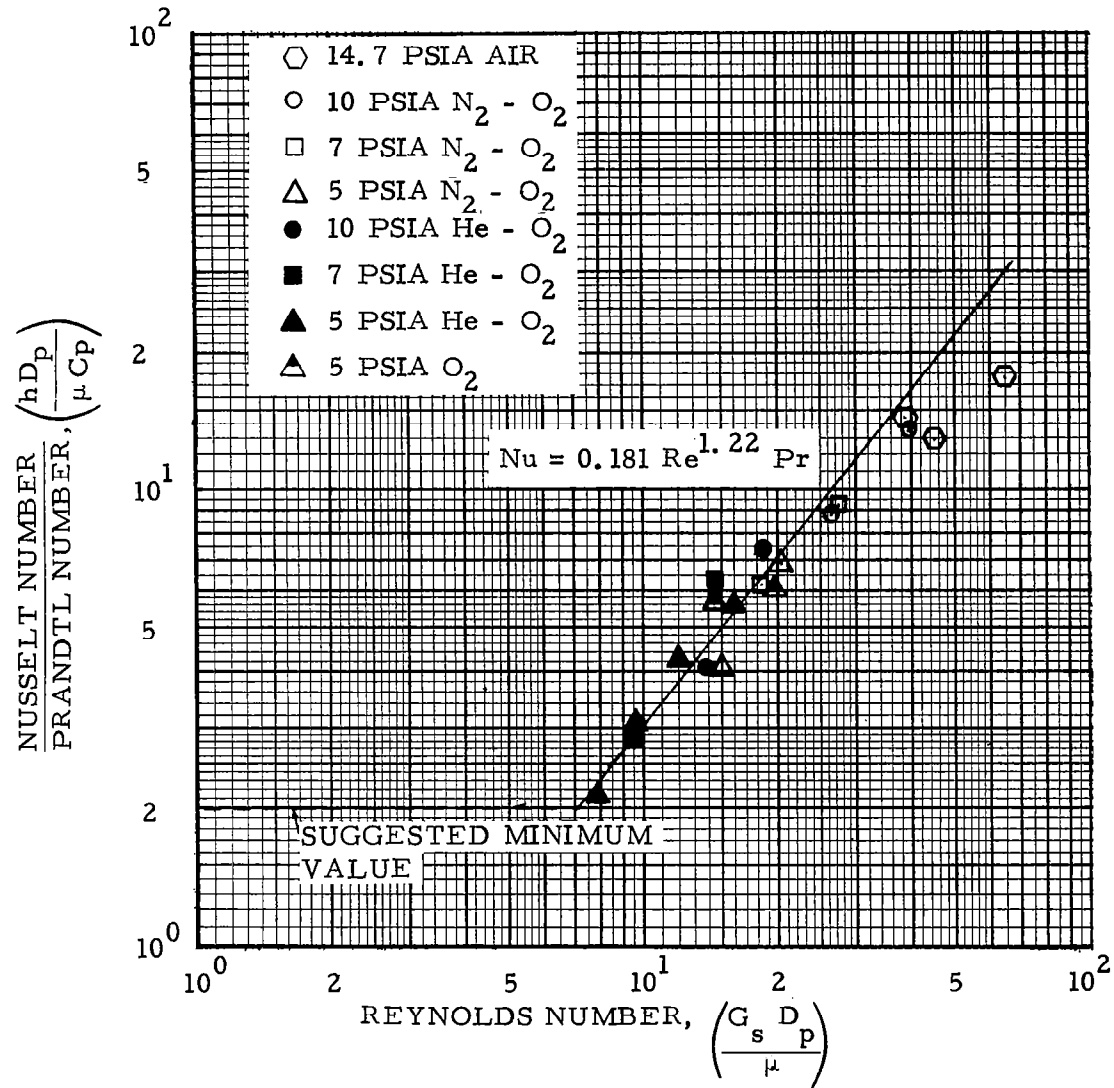


FIGURE 6-3 HEAT TRANSFER DATA FOR SILICA GEL AND ZEOLITE PELLETS

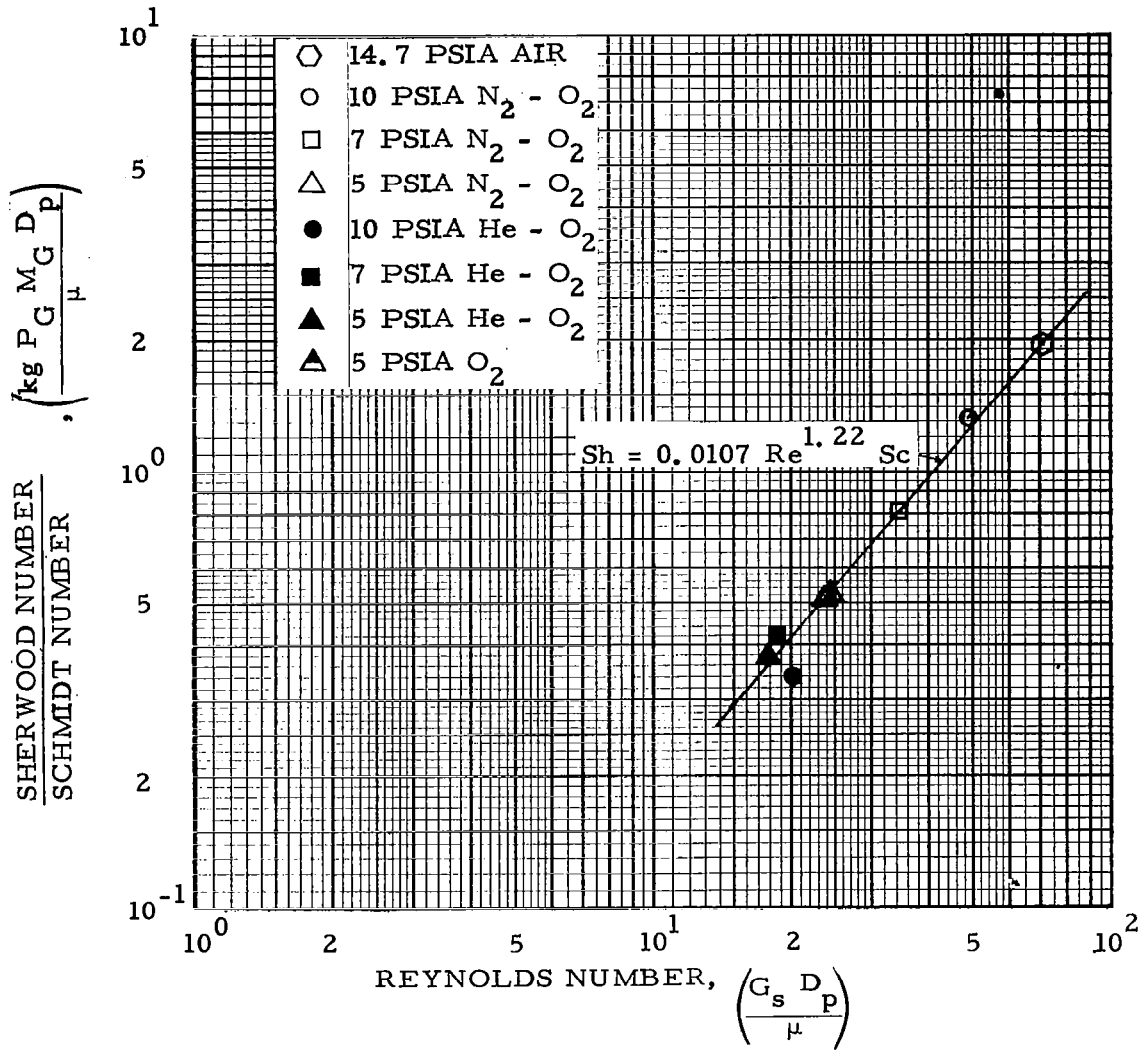


FIGURE 6-4 MASS TRANSFER DATA FOR ZEOLITE PELLETS

Adsorption Bed Mass Transfer Data Correlation. --Mass transfer coefficients for the various atmospheres and the zeolite bed material were determined using the methods outlined in ref. 6-8. The silica gel mass transfer data could not be reduced in this manner because of inadequate control of the inlet pressure of the water vapor and the large temperature changes that occurred in the bed because of the high heat of adsorption for water vapor and the large amounts of water adsorbed. Correlation of the silica gel mass transfer data would require the use of a computer program to allow for the large variations in the inlet conditions and bed temperatures together with a trial-and-error method of data correlation. The dimensionless groups specified in eq. (6-30) were calculated for the zeolite mass transfer data. Since there is a similarity in heat and mass transfer, the logical correlation to try appeared to be  $Sh/Sc$  vs  $Re$ . The data are plotted for these coordinates in fig. 6-4. A good correlation of these data appears to be represented by the following equation:

$$Sh = 0.0107 Re^{1.22} Sc \quad (6-34)$$

Again, an attempt was made to correlate the data using a Colburn mass transfer modulus,  $j_m$ , and to match the data in ref. 6-3. This also proved to be an inadequate method of correlation and the mass transfer data did not correlate with that given in ref. 6-3. Even at the higher Reynolds numbers, the  $j_m$  values appeared to be an order of magnitude lower than those of ref. 6-3.

Eqs. (6-33) and (6-34) were solved for Reynolds number and combined to yield a relationship between the heat and mass transfer coefficients to compare with eq. (6-31). This combination produced the following relationship:

$$k_G = \frac{1}{16.9} \left( \frac{h}{C_p P_G M_G} \right) \quad (6-35)$$

where the gas properties are those pertaining to the carrier gas.

Heat and mass transfer correlations were used in an adsorption bed computer program to verify the zeolite adsorption test data. The case chosen for verification was the 14.7-psia air atmosphere. Inlet carbon dioxide was assumed to have a constant value of 5.10 mmHg. The test data and results of the analysis are shown in fig. 6-5 and are in good agreement.

Adsorption Bed Pressure Drop Data Correlation. --Pressure drop data were reduced and plotted in the two forms discussed in the pressure drop theory section. Figs. 6-6 and 6-7 show the  $\sigma_g \Delta P/L_B$  as a function of  $G_s$  data for Davidson, grade 40, 6-12 mesh silica gel and Linde, type 5A, 1/8-in. zeolite pellets. Fig. 6-8 shows the data in a more general form ( $f$  versus  $Re$ ), which can be applied to all bed materials. The  $\sigma_g \Delta P/L_B$  curves are in good agreement with similar data presented in refs. 6-6 and 6-7 and the  $f$  data are in excellent agreement with the data of ref. 6-3. In both cases, the new test data extended into the lower flow rate and Reynolds number regions, which are of interest in the design of spacecraft ECS systems.

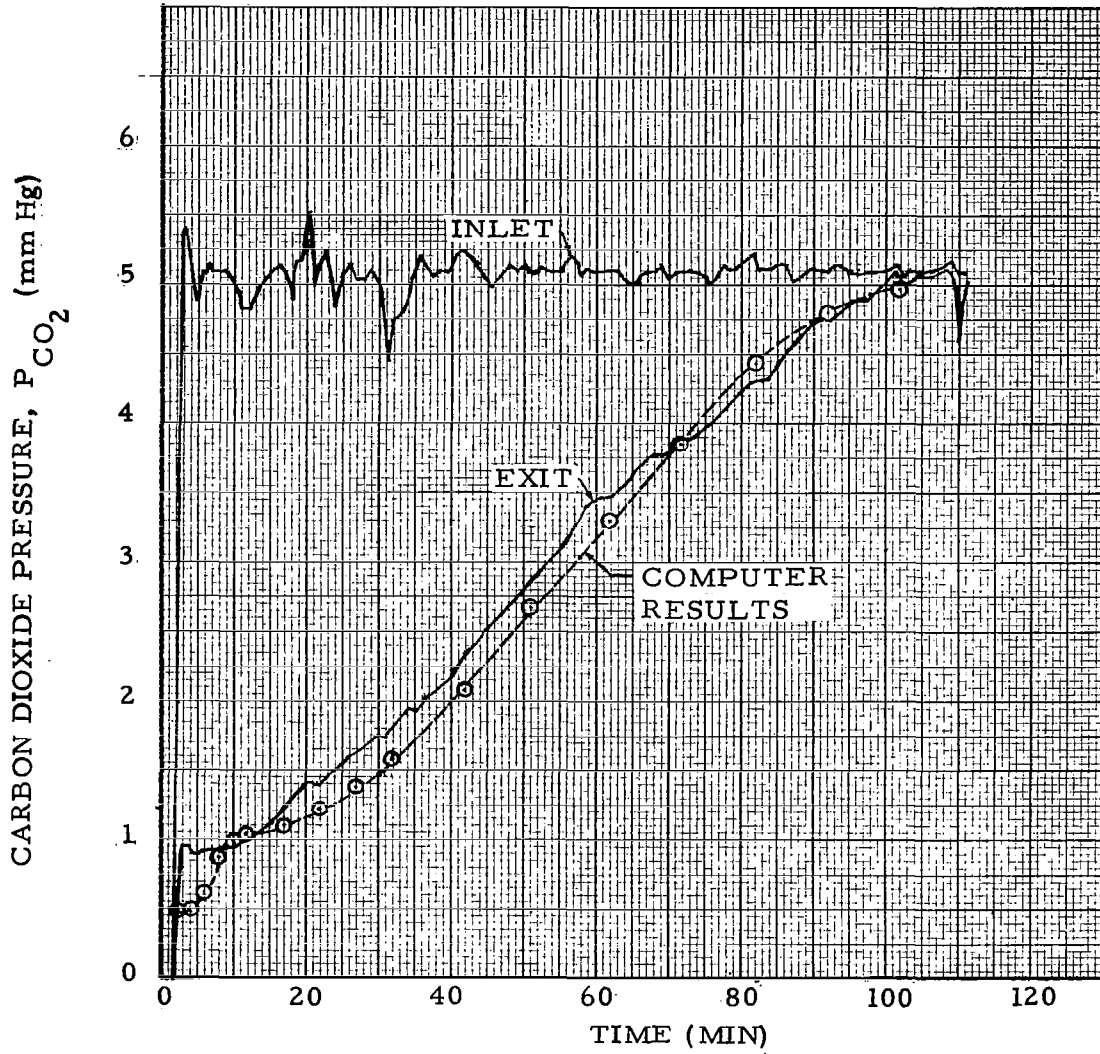


FIGURE 6-5 ZEOLITE ADSORPTION BED DATA FOR 14.7 PSIA AIR

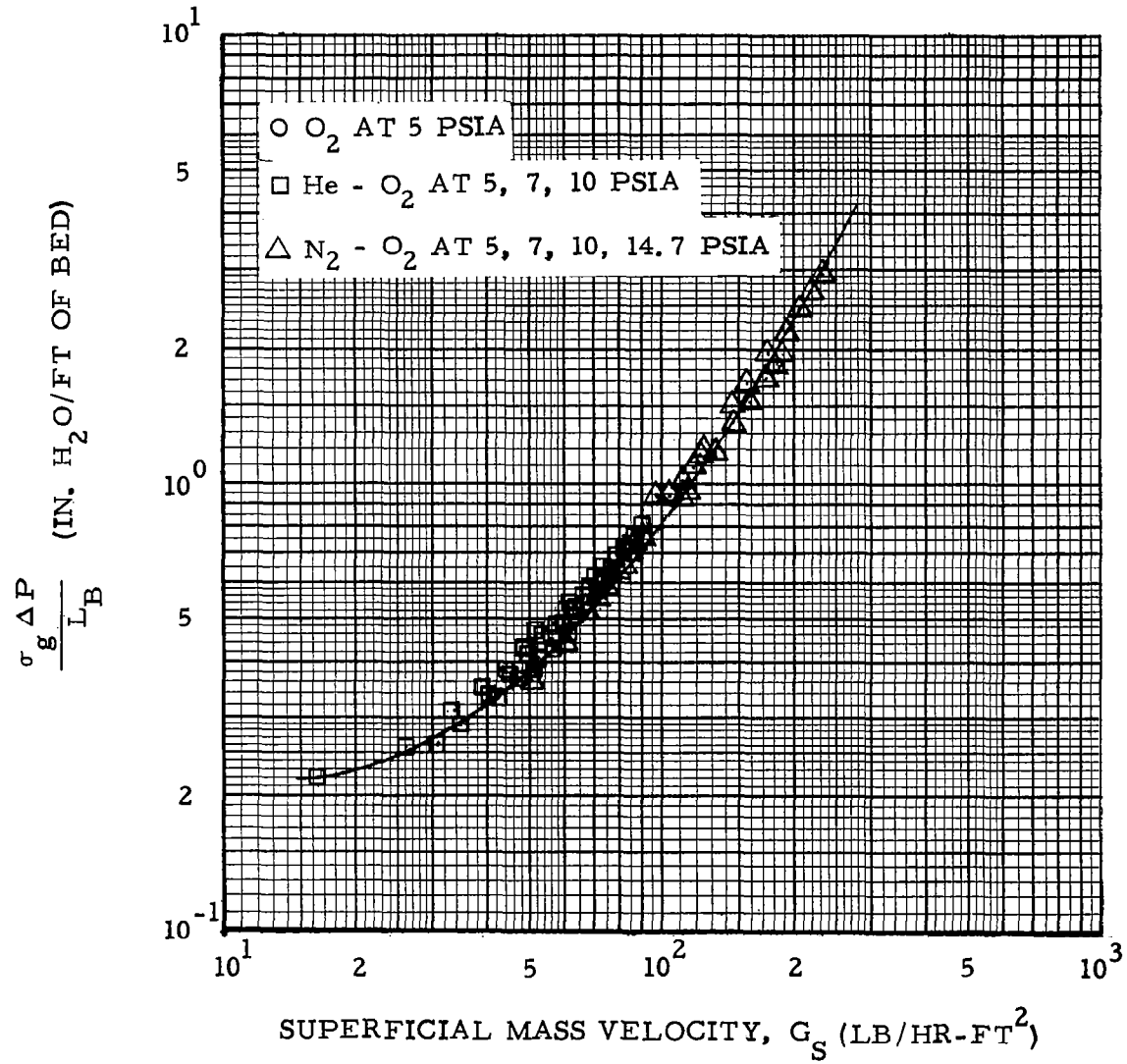


FIGURE 6-6 PRESSURE DROP DATA FOR DAVIDSON, GRADE 40, 6-12 MESH SILICA GEL

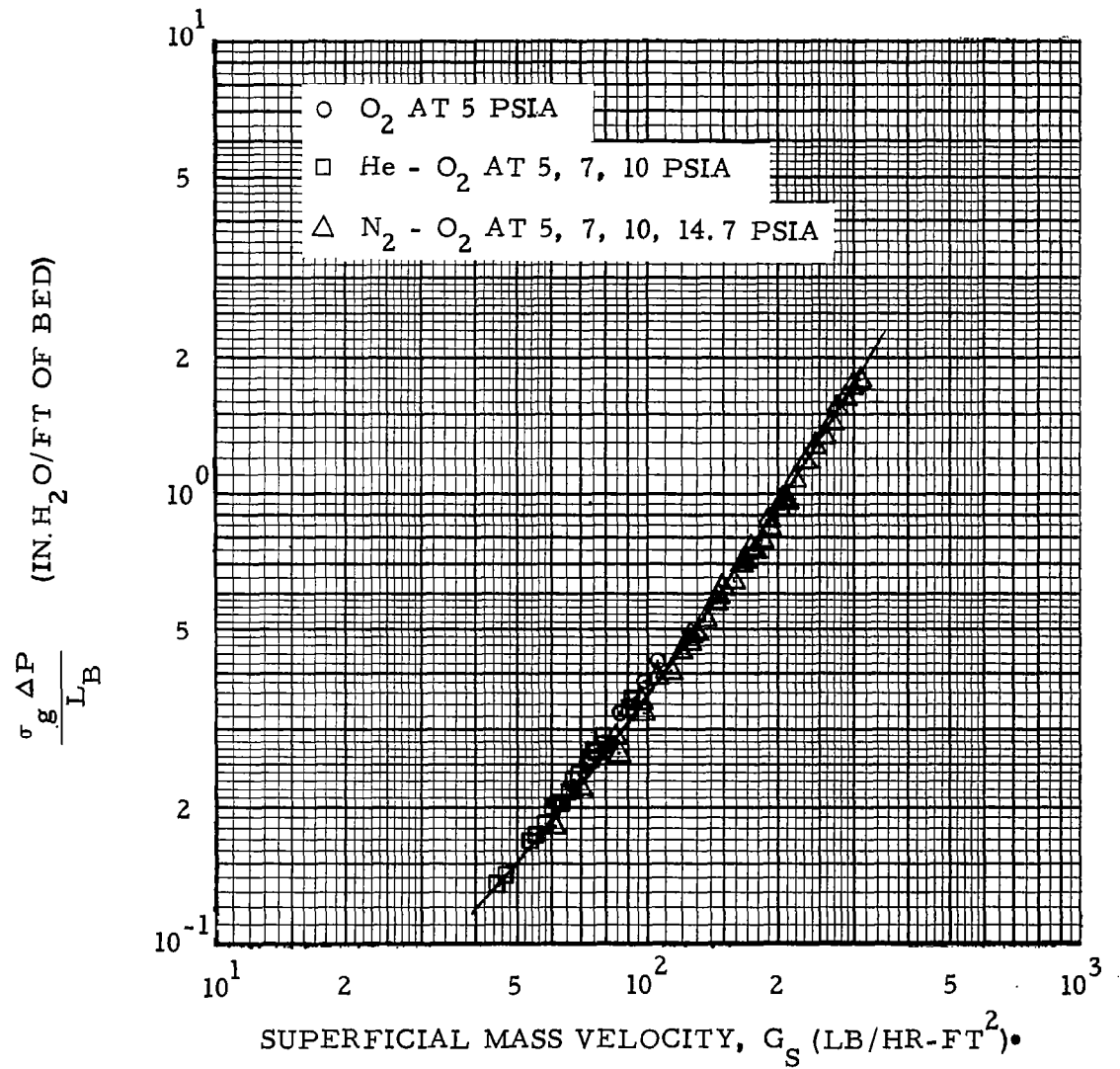


FIGURE 6-7 PRESSURE DROP DATA FOR LINDE, TYPE 5A, 1/8" ZEOLITE PELLETS

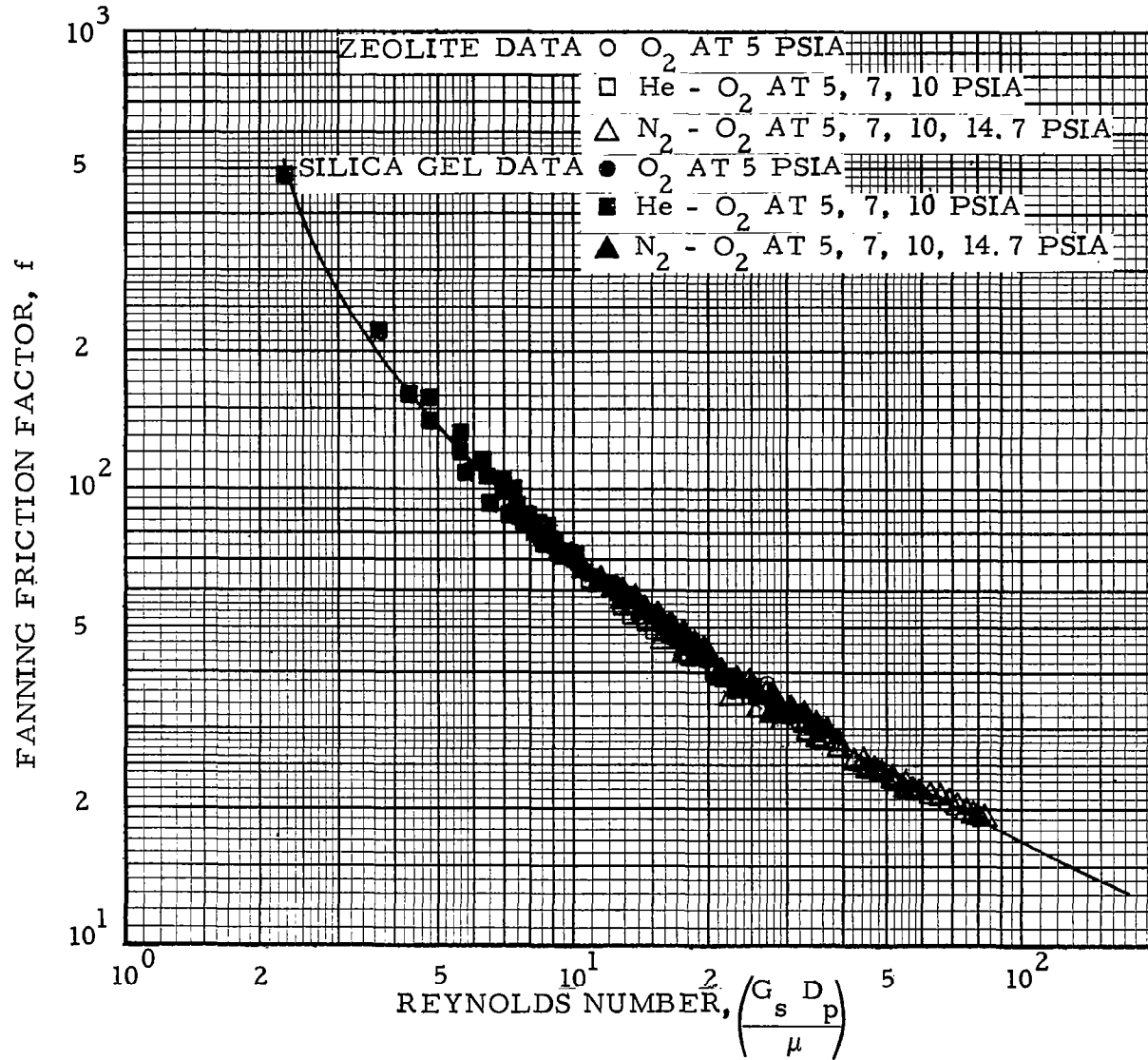


FIGURE 6-8 FANNING FRICTION FACTOR DATA FOR SILICA GEL AND ZEOLITE PELLETS

## Application of Experimental Data to Adsorption Bed Design

The following discussion considers molecular sieve/silica gel bed combinations for various gas atmospheres and pressures at a component level. A comparison of the effect of atmosphere composition and pressure on weight penalty for an integrated CO<sub>2</sub> regenerative molecular sieve/silica gel system, using the test data presented, is given in Sec. 7. The experimental heat transfer, and pressure drop data presented in fig. 6-3, 6-4, 6-6, and 6-7 were used together with a computer to arrive at typical adsorption bed designs for a three-man life support system. These results may be linearly scaled, with respect to the number of men in the system, if the design conditions are similar. A bed weight and power penalty comparison, based on these designs, is presented to illustrate the effect of atmosphere composition and pressure. A hand calculation method may be used to determine approximate adsorption bed designs (ref. 6-8). A sample problem using this method is presented and the results are compared to the computer generated designs to give an indication of the accuracy and consequences of the simplifying assumptions inherent in the readily usable hand calculation method.

The molecular sieve/silica gel beds were designed for the following set of conditions:

- (1) Three-man system (also a nine-man system for molecular sieve).
- (2) Carrier gas flow rate through bed for three-man unit = 10 cu ft/min.  
Carrier gas flow rate through bed for nine-man unit = 30 cu ft/min.
- (3) Bed superficial gas velocity = 60 ft/min.
- (4) Carrier gas temperature at bed inlet = 52.5°F. saturated gas for  
silica gel  
= 50 °F. for molecular sieve
- (5) Carbon dioxide pressure in cabin = 5 mmHg.
- (6) Carbon dioxide generation rate = 2.25 lb/man-day.
- (7) Regenerative silica gel for H<sub>2</sub>O removal and regenerative molecular sieve for CO<sub>2</sub> removal.
- (8) Silica gel bed is designed to limit the amount of water passing through the bed to 0.5% of the downstream molecular sieve bed weight.  
(This is done to prevent poisoning of the molecular sieve.)
- (9) One of two molecular sieve/silica gel bed combinations is always desorbing.

The independent variables chosen for the bed designs were atmospheric gas composition and initial bed concentration. Gas mixtures of N<sub>2</sub>-O<sub>2</sub> and He-O<sub>2</sub> at 5, 7, and 10 psia were used for the molecular sieve designs and mixtures at 5 and 7 psia were used for the silica gel designs. Initial bed

concentrations were varied from 0 to 3% for molecular sieve designs and from 1 to 6% for silica gel designs. A nine-man system, using a carrier gas flow rate of 30 cu ft/min was also designed for molecular sieve beds. These data verified the supposition that the bed designs could be scaled linearly in direct proportion to the number of men in the system. Adiabatic bed designs were assumed for the molecular sieve and, for the design conditions, the bed temperature changes were small; therefore, a cooled bed design would not be significantly different in size. However, because of the high heat of adsorption of water vapor and the large amounts of water entering the silica gel bed, it was necessary to run both adiabatic and isothermal bed designs for silica gel. These data provide bounds for the size of an actual cooled silica gel bed design.

The basic equations, presented in ref. 6-8, governing the heat and mass transfer relationships in an adsorbing bed were placed in a finite difference form and combined using a lumped capacitance representation of the bed material. A computer program using these equations was prepared for rapid analysis of bed designs. The program allows for convective heat and mass transfer between the carrier gas and the bed, the heat of adsorption released during the adsorption process, and the use of equilibrium isotherm test data. It also allows for uniform heat addition so that it can be used to analyze purge gas desorption. Another program, which uses experimentally determined coefficients, was used to predict the amount of heat required for vacuum desorption of the molecular sieve beds. Fan power required to overcome pressure drop in the beds was computed by hand from the design conditions and the data presented in figs. 6-6 and 6-7.

First, the molecular sieve bed sizes were calculated using the design conditions and the experimental heat and mass transfer data. The molecular sieve bed weights provided the necessary design conditions for the silica gel beds (i. e., the amount of water passing through the silica gel bed is limited to 0.5% of the weight of the downstream molecular sieve bed). After the molecular sieve and silica gel bed sizes were determined, the heat required for desorption and the fan power required for overcoming the pressure drop in the beds were calculated.

The molecular sieve bed designs for a three-man system are presented in table 6-I. Bed length and weight together with fan power to overcome bed pressure drop and thermal power required for vacuum desorption are shown for the independent variables of atmospheric gas and initial bed concentrations. It should be noted that, for indicated design conditions, the He-O<sub>2</sub> bed designs are generally larger than the beds designed for N<sub>2</sub>-O<sub>2</sub>, but they require less fan power. The lightest beds correspond to low initial concentrations, but they require more thermal power for desorption. Higher pressure atmospheres result in smaller beds; however, as initial bed concentration decreases this effect is less significant.

Table 6-II presents the same data as 6-I except it is for a nine-man system and considers only the 5- and 7-psia pressure levels. These designs were presented to demonstrate the feasibility of linearly scaling the designs on the basis of the number of men. The same superficial face velocity was used as in the three-man system, but the gas flow rate was varied in

TABLE 6-1 (page 1 of 2)

## EFFECT OF ATMOSPHERIC COMPOSITION AND PRESSURE ON A THREE-MAN ADIABATIC MOLECULAR SIEVE BED DESIGN

[ Designs based on experimental data of figs. 6-3 through 6-8 ]

Atmosphere	<sup>a</sup> Initial bed concentration (lb adsorbate/lb bed)	<sup>b</sup> Adiabatic bed length (ft)	Bed material weight (lb)	Fan power to overcome pressure drop (W)	Thermal power for 30-min vacuum desorption of CO <sub>2</sub> (W)
5 psia N <sub>2</sub> -O <sub>2</sub>	0	0.375	2.69	0.424	102.5
	0.01	0.485	3.47	0.545	65.9
	0.02	0.727	5.21	0.818	48.3
	0.03	1.320	9.46	1.485	0
5 psia He-O <sub>2</sub>	0	0.393	2.82	0.414	102.5
	0.01	0.520	3.73	0.548	67.4
	0.02	0.780	5.59	0.823	45.4
	0.03	1.430	10.23	1.509	0
7 psia N <sub>2</sub> -O <sub>2</sub>	0	0.337	2.41	0.423	102.5
	0.01	0.417	2.98	0.524	63.0
	0.02	0.567	4.06	0.712	49.8
	0.03	1.030	7.38	1.293	0

TABLE 6-1 (page 2 of 2)

Atmosphere	<sup>a</sup> Initial bed concentration (lb adsorbate/lb bed)	<sup>b</sup> Adiabatic bed length (ft)	Bed material weight (lb)	Fan power to overcome pressure drop (W)	Thermal power for 30-min vacuum desorption of CO <sub>2</sub> (W)
7 psia He-O <sub>2</sub>	0	0.363	2.60	0.395	102.5
	0.01	0.457	3.27	0.496	64.4
	0.02	0.653	4.68	0.710	48.3
	0.03	1.220	8.74	1.324	0
10 psia N <sub>2</sub> -O <sub>2</sub>	0	0.310	2.22	0.463	102.5
	0.01	0.370	2.65	0.552	60.6
	0.02	0.470	3.37	0.701	50.7
	0.03	0.720	5.16	1.074	26.4
10 psia He-O <sub>2</sub>	0	0.335	2.40	0.368	102.5
	0.01	0.410	2.94	0.450	62.9
	0.02	0.555	3.98	0.609	50.6
	0.03	0.910	6.52	0.998	9.4

<sup>a</sup>Initial gas temperature entering bed from silica gel bed and condenser  $\approx 50^{\circ}\text{F}$ .

<sup>b</sup>Cross-sectional area of all beds is  $1/6 \text{ ft}^2$ , based on the design conditions.

TABLE 6-II

## EFFECT OF ATMOSPHERIC COMPOSITION AND PRESSURE ON A NINE-MAN ADIABATIC MOLECULAR SIEVE BED DESIGN

[Designs based on experimental data of figs. 6-3 through 6-8]

Atmosphere	<sup>a</sup> Initial bed concentration (lb adsorbate/lb bed)	<sup>b</sup> Adiabatic bed length (ft)	Bed material weight (lb)	Fan power to overcome pressure drop (W)	Thermal power for 30-min vacuum desorption of CO <sub>2</sub> (W)
5 psia N <sub>2</sub> -O <sub>2</sub>	0	0.360	7.74	1.210	293
	0.01	0.468	10.06	1.578	194
	0.02	0.728	15.63	2.455	138
	0.03	1.424	30.60	4.80	0
5 psia He-O <sub>2</sub>	0	0.380	8.21	1.200	293
	0.01	0.500	10.75	1.580	195
	0.02	0.796	17.10	2.520	138
	0.03	1.520	32.70	4.81	0
7 psia N <sub>2</sub> -O <sub>2</sub>	0	0.324	6.97	1.220	293
	0.01	0.400	8.60	1.505	188
	0.02	0.548	11.78	2.065	150
	0.03	1.064	22.90	4.01	0
7 psia He-O <sub>2</sub>	0	0.348	7.48	1.132	293
	0.01	0.440	9.46	1.432	191
	0.02	0.640	13.75	2.083	144
	0.03	1.280	27.50	4.17	0

<sup>a</sup>Initial gas temperature entering bed from silica gel bed and condenser  $\approx 50^{\circ}\text{F}$ .<sup>b</sup>Cross-sectional area of all beds is  $1/2\text{ ft}^2$ , based on the design conditions.

proportion to the number of men. As shown in table 6-II the bed frontal area for the nine-man system is three times as large as that for the three-man system. The fan powers and thermal powers for desorption are approximately three times as large as the three-man system, and the bed lengths are about equal.

Table 6-III presents the adiabatic silica gel bed designs that complement the 5- and 7-psia molecular sieve designs shown in table 6-I. A complementary silica gel bed design (using initial concentrations of 0.01, 0.02, 0.04, and 0.06) was attempted for each molecular sieve design. In some cases, the silica gel beds designs were unable to remove the required amount of water, and no designs were obtained. The silica gel bed designs indicate the same general trends as did the molecular sieves: (1) the He-O<sub>2</sub> bed designs are larger, but require less fan power, and (2) a low initial concentration results in a lighter bed. The required weight of silica gel decreases as the initial concentration of the molecular sieve increases. This results from the fact that higher initial CO<sub>2</sub> concentrations result in heavier molecular sieve weights. Therefore, the silica gel beds are smaller because they retain less water (that is, the silica gel design is based on passing an amount of water equal to 0.5% of the downstream molecular sieve bed weight). Table 6-III also tabulates the amount of thermal power required for purge gas desorption of the silica gel beds.

The purge gas desorption of silica gel beds requires the addition of relatively large amounts of heat, which results in significant temperature rises in the bed material. Because the thermal capacity of the carrier gas is small, this requires the use of a heat exchanger to heat the bed directly and also to pre-cool it before the adsorption cycle. A heating period of 20 min and a pre-cooling period of 10 min was chosen for the silica gel desorption analysis. After considering the results presented in table 6-III and noting the necessity for a heat exchanger to heat and pre-cool the bed during desorption, it became obvious that the heat exchanger should also be used during the adsorption cycle to cool the bed. A cooled bed greatly reduces the amount of bed material required during adsorption, therefore, a series of cases which considered the bed to be isothermal were run. Table 6-IV presents the data for the isothermal cases. The actual design for a silica gel bed with an integral heat exchanger should lie between the bounds described by the data in tables 6-III and 6-IV.

The molecular sieve bed data presented in table 6-I and the silica gel data presented in table 6-III were used to develop weight penalty trends. The minimum weight bed will depend upon the penalty factors assigned to fan power to overcome bed pressure drop and thermal power required for desorption, together with bed material weight and associated heat transfer equipment required for desorption. The following equation was used to arrive at weight penalties:

$$WT_T = \left[ \frac{PWR_F}{\eta_F} + \text{Thermal Power for Desorption} \right] PPF + 1.75 WT_B \quad (6-36)$$

TABLE 6-III.

EFFECT OF ATMOSPHERIC COMPOSITION, PRESSURE, AND MOLECULAR SIEVE DESIGN ON  
A 3-MAH ADIABATIC SILICA GEL BED DESIGN

(Designs based on experimental data of figures 6-3 through 6-8)

Atmosphere	*Initial Bed Concentrations (lb adsorbate/lb bed)		**Adiabatic Bed Length (ft)	Bed Material Weight (lb)	Fan Power to Overcome Pressure Drop (watts)	Thermal Power for 20 Minute Purge Gas Desorption (watts)
	Molecular Sieve	Silica Gel				
5 psia N <sub>2</sub> -O <sub>2</sub>	0	0.01	1.230	9.23	3.41	359
		0.02	1.511	11.33	4.20	315
		0.04	2.03	15.21	5.63	293
		0.06	ND	-	-	-
	0.01	0.01	1.152	8.64	3.20	337
		0.02	1.425	10.68	3.95	308
		0.04	1.900	14.24	5.26	278
		0.06	2.55	19.11	7.06	266
	0.02	0.01	0.990	7.42	2.75	322
		0.02	1.260	9.45	3.49	286
		0.04	1.702	12.75	4.72	256
		0.06	2.15	16.12	5.96	242
0.03	0.01	0.612	4.59	1.70	271	
	0.02	0.858	6.43	2.37	242	
	0.04	1.278	9.58	3.55	220	
	0.06	1.680	12.60	4.66	198	
5 psia He-O <sub>2</sub>	0	0.01	1.236	9.27	3.24	359
		0.02	1.494	11.20	3.93	308
		0.04	1.992	14.93	5.24	286
		0.06	ND	-	-	-
	0.01	0.01	1.157	8.68	3.05	344
		0.02	1.405	10.53	3.69	293
		0.04	1.855	13.91	4.88	271
		0.06	2.42	18.13	6.36	278
	0.02	0.01	0.978	7.34	2.57	315
		0.02	1.247	9.35	3.28	278
		0.04	1.645	12.33	4.33	242
		0.06	2.09	15.67	5.49	242
0.03	0.01	0.618	4.63	1.62	256	
	0.02	0.852	6.39	2.24	234	
	0.04	1.219	9.14	3.21	205	
	0.06	1.595	11.96	4.20	198	
7 psia N <sub>2</sub> -O <sub>2</sub>	0	0.01	1.122	8.42	3.41	366
		0.02	1.572	11.78	4.78	337
		0.04	2.25	16.87	6.85	337
		0.06	ND	-	-	-
	0.01	0.01	1.015	7.61	3.08	359
		0.02	1.476	11.07	4.49	330
		0.04	2.11	15.82	6.42	315
		0.06	ND	-	-	-
	0.02	0.01	0.835	6.26	2.54	344
		0.02	1.295	9.72	3.94	315
		0.04	1.920	14.40	5.83	293
		0.06	2.48	18.60	7.54	293
0.03	0.01	0.492	3.69	1.50	322	
	0.02	0.795	5.96	2.42	271	
	0.04	1.440	10.80	4.37	256	
	0.06	1.920	14.40	5.83	249	
7 psia He-O <sub>2</sub>	0	0.01	1.200	9.00	3.16	366
		0.02	1.545	11.59	4.08	337
		0.04	2.14	16.05	5.64	322
		0.06	ND	-	-	-
	0.01	0.01	1.158	8.69	3.06	359
		0.02	1.460	10.95	3.86	322
		0.04	2.01	15.07	5.30	308
		0.06	3.00	22.50	7.92	337
	0.02	0.01	0.918	6.88	2.42	337
		0.02	1.278	9.59	3.37	300
		0.04	1.800	13.50	4.75	266
		0.06	2.30	17.25	6.07	256
0.03	0.01	0.521	3.91	1.38	286	
	0.02	0.793	5.95	2.09	264	
	0.04	1.320	9.90	3.48	242	
	0.06	1.752	13.14	4.62	205	

\* Initial gas conditions entering the silica gel bed from the condenser  $\approx 52.5^{\circ}\text{F}$  saturated gas.\*\* Cross-sectional area of all beds is  $1/6\text{ ft}^2$ , based on the design conditions. Silica gel beds are sized to limit the amount of water passing through the bed to 0.5%, by weight, of the corresponding molecular sieve bed weight.

† Design data for molecular sieves are tabulated in Table 6-I.

ND No design is obtainable (i.e., equilibrium pressure, corresponding to initial concentration, limits the amount of water which can be removed).

TABLE 6-IV.

EFFECT OF ATMOSPHERIC COMPOSITION, PRESSURE, AND MOLECULAR SIEVE DESIGN ON  
A 3-MAN ISOTHERMAL SILICA GEL BED DESIGN

(Designs based on experimental data of figures 6-3 through 6-8)

Atmosphere	*Initial Bed Concentrations (lb adsorbate/lb bed)		**Isothermal Bed Length (ft)	Bed Material Weight (lb)	Fan Power to Overcome Pressure Drop (watts)
	Molecular Sieve	Silica Gel			
5 psia N <sub>2</sub> -O <sub>2</sub>	0	0.01	0.394	2.95	1.092
		0.02	0.435	3.26	1.205
		0.04	0.564	4.23	1.564
		0.06	ND	-	-
	0.01	0.01	0.360	2.70	0.997
		0.02	0.384	2.88	1.063
		0.04	0.468	3.51	1.297
		0.06	0.720	5.40	1.995
	0.02	0.01	0.300	2.25	0.831
		0.02	0.318	2.39	0.882
		0.04	0.366	2.74	1.015
		0.06	0.444	3.33	1.230
0.03	0.01	0.210	1.58	0.582	
	0.02	0.222	1.67	0.614	
	0.04	0.240	1.80	0.665	
	0.06	0.270	2.02	0.748	
5 psia He-O <sub>2</sub>	0	0.01	0.420	3.15	1.103
		0.02	0.456	3.42	1.198
		0.04	0.588	4.41	1.545
		0.06	ND	-	-
	0.01	0.01	0.372	2.79	0.976
		0.02	0.405	3.04	1.064
		0.04	0.480	3.60	1.261
		0.06	0.690	5.18	1.812
	0.02	0.01	0.309	2.32	0.812
		0.02	0.324	2.43	0.851
		0.04	0.372	2.79	0.977
		0.06	0.444	3.33	1.166
0.03	0.01	0.210	1.58	0.551	
	0.02	0.222	1.67	0.583	
	0.04	0.246	1.84	0.647	
	0.06	0.270	2.03	0.709	
7 psia N <sub>2</sub> -O <sub>2</sub>	0	0.01	0.390	2.92	1.185
		0.02	0.426	3.20	1.189
		0.04	0.588	4.41	1.787
		0.06	ND	-	-
	0.01	0.01	0.360	2.70	1.094
		0.02	0.390	2.93	1.185
		0.04	0.492	3.69	1.495
		0.06	ND	-	-
	0.02	0.01	0.318	2.38	0.966
		0.02	0.342	2.56	1.040
		0.04	0.396	2.97	1.205
		0.06	0.540	4.05	1.641
0.03	0.01	0.228	1.71	0.692	
	0.02	0.252	1.89	0.766	
	0.04	0.270	2.03	0.821	
	0.06	0.312	2.34	0.948	
7 psia He-O <sub>2</sub>	0	0.01	0.432	3.24	1.140
		0.02	0.465	3.49	1.227
		0.04	0.612	4.59	1.615
		0.06	ND	-	-
	0.01	0.01	0.390	2.92	1.030
		0.02	0.420	3.15	1.108
		0.04	0.522	3.91	1.377
		0.06	1.020	7.65	1.900
	0.02	0.01	0.330	2.47	0.871
		0.02	0.348	2.61	0.919
		0.04	0.408	3.06	1.076
		0.06	0.622	3.91	1.171
0.03	0.01	0.234	1.76	0.618	
	0.02	0.246	1.84	0.649	
	0.04	0.270	2.03	0.712	
	0.06	0.306	2.29	0.807	

\* Initial gas conditions entering the silica gel bed from the condenser  $\approx 52.5^{\circ}\text{F}$  saturated gas.\*\* Cross-sectional area of all beds is  $1/6 \text{ ft}^2$ , based on the design conditions. Silica gel beds are sized to limit the amount of water passing through the bed to 0.5%, by weight, of the corresponding molecular sieve bed weight.

/ Design data for molecular sieves are tabulated in Table 6-I.

ND No design is obtainable (i.e., equilibrium pressure, corresponding to initial concentration, limits the amount of water which can be removed).

A fan efficiency of  $\eta_F = 0.20$  and a power penalty factor for an isotope Brayton electrical power system of  $PPF = 0.503 \text{ lb/W}$  were assumed. The fan power to overcome bed pressure drop,  $PWR_F$ , may be read directly from the tables. The second term in the brackets is assumed to be zero if waste heat is available. If electrical heat is used for desorption, the value may be obtained directly from the table for the case of silica gel. However, for the molecular sieve beds an additional amount of heat is added to account for desorption of the 0.5% concentration of water which passed through the silica gel bed. The heat of desorption for water was assumed to be 1400 Btu/lb and the 0.5% concentration of water was assumed to be desorbed over the 30 min vacuum desorption cycle. This resulted in an additional amount of thermal power for the molecular sieves which was added to the value in table 6-I. The 1.75 multiplying factor on the last term of the above equation was assumed to account for an integral heat exchanger, enclosing canister, and weight of the bed material. Table 6-V presents the results of the weight penalty trends.

The weight penalty trend data, for the case of waste heat desorption, indicate that low initial concentrations for both beds are desirable. For this case the effect of the atmospheric gas is small with the higher pressure, more dense gas yielding a slight weight advantage. The weight penalty data using electrical heat for desorption indicates an opposite trend with high initial bed concentrations yielding the minimum weight penalties.

An approximate bed design can be determined by hand calculations using data presented in ref. 6-8 together with the experimental mass transfer data. The following discussion will explain the necessary steps and calculations required to obtain a bed design that should approach the isothermal case. Fig. 6-9, taken from ref. 6-8, presents the necessary dimensionless mass transfer relationships, nomenclature, and basic assumptions required for the use of the data. Probably the most stringent of the assumptions is that the slope of the isotherm be constant. If inlet gas concentrations are large and/or the heat of adsorption for the adsorbate gas is high, the bed heats up and is not isothermal, therefore, the assumption of a linear isotherm is invalid. This will become apparent when the results of the example below are compared to the computer designs which are not restricted to the linear isotherm assumption and which account for the heat of adsorption and convective heat transfer.

The first example chosen was the design of a molecular sieve bed for a 7 psia  $N_2-O_2$  gas mixture with an initial bed concentration  $w_i = 0$ . The design criteria used is identical to that described above for the computer cases. The following gas and bed properties were used.

$$T_G = 50^\circ\text{F}$$

$$C_P = 0.233 \text{ Btu/lb}^\circ\text{F}$$

$$\mu = 0.0446 \text{ lb/ft-hr}$$

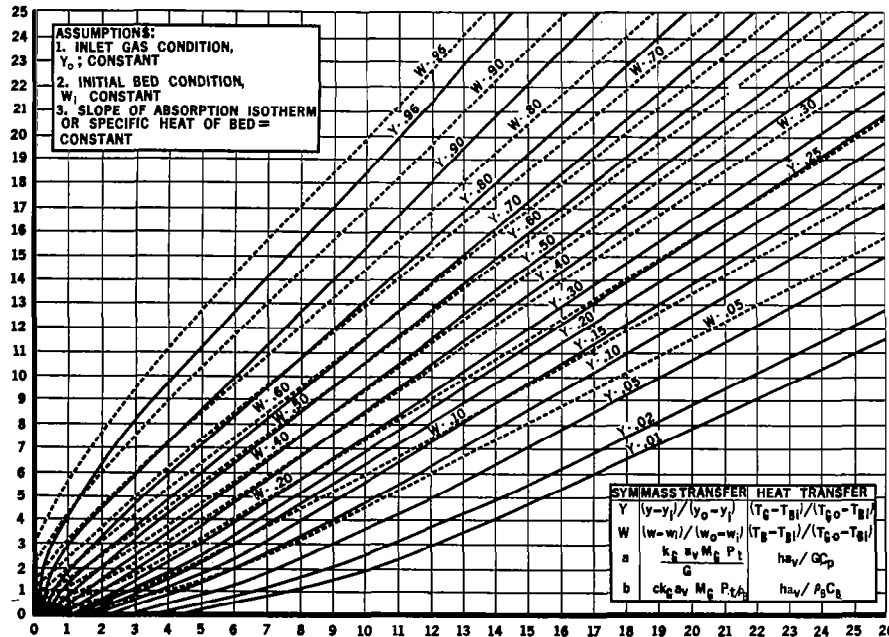
$$k = 0.0144 \text{ Btu/hr-ft}^\circ\text{F}$$

TABLE 6-V.  
TOTAL WEIGHT PENALTY TRENDS FOR 3-MAH ADIABATIC MOLECULAR SIEVE  
AND SILICA GEL BED DESIGNS

Atmosphere	Total Weight Penalty (lb)					
	Initial Bed Concentrations (lb adsorbate/lb bed)		Using Waste Heat for Desorption		Using Electrical Heat for Desorption	
	Molecular Sieve	Silica Gel	Molecular Sieve	Silica Gel	Molecular Sieve	Silica Gel
5 psia N <sub>2</sub> -O <sub>2</sub>	0	0.01	5.78	24.73	62.8	205.2
		0.02		30.22		188.7
		0.04		40.77		188.1
		0.06		-		-
	0.01	0.01	7.44	23.16	47.5	192.6
		0.02		28.62		183.4
		0.04		38.13		177.9
		0.06		51.15		195.0
	0.02	0.01	11.18	19.92	46.2	181.9
		0.02		25.21		169.0
		0.04		34.17		163.0
		0.06		43.20		164.8
0.03	0.01	20.29	12.29	39.8	148.6	
	0.02		17.21		138.8	
	0.04		25.68		136.3	
	0.06		33.82		133.4	
5 psia He-O <sub>2</sub>	0	0.01	5.98	24.37	63.4	204.9
		0.02		29.48		184.4
		0.04		39.31		183.1
		0.06		-		-
	0.01	0.01	7.90	22.85	49.5	195.5
		0.02		27.70		175.0
		0.04		36.62		172.9
		0.06		47.75		187.6
	0.02	0.01	11.86	19.31	46.3	177.7
		0.02		24.61		164.4
		0.04		32.49		154.2
		0.06		41.23		162.9
0.03	0.01	21.72	12.19	42.8	141.0	
	0.02		16.82		134.5	
	0.04		24.07		137.2	
	0.06		31.49		131.1	
7 psia N <sub>2</sub> -O <sub>2</sub>	0	0.01	5.28	23.31	61.9	207.3
		0.02		32.64		202.1
		0.04		46.73		216.2
		0.06		-		-
	0.01	0.01	6.54	21.07	44.4	201.6
		0.02		30.68		196.7
		0.04		43.85		202.3
		0.06		-		-
	0.02	0.01	8.90	17.34	42.4	190.3
		0.02		26.90		185.3
		0.04		39.85		187.2
		0.06		51.53		198.8
0.03	0.01	16.18	10.22	31.4	172.2	
	0.02		16.52		152.8	
	0.04		29.88		158.6	
	0.06		39.86		165.1	
7 psia He-O <sub>2</sub>	0	0.01	5.54	23.70	62.5	207.7
		0.02		30.56		200.1
		0.04		42.28		204.3
		0.06		-		-
	0.01	0.01	6.97	22.89	46.1	203.4
		0.02		28.88		190.9
		0.04		39.73		194.7
		0.06		49.25		218.8
	0.02	0.01	9.98	18.13	43.9	187.6
		0.02		25.26		176.1
		0.04		35.58		179.4
		0.06		45.46		174.2
0.03	0.01	18.62	10.30	36.7	154.1	
	0.02		15.68		148.5	
	0.04		26.09		147.8	
	0.06		34.61		137.7	

# HEAT OR MASS TRANSFER IN A PACKED BED

DIMENSIONLESS TIME PARAMETER, bt



DIMENSIONLESS LENGTH PARAMETER, ax

Symbol	Definition	Dimensions
$a_v$	Bed material superficial surface area	Sq. Ft./Cu. Ft.
$c$	Absorption isotherm effective slope	$\frac{\text{lb. adsorbate in gas/lb. gas}}{\text{lb. adsorbate in bed/lb. bed}}$
$C_B$	Effective specific heat of bed material	BTU/lb. °F
$C_p$	Specific heat of carrier gas at constant pressure	BTU/lb. °F
$G$	Mass velocity	lb./hr. sq. ft.
$h$	Heat transfer coefficient	BTU/hr.-sq. ft.-°F
$k_G$	Mass transfer coefficient	lb. moles/hr.-sq. ft. atmos.
$M_G$	Molecular weight of carrier gas	lb./lb. mole
$P_t$	Total pressure of gas	atmospheres
$t$	Time	hrs.
$T_B$	Temperature of bed	°F
$T_{Bi}$	Initial temperature of bed at $t=0$	°F
$T_G$	Temperature of gas stream	°F
$T_{Go}$	Inlet temperature of gas stream at $x=0$	°F
$w$	Adsorbate concentration in bed	lb. adsorbate/lb. bed
$w_i$	Initial adsorbate concentration in bed at $t=0$	lb./lb.
$w_0$	Equilibrium concentration of adsorbate in bed corresponding to $y_0$	lb./lb.
$x$	Bed length	ft.
$y$	Adsorbate concentration in carrier gas	lb. adsorbate/lb. carrier gas
$y_i$	Adsorbate concentration in carrier gas corresponding to equilibrium with initial bed conditions $w_i$	lb./lb. carrier gas
$y_0$	Adsorbate concentration in carrier gas at inlet of bed, $x=0$	lb./lb. carrier gas
$\rho_B$	Bed density	lb./cu. ft. bed

Figure 6-9 Heat or Mass Transfer in a Packed Bed

$$\begin{aligned}\rho &= 0.0384 \text{ lb/ft}^3 \\ D_p &= 0.0119 \text{ ft} \\ a_v &= 309 \text{ ft}^2/\text{ft}^3 \\ \rho_B &= 43 \text{ lb/ft}^3\end{aligned}$$

from the design criteria

$$V_s A_F = 10 \text{ cu ft/min}$$

$$V_s = 60 \text{ ft/min} = 3600 \text{ ft/hr}$$

$$\begin{aligned}Re &= \frac{\rho V_s D_p}{\mu} \\ &= \frac{0.0384(3600)0.0119}{0.0446} \\ &= 36.9\end{aligned}$$

from the mass transfer data in fig. 6-4

$$\begin{aligned}\frac{k_G P_t M_G D_p}{\mu} &= 0.87 \\ k_G P_t M_G &= 0.87 \left( \frac{0.0446}{0.0119} \right) \\ &= 3.26\end{aligned}$$

To use the dimensionless mass transfer data presented in fig. 6-9, the dimensionless time parameter (bt) must be determined.

$$bt = \frac{c k_G a_v M_G P_t t}{\rho_B}$$

for the adsorption cycle,  $t = 0.5 \text{ hr}$ .

$$\begin{aligned}bt &= \frac{c(309)3.26(0.5)}{4.3} \\ &= 11.73 \text{ c}\end{aligned}$$

Fig. 6-10 presents carbon dioxide isotherm test data for Linde 5A molecular sieve material obtained from NASA Contract No. NAS9-3541. These data are required to determine the slope of the isotherm (c). The slope is determined by picking two values from the isotherm on which the bed operates. One value should be near the initial bed concentration and the other value should correspond to a bed saturated at the inlet adsorbate pressure or, if known, the average bed concentration at the end of the run.

From fig. 6-10 at a bed temperature of  $T_G = 50^\circ\text{F}$

$$\begin{aligned} w_1 &= 0.008 \text{ lb adsorbate/lb bed} & w_2 &= 0.079 \text{ lb adsorbate/lb bed} \\ P_1 &= 0.1 \text{ mmHg} & P_2 &= 5 \text{ mmHg} \end{aligned}$$

for dilute solutions of adsorbate gas, the inlet gas concentration is

$$\begin{aligned} y &= P \left( \frac{M_A}{P_t M_G} \right) \\ &= P \frac{44}{362(30)} \\ &= 0.00405P \end{aligned}$$

$$\therefore y_1 = 0.00041 \text{ lb adsorbate/lb gas}$$

$$y_2 = 0.02025 \text{ lb adsorbate/lb gas}$$

$$\begin{aligned} c &= \frac{y_2 - y_1}{w_2 - w_1} = \frac{0.02025 - 0.00041}{0.079 - 0.008} \\ &= 0.2795 \end{aligned}$$

$$\therefore bt = 11.73 (0.2795)$$

$$\underline{\underline{bt = 3.28}}$$

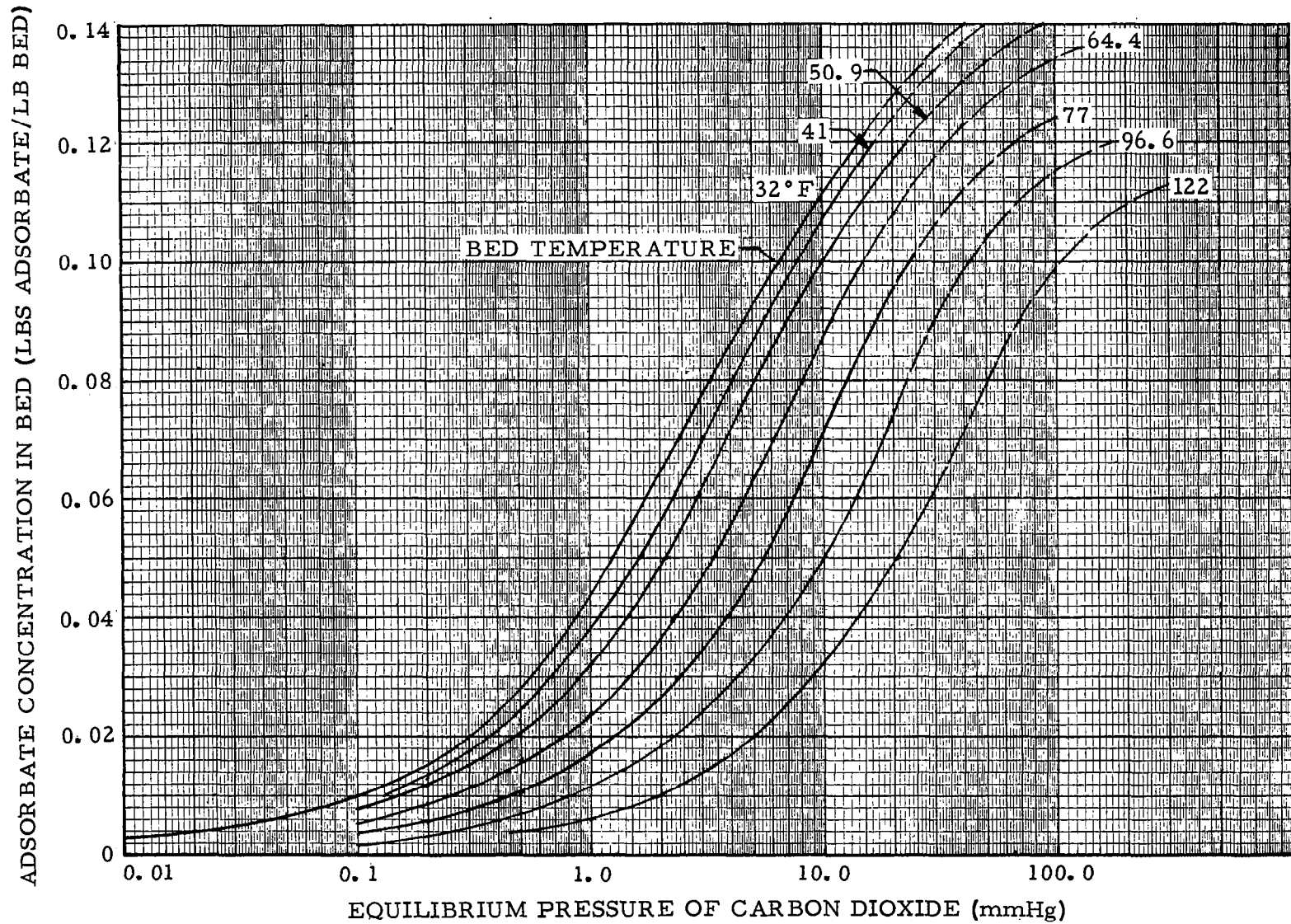


FIGURE 6-10 CARBON DIOXIDE ISOTHERM TEST DATA FOR LINDE 5A, 1/16" DIA. PELLETS

next, the dimensionless length parameter ( $ax$ ) is evaluated

$$\begin{aligned} ax &= \frac{k_G a_v M_G P_t x}{G_s} \\ &= \frac{3.26(309) x}{0.0384 (3600)} \\ &= 7.31 x \end{aligned}$$

solving for  $x$

$$x = \frac{ax}{7.31} \text{ ft}$$

next, the equation for the dimensionless bed concentration parameter ( $W$ ) is solved for  $w$

$$\begin{aligned} W &= \frac{w - w_i}{w_o - w_i} \\ w &= w_i - W (w_o - w_i) \end{aligned}$$

for this case

$$w_i = 0$$

and

$$w_o = 0.079$$

$$\therefore \underline{w = 0.079 W} \quad \text{lb adsorbate/lb bed}$$

By using the calculated value of  $bt$ , corresponding values of  $W$  and  $ax$  are read from fig. 6-9. These values are tabulated, and, then, values for  $x$  and  $w$  are determined. The results for this case are shown in table 6-VI.

Fig. 6-11 presents a plot of bed concentration ( $w$ ) versus bed length ( $x$ ) after the 30-min adsorption cycle. The difference between  $w$  and  $w_i$  can be

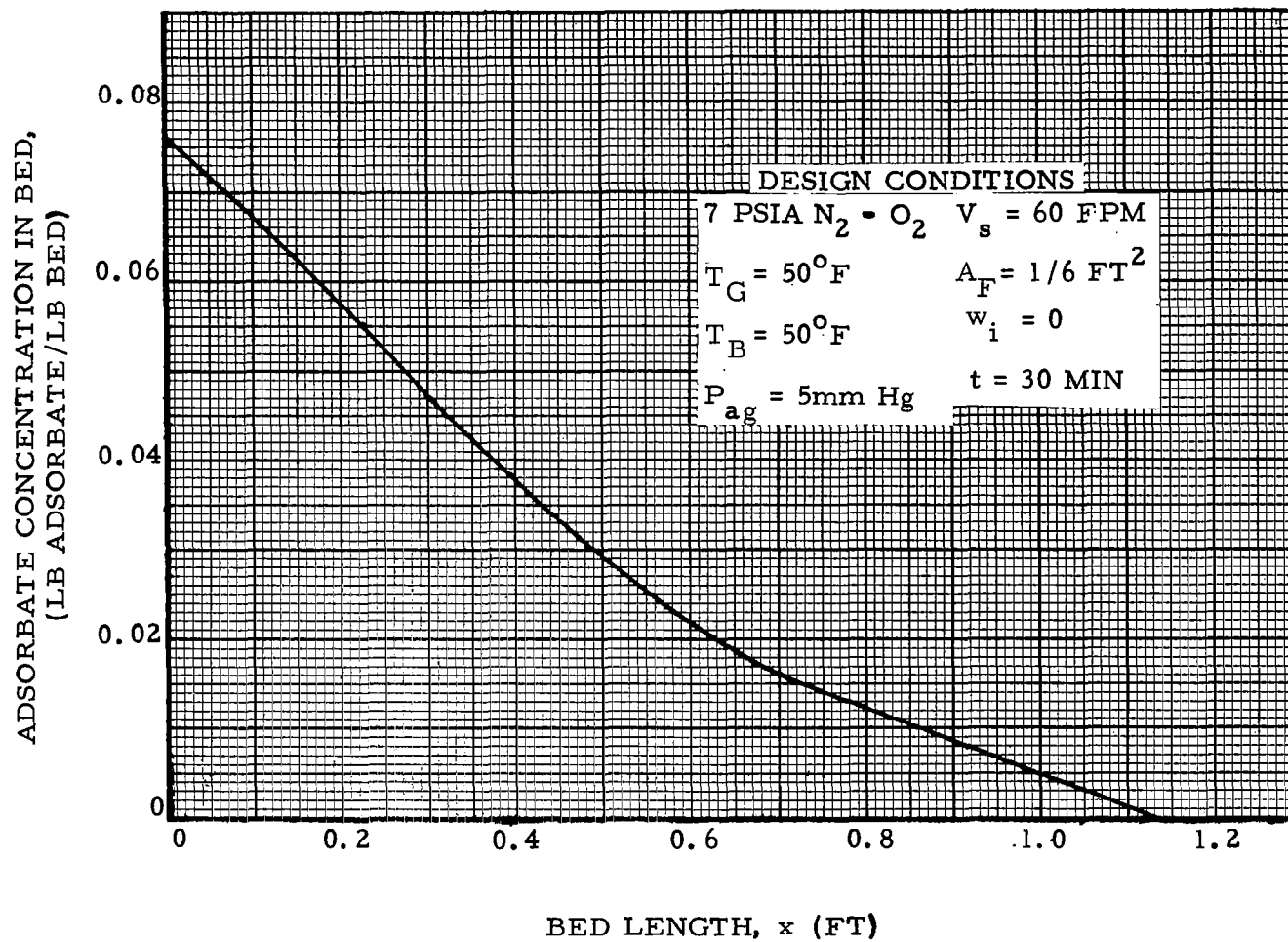


FIGURE 6-11  $CO_2$  LOADING FOR MOLECULAR SIEVE EXAMPLE - CALCULATED USING FIGURE 6-9

TABLE 6-VI  
 MASS TRANSFER DATA FOR A 7-PSIA N<sub>2</sub>-O<sub>2</sub> MOLECULAR  
 SIEVE BED FROM FIG. 6-9

Dimensionless bed concentration parameter, W	Dimensionless length, parameter, ax	Bed length, x (ft)	Bed concentration, w (lb adsorbate/ lb bed)
0.96	0.03	0.0041	0.0758
0.90	0.45	0.0616	0.0711
0.80	1.05	0.1437	0.0632
0.70	1.65	0.226	0.0553
0.60	2.17	0.297	0.0474
0.50	2.80	0.383	0.0395
0.40	3.45	0.472	0.0316
0.30	4.17	0.571	0.0237
0.20	5.20	0.712	0.0158
0.10	6.70	0.917	0.0079
0.05	8.20	1.122	0.0004

integrated along the length of the bed and multiplied by the weight of the bed per unit length to yield the weight of gas adsorbed. The equation describing this procedure is

$$WT_A = \int_0^L (w - w_i) \rho_B A_F dx \quad (6-37)$$

Fig. 6-12 presents the results of this integration as a plot of adsorbed gas weight ( $WT_A$ ) versus bed length ( $x$ ).

To satisfy the bed design conditions, it is necessary to find the length of bed that yields the proper amount of adsorbed gas ( $WT_A$ ). For the molecular sieve designs,  $WT_A$  is calculated by the following equation:

$$WT_A = \frac{(\text{no. of men}) (\text{CO}_2 \text{ generation rate/man})}{(\text{adsorption cycle time})}$$

$$= 3 \left( \frac{2.25}{24} \right) 0.5$$

$$\underline{\underline{WT_A = 0.1405 \text{ lb}}}$$

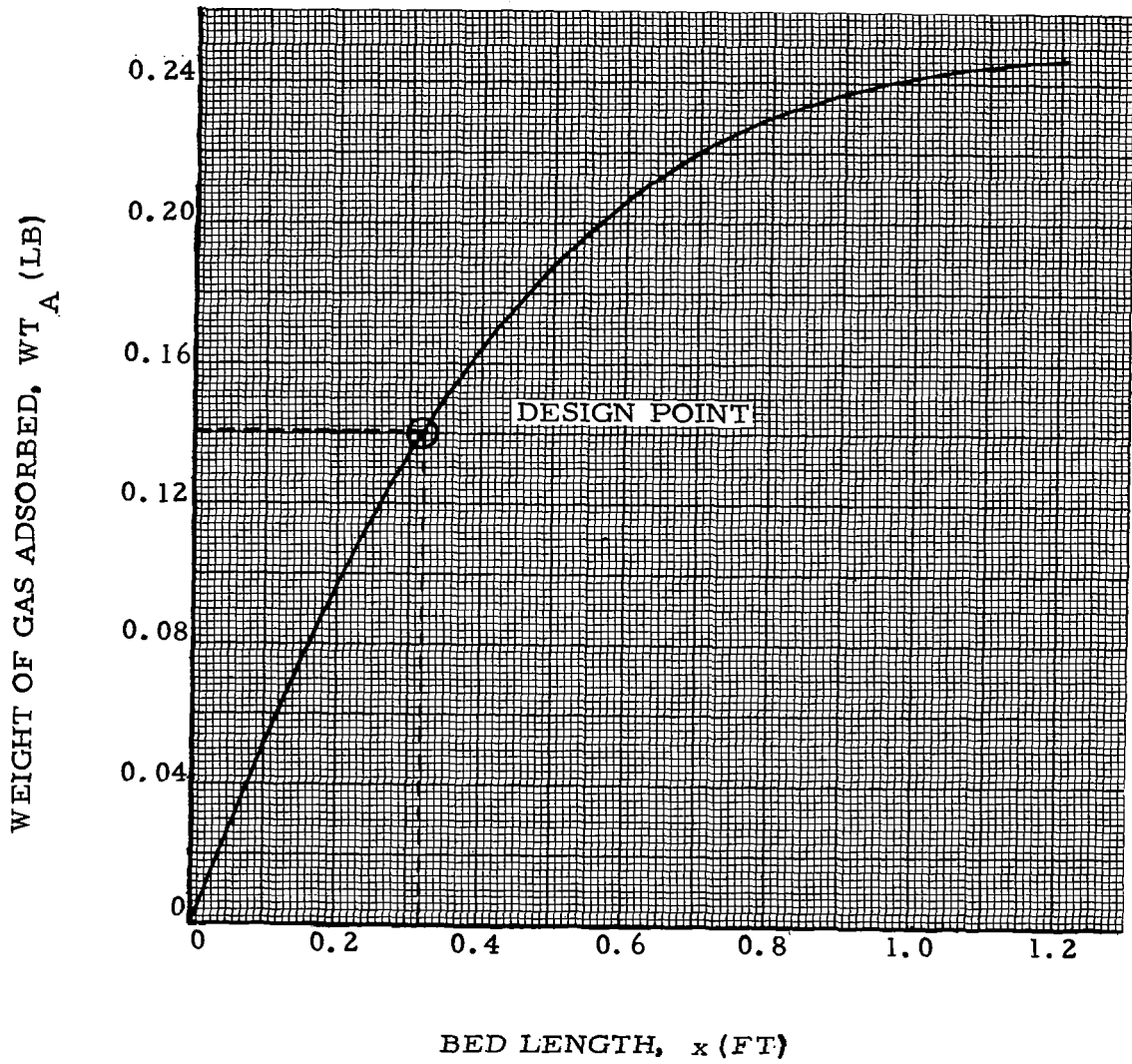


FIGURE 6-12 WEIGHT OF CO<sub>2</sub> ADSORBED VERSUS BED LENGTH FOR MOLECULAR SIEVE EXAMPLE

The bed length corresponding to this value of  $WT_A$  is read from fig. 6-12.

$$\underline{\underline{L_B = 0.320 \text{ ft}}}$$

The procedure outlined above was also used for a bed with an initial concentration of  $w_i = 0.03$ . Table 6-VII presents the results and shows the comparison between the computer designs and the hand-calculation method.

TABLE 6-VII  
COMPARISON OF MOLECULAR SIEVE BED LENGTHS

Atmosphere	Initial bed concentration (lb adsorbate/lb bed)	Bed length (ft)	
		Hand-calculated design	Adiabatic computer design
7 psia N <sub>2</sub> -O <sub>2</sub>	0	0.320	0.337
	0.03	0.567	1.030

The bed length obtained by hand calculation is smaller than that determined by the computer, which accounts for the heat of adsorption and convective heat transfer. To determine the slope of the isotherm (required for the hand-calculation method), the bed was assumed to be isothermal. Therefore, this design is expected to be smaller than the adiabatic computer design. If the bed is adiabatic, it is difficult to estimate the effective slope of the isotherm that would yield the proper bed size; however, if the bed is cooled, the hand-calculation method should yield a reasonable bed design.

Several silica gel beds for a 7-psia N<sub>2</sub>-O<sub>2</sub> gas mixture were also designed from the data on fig. 6-9. Table 6-VIII shows the results of these designs and also tabulates the adiabatic and isothermal computer designs for a comparison. Silica gel isotherm data were taken from ref. 6-7.

TABLE 6-VIII  
COMPARISON OF SILICA GEL BED LENGTHS

Initial bed concentration (lb adsorbate/lb bed)			Bed length (ft)			
Atmosphere	Molecular sieve	Silica gel	Hand-calculated design	Isothermal computer design	Adiabatic computer design	
7 psia N <sub>2</sub> -O <sub>2</sub>	0	0.01	0.700	0.390	1.122	
		0.04	ND	0.588	2.25	
	0.03	0.01	0.370	0.228	0.492	
			0.735	0.312	1.440	
		0.04				

ND = No design is obtainable.

The silica gel bed lengths obtained by the hand-calculation method lie between the isothermal and adiabatic bed lengths obtained from the computer program. This probably yields a reasonable design for a cooled bed. It was anticipated that the bed length for the hand-calculated design would more closely match the isothermal computer design; however, the significant difference indicated in table 6-VIII might result from the large amount of extrapolation required on the plot of silica gel concentration versus bed length. Only four points were available from fig. 6-9 because the slopes of the silica gel isotherm are an order of magnitude smaller than molecular sieve isotherm slopes. The small slopes of the silica gel isotherms result in small values of the dimensionless time parameters (for the cases taken  $bt = 0.044, 0.047$ ). These small values of  $bt$  yield only four pairs of  $W$  and  $ax$  for each case (see fig. 6-9). The largest  $x$  value obtained was  $x = 0.281$  ft. It is apparent, for these cases, that the dimensionless bed concentration parameter ( $W$ ) on fig. 6-9 needs to be extended to lower values of  $W = 0.02, 0.01$ . This may be done by using the method outlined in ref. 6-8.

### CONCLUSIONS AND RECOMMENDATIONS

The major components affected by cabin atmosphere selection are those which are found in the cabin ventilation, humidification, temperature control, and purification systems. Analysis and simple tests were performed on a molecular sieve bed, a silica gel bed, and a heat exchanger configuration which could be used in a spacecraft life support system. The theory, experimental data, and typical design data presented can be used to determine the effect of cabin atmosphere and pressure level selection on the major life

support system components. Sec. 7 applies the data presented herein to determine effect of atmospheric selection on a total integrated life support. The weight penalty data presented in Sec. 7 indicates that the heat and mass transfer components provide very little influence upon the total system weight penalty. Table 6-IX indicates the effect of atmospheric selection on component weight, fan power, and total weight penalty for a typical three-man system.

For the example heat exchanger cases evaluated, overall weight penalty savings were obtained for He-O<sub>2</sub> gas mixtures at increased cabin pressure level. The heat exchangers for N<sub>2</sub>-O<sub>2</sub> gas mixtures at equivalent design conditions weighed less; however, the pressure drop and power requirement were generally higher. The actual magnitude of weights for cabin air to liquid heat exchangers are very dependent upon the particular design application.

For the example adsorption bed designs evaluated, overall weight penalty savings were generally obtained for N<sub>2</sub>-O<sub>2</sub> gas mixtures at increased cabin pressure level. Total weight penalties generally differ less than 5% between the He-O<sub>2</sub> and N<sub>2</sub>-O<sub>2</sub> atmospheres at equivalent design conditions. The example designs were generated by a computer program which used the experimental heat and mass transfer data. Molecular sieve designs were based on an adiabatic bed design, and, because the bed temperature did not increase significantly, no isothermal cases were run. However, both adiabatic and isothermal bed designs were used for silica gel. The high heat of adsorption and large amounts of water entering the silica gel bed produced significant changes in the bed temperatures for the adiabatic design, thereby requiring large beds. The isothermal silica gel bed designs were run to provide the minimum bed sizes, which were approximately 1/3 to 1/6 the size of the adiabatic designs. An actual spacecraft silica gel bed design will probably be cooled during adsorption and, therefore, lie between size limits determined for the adiabatic and isothermal bed designs.

From a comparison of the computer cases to hand-calculation cases based on ref. 6-8 and fig. 6-9, it was determined that the hand-calculation method was adequate for the design of cooled beds (nearly isothermal) but could give erroneous answers if applied to adiabatic bed design. This is mainly the result of the assumption of a linearized isotherm inherent in the derivation of the data presented in fig. 6-9 and in the difficulty of defining an effective isotherm slope for a nonisothermal bed design.

The adsorption bed test data indicate a need for more heat and mass transfer testing in the lower Reynolds number regions which encompass spacecraft ECS bed designs. It is recommended that low adsorbate gas concentrations be used and/or that the beds be cooled when future mass transfer tests are run. This will enable the bed to remain nearly isothermal and result in more accurate determination of the mass transfer coefficients and ease the task of data reduction. Following these tests, it is suggested that tests be conducted with bed material packed into a compact heat exchanger core. It is desirable that the adsorbent materials be cooled during adsorption (to increase adsorption capability and reduce required bed material weight)

TABLE 6-IX  
EFFECT OF CABIN ATMOSPHERE ON TYPICAL COMPONENTS FOR A  
THREE-MAN SYSTEM

Component	Pressure level (psia)	Nominal weight for N <sub>2</sub> -O <sub>2</sub> (lb)	Nominal fan power for N <sub>2</sub> -O <sub>2</sub> (W)	Weight Ratio WT <sub>N<sub>2</sub></sub> / WT <sub>He</sub>	Fan power ratio PWR <sub>N<sub>2</sub></sub> / PWR <sub>He</sub>	<sup>b</sup> Net weight penalty saving for He-O <sub>2</sub> gas mixture (lb)
Heat exchanger	5	10	15	0.893	1.63	1.69
	7	10	15	0.926	1.43	1.47
<sup>a</sup> Molecular sieve canister	5	4.7	0.42	0.952	1.03	-0.20
	7	4.2	0.42	0.924	1.07	0.36
<sup>a</sup> Silica gel canister	5	43	3.41	0.996	1.05	-0.26
	7	41	3.41	0.936	1.08	-0.39
Total system	5					1.23
	7					1.44

<sup>a</sup>Adiabatic bed designs with low initial bed concentrations and waste heat available for desorption.

<sup>b</sup>A Brayton isotope power penalty of 0.503 lb/W was assumed.

and heated during desorption (to decrease desorption time, pumping power, and final bed concentration). This requires the use of a compact heat exchanger core in direct contact with the adsorbent and having a surface area comparable to the surface area of the adsorbent. This design appears to be the most probable for future spacecraft vehicles. Other areas of testing which need to be investigated in regard to molecular sieve bed design are the thermal/vacuum desorption characteristics, the effect of coadsorption of water vapor and carbon dioxide, and the possibilities of using molecular sieves in place of silica gel as a desiccant. Another area of testing required for silica gel is the study of purge gas desorption with heat addition. These tests are necessary to generate the data required for performing valid weight penalty tradeoffs and adsorption system studies.

## REFERENCES

- 6-1. Krieth, F.; Principles of Heat Transfer. Second ed., International Textbook Company, 1965.
- 6-2. Chapman, A.; Heat Transfer. First ed., The MacMillan Company, New York, 1960.
- 6-3. Integration and Optimization of Space Vehicle Environmental Control Systems. ASD-TR-61-176, Part II. Wright-Patterson Air Force Base, Ohio, April 1963.
- 6-4. Chemical Engineer's Handbook. Fourth ed., McGraw-Hill Book Company, Inc., 1963.
- 6-5. Ind. Eng. Chem., 26, 1183, Chilton and Colburn, 1934.
- 6-6. Low Temperature Adsorption of Carbon Dioxide. ASD-TR-62-560. Wright-Patterson Air Force Base, Ohio, September 1962.
- 6-7. Adsorption and Dehydration with Silica Gel. Technical Bulletin 202. W. R. Grace & Co., Davidson Chemical Division, 1958.
- 6-8. Jackson, J. K.; Heat and Mass Transfer Analysis of Adsorption Beds Used in Spacecraft Life Support Systems. Douglas Report No. SM-47721, September 1964.

## Section 7

### THE EFFECT OF ATMOSPHERE SELECTION ON LIFE SUPPORT SYSTEM PENALTY

The experimental data and analyses from previous sections will be applied to an example problem to show the effect on an integrated life support system resulting from the selection of cabin atmosphere composition and pressure. Based on the review of experimental data and analysis, the major life support subsystems that are the most influenced by the selection of atmosphere composition and pressure are the following:

- (1) Atmospheric Supply and Pressurization System.
- (2) Thermal Control System.
- (3) Atmospheric Purification and Control System.

The following definitions of the functions of the above life support subsystems will be used in the example problem. The atmospheric supply and pressurization system is used to provide oxygen for crew breathing as well as gas to compensate for leakage losses, recompression, and airlock loss. The thermal control system provides cooling for the cabin gas, humidity control for the cabin and other equipment, as well as most of the ventilation. The atmosphere purification and control system is used to remove carbon dioxide, odors, and other contaminants from the processed gas.

It is not intended to present material in this section for the development of a detailed life support computer program to complete general tradeoff and performance studies. The NASA/Douglas "G-189 Generalized Environmental Control and Life Support Computer Program," and Air Force ASD TDR-63-328 computer program, "Transient Performance of Atmosphere Control Systems," and similar programs can be used to complete this type of task. Therefore, simplified analyses and data were used to evaluate the thermal control system heat exchanger, condenser, fans, and distribution system penalty for the example problem to determine the differences in equivalent system weight caused by the choice of atmosphere composition and pressure. The procedure for evaluating the atmosphere supply and pressurization system penalty, airlock penalty, and CO<sub>2</sub> removal penalty was presented in secs. 1 through 6. The methodology for penalty evaluation for the example problem is given in the following discussion.

## METHODOLOGY FOR PENALTY EVALUATION

### Atmospheric Supply and Pressurization System

Cabin pressure level, gas composition, and temperature level for comfort can be selected as a starting point from comfort zone test data in sec. 2. Spacecraft gas makeup to compensate for leakage, repressurization, and makeup requirements can be evaluated using sec. 3. Airlock penalty for a system which conserves gas by pumping it into the main cabin for eventual use is also given. Other types of airlock configurations may be evaluated by using the information given in sec. 4. The atmospheric supply and pressurization system weight to supply makeup gas and metabolic oxygen can be determined for different types of storage by using the data in sec. 5. A representative atmospheric supply and pressurization system weight and penalty comparison for helium-oxygen and nitrogen-oxygen gas mixtures is presented in the example problem in this section.

### Thermal Control System

The thermal control system includes the cabin heat exchanger, condenser, fans, and liquid coolant from a radiator. The system arrangement analyzed, as shown in fig. 7-1, is a representative arrangement proposed for many vehicles under consideration.

Thermal and Mass Balance. -- Thermal and mass balances were obtained using the procedure discussed below for the system shown in fig. 7-1. For the thermal and mass balance evaluation, the condenser was considered to remove the water generated by the crew in the cabin, the CO<sub>2</sub> adsorption subsystem to remove the CO<sub>2</sub>, and the cabin heat exchanger to remove the total cabin sensible heat load minus the sensible load removed by the condenser. Heat loads generated by the fans were also removed by the condenser and the heat exchanger. The fan heat loads effectively increased the specified total sensible heat load.

The required effectiveness values were determined for the condenser and the heat exchangers based on the thermal balance. The effectiveness values were used to obtain corresponding values of heat exchanger UA from data for single-pass crossflow heat exchangers given in fig. 7-2 (ref. 7-1). This condenser and heat exchanger configuration was used because it represents the typical method of fabrication for this type of heat exchanger.

Representative correction factors for heat exchanger hardware weight difference, fan power penalty, and pressure drop differences using helium-oxygen and nitrogen-oxygen between 5 and 10 psia pressure are given in sec. 6. The correction factors indicate, in most instances, that a negligible weight and power penalty difference is incurred due to choice of atmosphere composition and pressure level as compared to the total thermal control system weight. The major savings in penalty in the thermal control system is

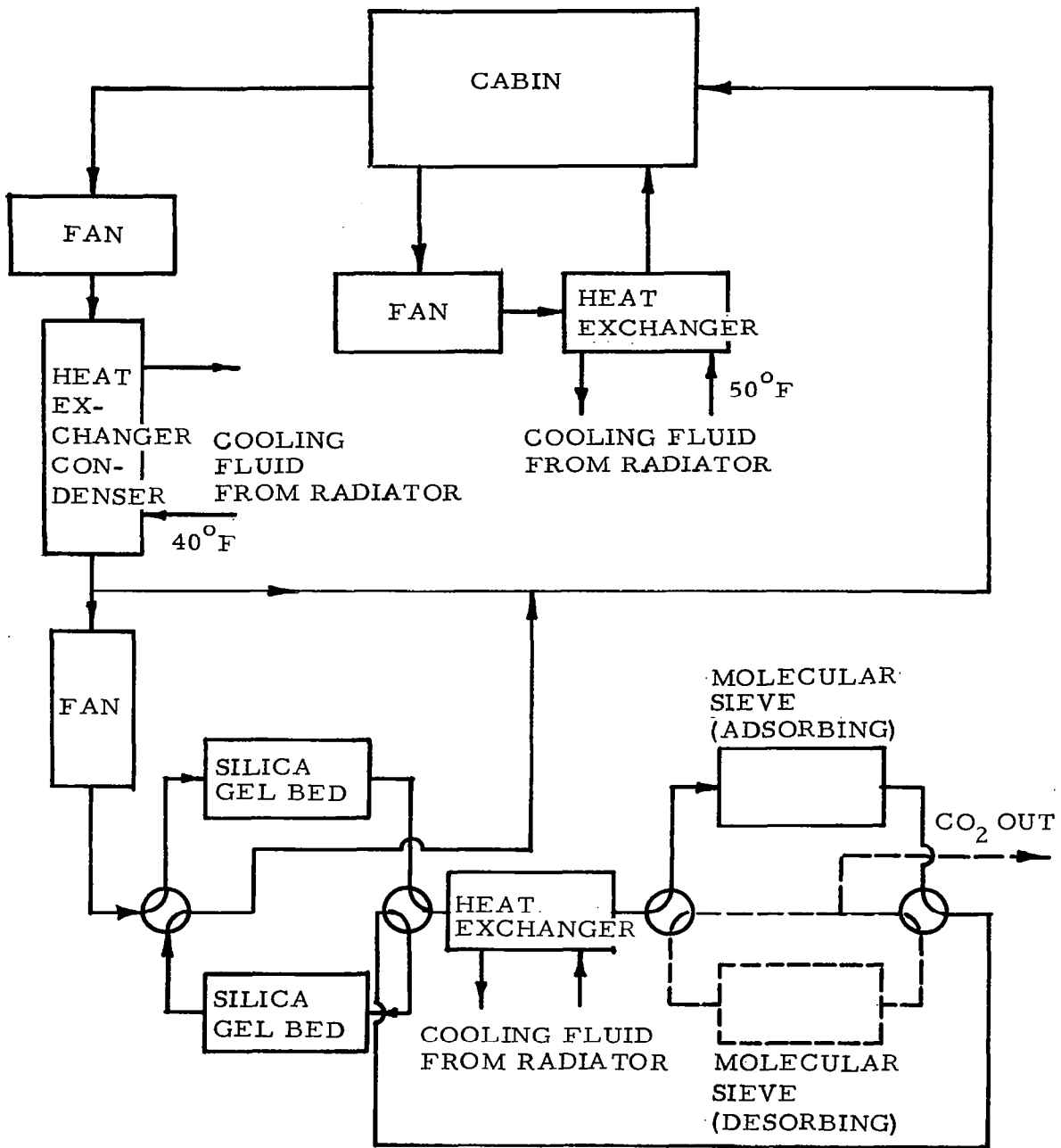


FIGURE 7-1 THERMAL AND ATMOSPHERIC CONTROL SYSTEM

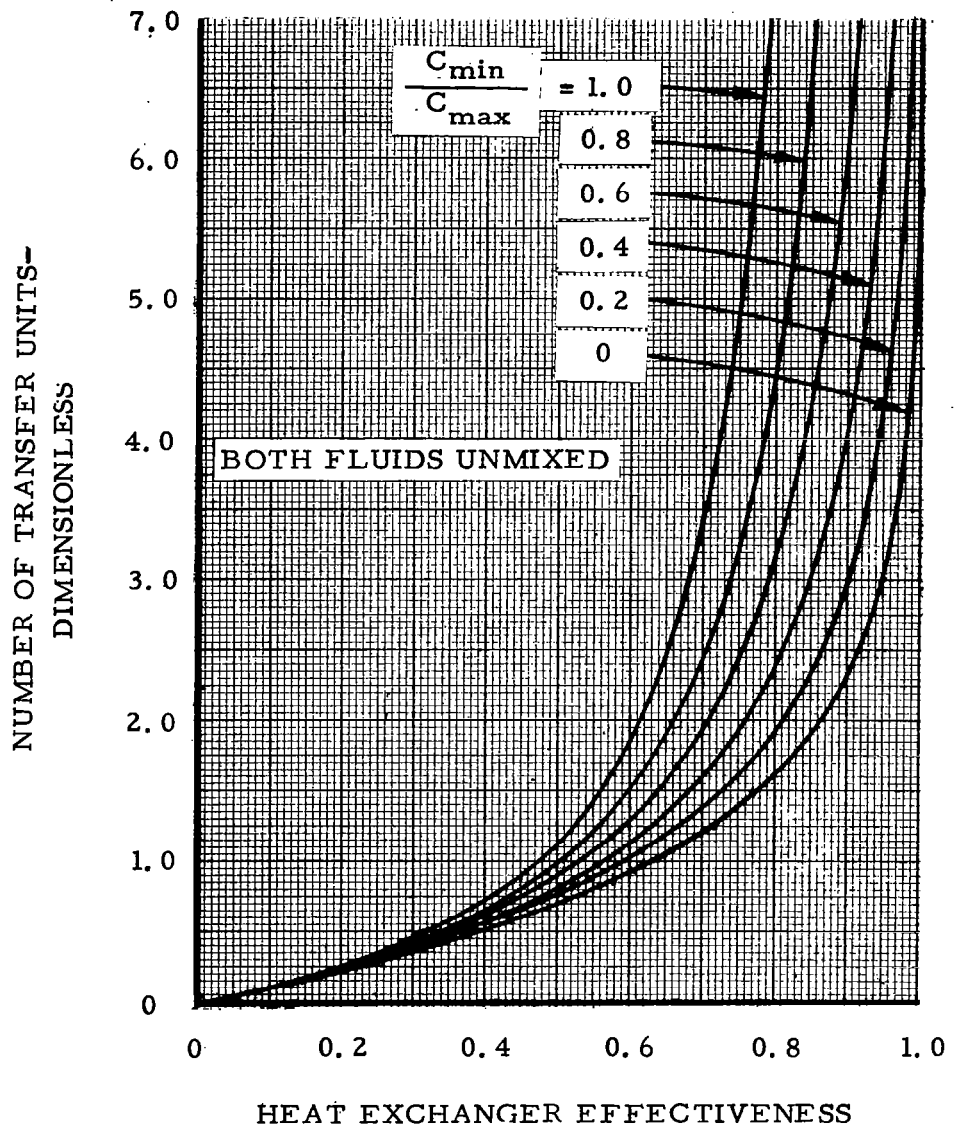


FIGURE 7-2 SINGLE-PASS CROSSFLOW HEAT EXCHANGER PERFORMANCE

achieved by increased allowable cabin temperature level, which reduces gas mass flow and therefore fan power. Comfort tests reported in sec. 2 indicate that helium diluent permits a 5° to 7°F higher allowable cabin temperature level for comfort and, hence, reduces fan power penalty as will be shown later.

Revised heat loads were determined from the heat exchanger/fan sizing computations. An iterative procedure was used to correct the thermal balances as a result of revised fan heat loads. Input data for the evaluation included boundary conditions and combinations of gas flow rates to the cabin heat exchanger and the condenser, temperature rises for the liquid sides of the heat exchangers, and trial temperature rises due to the fans. Thermal/physical property data for the fluids from tables 7-I and 7-II were also used. The following steps were used in determining UA values for both cabin condenser and heat exchanger.

Water vapor flow rates into and out of the condenser were determined from the required condensing rate and the condenser gas flow rate as follows. From Dalton's Law

$$\dot{w}_{v, i} = \dot{w}_g \frac{M_v}{M_g} \left( \frac{P_k}{P_{v, k}} - 1 \right)^{-1} \quad (7-1)$$

$$\dot{w}_{v, o} = \dot{w}_{v, i} - \dot{w}_{v, gen} \quad (7-2)$$

Vapor pressure and corresponding saturation temperature at the condenser exit were determined by the vapor flow. The condensing rate and sensible heat rate were added and a corresponding effective specific heat was obtained.

$$P_{v, o} = \frac{P_k}{1 + \frac{\dot{w}_g M_y}{\dot{w}_{v, o} M_g}} \quad (7-3)$$

$T_{v, o}$ , the saturation temperature corresponding to  $P_{v, o}$ , was obtained from the relationships in ref. 7-2.

$$\dot{q}_c = \dot{w}_{v, gen} \Delta H_v + \dot{w}_g C_{p, g} (T_k + \Delta T_{F, c} - T_{v, o}) \quad (7-4)$$

$$\bar{C}_{p, c} = \frac{\dot{q}_c}{\dot{w}_g (T_k + \Delta T_{F, c} - T_{v, o})} \quad (7-5)$$

TABLE 7-I  
ATMOSPHERE AND HEAT EXCHANGER PROPERTIES

Atmosphere									
Atmosphere	Viscosity $\mu$	Specific heat $C_p$	Ratio of specific heats $\gamma$	Thermal conductivity $k$	Molecular weight $M$	Gas constant $R$	Prandl number $Pr$	$Pr^{2/3}$	
1.5 psia $O_2$ - 3.5 psia He	0.0515	0.273	1.44	0.0255	23.6	65.5	0.499	0.671	
3.5 psia He - 3.5 psia $O_2$	0.0526	0.332	1.50	0.0355	18.0	85.8	0.493	0.624	
6.5 psia $O_2$ - 3.5 psia He	0.0533	0.413	1.51	0.0450	13.8	112	0.486	0.618	
1.5 psia $O_2$ - 3.5 psia $N_2$	0.0497	0.227	1.40	0.0152	30.8	50.1	0.725	0.807	
3.5 psia $N_2$ - 3.5 psia $O_2$	0.0480	0.233	1.40	0.0152	30.0	51.5	0.718	0.804	
6.5 psia $O_2$ - 3.5 psia $N_2$	0.0470	0.237	1.40	0.0152	29.4	52.5	0.714	0.799	
5.0 psia $O_2$	0.0520	0.220	1.40	0.0152	32.0	48.0	0.731	0.811	
14.7 psia Air	0.0460	0.240	1.40	0.0152	39.0	53.3	0.709	0.795	
Heat Exchanger	Fin effectiveness $\eta$	Hydraulic diameter $D_H$ -ft		Surface density $K_m$ -lb/ft <sup>2</sup>					
Gas side	0.99	0.0085		100.0					
Liquid side	0.97	0.0050		100.0					

TABLE 7-II  
HEAT EXCHANGER OPTIMIZATION DATA

Fluid	$K_j F_j$ (hr-° F-lb/Btu)	$K_f F_f$ (ft/hr)
3.5 psia He - 1.5 psia O <sub>2</sub>	0.0400	0.00663
3.5 psia He - 3.5 psia O <sub>2</sub>	0.0288	0.00630
3.5 psia He - 6.5 psia O <sub>2</sub>	0.0226	0.00520
3.5 psia N <sub>2</sub> - 1.5 psia O <sub>2</sub>	0.0576	0.00326
3.5 psia N <sub>2</sub> - 3.5 psia O <sub>2</sub>	0.0579	0.00171
3.5 psia N <sub>2</sub> - 6.5 psia O <sub>2</sub>	0.0580	0.00079
5.0 psia O <sub>2</sub>	0.0574	0.00376
14.7 psia Air	0.0580	0.00037
Water	0.0016	0.00056

The sensible heat load imposed on the cabin heat exchanger was determined from the specified sensible heat load, the sensible heat load removed by the condenser, and temperature rise at the heat exchanger fan. The coolant flow rates, corresponding to the specified coolant temperature rises, and for given heat loads are determined for the condenser and the heat exchanger. The flow capacitance terms  $\dot{w}C_p$ , were obtained for both flow streams in each unit. The required effectiveness for each unit is expressed by the following:

$$E = \frac{(\dot{w}C_p)_{\text{pri}} (T_k + \Delta T_{F, \text{pri}} - T_{\text{pri}, o})}{(\dot{w}C_p)_{\text{min}} (T_k + \Delta T_{F, \text{pri}} - T_{\text{sec}, i})} \quad (7-6)$$

Based on the values for flow capacitance and effectiveness, the corresponding values of UA were determined from the data in fig. 7-2.

Condenser and Cabin Heat Exchanger. -- The procedure presented by Paselk was used to determine the weights and the fan power requirements for the cabin condenser and heat exchanger (ref. 7-3).

This procedure provides general relationships used to determine heat exchanger weights and power requirements. Methods for suboptimizing heat exchangers on the basis of the Reynolds numbers on each side of the heat exchanger are included. The term suboptimization, refers to an optimum solution based on variables which directly influence the component considered, the suboptimized solution does not reflect the effects of variables which provide indirect influences. The suboptimum solution based on Reynolds numbers is obtainable because increasing the Reynolds number improves the heat transfer coefficient at the expense of increased pressure drop. An improved heat transfer coefficient permits reduced heat transfer area, with consequent reduced heat exchanger weight. Increased pressure drop increases fan power requirements, with a consequent increased system weight penalty through the weight/power penalty factor. The suboptimization relationships considered are based on the assumption that variables other than the Reynolds numbers on each side of the heat exchanger remain essentially constant. Both the Reynolds number optimization relationships and the general relationships discussed below are considered in the application of the heat exchanger test data from sec. 6.

The general heat exchanger weight equation from, ref. 7-3 is as follows:

$$WT_T = UA \left[ \left( \frac{K_j F_j}{j' Re} \right)_{\text{pri}} + \left( \frac{K_j F_j}{j' Re} \right)_{\text{sec}} \right] \\ \times \left[ 1 + (f' Re^3)_{\text{pri}} (PPF \cdot K_f F_f)_{\text{pri}} \right. \\ \left. + (f' Re^3)_{\text{sec}} (PPF \cdot K_f F_f)_{\text{sec}} \right] \quad (7-7)$$

The quantities  $K_j$ ,  $F_j$ ,  $K_f$ , and  $F_f$  are the core and fluid heat transfer and power parameters. The quantities are comprised of physical quantities unique to the test heat exchanger core and the fluids from section 6. Some of the quantities can be considered constant. One of the quantities, the fin effectiveness of the core, is a function of the local convective heat transfer coefficient and fin material thermal conductivity. The thermal/physical properties of the fluids used are temperature dependent. The gas density is pressure dependent. A review of test data in sec. 6 indicates that the use of average values for these dependent quantities would produce negligible error. The quantities  $K_j$ ,  $F_j$ ,  $K_f$ , and  $F_f$  were therefore evaluated for average conditions and maintained constant. The average physical properties used, and resultant values for the products  $(K_j F_j)_{pri}$ ,  $(K_j F_j)_{sec}$ ,  $(K_f F_f)_{pri}$ , and  $(K_f F_f)_{sec}$ , are listed in tables 7-I and 7-II

The relationships developed from the heat exchanger test data in sec. 6 for the quantities  $j'$  and  $f'$ , as functions of Reynolds numbers, for each side of the heat exchangers were used in the above weight equation. As eq. 6-14 and 6-15 for  $j'$  and eq. 6-17 for  $f'$  indicate, a significant Prandtl number influence due to the different atmospheres was found in the correlations of these test data. Fig. 6-1 and 6-2 show the correlated values of  $j'$  and  $f'$ . The power penalty factors  $(PPF)_{pri}$  and  $(PPF)_{sec}$  as used in this analysis were defined as follows:

$$(PPF)_{pri} = \left( \frac{PWR_E \cdot \phi + W_F}{PWR_H} \right)_{pri} \quad (7-8)$$

$$(PPF)_{sec} = \left( \frac{PWR_E \cdot \phi + W_P}{PWR_H} \right)_{sec} \quad (7-9)$$

The total weight,  $WT_T$ , includes equivalent weights for the power used and weights for the fan and the pump. It was desirable to include the fan and pump weights, as well as the power requirements, in the above expressions in the suboptimization relationships.

The suboptimized weight therefore included heat exchanger weight, fan and pump weight, and equivalent electrical power weight. To obtain these relationships, the derivatives of the total weight,  $WT_T$ , with respect to the primary and secondary flow Reynolds numbers, were set to zero, and the corresponding Reynolds numbers were computed. From ref. 7-3, these Reynolds numbers are:

$$Re_{pri} = \left( \frac{A_{pri}}{b_{pri}} \right)^{1/4} \left[ 2 \left( A_{pri}^{3/4} b_{pri}^{1/4} + A_{sec}^{3/4} b_{sec}^{1/4} \right) \right]^{-1/3} \quad (7-10)$$

$$\text{Re}_{\text{sec}} = \left( \frac{A_{\text{sec}}}{b_{\text{sec}}} \right)^{1/4} \left[ 2 \left( A_{\text{pri}}^{3/4} b_{\text{pri}}^{1/4} + A_{\text{sec}}^{3/4} b_{\text{sec}}^{1/4} \right) \right]^{-1/3} \quad (7-11)$$

where:

$$A_{\text{pri}} = \left( \frac{UA K_j F_j}{j'} \right)_{\text{pri}} \quad A_{\text{sec}} = \left( \frac{UA K_j F_j}{j'} \right)_{\text{sec}}$$

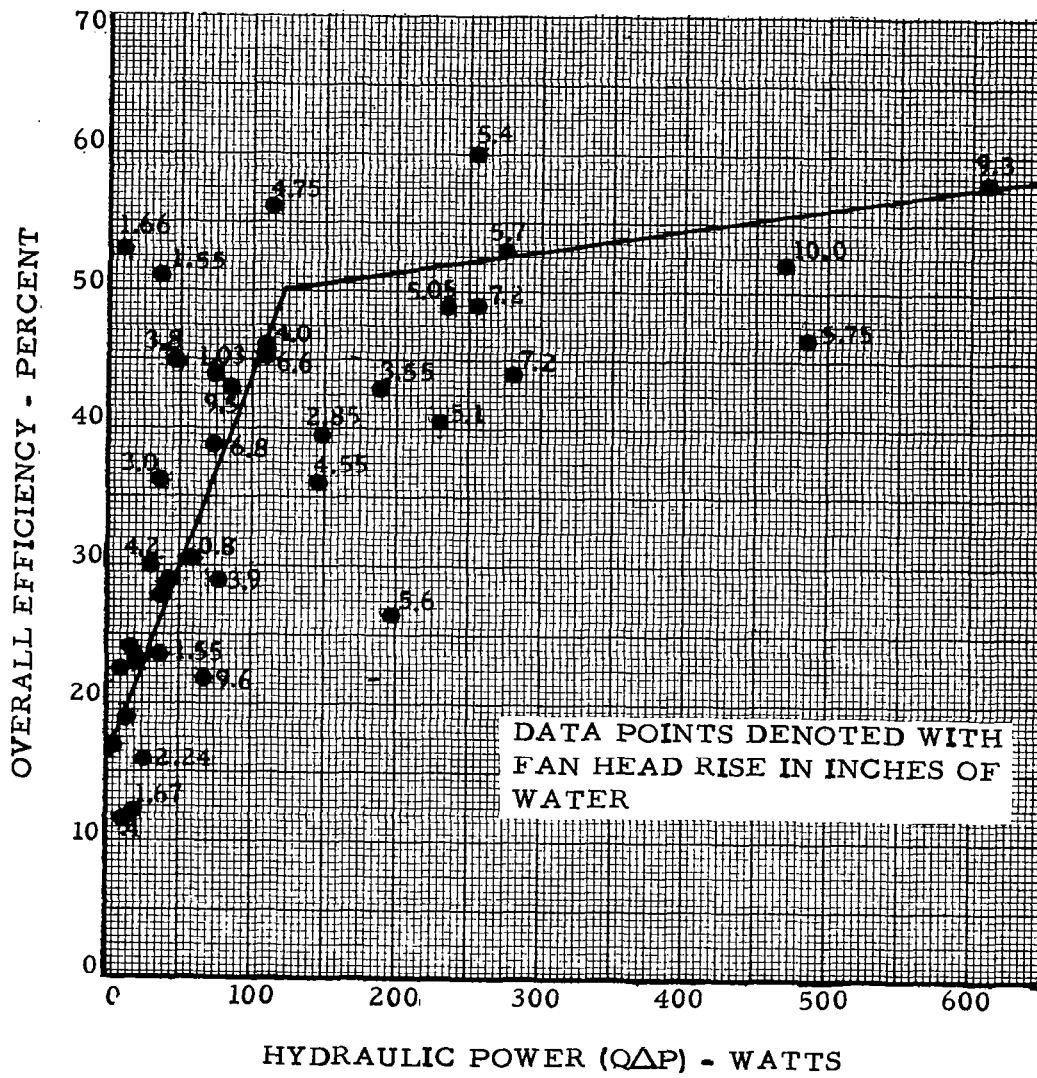
$$b_{\text{pri}} = (f' \text{ PPF } K_f F_f)_{\text{pri}} \quad b_{\text{sec}} = (f' \text{ PPF } K_f F_f)_{\text{sec}}$$

The suboptimized weight expression is:

$$\left( \text{WT}_T \right)_{\text{Re}} = \frac{3}{(2)^{2/3}} \left[ A_{\text{pri}}^{3/4} b_{\text{pri}}^{1/4} + A_{\text{sec}}^{3/4} b_{\text{sec}}^{1/4} \right]^{4/3} \quad (7-12)$$

The suboptimized solutions were often geometrically impractical for the example problem because the no-flow dimension was generally excessive. The above solution is given for usage in making penalty comparisons where the answers result in a reasonable heat exchanger weight and shape. In cases where the solutions appear impractical, such as producing a narrow frontal area and/or an extremely long heat exchanger, or excessive weight, bounds must be set for the liquid-flow length and for the no-flow length. These bounds were both set equal to 1.0 ft for the example problem. For all of the cases evaluated, the suboptimized solutions exceeded at least one of these bounds. The violating length was set equal to the bound value when the bound was exceeded. When only one bound was exceeded, the violating length was set equal to the bound, and with the gas flow cross-sectional area constant, the remaining new length was found. This value was compared with the appropriate bound value and subsequently was set equal to the bound value if it was too large. A bound can be set equal to any reasonable length, such as that established by the allowable heat exchanger envelope, and the same procedure as outlined above can be used.

Fans. -- The performance and weight of fans were determined on the basis of piecewise linear curves shown in fig. 7-3 and 7-4. The data are specified by the design pressure rise in inches of water. The flow is proportional to the square of the fan-impeller diameter, for axial fans with constant tip speed (ref. 7-4). Ref. 7-4 and 7-5 indicate that fan weight is approximately equal to the square of the fan impeller diameter. These factors lead to a linear relationship between flow and weight. The basis for plotting overall efficiency as a function of power is based on the general trends of (1) improved electrical motor efficiencies, and (2) reduced entrance, internal, and exit losses in fans with increased power levels. The efficiency and weight data from these curves were used to obtain the electrical power terms,  $\text{PWR}_E$ , and the fan weight term,  $W_F$ .



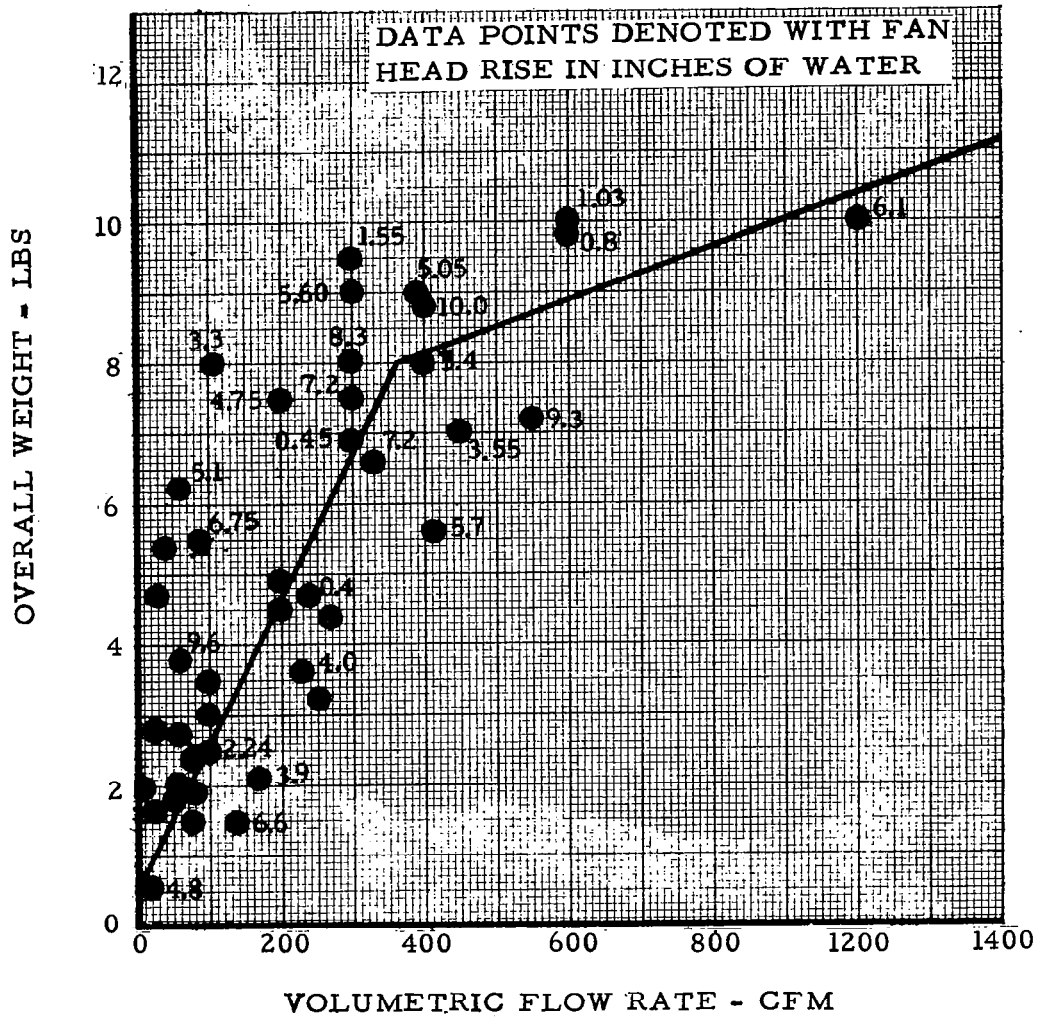


FIGURE 7-4 FAN OVERALL WEIGHT VS VOLUMETRIC FLOW RATE

## Atmospheric Purification and Control System

CO<sub>2</sub> Removal System. --A representative carbon dioxide adsorption system integrated with the thermal control system is shown in fig. 7-1. The procedure used for determining component weights and system power requirements is given. Molecular-sieve and silica-gel bed sizes, pressure drops, and desorption heat requirements can be obtained from the adsorption bed data reduced and presented in sec. 6. The experimentally obtained adsorption bed heat transfer coefficients, mass transfer coefficients, and friction factors for adiabatic conditions were used in the analyses in the example problem, since the bed did not contain an internal heat exchanger for cooling or heating. System weights were obtained by estimating the weight of valves, ducting, and mounting structure, and by adding to this weight the result of the computed weights of the packaged silica-gel beds, molecular-sieve beds, fan, and heat exchanger for each atmosphere examined.

System pressure drop was obtained by evaluating the system pressure drop, exclusive of the silica-gel and molecular-sieve beds, and then adding the bed-pressure drops for each atmosphere evaluated. The system heat exchanger was sized with the assumptions that (1) the heat load imposed on the heat exchanger was equal to the sum of the adsorption heat load for the upstream silica-gel bed and the heat load due to the fan and (2) the gas stream Reynolds number in this heat exchanger was equal to the Reynolds number in the condenser. The latter assumption permitted the heat exchanger size to be determined from the condenser size through the ratio of UA values required for the two units as previously discussed in the thermal control presentation. Heat exchanger effectiveness data from fig. 7-2 were used to obtain the required UA value. Fan performance and weight can be obtained in the fan and blower presentation previously given.

A weight of 80 lb for the valves, ducts, and supporting structure was estimated for the CO<sub>2</sub> adsorption subsystem. This weight was estimated from an existing prototype unit with allowance for predicted flight weight system development.

Pressure drops incurred in the prototype unit silica-gel bed and the molecular-sieve bed were obtained using the test data in sec. 6 and from bed dimensions. The predicted pressure drops were as follows:

<u>Adsorption bed</u>	<u>Silica-gel</u>	<u>Molecular-sieve</u>
Pressure drop for N <sub>2</sub> -O <sub>2</sub> at 10 psia at 10 cfm	0.57 in. of water	0.69 in. of water

The resulting prototype unit CO<sub>2</sub> removal subsystem pressure drop, exclusive of the adsorption-bed pressure drop, was 13.1 in. of water for 10 cfm of gas flow for a 10-psia N<sub>2</sub> - O<sub>2</sub> atmosphere and is adjusted for the various other gas densities used. This pressure drop versus flow rate is comparable to that obtained from prototype units for space cabin simulators.

**EXAMPLE PROBLEM COMPARING LIFE SUPPORT SYSTEM  
PENALTY FOR DIFFERENT CABIN ATMOSPHERES**

A representative space laboratory life support system was established to evaluate the effects of the atmosphere selection on the design with the analysis and test data previously discussed in secs. 2 through 6 and with the analytical techniques previously presented in this section. Fig. 7-1 presents an integrated atmospheric purification and thermal control part of the support system. The design conditions and assumptions for the example problem are as follows:

Mission--Earth-orbital laboratory having a 90-day period without resupply.

Crew--3 to 4 men.

Cabin volume--5360 cu ft.

Airlock size--100 cu ft.

Cabin leakage assumed to be 2 lb/day based on a 7-psia N<sub>2</sub>-O<sub>2</sub> condition.

Cabin repressurization penalty for emergency allows for 1 repressurization.

Airlock usage--once per day.

Airlock pump-down to cabin and return will be used for gas conservation.

Oxygen consumption--2 lb/day/man.

Crew average clothing factor--0.70 clo in N<sub>2</sub>-O<sub>2</sub> atmosphere (same suit used in He-O<sub>2</sub> atmosphere).

Average metabolic load based on 24 hr--460 Btu/hr/man.

Cabin average ventilation rate--50 fpm.

Cabin pressure levels and average temperature for comfort that will be used for the penalty comparison is as follows (see sec. 2).

	<u>5 psia</u>	<u>7 psia</u>	<u>10 psia</u>
O <sub>2</sub>	70 °F	--	--
N <sub>2</sub> O <sub>2</sub>	70 °F	70 °F	71 °F
He O <sub>2</sub>	73.5 °F	76.5 °F	78 °F

Total cabin sensible heat load--2000 Btu/hr.

Cabin dew point temperature--60 °F.

Water vapor generation rate--0.4 lb/hr.

Carbon dioxide generation rate--0.281 lb/hr.

Power system--isotope-Brayton.

Power system penalty--503 lb/kW.

The major life support systems that could be directly affected by the selection of atmosphere composition and pressure, as previously discussed, are the atmospheric supply and pressurization, airlock, atmospheric purification and control, and thermal control systems. Separate examples on the use of the presented data from the study are also presented in each of the related secs. 2 through 6. The sample problem presented below is for each of the systems noted and uses the given design conditions and assumptions.

#### Atmosphere Supply and Pressurization System

Spacecraft penalty for gas makeup to compensate for leakage, repressurization, and for metabolic use is shown in table 7-III. Airlock operation penalty is given in table 7-IV. Supercritical gas storage was used for this penalty tradeoff because it represents current technology.

#### Atmosphere Purification System and Thermal Control System

Fig. 7-1 shows the arrangement of the regenerative CO<sub>2</sub> removal and humidity control loop, as it is integrated with the thermal control system. The atmospheric and thermal control system weight and power requirements were taken from fig. 7-5 through 7-9 and tables 7-V and 7-VI.

Solutions were obtained for gas flow rates of 25, 50, and 100 lb/hr and coolant temperature rises of 1° and 7°F for the condenser loop, based on condenser characteristics given in tables 7-I and 7-II. The combined penalty of condenser weight, fan weight, and fan power was generally lowest for the 50 lb/hr gas flow rate except for the 10-psia N<sub>2</sub>-O<sub>2</sub> atmosphere where the lowest combined penalty occurred at the 100-lb/hr flow rate. Tabulated data for these solutions are shown in table 7-V. The condenser weights are wet and include a 20% weight increase for headers and support structure. The condenser and heat exchanger characteristics used are given in tables 7-I and 7-II. A gas flow rate to the regenerative CO<sub>2</sub> adsorption system was 10 cfm, which produces a 60 fpm bed face velocity. The remainder of the gas flow leaving the condenser bypassed the CO<sub>2</sub> adsorption system. The adsorption system weight and power requirements were obtained as outlined previously, and from the data in sec. 6 and table 7-VI.

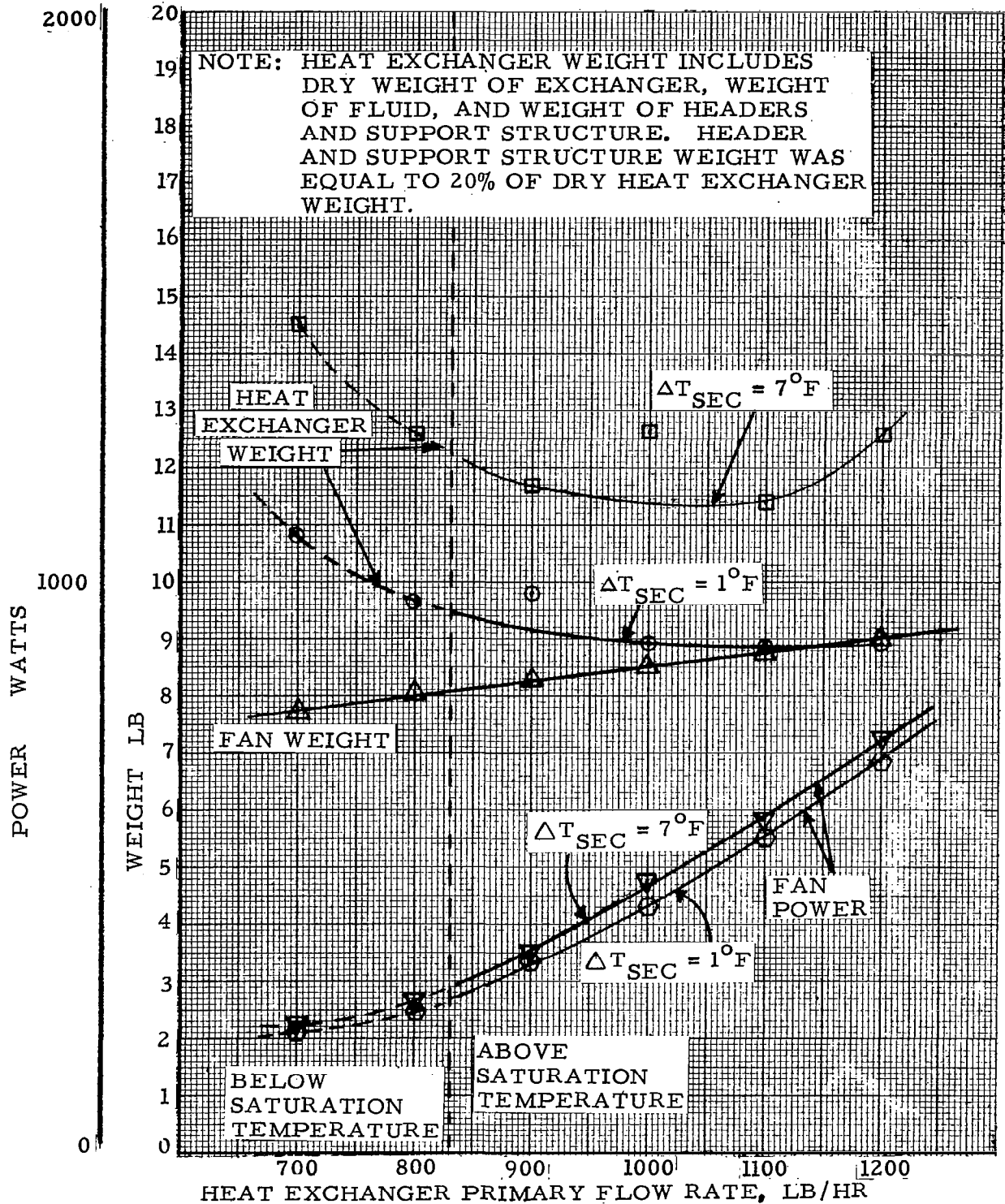


FIGURE 7-5 CABIN THERMAL CONTROL WEIGHT AND POWER REQUIREMENTS - 5 PSIA O<sub>2</sub>

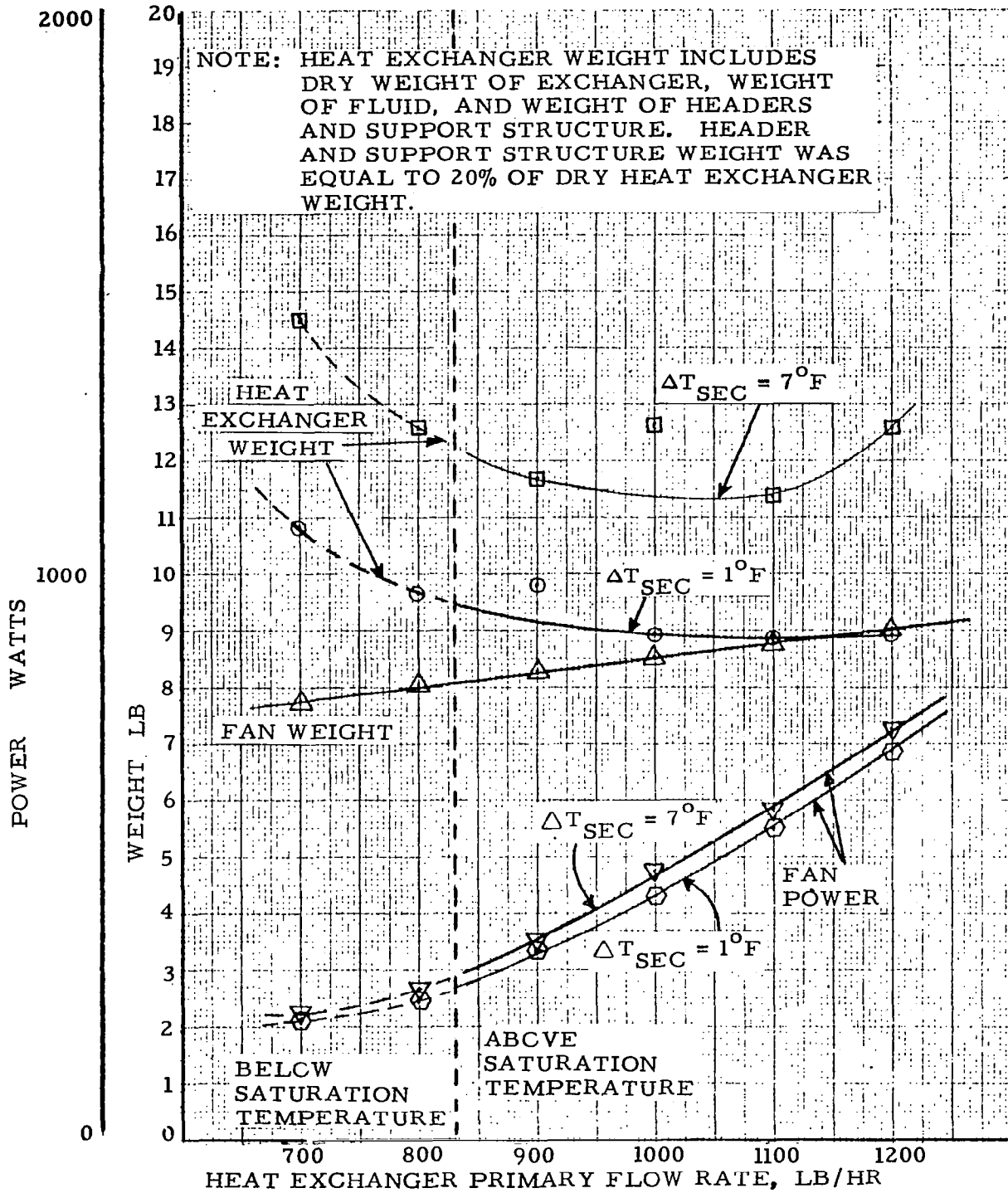


FIGURE 7-6 CABIN THERMAL CONTROL WEIGHT AND POWER REQUIREMENTS - 5 PSIA N<sub>2</sub> - O<sub>2</sub>

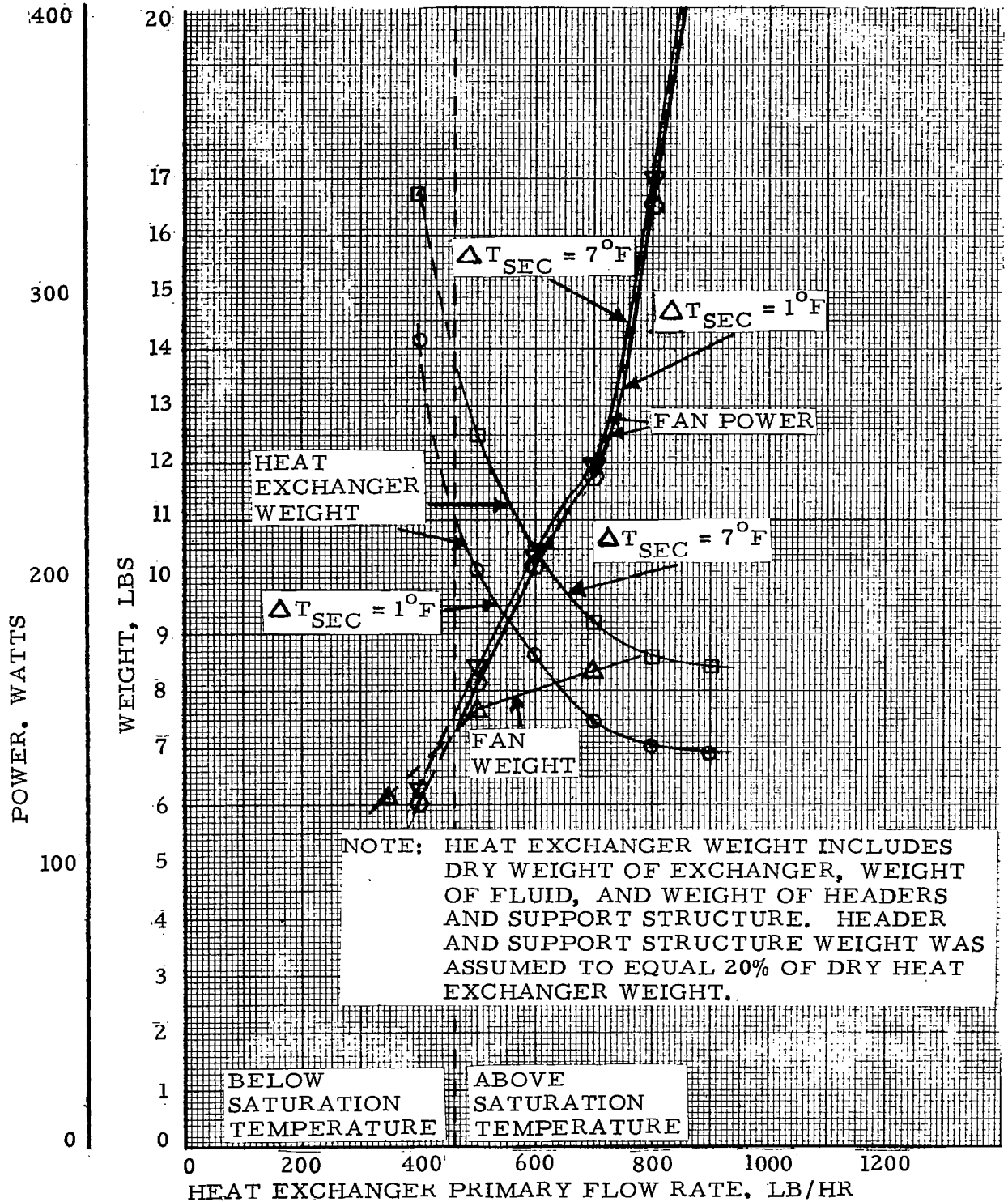


FIGURE 7-7 CABIN THERMAL CONTROL WEIGHT AND POWER REQUIREMENTS - 5 PSIA He - O<sub>2</sub>

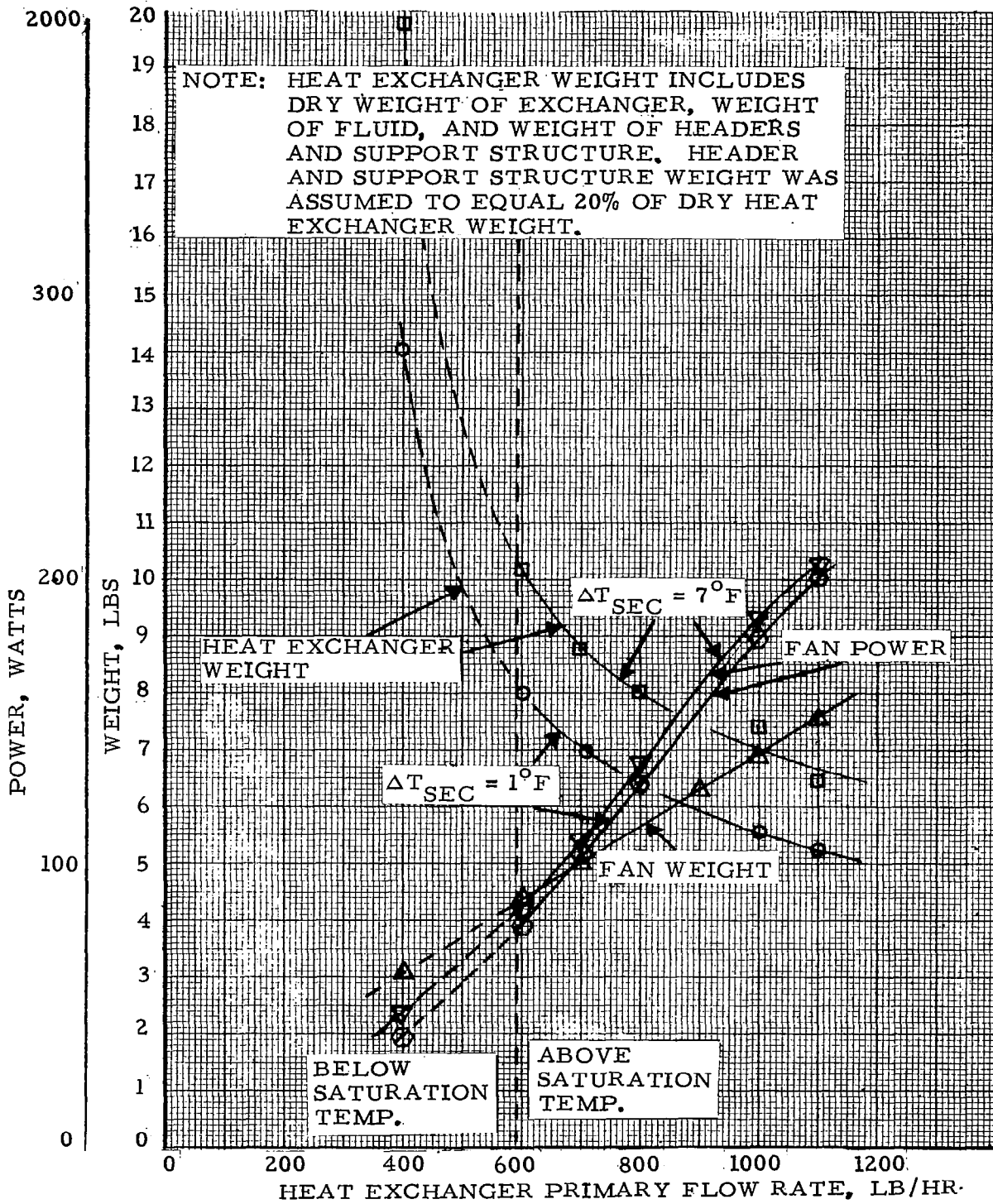


FIGURE 7-8 CABIN THERMAL CONTROL WEIGHT AND POWER REQUIREMENTS - 10 PSIA N<sub>2</sub> - O<sub>2</sub>

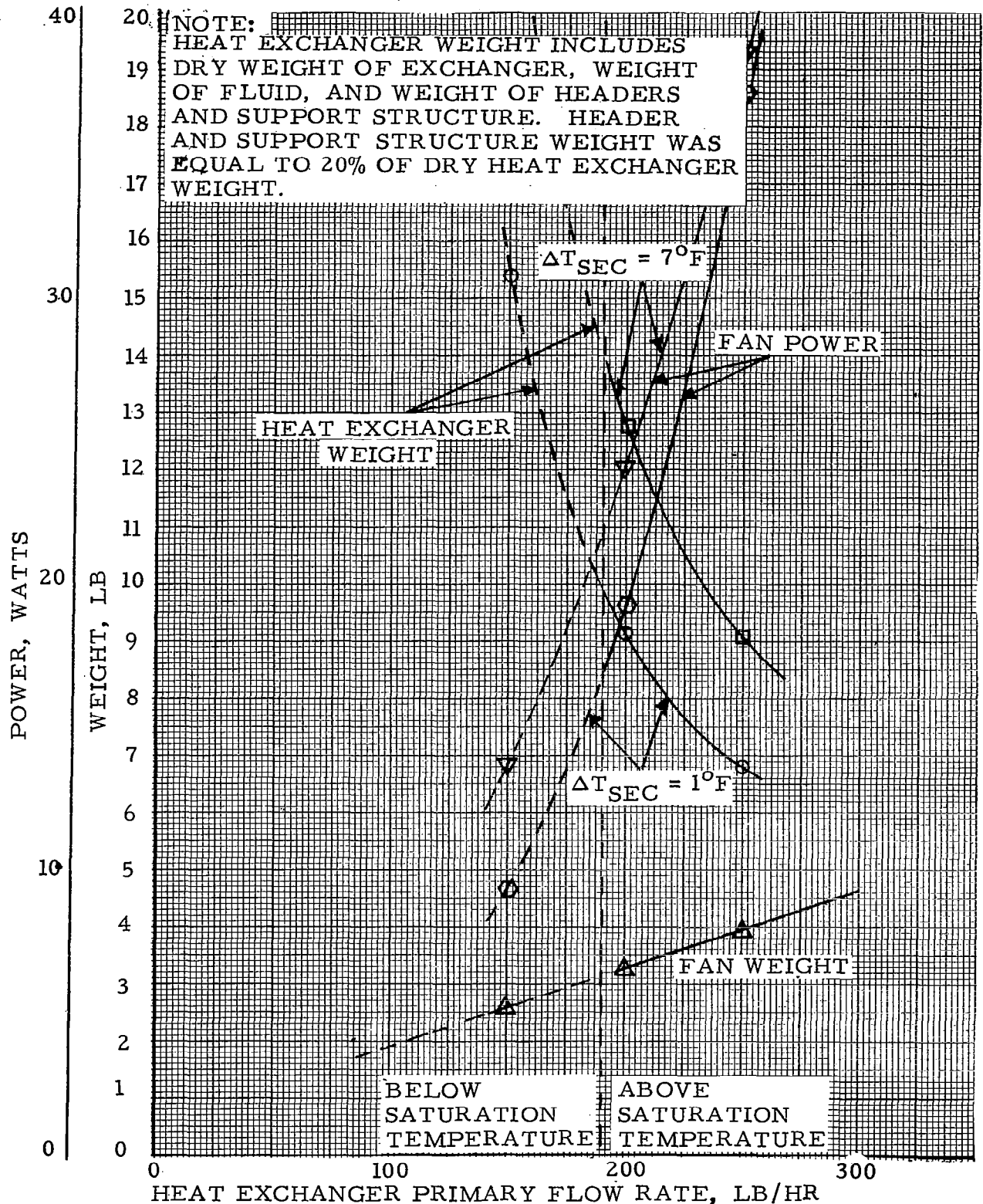


FIGURE 7-9 CABIN THERMAL CONTROL WEIGHT AND POWER REQUIREMENTS - 10 PSIA He - O<sub>2</sub>

TABLE 7-III  
WEIGHT REQUIREMENTS FOR STORED  
ATMOSPHERIC CONSTITUENTS

Atmosphere	Pressure (psia)	Oxygen storage weight (lb)	Diluent storage weight (lb)	Total atmosphere storage weight (lb)
N <sub>2</sub> -O <sub>2</sub>	5	953	130	1083
	7	978	269	1247
	10	1003	482	1485
He-O <sub>2</sub>	5	956	90	1046
	7	975	153	1128
	10	1003	206	1209
O <sub>2</sub>	5	1052	0	1052

Notes:

1. Exclusive of storage vessel penalty due to airlock operation (see Table 7-IV).
2. Total storage vessel weight includes stored supercritical atmospheric constituent, tankage, and insulation taken from section 5.
3. Gas use rates include oxygen consumption, cabin leakage, and a single repressurization for a 90-day mission.

TABLE 7-IV  
WEIGHT AND POWER REQUIREMENTS  
FOR AIRLOCK OPERATION

Atmosphere	Pressure (psia)	Average Pump power (kW)	Pump weight (lb)	Total storage vessel weight (lb)
N <sub>2</sub> -O <sub>2</sub>	5	0.23	12.3	19.9
	7	0.33	12.7	23.3
	10	0.48	13.3	26.8
He-O <sub>2</sub>	5	0.22	11.9	19.9
	7	0.33	12.3	21.74
	10	0.46	12.7	23.8
O <sub>2</sub>	5	0.23	12.3	19.6

Notes:

1. Total storage vessel weight includes stored supercritical fluid atmospheric constituents, tankage, and insulation taken from sections 4 and 5.
2. Airlock operation is based on the 90-day mission with a single airlock usage per day, with airlock pumping into cabin (see section 4).

TABLE 7-V  
CONDENSER LOOP WEIGHT AND  
POWER REQUIREMENTS

Atmo- sphere	Press. (psia)	w <sub>pri</sub> (lb/hr)	$\Delta T_{sec}$ (°F)	Con- denser weight (lb)	Con- denser UA (btu/hr °F)	Con- denser outlet temp (°F)	Con- denser effec- tiveness	R <sub>e_g</sub>	W <sub>sec</sub> (lb/hr)	Fan power (W)	Fan weight (lb)
N <sub>2</sub> - O <sub>2</sub>	5	50	1°	8.6	30.17	52.6	0.59	23.0	628.	4.4	1.1
		50	7°	9.6	35.62	52.6	0.59	24.2	126.	5.2	1.1
	10	100	1°	9.90	43.86	52.4	0.61	30.1	881.	6.0	1.2
		100	7°	11.1	51.49	52.4	0.61	33.2	126.	6.5	1.2
He - O <sub>2</sub>	5	50	1°	10.4	35.99	52.1	0.65	22.1	730.	5.8	1.3
		50	7°	11.75	39.1	52.1	0.65	22.9	105.	6.4	1.3
	10	50	1°	8.15	40.9	52.96	0.67	20.8	962.	4.0	1.2
		50	7°	9.3	50.7	52.96	0.67	23.3	138.	4.7	1.2
O <sub>2</sub>	5	50	1°	9.4	31.8	52.3	0.60	20.7	627.	4.6	1.1
		50	7°	10.7	37.52	52.3	0.60	21.9	90.	6.9	1.1

TABLE 7-VI  
 CARBON DIOXIDE ADSORPTION SYSTEM  
 WEIGHT AND POWER REQUIREMENTS

Atmosphere	<sup>a</sup> 2 molecular sieve beds (lb)	<sup>a</sup> 2 Silica gel beds (lb)	Fan (lb)	Heat exchanger (lb)	<sup>b</sup> Fixed weight	Total system weight (lb)	Total system pressure drop (in. of water)	Fan power (W)
N <sub>2</sub> - O <sub>2</sub>								
7 psia	14.2	21.9	1.0	3.9	80	121.0	14.48	85.0
5 psia	9.4	32.2	1.0	3.1	80	125.7	13.06	77.0
He - O <sub>2</sub>								
7 psia	16.4	24.1	1.0	1.5	80	123.0	10.44	61.5
5 psia	9.85	32.4	1.0	3.3	80	126.6	11.09	65.5

<sup>a</sup>Includes canister weight.

<sup>b</sup>Ducts, controls, valves, supporting structure, and other fixed weight.

The adsorption system selected for each atmosphere has the lowest weight penalty due to fixed weight and fan power. Molecular-sieve and silica-gel bed weights and fan power to overcome pressure drop requirements were taken from tables 6-I and 6-III. It was assumed that waste heat for desorption was available from the vehicle power system. As noted in sec. 6, and by comparing the data in tables 6-III and 6-IV, cooling the silica gel beds during adsorption reduces the amount of bed material required. Therefore, the bed weights used in this adiabatic design are somewhat conservative.

The minimum penalty systems selected correspond to molecular sieve bed initial loadings of 0 lb adsorbate/lb bed for the 5-psia atmospheres and 0.02 lb adsorbate/lb bed for the 7-psia atmospheres. Initial bed loading of 0.01 lb adsorbate/lb bed was used for the silica gel beds for all atmospheres.

The sums of the desorption heat requirements from tables 6-I and 6-III for a molecular sieve bed and a silica gel bed for each of these systems vary between 380 to 460W. If electrical power were used instead of waste heat it would add an additional weight penalty of from 190 to 230 lb.

The molecular sieve can be optimized by considering the use of vacuum only at the expense of increased bed size and/or cycle time, the use of a combination of thermal heat and vacuum for smaller bed sizes and/or shorter cycle times and by increasing the allowable concentration in the bed at the start of adsorption. Sec. 6 data and procedures can be used to evaluate these conditions. Normally, computer optimization is required to accomplish this task. Approximations can be made by scaling the data shown in sec. 6. The inlet temperatures and flow rates entering the silica-gel bed that precedes the molecular sieve were determined from the outlet conditions of the condenser.

Total packaged bed weights, including canisters and liquid coolant provisions, were assumed to be 1.75 times the weights of bed material. Table 7-VI shows a detailed breakdown of the variation in penalty for the CO<sub>2</sub> adsorption system.

Most thermal control systems are designed to achieve a cabin heat exchanger outlet temperature above the saturation temperature to preclude condensing in the heat exchanger. Achieving outlet temperatures above the saturation temperature is more easily achieved with some of the candidate atmospheres than with others, as shown in fig. 7-10. A partial explanation of the differences in heat exchanger weights and fan powers, shown in figs. 7-5 through 7-9, follows. The combination of high specific heat and high cabin temperature for the 10-psia helium-oxygen atmosphere results in the lowest required gas weight flow rate. This, in turn, results in the lowest fan power requirement. The higher density for the 10-psia nitrogen-oxygen atmosphere results in reduced fan power, compared to the 5-psia helium-oxygen atmosphere even though in this latter case there is a somewhat lower flow rate. The low density and high flow rate for the 5-psia nitrogen-oxygen atmosphere and 5-psia oxygen atmosphere result in the largest fan power. The heavier heat exchangers obtained for the helium-oxygen atmospheres were largely due to the Reynold's number which resulted from the lower gas flow rates. Reduction in these heat exchanger weights could be achieved with liquid flow and no-flow lengths less than 1.0 ft.

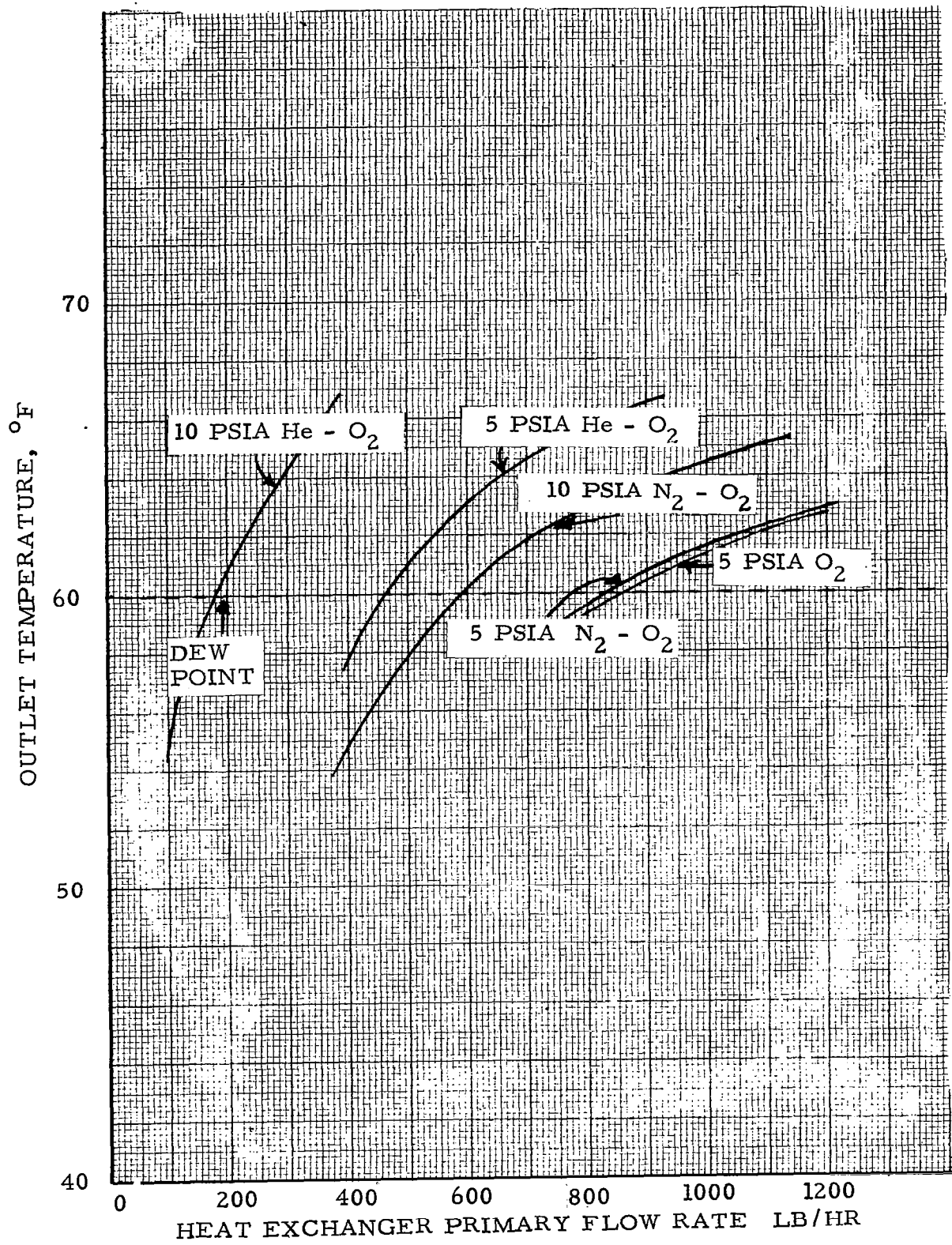


FIGURE 7-10 HEAT EXCHANGER OUTLET TEMPERATURE

System pressure drops include the effect of entrance losses, internal losses, and exit losses at the condenser and at the cabin exchanger, and pressure drop of a water separator, based on 2-in. circulator distribution ducts for the condenser and a 4-in. duct for the cabin heat exchanger.

### Summary of Penalty Comparison for Different Atmospheres

Table 7-VII presents a review of the penalty difference that was incurred by the change in atmospheric composition and pressure level for oxygen at 5 psia, helium-oxygen at 5, 7, and 10 psia, and nitrogen-oxygen at 5, 7, and 10 psia, with a 3.5-psia partial pressure of oxygen. The example problem indicates that a helium-oxygen system can be designed for lower total system weight rather than either a nitrogen-oxygen or pure oxygen system. Furthermore, the penalty incurred by increasing pressures, and diluent concentration, is not large for helium diluent but is significant if the diluent is nitrogen.

A lower atmosphere supply system storage weight exists for helium-oxygen because of the lower gas weight requirements for leakage makeup and repressurization. For example, 1046 lb are required as noted in table 7-VII for helium oxygen at 5 psia as compared to 1083 lb for nitrogen-oxygen or 1052 lb for pure oxygen at the same pressure. The airlock penalty difference for a different gas mixture is primarily dependent on the airlock repressurization system used and on the gas density. Therefore, the airlock system used is more important than the gas used. Sec. 4 presents the tradeoff parameters for various airlock systems that have been proposed for spacecraft.

Weight of the basic heat and mass transfer equipment is nearly independent of the atmosphere composition and pressure for the atmosphere purification system and the thermal control system. The total penalty difference is primarily caused by fan power to overcome system pressure drop. Fan power decreases with increased cabin pressures and is less with helium diluent than with nitrogen at equivalent pressures. The most significant decrease in power occurs in the thermal control systems. Blower power penalty for the helium-oxygen compared to nitrogen-oxygen and oxygen atmospheres is decreased because of the increased specific heat of the gas and the higher allowable cabin heat rejection temperature. This combination permits a decrease in gas flow rate and, thereby, significantly reduces blower power in the thermal control system. Increased sensible heat load above the 2000 Btu/hr design point can significantly increase the savings for helium-oxygen atmospheres. The thermal control system weight penalty for the example problem is shown in fig. 7-11.

### CONCLUSIONS AND RECOMMENDATIONS

The major systems influenced by the atmosphere composition and pressure level from a penalty standpoint are the atmosphere supply and pressurization and thermal control systems. The atmosphere purification and control system and the airlock system are influenced to a much lesser degree, as was illustrated in the example problem.

TABLE 7-VII  
LIFE SUPPORT SYSTEM WEIGHTS FOR EXAMPLE PROBLEM

System Type	Atmosphere →	O <sub>2</sub>		N <sub>2</sub> - O <sub>2</sub>		He - O <sub>2</sub>		
	Pressure (psia) →	5	5	7	10	5	7	10
Atmospheric supply and pressurization <sup>a</sup>								
Storage vessel and atmosphere weight (lb)		1052.0	1083.0	1247.0	1485.0	1046.0	1128.0	1209.0
Airlock penalty								
Storage vessel and atmosphere weight (lb)		19.6	19.9	23.3	26.8	19.9	21.7	23.8
Pump weight (lb)		12.3	12.3	12.7	13.3	11.9	12.3	12.7
Pump power penalty (lb) <sup>b</sup>		<u>1.1</u>	<u>1.2</u>	<u>1.7</u>	<u>2.4</u>	<u>1.1</u>	<u>1.7</u>	<u>2.3</u>
		33.0	33.4	37.7	42.5	32.9	35.7	38.8
Atmosphere purification and control system								
CO <sub>2</sub> control system weight (lb)		126.0	125.7	121.0	117.0	126.6	123.0	120.0
CO <sub>2</sub> control system fan power (lb) <sup>b</sup>		39.0	38.6	42.8	46.0	32.8	31.0	30.2
Condenser weight (lb)		10.7	9.6	12.2	11.1	11.8	8.4	9.3
Fan weight (lb)		1.1	1.1	1.2	1.2	1.3	1.2	1.2
Fan power (lb) <sup>b</sup>		<u>2.0</u>	<u>2.2</u>	<u>3.0</u>	<u>3.3</u>	<u>2.9</u>	<u>2.0</u>	<u>2.4</u>
		178.8	177.2	180.2	178.6	175.4	165.6	163.1
Thermal control system								
Heat exchanger weight (lb)		12.3	12.3	11.5	10.3	13.8	13.9	13.9
Fan weight (lb)		8.1	8.1	7.5	4.3	7.2	5.2	3.1
Fan power (lb) <sup>b</sup>		<u>146.0</u>	<u>146.0</u>	<u>90.5</u>	<u>41.8</u>	<u>75.5</u>	<u>35.0</u>	<u>10.9</u>
		166.4	166.4	109.5	56.4	96.5	54.1	27.9
Total system weight (lb)		1430.2	1460.0	1574.4	1762.5	1350.8	1383.4	1438.8

<sup>a</sup>Values for metabolic use, leakage, and repressurization.

<sup>b</sup>Brayton - Isotope power system penalty = 0.503 lb/watt.

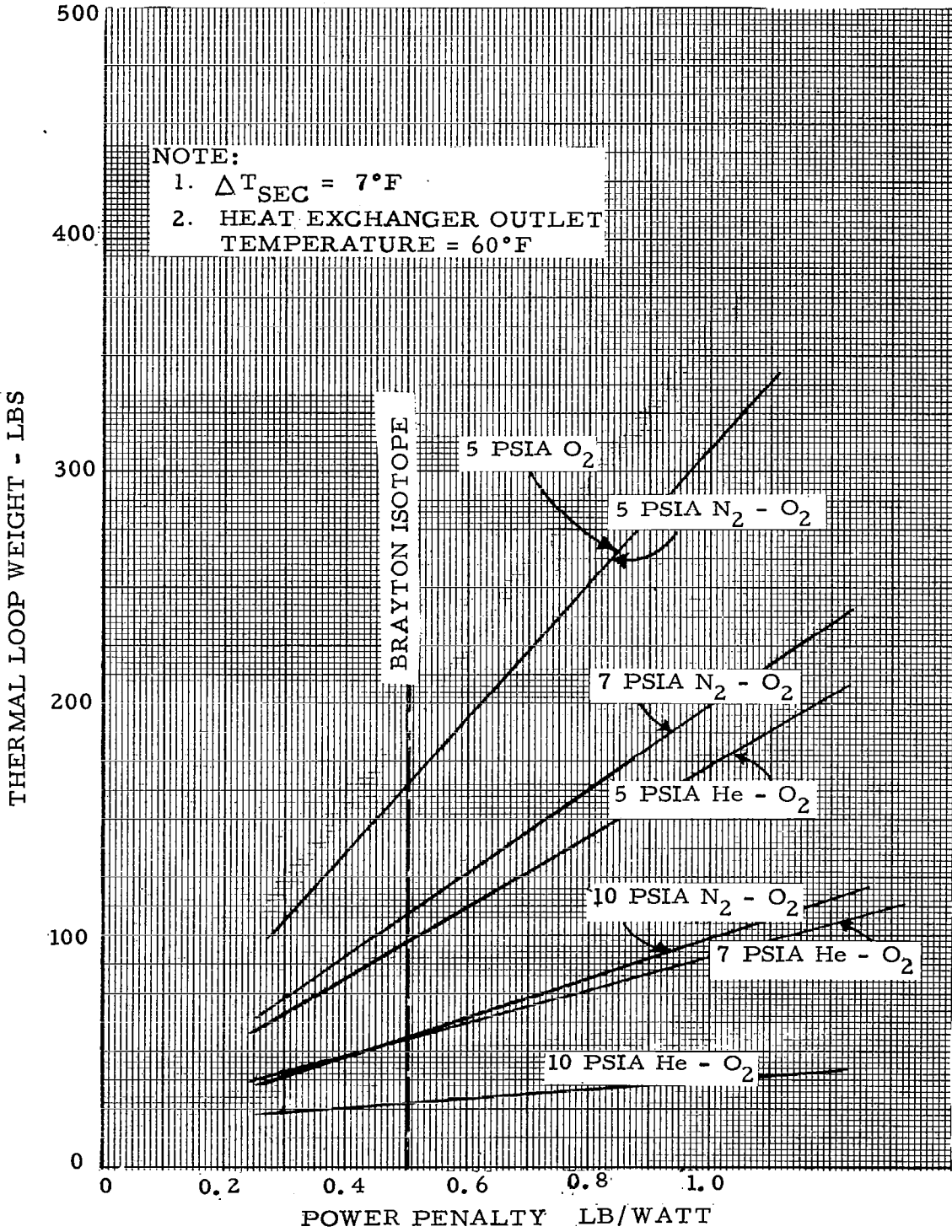


FIGURE 7-11 THERMAL CONTROL LOOP WEIGHT PENALTY

The data presented in secs. 6 and 7 can be best applied by using a Fortran program, such as the NASA G-189 Generalized Environmental Control and Life Support Fortran Program, or the Air Force ASD TDR-63-328 for Atmospheric Control Systems, that defines the particular component arrangement and components for the life support system under evaluation. However, approximations in the penalty difference incurred by atmosphere selection can be made by applying the procedures and data contained in this report.

Data for the evaluation for all life support systems can be obtained from secs. 2 through 6 which are entitled as follows:

- Comfort Zone.
- Leakage.
- Airlock System.
- Atmosphere Supply System.
- The Effect of Atmosphere Selection on Component Heat and Mass Transfer.

For the conditions considered in the sample problem there is a weight advantage in using helium-oxygen atmospheres. This advantage increases if higher atmospheric pressures (higher diluent percentages) are considered. The primary advantage of helium-oxygen is that a lower weight of gas is required for low leakage rates and fan and blower power is reduced. The savings in blower power are caused by the higher allowable comfort zone temperature which reduces volumetric flow rates in the cabin conditioning system. More test data are required for a greater number of subjects with varying degrees of clothing and for different wall temperatures to refine the allowable comfort zone data. Criteria that also must be considered, in addition to weight penalty, are the availability of hardware, cost, reliability, design risk, and fire protection. A discussion of the fire problem associated with atmosphere selection is presented in sec. 8.

## REFERENCES

- 7-1. Stevens, R. A. ; Fernandez, J. ; Woolf, J. R. : Mean-Temperature Difference in One-, Two-, and Three-Pass Crossflow Heat Exchangers. Trans. of the ASME 79, Feb. 1957, pp. 287-297.
- 7-2. Zahn, W. R. : Properties of Humid Air at Other than Standard Atmosphere in Symposium on Air-Cooled Heat Exchangers. Compiled from 7th National Heat Transfer Conference, Cleveland, Ohio, Aug. 10, 1964. Published by the ASME, New York, New York.
- 7-3. Paselk, R. A. : Integration and Optimization of Space Vehicle Environmental Control Systems. Rept. No. ASD-RE-61-176, Part II, Wright Patterson AFB, Ohio, April 1963.
- 7-4. Coe, C. S. ; Rousseau, J. ; and Shaffer, A. : Analytical Methods for Space Vehicle Atmospheric Control Processes. Rept. No. ASD-TR-61-162, Part II, Wright Patterson AFB, Ohio, Nov. 1962.
- 7-5. Blakely, R. L. ; and Barker, R. S. : Generalized Environmental Control and Life Support System Fortran Programs, Vol. IV, Fan, Blower, and Pump Data Reduction and Design Fortran Programs.



## Section 8

### COMPARISON OF ATMOSPHERES FOR FIRE PREVENTION

A vehicle designer normally selects the cabin atmosphere mixture and pressure level based on either one or a combination of design requirements that involve human physiology, low weight penalty, cost, hardware availability and vehicle compatibility with other associated vehicle systems. This can be done if the more flammable materials are not used in vehicle design or if these materials are isolated behind panels. Many of the most favorable heat transport fluids, lubricants, and materials cannot be used aboard a spacecraft because of the increase in fire potential. The cabin ventilation rate must also be held to a minimum to retard the fire potential. The weight and cost difference for a vehicle because of the material selection and test program varies with each design. The selection and testing of materials for the larger vehicles becomes even more stringent if 100 percent oxygen is used. The material and fluid selection program could be extremely costly when considering the larger planned space laboratories and the ever increasing number of experiments.

Logic indicates that even using utmost care, the materials, the power source, and the ventilation rate aboard a manned spacecraft in null gravity could still potentially cause some material to ignite and fire propagation in any atmosphere. Therefore, common low ignition materials were selected to determine the effect of cabin atmosphere on the probable burning phenomena. Test data for cotton cloth, insulated wire and other materials in the literature were reviewed. The published test procedures and specimens were not especially directed toward null gravity "burning rate tests." Therefore, specimens and tests were established to obtain one g baseline correlation data and also to be compatible with an 18 to 22 second null gravity flight time. The test specimens and procedures were additionally tailored to permit extension to orbital flight.

Atmosphere selection must consider all aspects of the proposed mission. In addition to flight operation, systems must be subjected to ground development and checkout tests. Exposure may be greater during these phases than in actual flight. In any event it is certain that characteristics in one g and the higher 'g' levels encountered during launch and entry, must be evaluated as well as those in null g. Necessary changes in pressure level must also be considered. It may well be that testing at sea level, one g will require an entirely different test atmosphere selection than flight operation. Certainly the use of a two gas atmosphere at sea level conditions to replace a five psia, pure oxygen atmosphere in space presents no greater compromise of engineering operation and much less hazard than a sea level, oxygen atmosphere.

Insight into the relationship of atmosphere selection to fire prevention aboard the spacecraft is provided by analysis and by test. Analysis of ignition and combustion characteristics will, in general, provide only limited qualitative results unless extremely complicated and detailed studies are performed.

Such general analyses, as presented in the following discussion, do provide valuable insight into the parameters influencing the combustion process and therefore are valuable in planning test programs and interpreting test results.

These analyses shown that ignition temperature is relatively independent of atmosphere selection, but is dependent upon oxygen partial pressure and, to a lesser extent, upon free or forced convection. Of course, for a given energy source, the time required to reach ignition temperature is dependent upon the conductivity of the atmosphere and therefore on the selection of diluent.

Once ignition has occurred, analysis indicates that rate of flame propagation depends upon the gravity forces present, the forced convection currents, nature of the material, oxygen partial pressure and the thermal diffusivity of the atmosphere selected.

Greater insight into the actual interaction of these variables is provided by tests reported on the following pages. These tests were conducted in atmospheres typical of those proposed for space cabin usage, including normal air at 14.7 psia, pure oxygen at 3.5, 5, 10, and 16 psia, and two gas mixtures of oxygen with nitrogen or helium at 5, 7, and 10 psia. Data were obtained on ignition temperatures and burning rates under varying convection conditions and oxygen partial pressure. In addition to one gravity, tests were run under short-term zero g in an airplane. In order to standardize on materials that are likely to be found in the space cabin, test items included cotton cloth patches, single insulated wires, and bundles of insulated wires.

The important conclusions of these tests include the following:

- Over the range tested, ignition temperature is independent of the type or partial pressure of diluent.
- Ignition temperature of cotton cloth is significantly decreased by increasing oxygen partial pressure (up to 7 psia).
- For a given input power, the heating rate of the ignition source is slower in a helium-oxygen atmosphere than an equivalent nitrogen-oxygen atmosphere. This is due to the higher thermal conductivity of the helium mixture and results in delayed ignition which may significantly reduce the probability of fire.
- At equivalent total pressures and oxygen partial pressures, cotton cloth burns faster in a helium-oxygen atmosphere than a nitrogen-oxygen atmosphere.
- Addition of diluent (helium or nitrogen) to atmospheres of equal oxygen partial pressure (3.5 psia) results in decreasing rates of combustion of cotton cloth.
- Overloaded electrical wires take the longest to smoke and/or burn-through in helium-oxygen mixtures, and second longest in nitrogen-oxygen. Shortest times were observed in pure oxygen.
- Effects of diluents (helium or nitrogen) on smoking and burn-through of overloaded wires are magnified when the wires are bundled.
- Burning characteristics of cotton cloth in null gravity were significantly influenced by type and amount of diluent.

## A DISCUSSION OF FIRE THEORY

Analyses of the ignition and combustion processes were completed to understand the influence of atmosphere selection and to help guide the test program and later data correlation.

Published analytical techniques used to define fire phenomena as they affect cabin atmosphere and potential cabin materials have been provided by Kimzey, Huggett, Klein and others. Each has made an important contribution which enables a better understanding of the total problem. These analyses and test data are given in references 8-1, 8-2 and 8-3.

A discussion is presented to help explain the effect of free and forced convection on ignition. A brief analysis is made also on the effects of gravity, oxygen concentration, atmospheric diluent and free stream velocity upon combustion rates.

### Gravity and Convection Effects on Ignition

A description of the parameters governing the ignition process is presented to describe the factors and processes involved. The information is intended to explain an interpretation of the general behavior of the most recognizable parameters.

The physical system describing a specimen to be tested is shown in figure 8-1. Shown is a single layer of cotton cloth folded over a wire. The following discussion will be primarily concerned with the region to the right of the Y axis. The system is assumed to be symmetrical around the Z axis, and distances are represented by the radius from the wire center. The wire when heated electrically with a step voltage input produces a time-temperature curve of the wire and cloth shown in figure 8-2. The dashed line represents the temperature at the outside surface of the cloth, designated as  $T_b$ . This curve is assumed to be essentially independent of the surrounding environment, which is probably valid at least during the first few seconds after application of power to the wire. Two cases are described, one involving no convection, representing null gravity, and one involving finite convection.

Figure 8-3 shows temperature profile shapes predicted at various times after power application for a null gravity condition. The temperature of the wire increases quite rapidly, the cloth somewhat more slowly, and the gas at a much slower rate at increased distance from the cloth surface.

Gaseous hydrocarbons are evolved as the cloth is heated past its decomposition temperature. These gases ignite and form a flame. The surrounding gases become less dense as they are heated before ignition if a constant

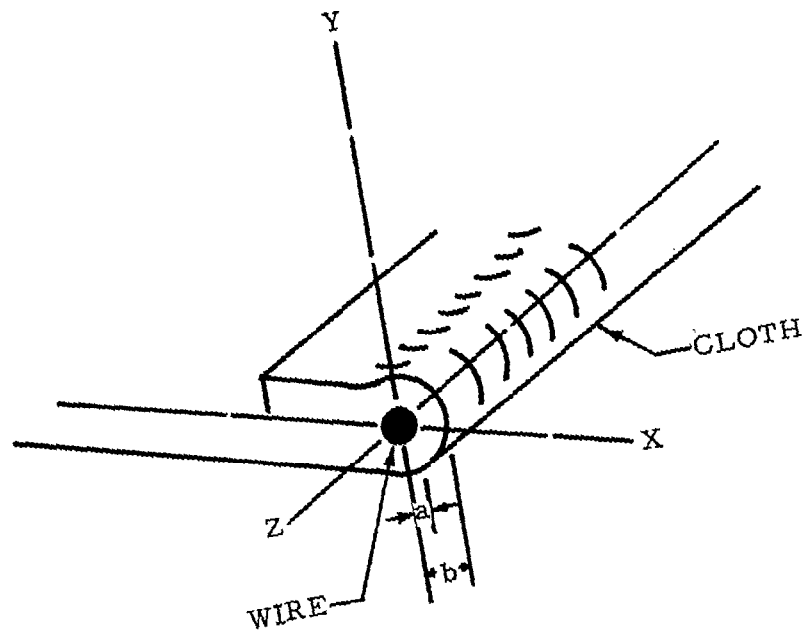


FIGURE 8-1 COTTON CLOTH AND IGNITION WIRE

TEMPERATURE

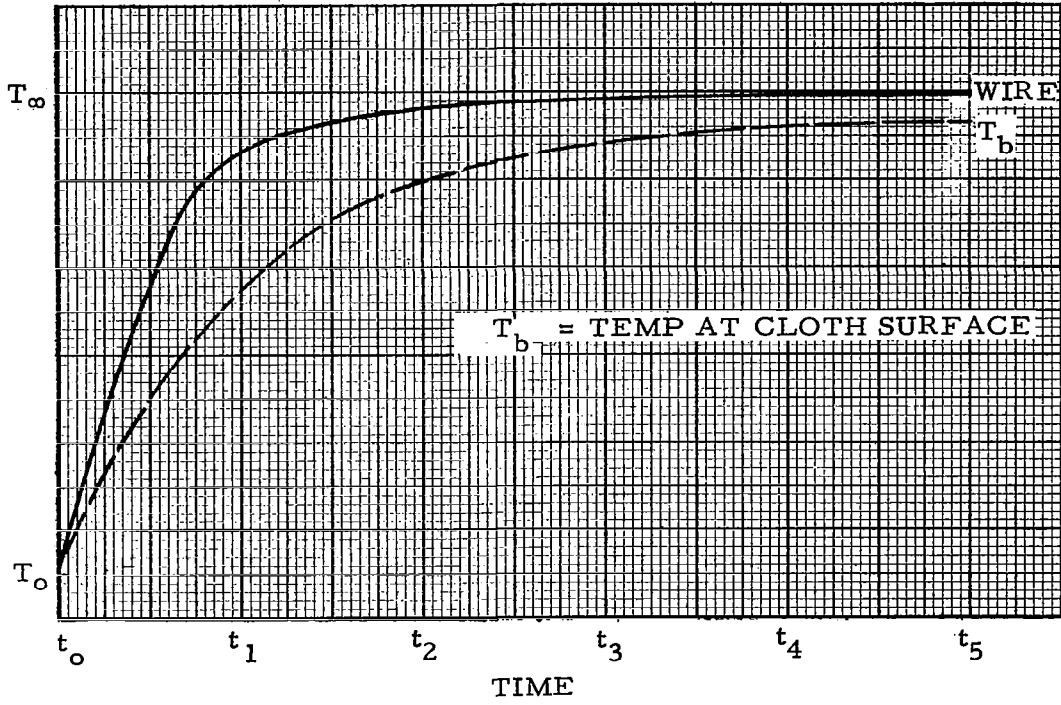


FIGURE 8-2 HEATING RATES OF WIRE AND CLOTH

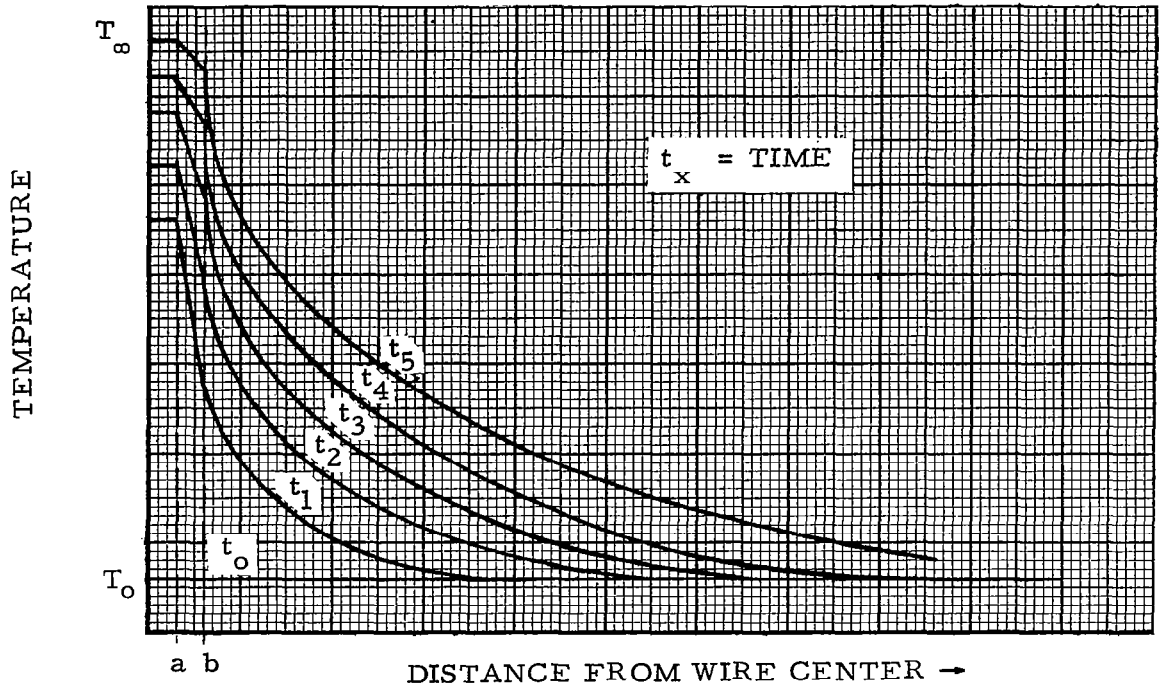


FIGURE 8-3 TEMPERATURE PROFILES (NO CONVECTION)

pressure system and negligible gas evolution is assumed. Density gradients appear as a function of time for ideal gas behavior as shown in figure 8-4. Assuming the application of Dalton's law, concentration gradients of oxygen in terms of moles of oxygen/liter shown in figure 8-5 can be calculated from the temperature profiles by the following equation:

$$C_{O_2} = C_{O_2}^{amb} \frac{T_o}{T} \quad (8-1)$$

Where  $C_{O_2}$  is the concentration of oxygen expressed in moles/liter at the appropriate temperature. The evolved gases will tend to reduce the oxygen concentration in the region near the cloth at an increased rate since a net flux of gases will be directed outward from the cloth surface. Now the oxygen concentration gradients in the system will actually appear as shown in figure 8-6. The oxygen concentration and temperature at any point in the system may be determined at any time from profiles similar to those of figures 8-3 and 8-6. The minimum temperature at which cotton cloth will ignite has been proven by test to be discussed later to be a function of the partial pressure of oxygen. This is consistent with the statistical kinetic models which indicate that self-sustaining oxidation depends upon the number of collisions of oxygen and fuel molecules (concentration dependent), and the energies at which they collide (temperature dependent). The experimental curve of minimum ignition temperature for cotton cloth as a function of the concentration of oxygen, corrected for temperature, is shown in figure 8-7. The region above the curve represents conditions which will result in ignition.

Neglecting the evolution of gases during the heating of the cloth, a temperature-concentration gradient will proceed up to the maximum wire temperature along line A. If this were the case, the surface would ignite when its temperature reached the minimum ignition temperature as evidenced by the intersection with the minimum ignition curve.

The effect of the evolution of gases by the decomposition of the cloth is seen by plotting points representing a region of gas immediately adjacent to the surface of the cloth at various times. The curve shifts toward lower oxygen concentrations corresponding to the change in oxygen concentration gradient shown in figure 8-6. Line B shown in figure 8-7 represents the temperature-concentration profile at various times for a point near the cloth surface. Line B does not cross the minimum ignition line. It is tangential with line A since the effect of evolved gases will become negligible at larger distances, and asymptotically approaches zero at the higher temperatures since there will be essentially no oxygen at the surface of the cloth. The dashed lines extending from each time point represent a temperature-composition gradient with the distance at that particular time. The distance scale is very non-linear since the point  $C_{O_2}^{amb}$  represents the bulk concentration and ambient temperature at an infinite distance away from the cloth surface. At time  $t_5$ , the gradient becomes tangential to the minimum ignition curve, and ignition occurs. Therefore, ignition takes place in the combustible gases some distance away from the surface of the cloth. If the time-temperature curve of the surface of the cloth can be obtained, the evolution rate of the gases from the cloth estimated, and the minimum ignition curve for the particular material obtained, the ignition time in null gravity can be calculated.

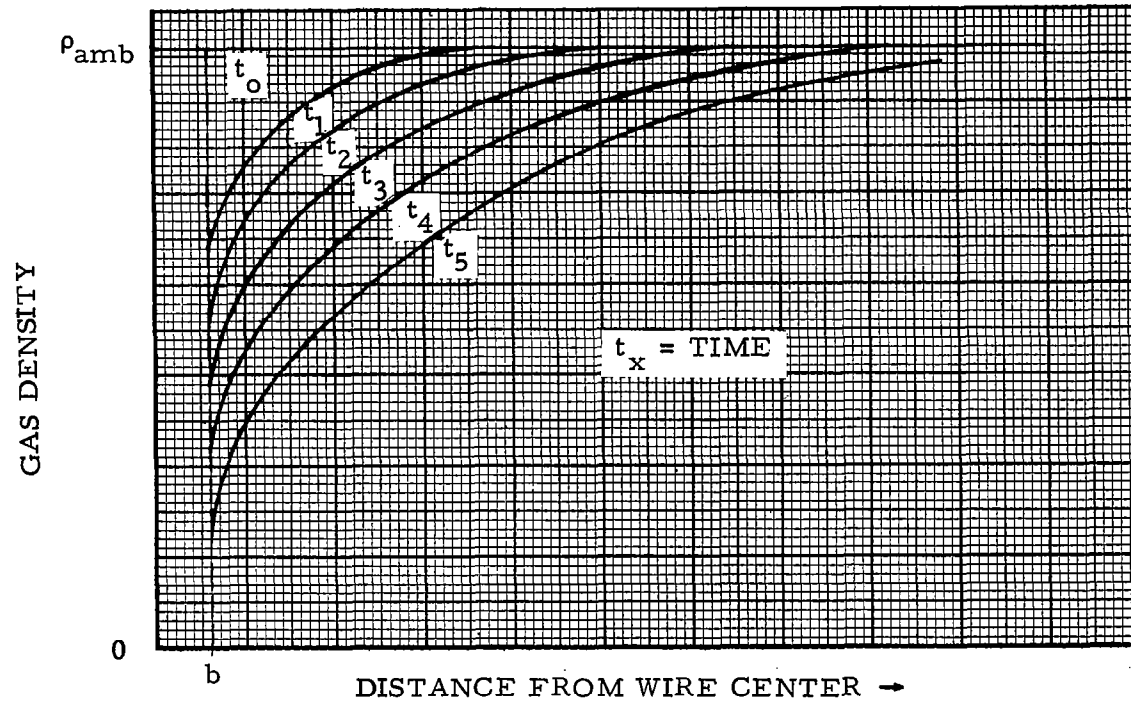


FIGURE 8-4 GAS DENSITY PROFILES (NO CONVECTION- EVOLVED GASES CONSIDERED NEGLIGIBLE)

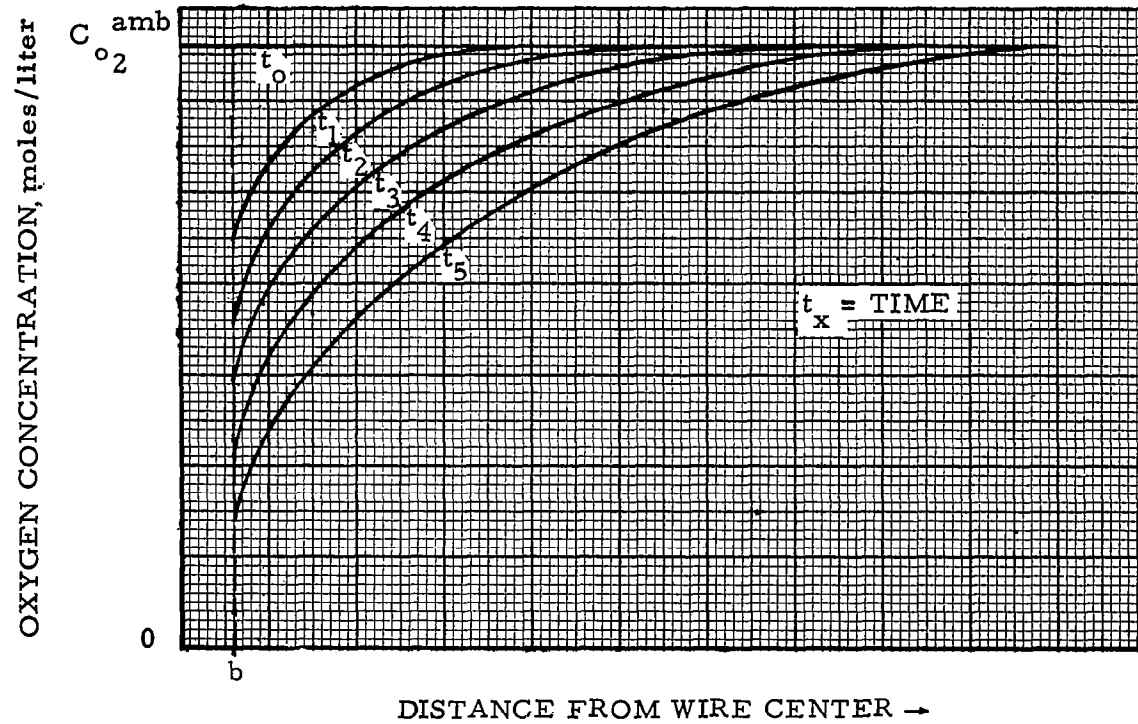


FIGURE 8-5 OXYGEN CONCENTRATION PROFILES (NO CONVECTION, NEGLECTING EVOLVED GASES)

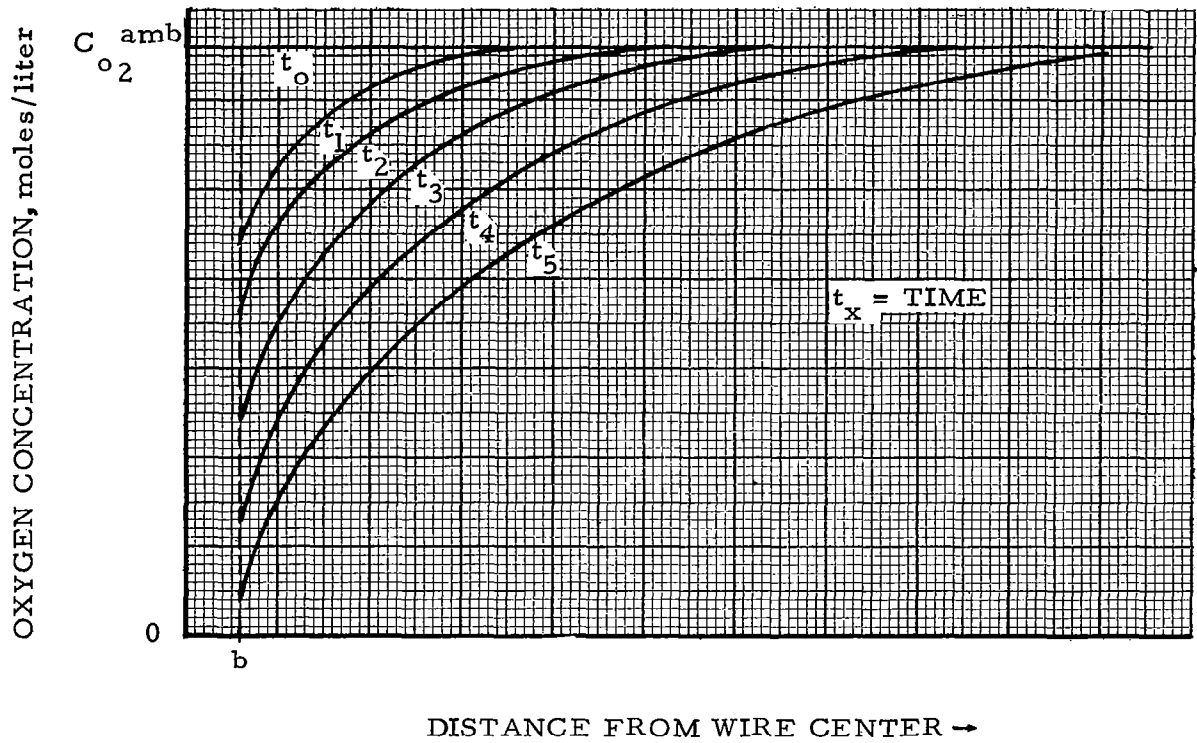


FIGURE 8-6 OXYGEN CONCENTRATION PROFILES (NO CONVECTION)

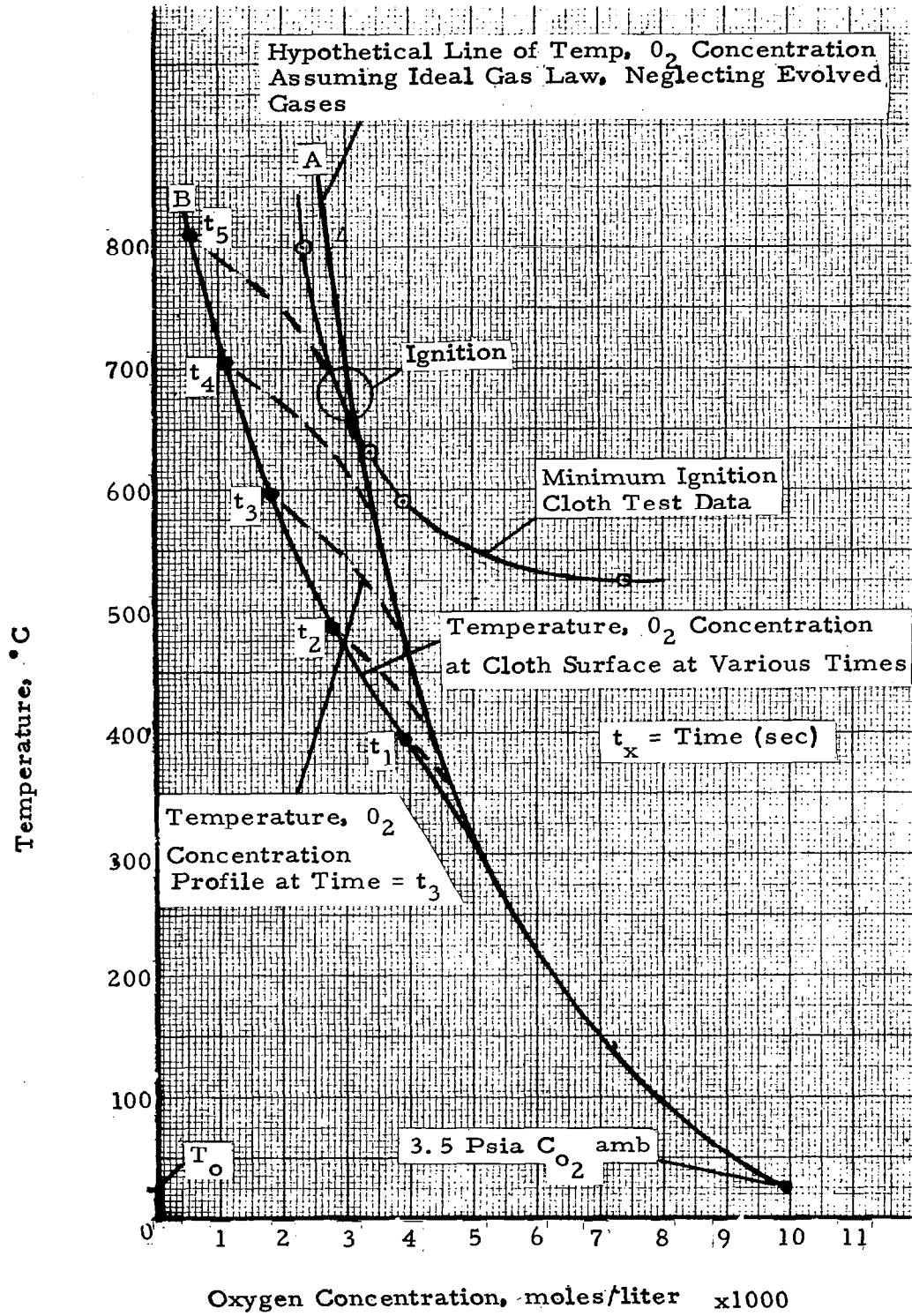


Figure 8-7 Ignition Process With No Convection Present

One of the major effects of free or forced convection will appear in the temperature profile. Figures 8-3 and 8-8 can be compared if the power is adjusted to permit the wire temperature to follow the same profile as in the case with no convection. The temperature will be lower at any point in the gas temperature profile with convection. Thus, ignition would be expected to take longer with convection due to the increased time required to reach the ignition temperature.

The effect of convection on the oxygen concentration profile is shown in figure 8-9. The density effect will be diminished due to the lower overall temperature conditions in the zone. The effect of evolved gases will not be as large since the gases will be physically removed by convection and replaced with oxygen-rich gas. The overall result will be to move the line representing the temperature-concentration conditions of a point near the cloth closer to the hypothetical line A of figure 8-7 which neglects evolved gases. Line B moves to the right for very high convection rates and eventually crosses the minimum ignition line. However, for normal convection rates as shown in figure 8-10, the gradients representing various times are closer to the curve and ignition occurs sooner with convection. Convection actually enhances ignition, a fact that also has many times been substantiated experimentally. Comparison of figure 8-7 and figure 8-10 also indicates the point of ignition occurs closer to the cloth surface with convection present, since oxygen is forced into the hot zone nearer the cloth. The ignition point occurs very close to the cloth surface for high convection rates since the predicted shape of the temperature profile of the cloth is no longer valid due to rapid cooling. Extremely high convection rates can sweep away and dilute the combustible evolved gases, and ignition will be retarded and in some cases prevented.

Gravity indirectly affects heat transfer rate through buoyancy forces. However, gravity should have no effect upon ignition temperature. Convective velocity and gas pressure may influence the heating rate and dilute the combustible gases but should have very little effect upon the ignition temperature. Null gravity test run 4, for N<sub>2</sub>-O<sub>2</sub> gas mixture of 7 psia, had a time to ignition the same as that obtained in one-g test for the same ignition temperature. More tests in null gravity are required to verify the above statements. However, Kimzey also recognized that the ignition phenomena difference between no convection in null gravity and free convection at one g is relatively small (ref. 8-1).

### Low Gravity Burning Characteristics

A general analysis of simple models has been considered in order to obtain some insight into the effects of gravity, diluent gas, oxygen concentration and convection velocity on combustion characteristics. A brief review of the literature indicates that the combustion of a material such as cotton cloth in a stagnant or low velocity atmosphere, takes place with a diffusion flame which usually is laminar.

The literature mainly discusses gas phase reactions. Although some consideration was given to the burning of liquid drops or wax pellets, very

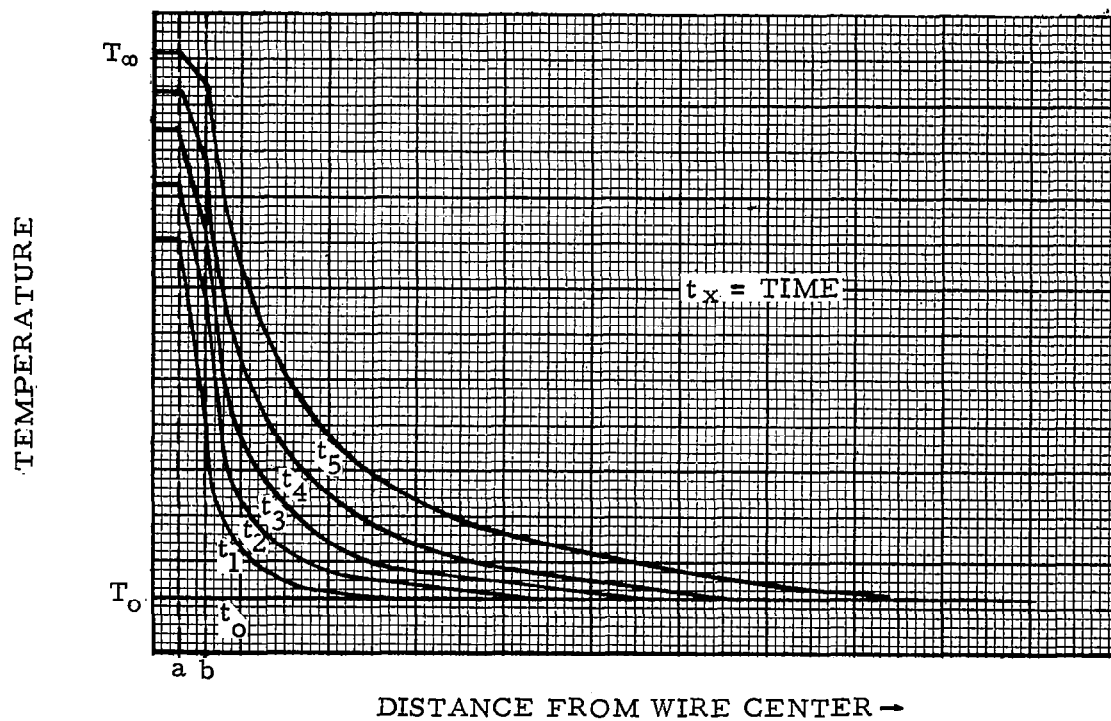


FIGURE 8-8 TEMPERATURE PROFILES (FREE AND/OR FORCED CONVECTION)

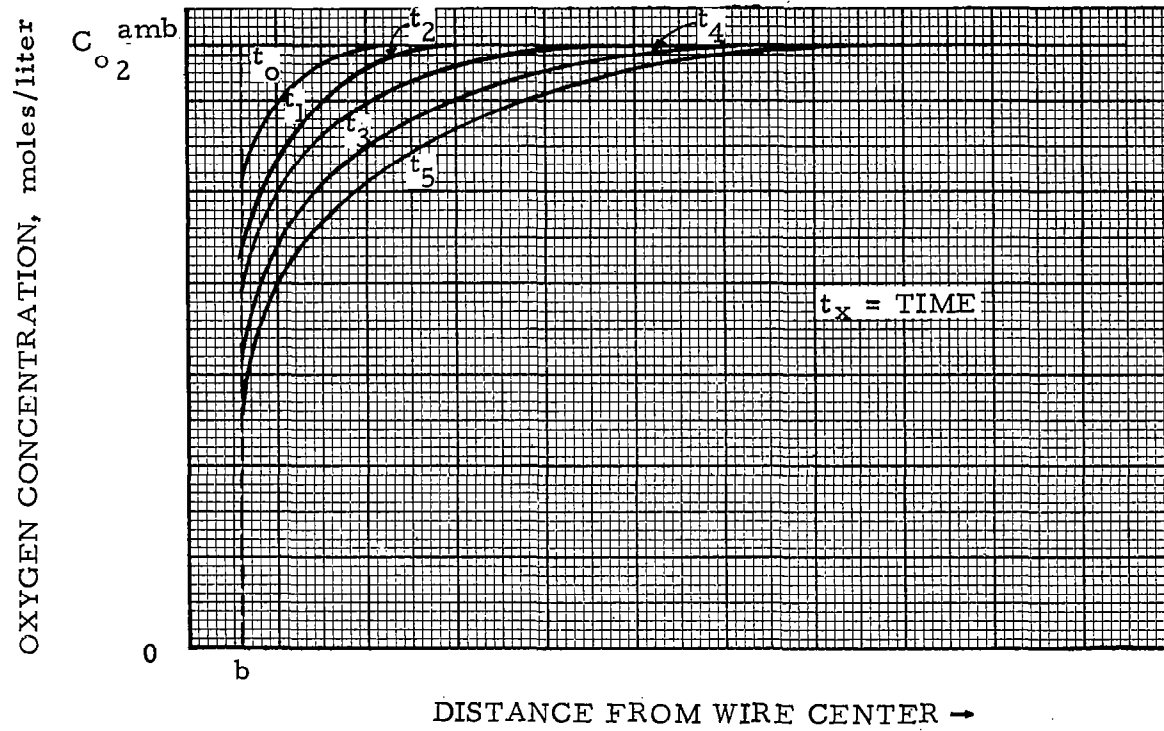


FIGURE 8-9 OXYGEN CONCENTRATION PROFILES (FREE AND/OR FORCED CONVECTION).

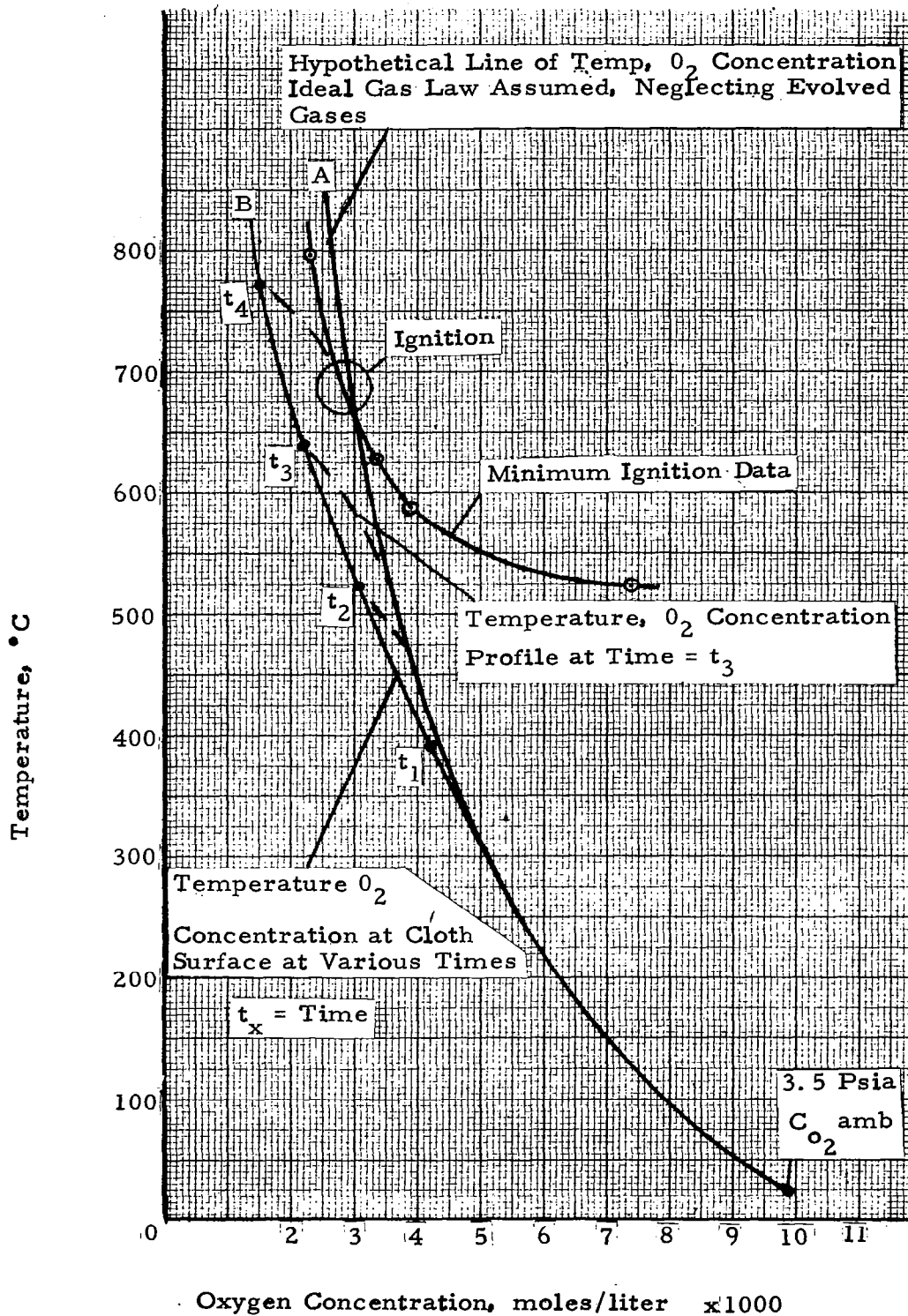


Figure 8-10 Ignition Process With Convection Present

little was found on the combustion of solids. There was general agreement that the ignition and combustion of alpha-cellulose was dominated by thermal diffusion.

The combustion of a solid such as alpha-cellulose or cotton cloth is characterized by a luminous flame. Heat transmitted from the flame front causes vaporization of the volatile gases in the solid material which form an expanding blanket over the solid surface to the flame front. The combustion of this expanding gas at the flame front produces combustion products at an even higher temperature and further outward expansion. However, oxygen from the free atmosphere must diffuse inward to the flame front in sufficient quantity to support the combustion reaction. The combustion mechanics therefore consists of:

1. The transfer of heat from the luminous flame to solid surface, vaporizing combustible gas.
2. Expansion of this gas during heating to reach the flame front.
3. Mass transfer of enough oxygen from the free atmosphere to the flame front to support combustion.
4. Combustion of the expanding combustible products.

Combustion is therefore a combination of heat transfer and mass transfer processes. If convection is present, the mass transfer process is aided. This convection may be self generated in a normal gravity field, supporting rapid combustion. However in null gravity, free convection will not occur. In the absence of outside gas circulation (forced convection), the mass transfer of oxygen into the flame front may then be inhibited to the point where combustion is considerably slowed or even extinguished. Since systems usually require checkout prior to flight, characteristics in both one g and null g must be considered, in any event.

The following analysis is based upon heat transfer concepts, although the process is known to include mass transfer as well. The considerations are similar, however, since Reynold's Analogy of heat and mass transfer shows that the two processes are closely related and governed by similar equations.

The heat transfer by convection from a horizontal heated flat plate is given by an equation of the form

$$\frac{hL}{k} = 0.54 (Gr Pr)^{1/4} \quad (8-2)$$

It has been shown that combustion involves a combination of convection (of oxygen into the flame front at least) and conduction (from the flame front to the burning material). For conduction into a semi-infinite medium due to a step rise in temperature at the interface (ignition), the following equation is given (ref. 8-4).

$$\frac{T - T_{\infty}}{T_o - T_{\infty}} = G \frac{X}{2 (a\theta)^{1/2}} \quad (8-3)$$

in which G is the Gaussian error integral.

A critical time and critical diffusion length can be derived in which the conduction heat transfer (time variant by equation 8-3) is equal to the convection heat transfer. In this derivation, the time is assumed arbitrarily to equal that for the temperature to reach 90 percent of the steady state value given by equation 8-3, or

$$\frac{T - T_{\infty}}{T_o - T_{\infty}} = 0.90 \quad (8-4)$$

Substitution of equation (8-4) into (8-3) and solution results in the following:

$$\frac{X_c}{2 (a \theta_c)^{1/2}} = 1.12$$

or

$$\theta_c = \frac{1}{a} \left[ \frac{X_c}{2.24} \right]^2 \quad (8-5)$$

In equation (8-5) the critical diffusion length,  $X_c$  is the distance in which the temperature transient has penetrated in the critical time period  $\theta_c$ . The heat transfer rate for conduction is given by

$$\dot{q} = \frac{kA (T_o - T_{\infty})}{(\pi a \theta_c)^{1/2}} \quad (8-6)$$

and for convection by

$$\dot{q} = hA (T_o - T_{\infty})$$

or, substituting from equation (8-2),

$$\dot{q} = A (T_o - T_{\infty}) \frac{k}{L} \times 0.54 (Gr Pr)^{1/4} \quad (8-7)$$

Equations (8-6) and (8-7) can be solved simultaneously, as shown in reference 8-5, to derive the following expression for critical time as a function of gravitational level,  $g_c$ ,

$$\theta_c = 1.04 \left[ \frac{L Pr}{g_c \beta (T_\infty - T_o)} \right]^{1/2} \quad (8-8)$$

Equations (8-5) and (8-8) may be equated and solved for  $g_c$  to derive the following expression for critical diffusion length as a function of gravitational acceleration:

$$X_c = 2.28 \left[ \frac{a^2 L Pr}{\beta g_c (T_\infty - T_o)} \right]^{1/4} \quad (8-9)$$

Equation (8-9) shows that, as gravitational forces are reduced, the critical diffusion length  $X_c$  must be increased. In other words, the region around the flame becomes more contaminated with combustion products, inhibiting transfer of fresh oxygen to maintain the flame. This is consistent with experimental observations in which combustion activity is greatly reduced in low  $g$  tests, compared with equivalent one  $g$  conditions. For example, during Test Run 12 reported subsequently, in a 7 psia helium-oxygen atmosphere, a fire which was started under one  $g$  was extinguished when the aircraft reached a near-null gravity condition (between  $10^{-3}$  and  $10^{-2}$   $g$ 's) and re-ignited a few seconds later after "pull out." Apparently the low gravity prevents visible combustion but does not allow sufficient cooling of the test item to bring it below the ignition temperature. It therefore is able to resume combustion when higher free convection rates are imposed. Of course, if null gravity is maintained long enough to allow cooling of the specimen, no re-ignition would take place.

To relate the conditions of free and forced convection, a critical velocity will be introduced. This critical velocity is that in which the heat transfer and corresponding mass transfer rates due to forced convection are equal to those due to free convection.

The heat transfer coefficient for laminar forced convection parallel to a flat plate is as follows:

$$h = 0.664 \frac{k}{L} (Re)^{1/2} (Pr)^{1/3} \quad (8-10)$$

The initial convective velocity can be found by equating (8-2) and (8-10):

$$V_c = 0.664 \left[ L g_c \beta (T_\infty - T_o) \right]^{1/2} \quad (8-11)$$

Figure 8-11 shows a representative plot of equation (8-11), for values of  $T_{\infty} - T_0 = 2000^{\circ}\text{F}$ . This plot shows the approximate convective velocities resulting from the combustion of a 2-in. specimen at a temperature of  $2000^{\circ}\text{F}$  and therefore is an indication of the boundary between free and forced convection as a function of  $g$  level. As an example, at 1  $g$  the value is given as approximately 1.5 ft/sec or 90 ft/min. Although this is slightly high it is not hard to visualize such a convective velocity being developed by a  $2000^{\circ}$  flame. At  $g_c = 10^{-2}$ ,  $V_c = 0.15$  ft/sec or 9 ft/min. If data with natural convection show flame extinguishment at  $10^{-2} g$ , then it would be reasonable to expect a forced convective velocity of 9 ft/min would be required to support combustion under true null gravity conditions. This is significant because the critical range of  $10^{-3}$  to  $10^{-2} g$  estimated previously represents critical velocities from 3 to 9 ft/min. Crew comfort considerations are almost certain to require substantially higher convective velocities than these. From this, it can be concluded that forced convection will be controlling combustion processes in spacecraft under null gravity, except in closed areas where cabin circulation fans do not reach.

## IGNITION AND BURNING TEST PROCEDURE AND DATA

So that data could be provided on representative inflammable samples, cotton cloth and insulated wire were selected to determine the effects of atmosphere and gravity on ignition time and burning phenomena. The cloth used was Flight-Text Grade A(MIL-C-5646C). A 2 in. x 2 in. cloth was selected as best suited in size for 6 to 22 sec null gravity tests. Propagation rates were evaluated using 8 in. x 2 in. specimens. The size is most adaptable to the longer null gravity flights.

The test description and representative results are reported as follows:

- Atmospheric effect of ignition temperature.
- Atmospheric effect on ignition and burning of cloth in 1  $g$ .
- Atmospheric effect on ignition and burning of insulated wire in 1  $g$ .
- Null gravity fire test procedures and data.

### Atmospheric Effect On Ignition Temperature

Analysis indicates that ignition temperature should be a unique number for each material and atmospheric composition. Therefore, if the ignition temperature for the test material is known then this parameter can be set for the null gravity flights, thus eliminating one very important variable. Ignition temperature tests were conducted using a 4 in. x 4.5 in. x 1/4 in. thick copper hot plate and the Space Cabin Simulator for containing the atmospheric mixture and gas pressure required for the test. The test set up is shown in Figure 8-12. Figure 8-13 shows the results of a test run.

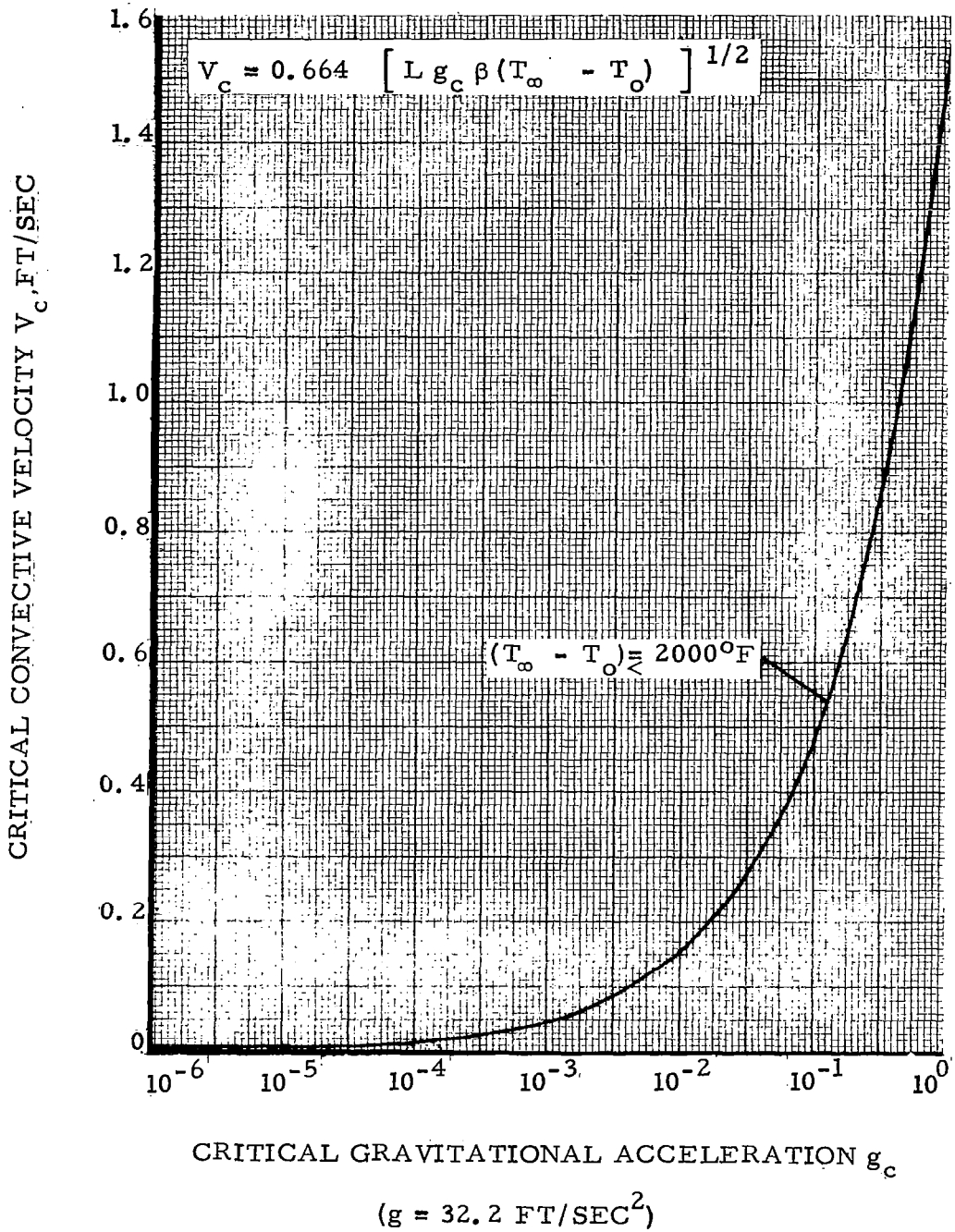


FIGURE 8-11 VARIATIONS OF CRITICAL CONVECTIVE VELOCITY AS A FUNCTION OF CRITICAL GRAVITATIONAL ACCELERATION

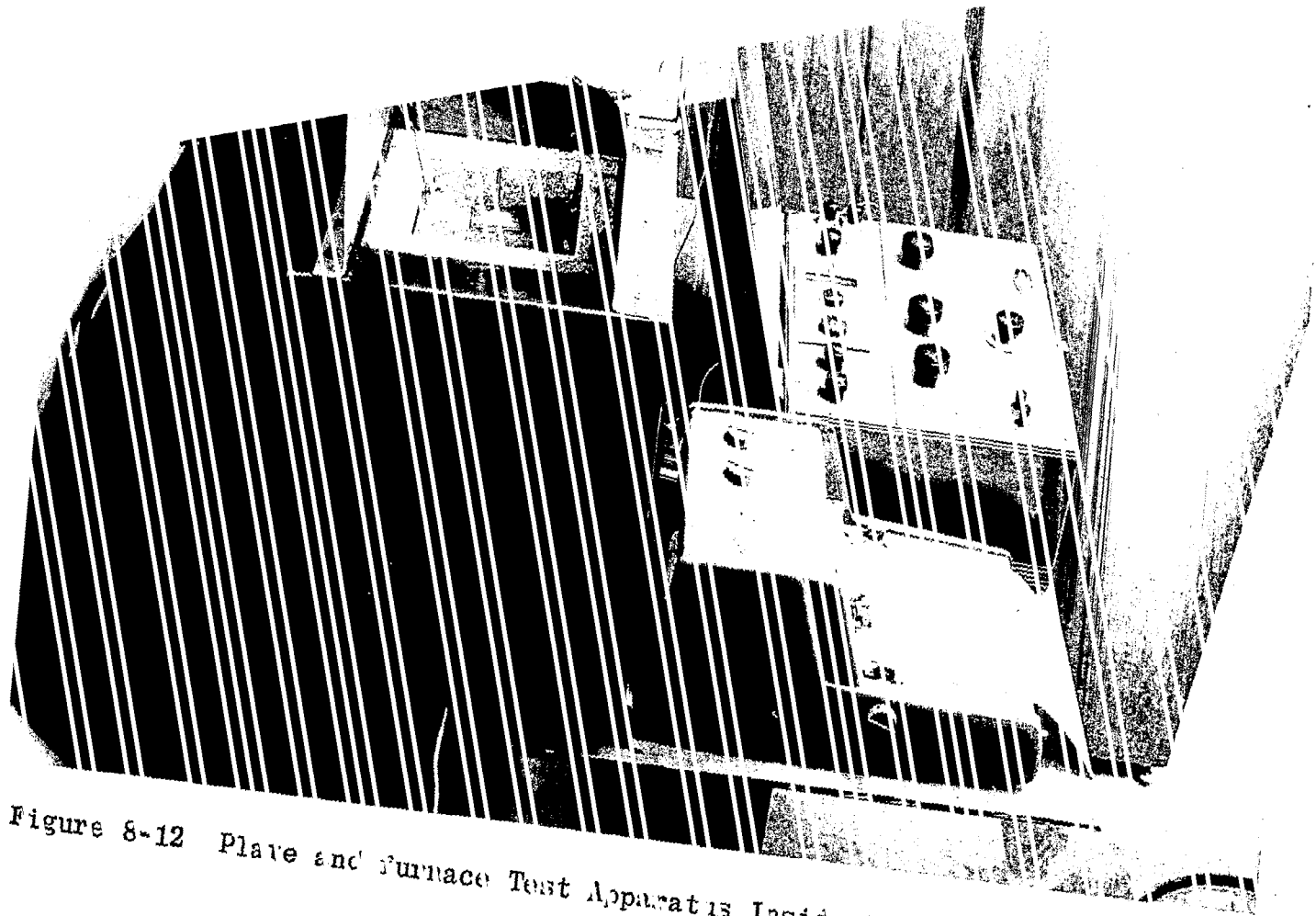


Figure 8-12 Plate and Furnace Test Apparatus Inside the Space Cabin Simulator



Figure 8-13 First Ignition of Cotton Cloth Specimen

A sample result of an ignition test run for cloth and the insulated wire with 50/50 nitrogen-oxygen at 7 psia is shown in figure 8-14. The triangles represent samples that did not ignite and the circles represent ignition. Figure 8-15 presents the ignition temperature data obtained for three minimum ignition temperature determinations for both cloth and wire insulation.

Figure 8-16 shows all averaged ignition temperatures for both cloth and wire specimens for the different atmospheric conditions. All of the minimum ignition temperatures for the cloth and all for the wire insulation appear to lie within relatively narrow limits, with the exception of some points reported at 5 psia with helium diluent.

The observers reported, at 5 psia with helium diluent, the appearance of a very small flame as the sample was almost decomposed at relatively low temperatures. This did not occur in any of the other tests, and thus these were not considered to be ignitions. The true ignition occurred almost immediately after the specimens were placed on the plate, and the entire sample was engulfed in a yellow flame.

These tests indicated that the minimum ignition temperature for cotton cloth, when the partial pressure of oxygen is between 3.1 and 3.5 psia, is between 630°C and 660°C and is independent of the amount of nitrogen or helium present at total pressures between 5 psia and 14.7 psia. The minimum ignition for the wire insulation under the identical atmospheric restraints mentioned above is between 680°C and 730°C.

The variation of ignition temperature with increased oxygen pressure was also determined and shown in figure 8-15. Figure 8-15 indicates that an increased oxygen pressure causes a rapid decrease in the ignition temperature up to about 7 psia pressure level. Additional ignition temperature tests were performed for 5, 7, and 10 psia nitrogen-oxygen and helium-oxygen mixtures, with 3.5 psia oxygen. The ignition temperatures obtained agreed with the pure oxygen test results given in figure 8-15. It is therefore concluded that the ignition temperature is not affected by the presence of the diluent, but rather by the concentration of oxygen present within the limits tested. Similar results were reported by Alvares and Fisher and Gerstein (ref. 8-6 and 8-9).

#### Atmospheric Effect on Ignition and Burning of Cloth in One g

The following discussion covers additional tests conducted in 72 liter Pyrex flasks on cotton cloth samples to determine the effect of atmospheric composition and pressure on ignition and burning. More tests were conducted for the cotton cloth than for the wire samples because of the ease of accurate measurement and the distinct separation of the burning phenomena. Figure 8-17 shows the test apparatus used for cotton cloth tests.

Ignition and Burning Time of Cotton Cloth. --The 2 in. x 2 in. test specimen was attached to the stainless steel grid at five points to prevent the lifting of the cloth from the grid by convective forces. The edge of the cloth specimen was folded over the nichrome wire to ensure good contact for ignition. After positioning the test specimen, the flask was purged with pure

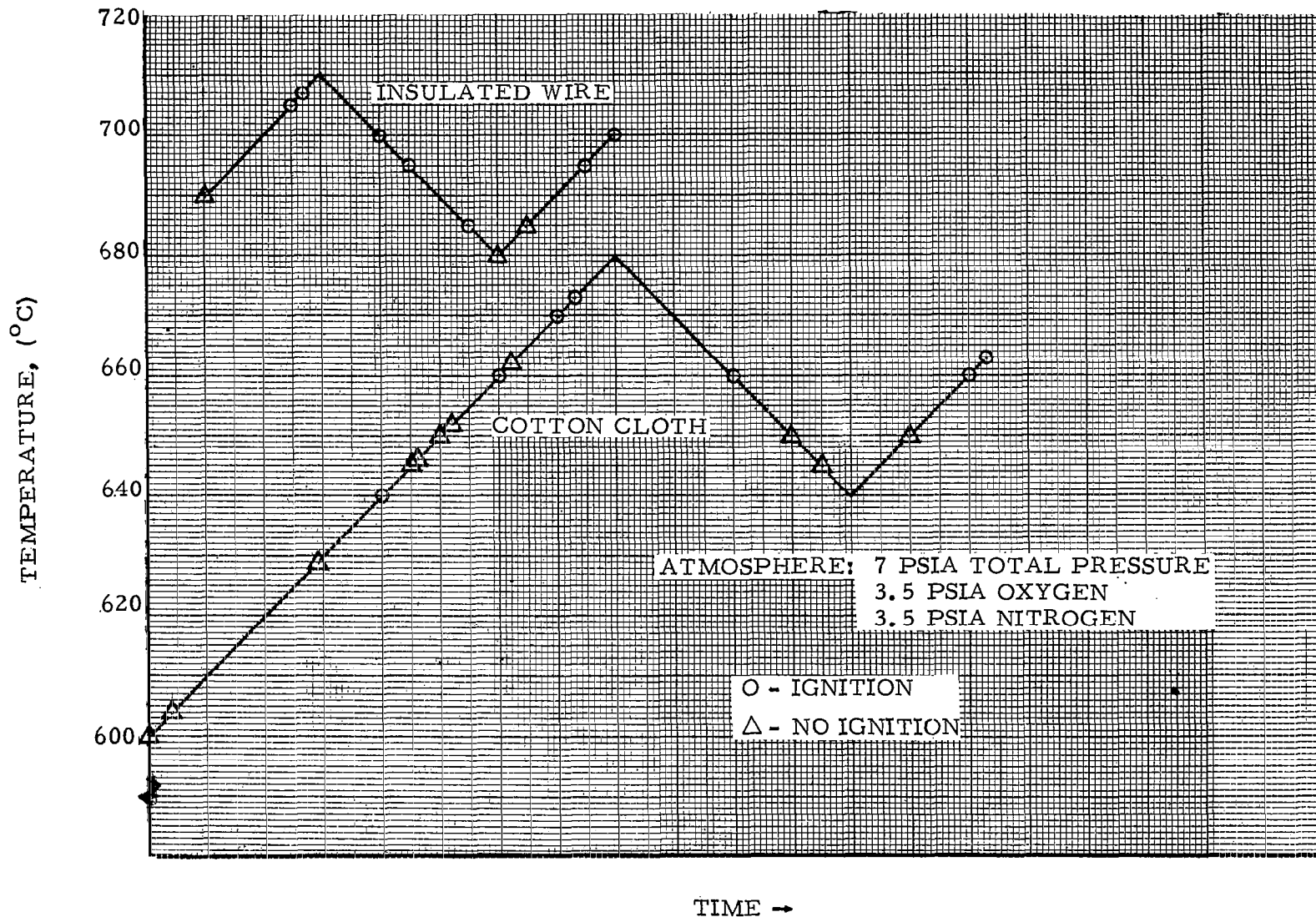


FIGURE 8-14 MINIMUM IGNITION TEMPERATURES OF SPECIFIC TEST SPECIMENS

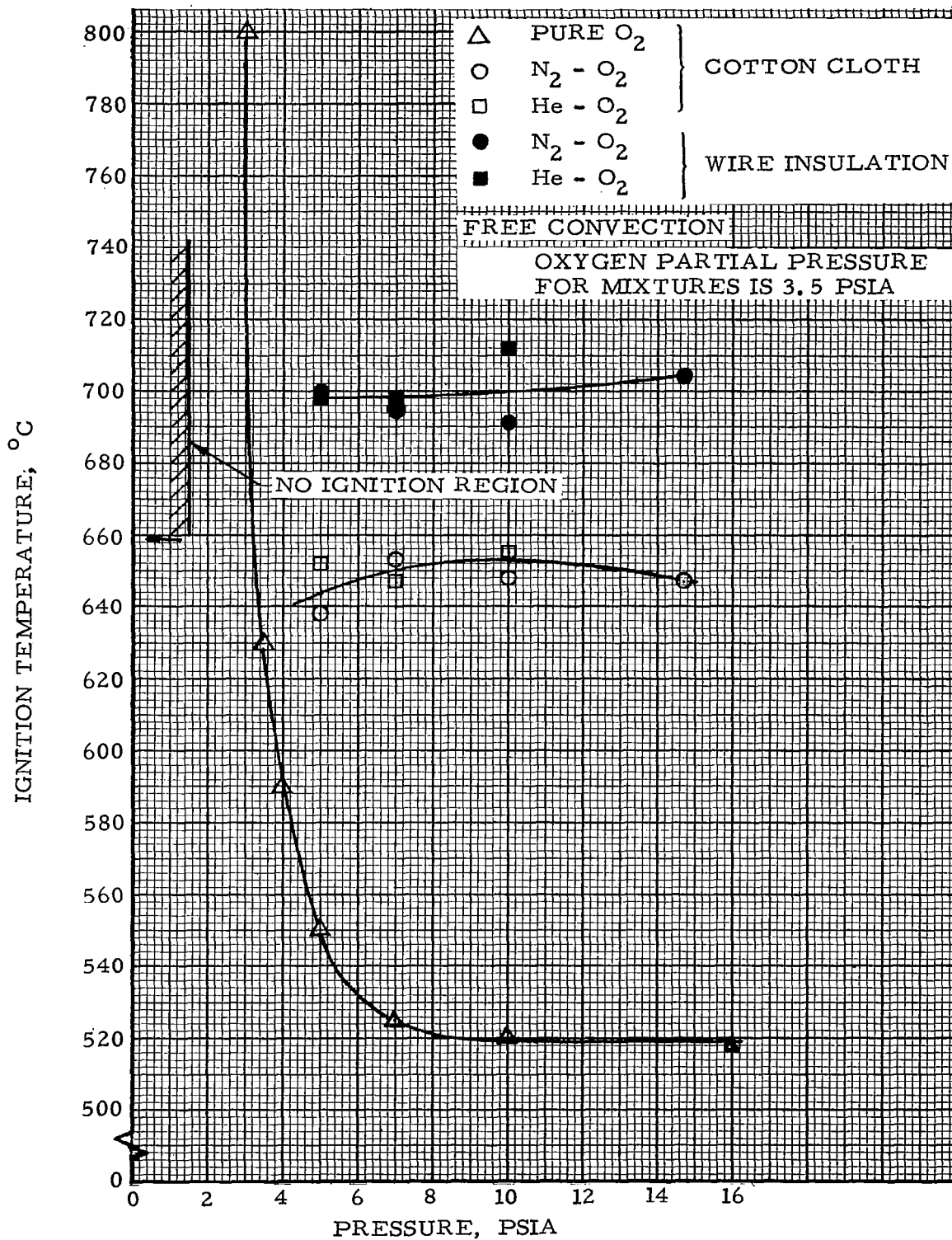


FIGURE 8-15 IGNITION TEMPERATURE FOR COTTON CLOTH AND WIRE INSULATION

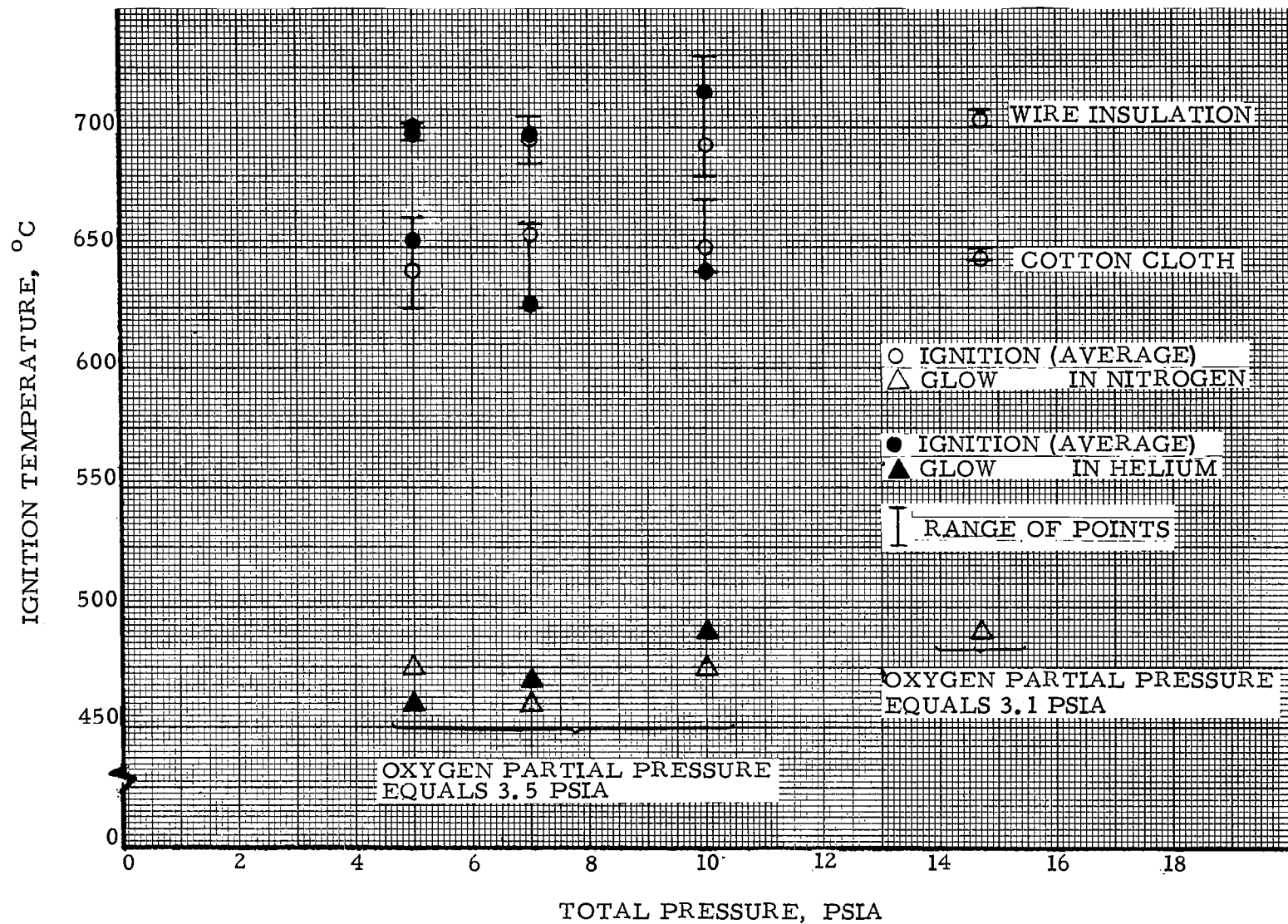


FIGURE 8-16 AVERAGE MINIMUM IGNITION TEMPERATURES

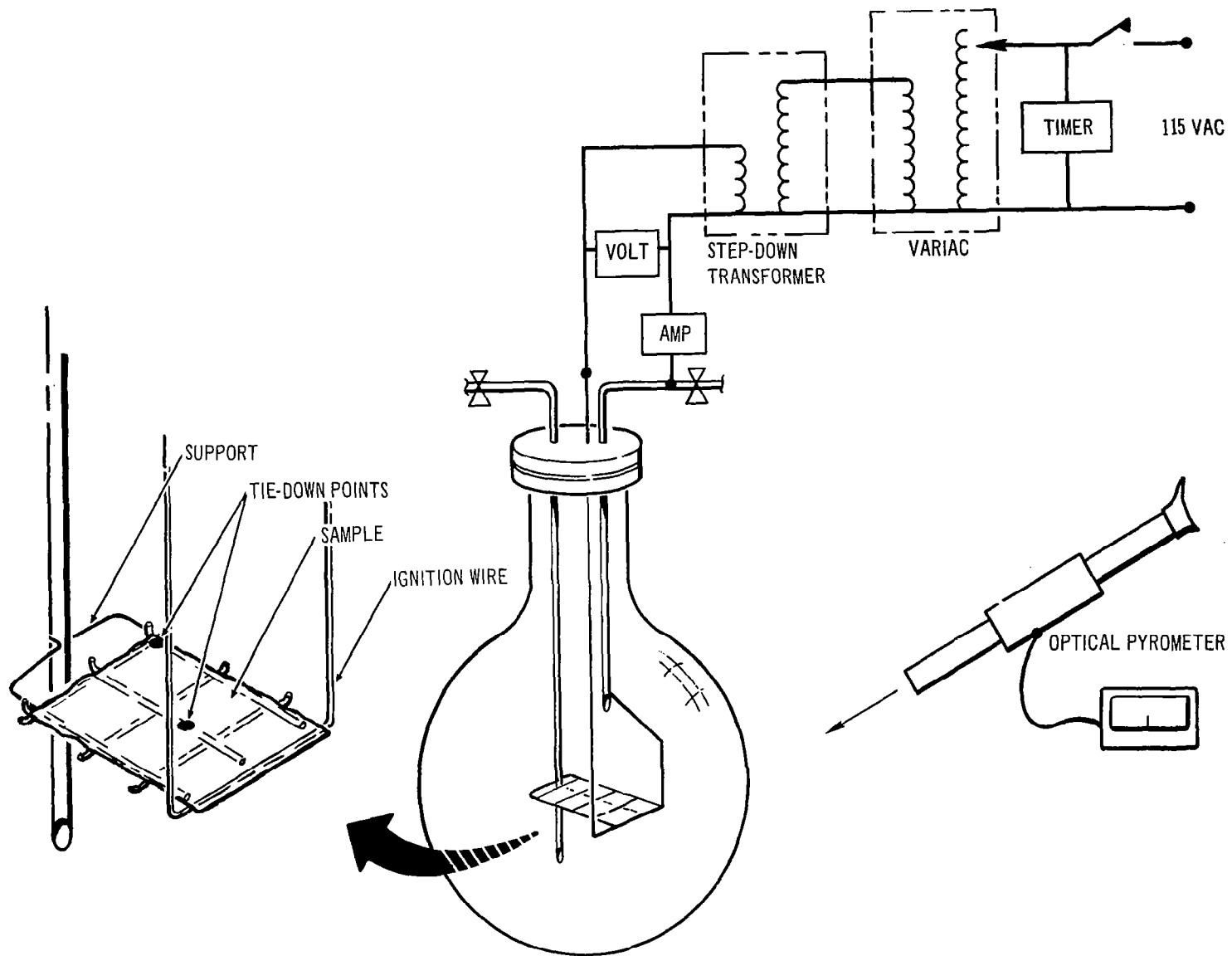


FIGURE 8-17 TEST SCHEMATIC

oxygen until gas samples indicated a nitrogen content of less than one percent. The flask was evacuated to the desired oxygen partial pressure. The diluent gas was added to obtain the desired composition and total pressure. Finally, the power was turned on to heat the ignition wire. Two stop watches were started simultaneously with power application. One watch was stopped at ignition and the second watch was stopped at the completion of combustion. The difference between the watches provided a measure of burning time. All runs were repeated four times and an average value was obtained. Table 8-I presents all of the atmospheric compositions tested and the results obtained.

The data in table 8-I illustrate the effect of oxygen partial pressure, as well as the presence of diluent gases, on the burning process. If data is compared for a particular atmospheric total pressure and wire temperature, it can be seen that the ignition times and burning times do not differ greatly, as shown in figure 8-18. The use of a constant wire temperature is somewhat misleading. In actual ignition conditions, the heat source is constant; thus, it was decided to repeat the tests with a constant power input and to allow the wire temperature to vary. In this situation, it is evident from figure 8-19 that the ignition times for the oxygen-helium atmospheres are significantly longer than for the oxygen-nitrogen atmospheres at both the 5- and the 7- psia total pressure conditions. These data seem to indicate that the higher thermal conductivity of the helium provides a greater cooling effect causing a lower cloth and wire temperature, and the result is a longer heat-up time for ignition.

Increasing the oxygen partial pressure causes a slight decrease in the ignition times. This is shown in figure 8-18 by comparing ignition of laboratory air that contains 3.1 psia of oxygen, 3.5 psia and 5.0 psia of pure oxygen, and the other atmospheric compositions containing 3.5 psia oxygen. This condition prevails when the wire temperature is held constant at 1035°C. If the power input is held constant as shown in figure 8-19, the effect of oxygen partial pressure is not apparent for the helium-oxygen atmospheres. The effect of diluent addition had a greater effect in increasing burning time than a slight change in oxygen pressure. The diluent gas would hinder the burning process not only by slowing the diffusion of oxygen into the flame area, but also by conducting heat away from the combustion area, thus slowing propagation. The large amount of nitrogen present in the laboratory air sample clearly illustrates this fact with the very long burning time. However at low diluent concentrations, the amount and the nature of the diluent apparently have little or no effect on the burning time as shown in table 8-I and figures 8-18 and 8-19. Although the foregoing discussion uses ignition time as an evaluation parameter, it is not the only measure of the different characteristics of an atmosphere. The wire temperature was kept low to emphasize the effect of ignition temperature. However, the power to the wire could have been increased to a level to minimize ignition time.

Determination of Combustion Rates. --The flask was modified to horizontally support a 2 in. wide by 8 in. long test sample of the same material described previously. The calibration of the flask and ignition wire rechecked and a test sample installed. The edges of these elongated samples were treated with a fire retardant solution Cal Flame Material Number 55. The time to burn each 2 in. interval was measured in addition to the ignition time, ignition temperature and total time to specimen consumption.

TABLE 8-I

## COTTON CLOTH BURN DATA FOR VARIOUS ATMOSPHERIC COMPOSITIONS

Atmospheric composition	Power input (watts)	Ignition temperature (°C)	Wire temperature (°C)	Ignition time (sec)	*Burning time (sec)	Total time (sec)
3.5 psia (100% O <sub>2</sub> )	51.3	630	1 035	7.5	12.9	20.4
5 psia (100% O <sub>2</sub> )	47.7	550	1 035	5.5	9.9	15.4
	37.2		880	10.3	10.2	20.5
5 psia N <sub>2</sub> (1.5 psia), O <sub>2</sub> (3.5 psia)	47.8	640	1 035	6.6	12.4	19.0
	39.0		880	10.2	13.6	23.8
5 psia He (1.5 psia), O <sub>2</sub> (3.5 psia)	64.7	652	1 035	5.8	11.5	17.3
	47.8		880	8.1	11.8	19.9
7 psia He (3.5 psia), O <sub>2</sub> (3.5 psia)	85.5	653	1 035	6.6	12.4	19.0
	57.1		880	10.2	11.6	21.8
7 psia N <sub>2</sub> (3.5 psia), O <sub>2</sub> (3.5 psia)	57.1	648	1 035	6.3	12.9	19.2
	44.8		880	9.5	12.7	22.2
Air N <sub>2</sub> (11.6 psia), O <sub>2</sub> (3.1 psia)	67.1	647	1 035	9.4	26.0	35.4

\*Time for complete combustion of the 2" x 2" specimen.

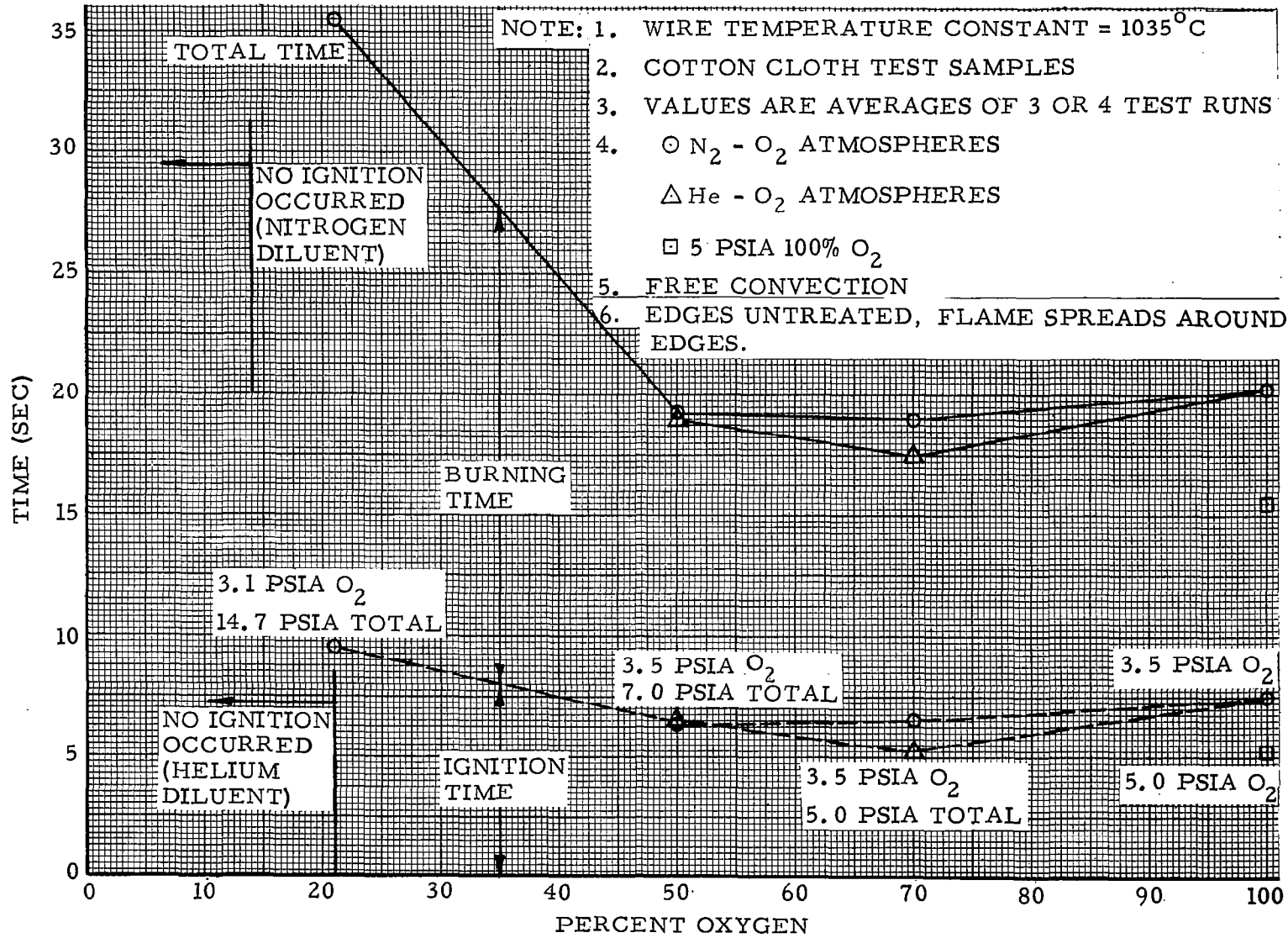


FIGURE 8-18 COMPARISON OF IGNITION AND BURNING TIME FOR COTTON CLOTH IN VARIOUS ATMOSPHERIC COMPOSITIONS (CONSTANT WIRE TEMPERATURE)

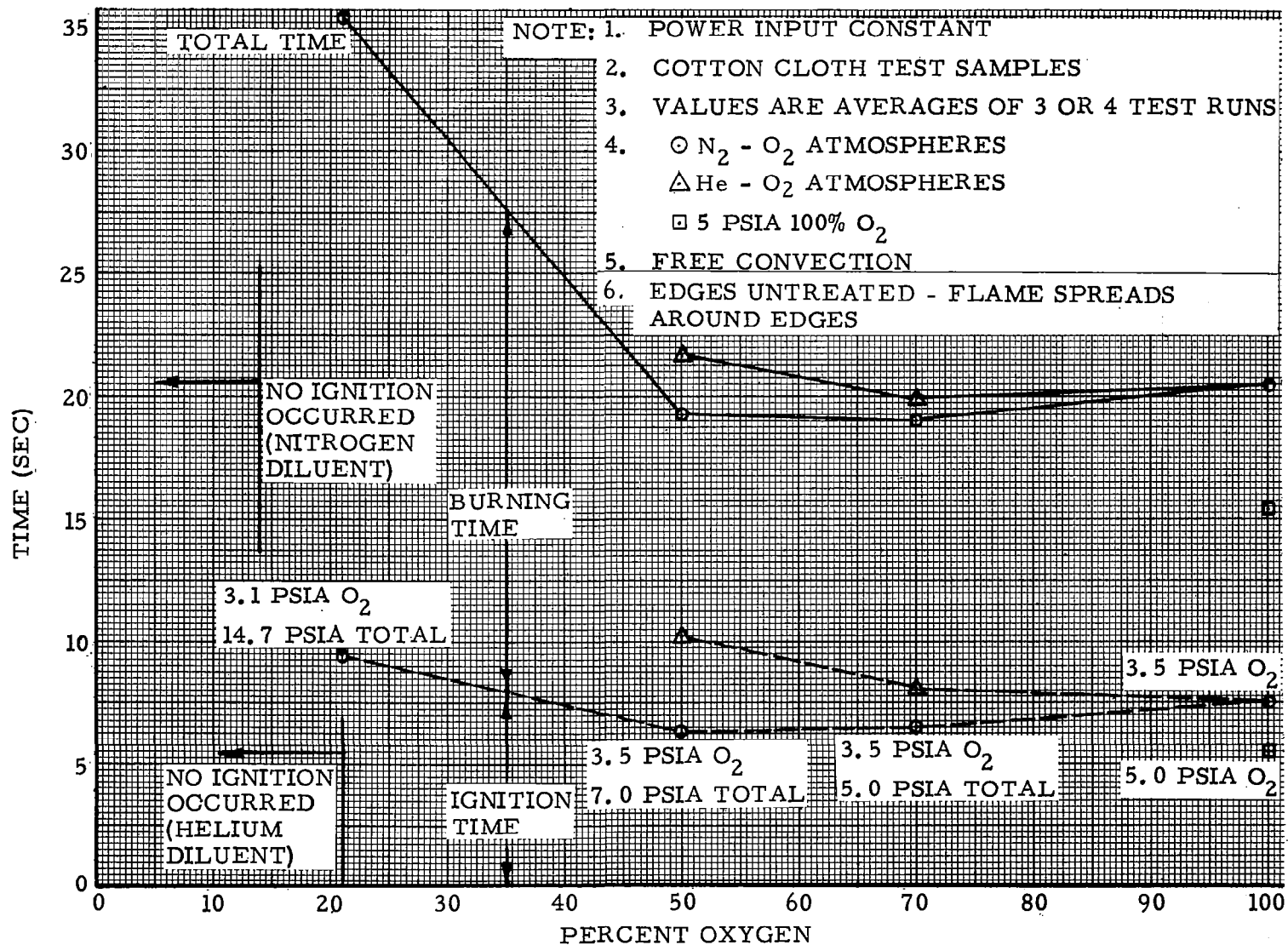


FIGURE 8-19 COMPARISON OF IGNITION AND BURNING TIME FOR COTTON CLOTH IN VARIOUS ATMOSPHERIC COMPOSITIONS (CONSTANT POWER INPUT)

Data presented in table 8-II show the different power inputs required to obtain a 1035°C wire temperature. The data is in good agreement with that previously reported. Helium diluent requires a larger power input for the ignition source to reach the ignition temperature than for nitrogen diluent. Once ignited, the burning rate in the presence of helium exceeds the burning rate in nitrogen by 20 to 30 percent. The burning rate in pure oxygen is from four to five times greater than for air, depending on the oxygen concentration.

The power required to reach the ignition temperature is not significantly higher in laboratory air than in pure oxygen atmospheres at 3.5 psia and 5 psia. The differences in power input between nitrogen and helium diluent, to reach the same operating temperature, are considerably greater. For example, 7 psia total pressure atmosphere containing equal concentrations of oxygen-nitrogen requires 42.5 w compared with 63.7 w for helium-oxygen mixtures under identical conditions.

It will be noted from figure 8-20 and table 8-II that combustion rates in oxygen-helium systems are higher than in nitrogen-oxygen. The addition of small amounts of helium up to 1.5 psi showed essentially no effect on burning rates. After further addition of helium the burning rate decreases below the value obtained with pure oxygen. The diffusion and thermal conductivity effects of helium become more pronounced with increased dilution and a sharp decrease in the rate of flame propagation results. The increased effect of nitrogen over helium in retarding burning rates is consistent with results reported by Chianta and Stoll (ref. 8-8).

The addition of 1.5 psia nitrogen to 3.5 psia pure oxygen had only a minor effect in reducing spread of fire. Not until the partial pressure of nitrogen was increased to 3.5 psia did a sizable reduction in burning rates occur. Tests by Klein also indicated that the first addition of diluent had only a minor effect on the reaction rate as compared with the burning rate in pure oxygen (ref. 8-3).

An effort was made to correlate the flame propagation rates with the heat capacity of the test gas mixtures per mole of oxygen. Huggett indicated the existence of a correlation between flame spread rate and molar heat capacities for the gas mixtures (ref. 8-2). The measurements of flame spread rates were limited to the surface of the test material without specimen consumption taking place. Table 8-III tabulates the computed heat capacities per mole of oxygen and the corresponding flame propagation rates. Figure 8-21 shows the two parameters placed on a semi-log scale. The straight line of regression obtained is similar to the relationship reported by Huggett.

Forced ventilation tests using the cotton cloth were completed to help correlate the effect of convection between the one g and planned null gravity tests. Burning tests involving forced convection into the flame zone were also completed using the 72-liter Pyrex flask. The blower was calibrated by determining the power input required to produce an air velocity of 50-ft/min at a vertical distance of 6 in. below the cloth. The power input was calibrated to provide the same air velocity for the different mixtures and pressures used in this test series.

TABLE 8-II

EFFECTS OF DIFFERENT ATMOSPHERES ON THE COMBUSTION RATE OF COTTON CLOTH  
(8 inch x 2 inch specimen) (Treated Edges)

Atmospheric composition	Power input (watts)	Ignition temperature (°C)	Wire temperature (°C)	Average propagation time per inch of cloth (sec)	Rate (inch/sec)	Total burning time (sec)
3.5 psia 100% O <sub>2</sub>	35.0	636	1 035	2.56	0.46	34.6
5 psia 100% O <sub>2</sub>	37.1	552	1 035	2.03	0.49	28.5
10 psia 100% O <sub>2</sub>	--	520	1 035	1.97	0.51	--
16 psia 100% O <sub>2</sub>	--	520	1 035	1.73	0.58	--
5 psia N <sub>2</sub> (1.5 psia), O <sub>2</sub> (3.5 psia)	34.7	641	1 035	2.71	0.37	33.1
5 psia He (1.5 psia), O <sub>2</sub> (3.5 psia)	46.4	651	1 035	2.34	0.43	30.9
7 psia N <sub>2</sub> (3.5 psia), O <sub>2</sub> (3.5 psia)	42.5	649	1 035	3.77	0.25	40.7
7 psia He (3.5 psia), O <sub>2</sub> (3.5 psia)	63.7	652	1 035	2.90	0.34	36.3
10 psia He (6.5 psia), O <sub>2</sub> (3.5 psia)	55.2	648	1 035	3.65	0.27	42.8
Air	47.2	650	1 035	10.0	0.1	95.4
N <sub>2</sub> (11.6 psia), O <sub>2</sub> (3.1 psia)						

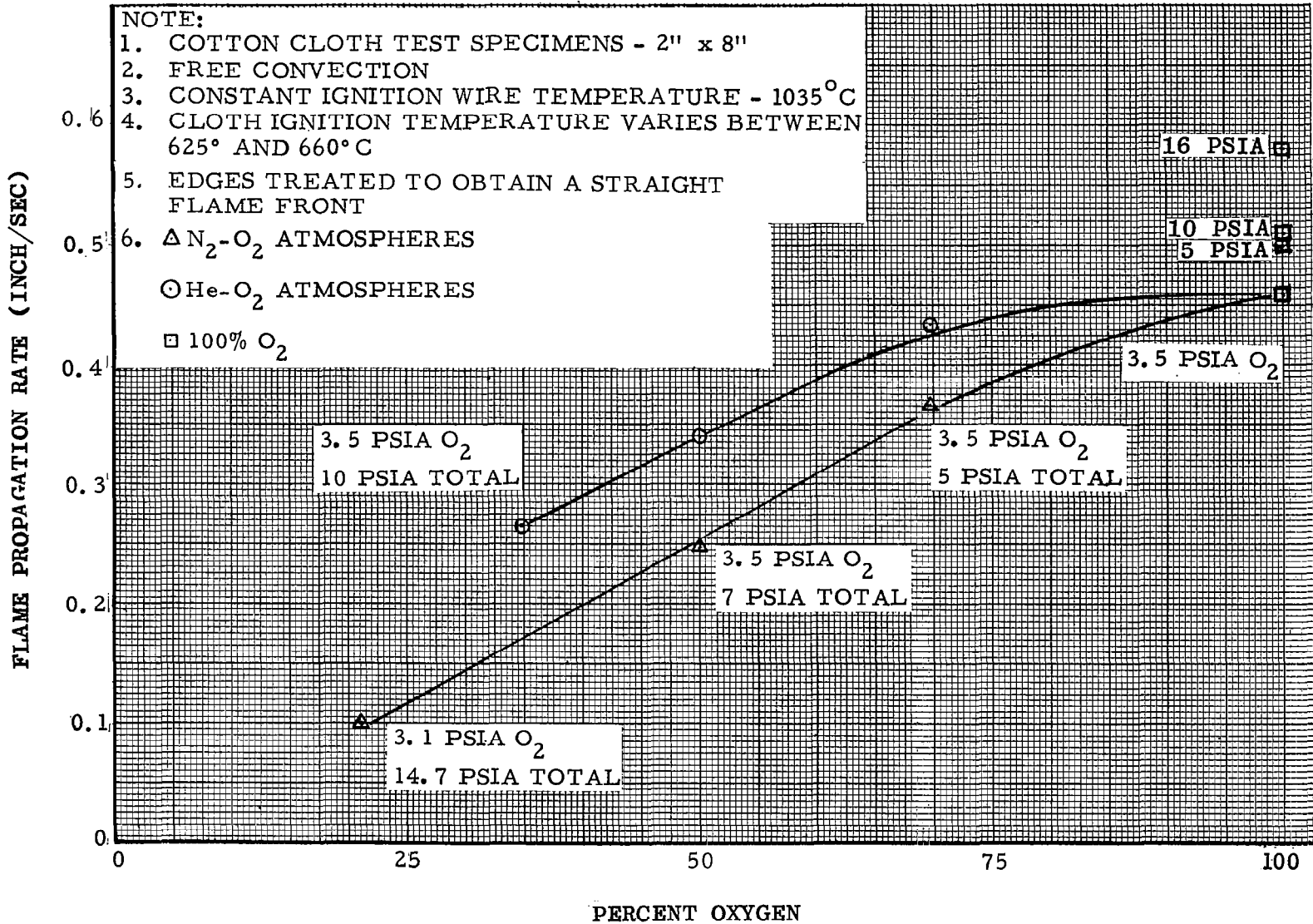


FIGURE 8-20 EFFECT OF INCREASING DILUENT PARTIAL PRESSURE ON FLAME PROPAGATION RATE

TABLE 8-III  
HEAT CAPACITIES OF GAS MIXTURES AT 25°C

Gas mixture	Heat capacity Cal/Mol, °C	Heat capacity Cal/Mol O <sub>2</sub> , °C	*Flame propagation rate, inch/ second
3.5 psia, 100% O <sub>2</sub>	7.0	7.0	0.46
5 psia, 100% O <sub>2</sub>	7.0	7.0	0.49
5 psia N <sub>2</sub> (1.5 psia), O <sub>2</sub> (3.5 psia)	7.0	10.0	0.37
5 psia He (1.5 psia), O <sub>2</sub> (3.5 psia)	6.41	9.2	0.43
7 psia N <sub>2</sub> (3.5 psia), O <sub>2</sub> (3.5 psia)	7.00	14.0	0.25
7 psia He (3.5 psia), O <sub>2</sub> (3.5 psia)	5.99	11.98	0.34
Air N <sub>2</sub> (11.6 psia), O <sub>2</sub> (3.1 psia)	8.26	39.30	0.10
*8 x 2 inch cotton cloth			

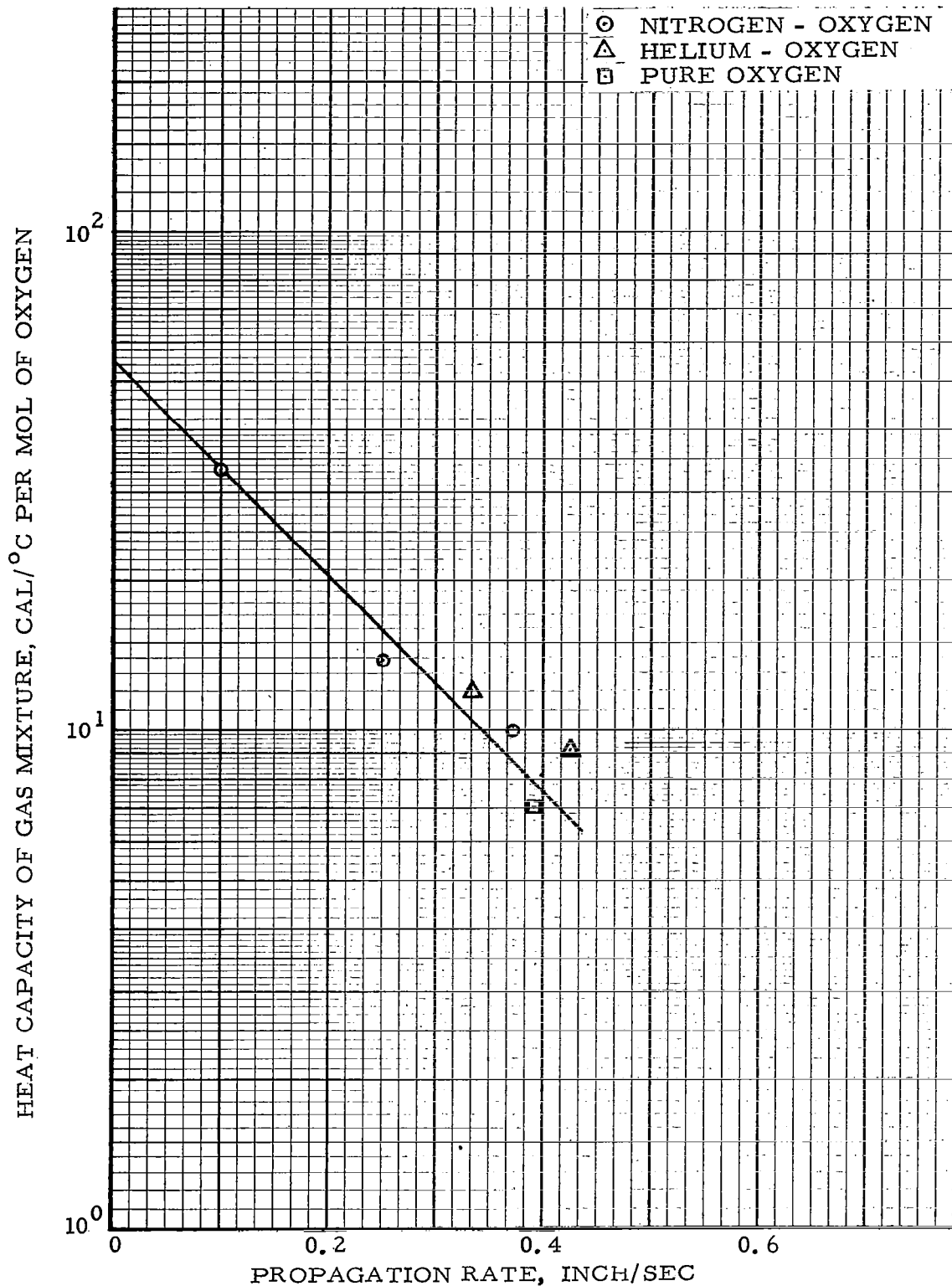


FIGURE 8-21 CORRELATION OF FLAME PROPAGATION RATE IN DIFFERENT GAS MIXTURES

The forced convection data obtained are tabulated in table 8-IV, which includes the free convection data previously reported to permit a direct comparison of the effects of forced convection. Figure 8-22 presents the burning times of the test specimen for normal and forced ventilation conditions.

A comparison of ignition times in the table indicates that forced ventilation produces slightly earlier ignition of the test specimen than free convection. Originally a longer ignition time was anticipated under the assumption that the blower action would significantly lower the temperature of the nichrome wire and thereby retard ignition of the cotton fabric. However, the consistently lower values suggest an interplay of other parameters, such as diffusion, heat transfer, and gas chemical composition. This trend agrees with theory presented earlier in this section.

Figure 8-22 indicates that the burning times decrease for all of the gas mixtures in 50 fpm forced convection. However, the diluent tended to have a greater relative effect under forced convection than under free convection conditions. This is caused by the diluent being forced into the flame front.

Null gravity tests have indicated increased burning time and smaller flames occur because of reduced free convection. Oxygen starvation tests were conducted on the cloth in one g to reproduce this burning behavior. The results of the tests are presented in table 8-V. The starvation of oxygen raises the required temperature for ignition. In the helium-oxygen atmosphere at 7 psia, 2 psia of oxygen was required to duplicate the burning effect produced by 1.5 psia oxygen in the nitrogen-oxygen atmosphere. The cooling effect of helium may have prevented the attainment of ignition temperature at 1.5 psia oxygen concentration or the diffusion rates of the products of combustion may be greater in a helium mixture. Slightly similar burning occurrences to those obtained in null gravity runs 4 and 12 were experienced for the 5.5 psia diluent and 1.5 psia oxygen cases.

It can be speculated from the data on table 8-V and from null gravity test runs 4 and 12, that with minimal free or forced convection and a diluent, a fire may be easier to put out in null gravity than on earth.

The cloth tests in one g indicated that helium-diluent retarded ignition better than nitrogen diluent but the fire propagated faster with helium diluent after ignition for mixtures containing 3.5 psia oxygen. Nitrogen, from the fire burning rate standpoint, would appear the best choice based on one g data. However, based on starvation data and meager null gravity tests for cloth, helium appears more attractive for the null gravity case from a fire propagation standpoint because the fire apparently will tend to extinguish itself more readily than in nitrogen when negligible convection is present. The "critical velocity" analysis using equation (8-11) presented previously would tend to partly substantiate the effect of a retardation of burning at the lower g levels. For example, it is assumed from figure 8-11 that an equivalent flame size of one g can be obtained at  $10^{-6}$  g by providing a forced ventilation rate of about 90 ft/min. The theory suggests that the flame for free convection would be small, if not extinguished, at some levels of reduced gravity. The forced convection in a vehicle must be kept very low to take advantage of the null gravity condition from a fire prevention standpoint. Further null gravity tests are required to correlate and evaluate the results of the oxygen starvation tests, both with and without forced convection.

Table 8-IV

TWO BY TWO INCH COTTON CLOTH BURN DATA FOR  
VARIOUS ATMOSPHERIC COMPOSITIONS WITH FREE AND FORCED CONVECTION

Atmospheric composition	Power input (watts)	Ignition temperature (°C)	Wire temperature (°C)	Free Convection			Forced Convection (50 fpm vertical)		
				Ignition time (sec)	Burning time (sec)	Total burning time (sec)	Ignition time (sec)	Burning time (sec)	Total burning time (sec)
3.5 psia, 100% O <sub>2</sub>	51.3	630	1 035	7.5	12.9	20.4	7.0	9.0	16.0
5 psia, 100% O <sub>2</sub>	47.7	551	1 035	5.5	9.9	15.4	5.2	7.3	12.5
5 psia N <sub>2</sub> (1.5 psia), O <sub>2</sub> (3.5 psia)	47.8	641	1 035	6.6	12.4	19.0	6.2	9.8	16.0
5 psia He(1.5 psia), O <sub>2</sub> (3.5 psia)	47.8	650	880	8.1	11.8	19.9	7.0	8.3	15.3
7 psia N <sub>2</sub> (5.5 psia), O <sub>2</sub> (1.5 psia)	45.8	-	1 035	15.4	45.5	incomplete burning	13.9	28.9	42.8
7 psia He(5.0 psia), O <sub>2</sub> (2.0 psia)	52.3	-	1 035	10.0	22.5	32.5	7.8	17.2	25.0
7 psia N <sub>2</sub> (3.5 psia), O <sub>2</sub> (3.5 psia)	57.1	650	1 035	6.3	12.9	19.2	6.0	11.4	17.4
7 psia He(3.5 psia), O <sub>2</sub> (3.5 psia)	57.1	653	880	10.2	11.6	21.8	9.4	8.2	17.6
10 psia He(6.5 psia), O <sub>2</sub> (3.5 psia)	75.6	647	880	8.1	13.7	21.8	10.1	9.5	19.6
14.7 psia N <sub>2</sub> (11.6 psia), O <sub>2</sub> (3.1 psia)	67.1	647	1 035	9.4	26.0	35.4	9.8	19.0	28.8

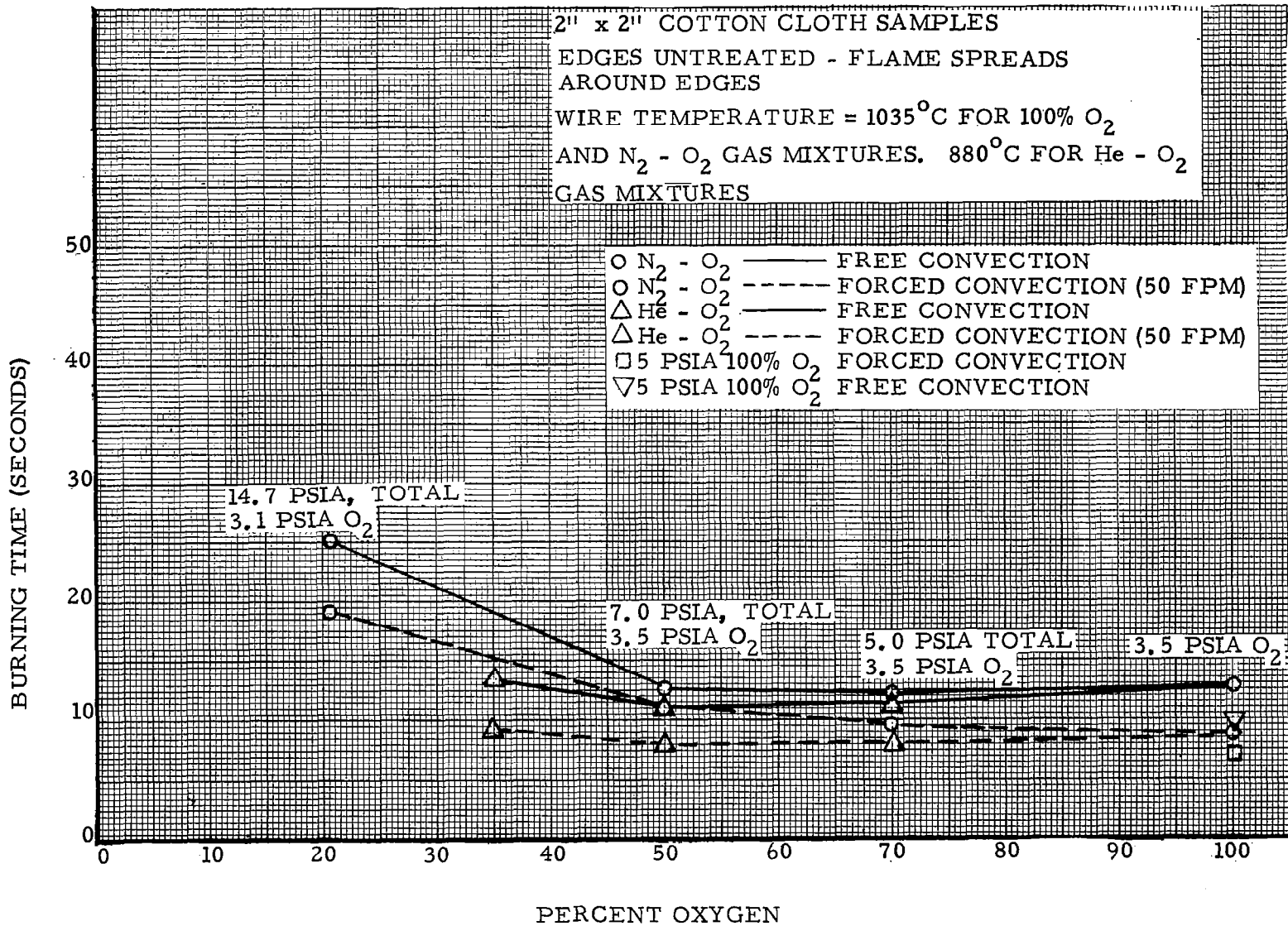


FIGURE 8-22 BURNING TIMES OF COTTON CLOTH IN DIFFERENT ATMOSPHERES WITH FREE AND FORCED CONVECTION

TABLE 8-V  
OXYGEN STARVATION TEST RESULTS FOR TWO BY TWO COTTON CLOTH

Atmosphere psia		Percent oxygen		Wire temperature °C	Ignition time (Sec)	Burning time (Sec)	Total burning time (Sec)	Remarks
N <sub>2</sub>	O <sub>2</sub>	Before	After					
6.0	- 1.0	14	13.1	1035	-	-	-	Wire red, no ignition <sup>(1)</sup>
5.5	- 1.5	21	20.5	1035	15.4	45.5	60.9	Ignition takes place <sup>(2)</sup>
5.0	- 2.0	28	27.1	1035	11.5	28.0	39.5	Fabric shows normal burning
He	- O <sub>2</sub>							
6.0	- 1.0	14	11.2	1035	-	-	-	Wire dull red, no ignition
5.5	- 1.5	21	18.4	1035	-	-	-	Red wire, no ignition, charring
5.0	- 2.0	28	25.6	1035	10.0	22.5	32.5	Fabric ignites, low flame <sup>(2)</sup>

(1) Black charring front moves along fabric; extinguishes itself after 0.25 inches

(2) Fabric ignites; flame about 0.5" high, moves slowly and after 1-1/2 inches extinguishes itself

## Atmosphere Effect on Burning of Insulated Wire in One G

This series of tests was conducted to determine the ignition and burning phenomena that could be expected from a single overloaded insulated wire either alone or in a wire bundle. It was necessary to select a wire-insulation combination that would smoke and burn freely when overloaded before any wire tests could be conducted. This would facilitate observing and recording any differences existing between atmospheric compositions. The three test wires used for preliminary testing were (1) a 20 gage wire with white Teflon insulation, Douglas specification 7869679 Class A, Nickel plated Teflon wire; (2) a 20 gage wire with red TFE insulation produced by Hi Temp Wire Co., Monrovia, California; and (3) a 20 gage wire insulated with cross-linked polyalkene and polyvinylidene fluoride, produced by Raychem Corp. The first two wires tested showed no burning of the insulation. In both instances the insulation curled, peeled off and dropped to the bottom of the flask, without any smoke formation. By contrast, overloading of the third wire resulted first in heavy smoke formation followed seconds later by the burn-through of the wire itself. Since both phenomena were readily reproducible, this wire was selected for use in all future burning tests.

The apparatus used for these tests is shown in figure 8-23. A 12-in. length of wire was installed in the circuit between the two low resistance copper terminals. A constant current of 50 amps at a voltage of 1.0 to 1.5 V was used. The atmospheric pressures and gases previously used for cotton cloth tests were also used for the wire insulation test. Nitrogen and helium were used as diluents. Partial pressure of the diluents varied from zero to 11.6 psia. During the tests measurements were taken of the time required to fill the bell jar with dense smoke (this point was reached when the opposite wall of the bell jar could not be seen) and the time until the glowing wire was free of insulation material. The latter point is hereafter referred to as burn-through. These measurements were selected because of their ease of recording and repeatability. At no time during these tests did an open flame appear and it was impossible to increase the power level to obtain more rapid oxidation. Any further increase would have caused wire melting and premature termination of the test.

Single Wire Data. The desired atmosphere within the bell jar was established after placing the selected wire in test position, as shown in figure 8-23. The partial pressure of oxygen was kept constant at 3.5 psia, and total pressures ranged from 4.1 to 14.7 psia. Helium or nitrogen were added to the basic oxygen content of 3.5 psia to arrive at the desired total pressures. In the case of pure oxygen, the required amounts of oxygen were introduced into an evacuated bell jar. The experiment was then activated by applying 50 amps to the electrical wire. This input was maintained until time readings of smoke density and burn-through had been reported. The results of this effort are tabulated in the first section of table 8-VI (single wires) and plotted in figure 8-24.

Inspection of the figure reveals that the choice of diluent has a significant effect on smoke development and burn-through of an overloaded electrical wire. The time required for a test wire to begin to smoke or burn through a helium-oxygen atmosphere is considerably greater than in a nitrogen-oxygen atmosphere. This difference increases as the amount of diluent is increased with a constant partial pressure of oxygen.

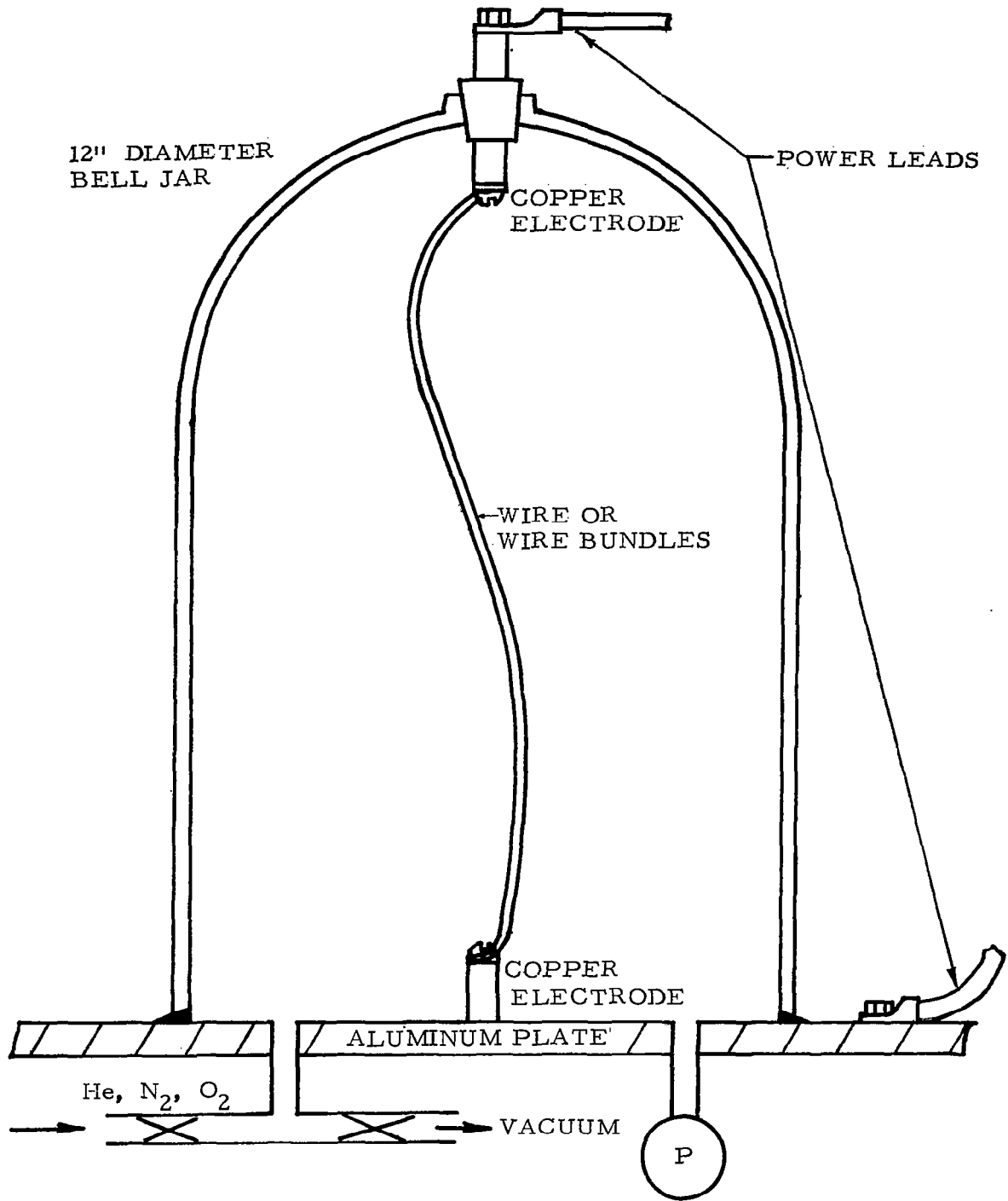


FIGURE 8-23 BELL JAR AND WIRE TEST APPARATUS

TABLE 8-VI

## SMOKE DEVELOPMENT AND BURN-THROUGH DATA FOR INSULATED WIRE SPECIMENS

Atmospheric composition				Single wire		Wire bundle	
				Constant density smoke development	Insulation Burn-Through	Constant density smoke development	Insulation Burn-Through
Total	O <sub>2</sub>	N <sub>2</sub>	He	(Seconds)		(Seconds)	
psia	psia	psia	psia				
3.5	3.5	-	-	23	24	33	36
5.0	5.0	-	-	24	24	42	44
4.1	3.5	0.6	-	20	22	33	37
4.1	3.5	-	0.6	25	28	38	49
5.0	3.5	1.5	-	18	20	36	39
5.0	3.5	-	1.5	25	28	60	80
7.0	3.5	3.5	-	22	28	51	60
7.0	3.5	-	3.5	37	45	76	110
10.0	3.5	6.5	-	25	35	63	74
10.0	3.5	-	6.5	46	62	105	142
14.7	3.1	11.6	-	29	40	75	90
14.7	3.1	-	11.6	57	82	146	no burning

TIME TO COMPLETION OF INSULATION BURN-THROUGH (SEC)  
 TIME TO CONSTANT SMOKE DENSITY (SEC)

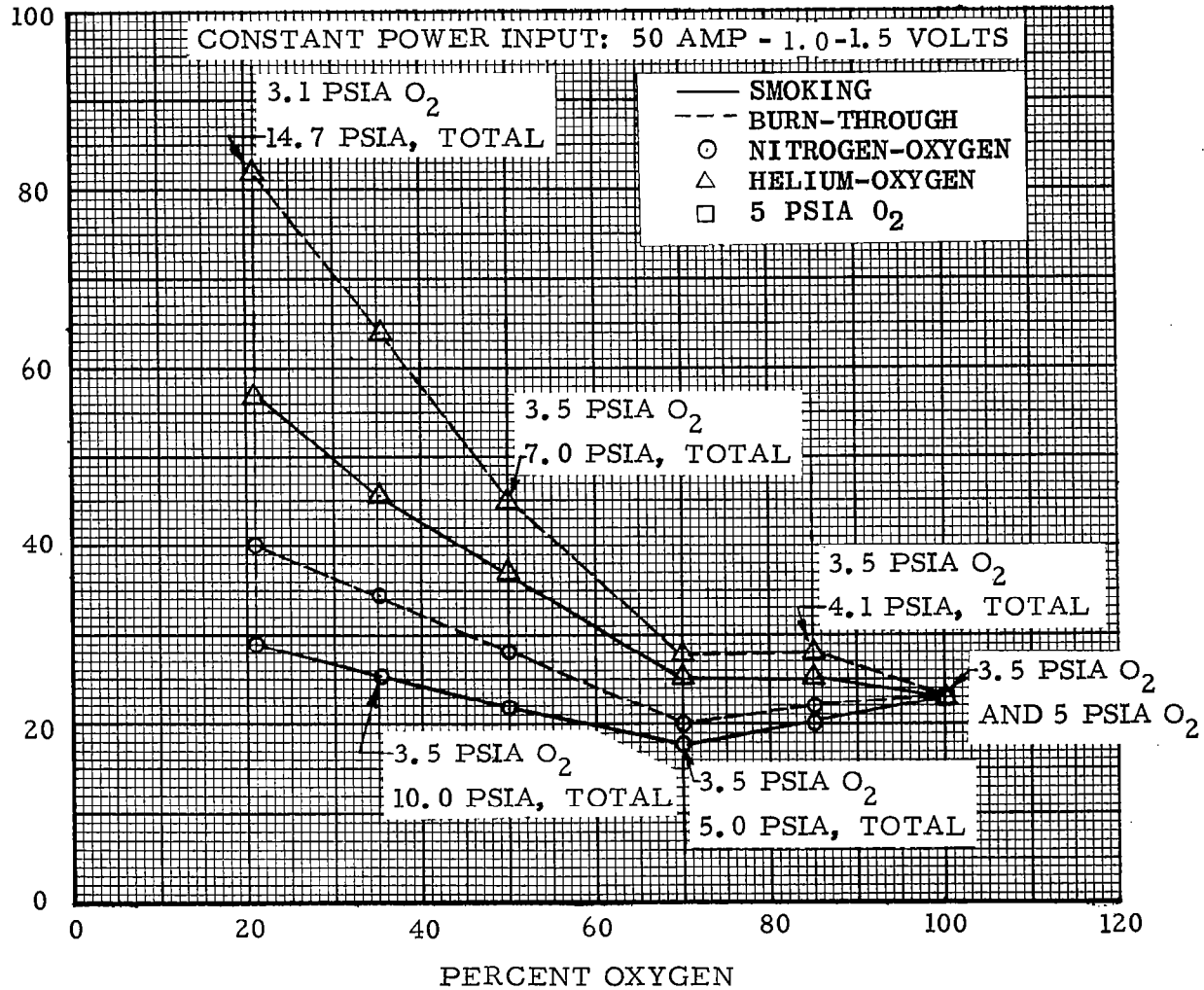


FIGURE 8-24 SMOKING AND BURN-THROUGH OF SINGLE INSULATED WIRE IN DIFFERENT ATMOSPHERES

In the presence of 3.5 psia of pure oxygen, an overloaded electrical wire begins smoking and burning almost simultaneously. As the total pressure of the atmospheric mixture increases by adding nitrogen, the time interval between smoking and burn-through of the wire increases. These time intervals between smoking and burn-through are even more pronounced in helium-oxygen atmospheres, also increasing as the partial pressure of the diluent increases.

More rapid smoke and fire development exists when small amounts of nitrogen (up to 1.5 psia) are added to oxygen than with pure oxygen. Upon addition of further quantities of nitrogen, or helium, the observed trend seems to reverse itself, resulting in longer times for smoke development and burn-through. This apparent bend in the curve, first promoting wire burning at low diluent concentrations and then retarding it, has not been previously observed by either Klein or Kimzey (ref. 8-3 and 8-1). The measurement of the time required until a bell jar appears to be "filled with smoke" is a subjective estimate. However, a series of replications indicated that reproducible values can be obtained. Frisco indicates that this measurement can be reliably used as an index of malfunction of equipment (ref. 8-9).

Wire Bundle Data. - The same Raychem electrical wire used for the testing of individual wires was also used in the preparation of wire bundles. Each bundle consisted of seven wires; the current carrying wire was 12 inches long, the other six wires were 1/8 in. shorter at each end. The current carrying wire was located at the periphery of the bundle rather than at its center. A few exploratory experiments indicated that the position in the bundle of the current carrying wire greatly affects the burning characteristics of the entire unit. The peripheral position was selected because it permitted the most area contact with the atmosphere. All measurements taken during these tests remained identical to the single wire test procedure. Results obtained are shown in figure 8-25. Comparison of the effects of helium-oxygen and nitrogen-oxygen atmospheres indicates the existence of significant differences in the burn-through and smoking times of the wire bundles tested. These differences are more pronounced than those observed with the use of single wires. For instance, at 7 psia, the time required for intense smoking in the presence of helium is 76 seconds compared to 51 seconds in a nitrogen-oxygen atmosphere. This difference of 25 seconds between the two atmospheres for wire bundles corresponds to a 14 second difference for a single wire. Specific times for all tests are shown in the second section of table 8-VI. Additional significant differences can also be seen in the time delay between smoking of the insulation and the actual start of burn-through. In a helium-oxygen atmosphere at 4.1 psia total pressure the time delay between heavy smoking and burning is 11 seconds. This time interval increases to 37 sec in a 10 psia total pressure helium-oxygen atmosphere. At 14.7 psia (3.1 psia oxygen + 11.6 psia helium) an overloaded circuit would only produce heavy smoke; burning of the wire did not take place. It is of course very unlikely that this atmospheric combination will ever be considered for space cabins. However it is of interest to note that with the use of larger size test samples (wire bundles instead of single wires) and higher total pressures 7, 10, 14.7 psia instead of 5 psia, the effects of diluents on burning properties assumes more significance.

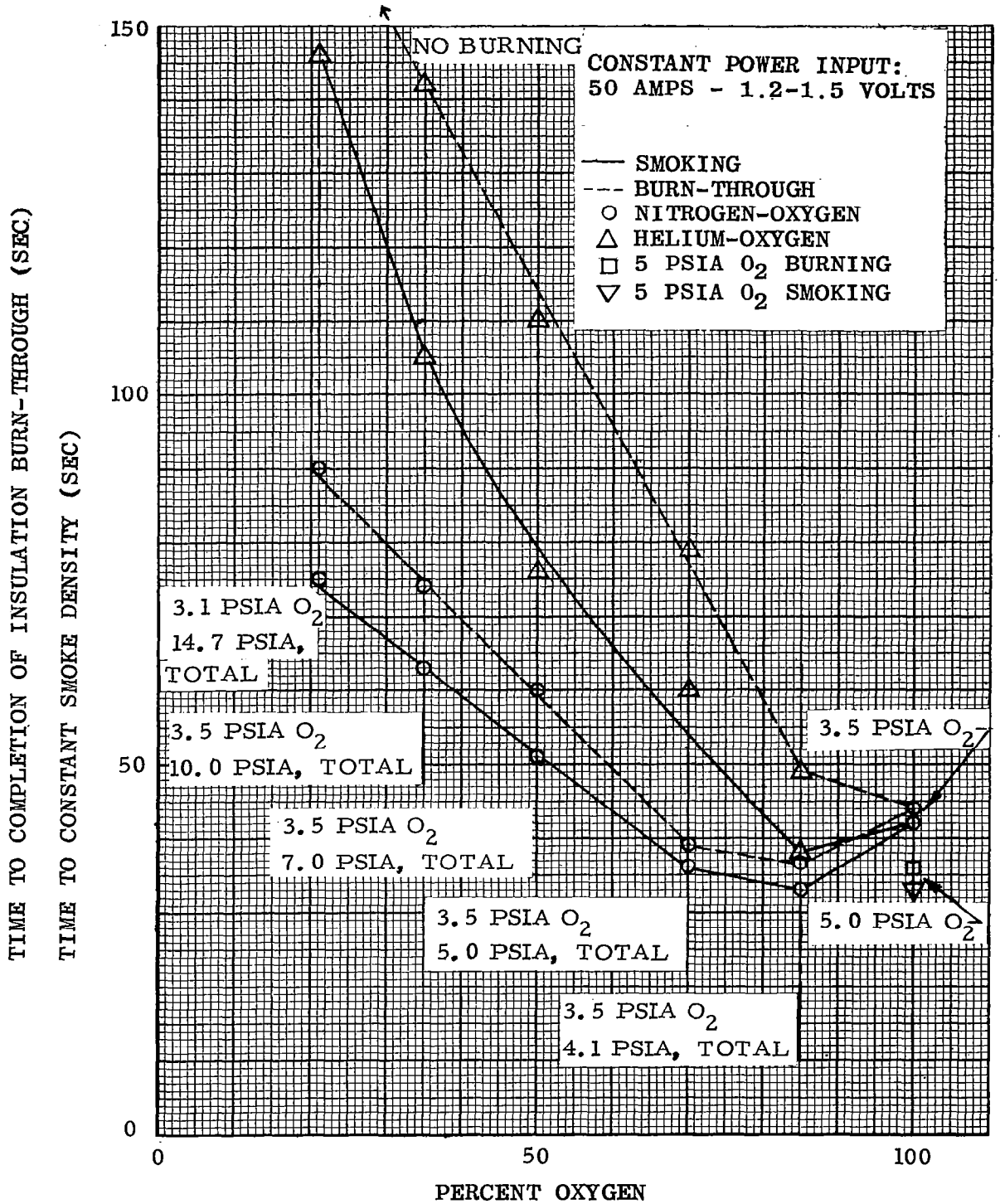


FIGURE 8-25 SMOKING AND BURN-THROUGH OF AN EXPOSED WIRE IN A WIRE BUNDLE IN DIFFERENT ATMOSPHERES

Helium diluent appears more attractive than nitrogen diluent for wire insulation heat up and burning, particularly for the wire bundle at 5 psia and above, and a single wire between 5 psia and 7 psia. The reason the Raychem insulated wire was used in the test was because it produced the most smoke and burned.

Wire and wire bundles aboard spacecraft in null gravity should not create a serious fire problem because, in most instances, wire and wire bundles will be isolated from the cabin behind panels. Several tests in null gravity should be performed to compare the smoke, burning and ignition characteristics of insulated wire and wire bundle specimens. The possibility of smoke creating an explosive or toxic mixture could be a problem.

#### Null Gravity Fire Test Procedure and Data

Further tests were performed at null gravity to obtain additional data. These tests were performed in an Aero Commander in order to establish a test procedure that could be used in future tests in a jet transport aircraft. The duration of null gravity that is obtainable in the Aero Commander is 6-8 seconds whereas 20-30 seconds is available in a KC-135. The 2 in. x 2 in. cotton cloth specimen, previously described, was used during these tests to provide a comparison of zero and one g data. Thirteen tests were performed in the 72 liter Pyrex flasks including nine at 7 psia 50/50 N<sub>2</sub>-O<sub>2</sub> and four at 7 psia 50/50 He-O<sub>2</sub>.

The test equipment previously calibrated and used in one g tests was placed into the special support used in the Aero Commander as shown in figure 8-26. The flask rested on a steel ring covered with 2 inches of foam rubber. It was held rigidly on the ring by a circular yoke of bungee cord with four tails. The tails were stretched to hook into eyelets at the bottom of the frame.

A 16 mm Milliken (DPM - 4/EP) movie camera with a wide-angle lens was used to photograph all of the tests. The camera was mounted at an angle of 45° above the horizontal such that the lens was perpendicular to the direction of flame propagation. The wide-angle lens was required to permit photographing the timer, accelerometer, identification sign, and burning cloth. All tests were photographed in color at a film speed of 200 frames/second. The entire support frame (including flask, camera, and instrumentation) was tethered at each corner to the floor of the aircraft. The tether lines allowed the apparatus to lift approximately 4 inches above the floor during the zero-g portion of the flight. This was intended to minimize the vibrations, accelerations, and small lateral movements expected of the aircraft. The shock load, caused by the support apparatus returning to the floor of the aircraft on pull-out, was absorbed by a 4-in. foam-rubber pad secured to the bottom of the support apparatus.

A control panel was built to indicate, by meter, the voltage and current. A power indicator-light, power-supply connection, and adjustable rheostat were also provided. Power was supplied to the apparatus by connecting the aircraft's 28 Vdc power supply to the control panel. The camera had a

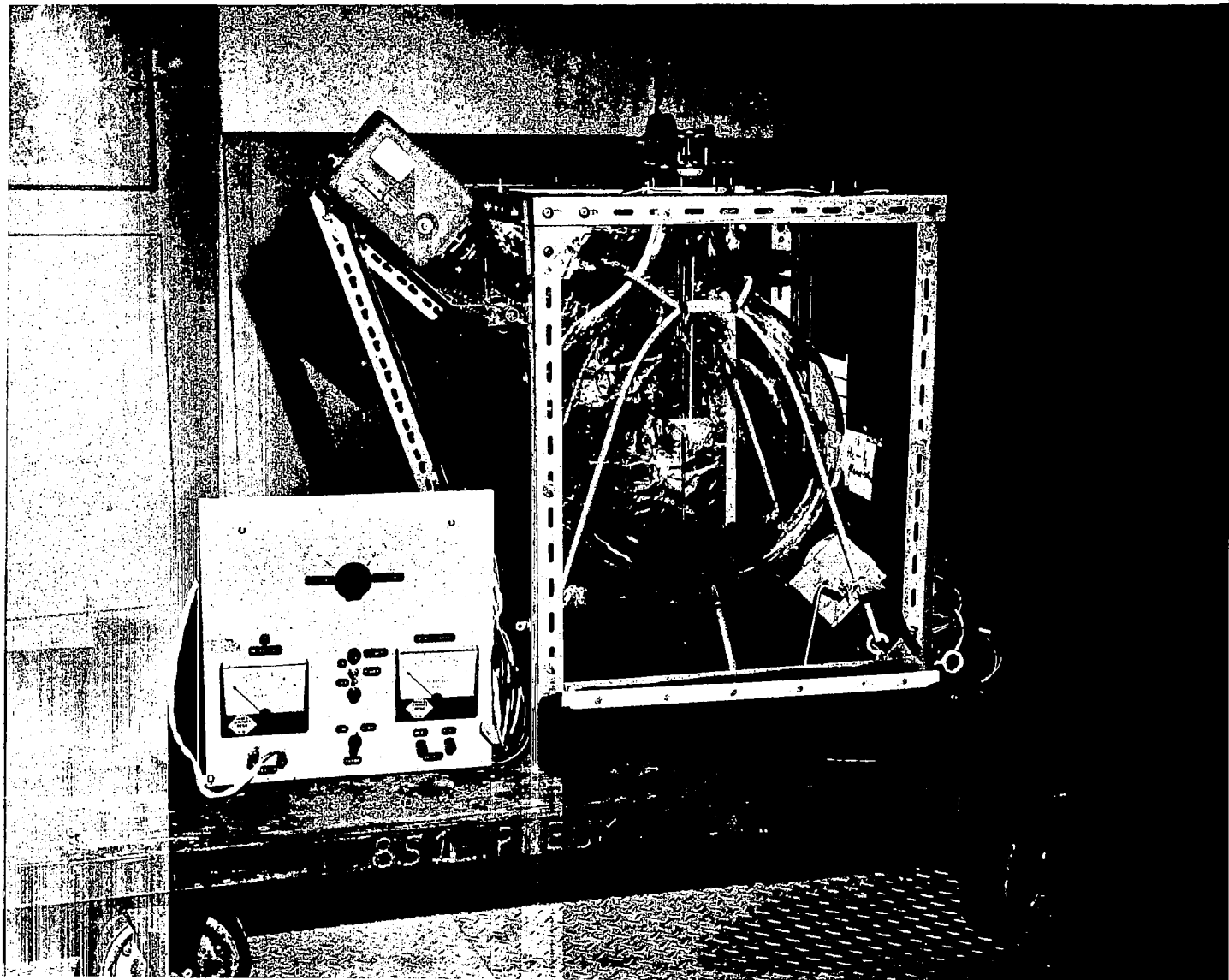


FIGURE 8-26. ZERO GRAVITY TEST APPARATUS

separate switch and was started 2 or 3 sec after power was supplied to the wire and timer. This delay in starting the camera was necessary to prevent overloading the circuit. Each resistance wire was calibrated in the laboratory with a power supply of 28 Vdc. Variable resistors were used to reduce the voltage to the level required to produce wire temperatures of 1035°C and 870°C for the N<sub>2</sub>-O<sub>2</sub> atmosphere and the He-O<sub>2</sub> atmosphere, respectively. During the zero-g flights it was observed that the actual voltage available in the Aero Commander was only 24 v. The test set-up required recalibration for 24 vdc. Null gravity experimental wire temperatures were found to be 870°C for the N<sub>2</sub>-O<sub>2</sub> atmospheres and 750°C for the He-O<sub>2</sub> atmospheres.

The Aero Commander has a zero-g flight time of approximately 6 to 8 sec. To record the maximum information at zero g, it was decided to initiate power to the apparatus 5 seconds before obtaining zero g. The value of 5 seconds was selected on the basis of tests performed at one g, which indicated an average ignition time of 6 sec. Thus, a part of the waiting time before ignition was spent under gravity conditions. This procedure was used for all test runs except runs 12 and 13. In these runs involving helium-oxygen mixtures, the power was actuated 10 and 15 seconds before attaining a low gravity condition.

A total of 13 experiments were conducted of which 8 of the more significant runs are summarized. The first four of these tests are for a mixture of nitrogen-oxygen and the remaining four are for a mixture of helium-oxygen. All tests were conducted in duplicate. Table 8-VII is a tabulation of the data collected from the films of each test run. The upper portion of the table contains all of the flask and atmospheric information pertinent to the tests and the lower portion of the table shows the data obtained from the films. Footnotes following the table provide data concerning the flame characteristics of each test run. It is difficult to compare the collected test data because of the different durations spent at the various gravitation levels while determining the correct flight and test procedure. However, certain consistencies were noted in the test results. The flame burned low and evenly on both sides of the fabric for the nitrogen-oxygen mixture during zero g. The ignition, during null gravity, of the combustible gases evolved during specimen heat-up for the helium-oxygen mixture created a "bright flash" that followed the pattern of the smoke cloud. No flame was visible after the cloud ignited. A char front propagated until the aircraft began to pull-out. A small flame occurred immediately and increased in size as the g level increased to two g's. During the helium-oxygen test, higher heat-source temperatures, difference in convection currents and longer time in null gravity could provide considerably different results. The flames observed at one and two g indicated that the nitrogen-oxygen atmosphere had a higher flame than the helium-oxygen atmosphere for the same gravity level. An evaluation of the ignition flash of the evolved combustibles in nitrogen-oxygen shows a much smaller flash, which remained close to the point of ignition, than the large extended flame observed with helium-oxygen mixtures. Future null gravity tests must evaluate the problem of smoke cloud generation, and the potential hazard of ignition flash propagation for pure oxygen, nitrogen-oxygen and helium oxygen mixtures. The tests should be conducted with varying degrees of ventilation.

Table 8-VII  
NULL GRAVITY TEST RESULTS (page 1 of 2)

Flask	1		2		3		4	
Gas mixture- 7 psi	N <sub>2</sub> -O <sub>2</sub>		N <sub>2</sub> -O <sub>2</sub>		N <sub>2</sub> -O <sub>2</sub>		N <sub>2</sub> -O <sub>2</sub>	
Material	Standard		Standard		Fire-Retardant on Edges Colombo		Fire-Retardant on Edges Mills	
Operator	Colombo		Colombo		Colombo		Mills	
Power input	2.4V-8.4 Amps		2.4V-8.4 Amps		2.4V-8.4 Amps		2.4V-8.4 Amps	
Wire temperature	870°C		870°C		870°C		870°C	
Data from film	G	Time (sec)	G	Time (sec)	G	Time (sec)	G	Time (sec)
At start	1.2	2.5	1.0	2.0 <sup>(1)</sup>	0.2	3.5	1.0	3
Reaching	0	7.5 <sup>(1)</sup>			0	3.9		
Ignites	0	12.0 <sup>(2)</sup>	0.4	12.25	0	8.8 <sup>(1)</sup>	0.1	6.25 <sup>(1)</sup>
			Reaching				Reaching	
			0	13.2 <sup>(2)</sup>			0	6.4 <sup>(2)</sup>
Loosing	0	13.3 <sup>(3)</sup>	0	20.5	0	10.4	0	13.1
Time in zero g		5.8		7.3		6.5		5.7
Reaches	1	14.6 <sup>(4)</sup>	1	20.8 <sup>(3)</sup>	1	11.0 <sup>(2)</sup>	1	14.5 <sup>(3)</sup>
Reaches	2	20.5 <sup>(5)</sup>	2	23.5	2	14.0 <sup>(2)</sup>	1.5	15.75 <sup>(3)</sup>
Flame out		24.0		23.5		20.0	2	19.0
Cinder out		28.3				23.4		
Burning time in zero g		1.3		7.3 <sup>(4)</sup>		1.6		6.7
Burning time		12.0		11.25		11.2		12.75

Notes:

Run 1 -- (1) Smoking starts; (2) Gases ignite in large flame for five film frames (1/40 sec) only, fabric then burns with low flame; (3) Flame remains low; (4) (5) Flame very high at 1 to 2 g's.

Run 2 -- (1) First to 2 g and returns to 1 g at 11 sec; small flash on one end at 11.8 sec and 0.7 g; (2) While in zero g flame low; (3) Flame high and bright in 1 to 2 g's; (4) The whole burning sequence can be observed while in zero g.

Run 3 -- (1) Burning in zero g with low flame, (2) Flame high and bright at 1 to 2 g's.

Run 4 -- (1) Fabric ignites before reaching zero g with brilliant flame, which lasts for five film frames (1/40 sec); (2) When zero g is reached, flame is low, burns evenly on both sides of fabric (3) At 1 and 2 g's flame is bright and high, with pulsing effect evident.

Table 8-VII (page 2 of 2)

Flask	9		10		12		13	
Gas mixture- 7 psi	He-O <sub>2</sub>		He-O <sub>2</sub>		He-O <sub>2</sub>		He-O <sub>2</sub>	
Material	Standard		Standard		Fire-Retardant on Edges		Fire-Retardant on Edges	
Operator	Mader		Colombo		Mader		Mills	
Power input	2.4V-8.4 Amps		2.4V-8.4 Amps		2.4V-8.4 Amps		2.4V-8.4 Amps	
Wire temperature	750°C		750°C		750°C		750°C	
	Start of Test: 10 Sec Before Going into Zero G				Start of Test: 15 Sec Before Going into Zero G			
Data from film	G	Time (sec)	G	Time (sec)	G	Time (sec)	G	Time (sec)
At start					0	10	0	9.2 <sup>(1)</sup>
Reaching			0	4.2	0	10		
Ignites					Glowing		Glowing	
					0	12 <sup>(1)</sup>	0	12.8
					0	13.75 <sup>(2)</sup>		
Loosing	0	7.5	0	11.7	0	15.6	Loosing	
							0	16.8
							Ignition	
	2	13.7 <sup>(1)</sup>	1.5	14.9 <sup>(1)</sup>			1	18.1 <sup>(2)</sup>
Time in zero g					Reignition			
					0.25	15.7 <sup>(3)</sup>		
Reaches			2.0	(2)				
Flame out	2	23.0	2.0	23.7	2	23.7	1-1/2	27.2
Cinder out		26.7		26.3	1-1/4	26.7		
Burning time in zero g		0		0		5.6		4.0 Glowing- not burning
Burning time		9.3		8.8		8.0		9.1

Run 9 -- (1) It took about 14 sec to ignition, by that time zero g had been passed; to be taken into consideration in Runs 12 and 13.

Run 10 -- (1) Sample ignite after 15 sec, after passing zero g; in 12 to 13 runs, the tests will be started 10 and 15 sec before zero g is approached; (2) After ignition at 1.5 g, very bright burning is noted.

Run 12 -- (1) Wire glows at 12 sec; (2) Ignition three frames later, no more burning at the wire, but burning in the smoke cloud for five film frames (1/40 sec); flame disappears while still at zero g and only char front propagates about 1/2 in; (3) Bright flame builds up after leaving zero g.

Run 13 -- (1) No flame front develops, only charring front propagates while in zero g; (2) Bright flame builds up after leaving zero g.

A pictorial presentation of two of the best test runs are shown in figure 8-27 (test run 4 for the nitrogen-oxygen atmosphere and test run 12 for the helium-oxygen atmosphere). Samples for both runs had the edges treated with a flame-retardant solution. Figure 8-27 shows the ignition and burning at zero, one, and two-g levels. It should be noted that the ignition time for helium-oxygen is considerably longer than that for nitrogen-oxygen. This was also observed during the one-g tests. Also, the flame in nitrogen-oxygen is considerably higher during all phases of the flight which was observed in all test runs. These figures are selected frames from the motion picture records of these test runs.

Table 8-VIII is a summary of trends observed during all of the laboratory tests and those tests conducted in the Aero Commander. These data are incomplete because of the limited number of test runs conducted and because of the short duration of zero g available in the Aero Commander. Longer periods of zero g, such as could be obtained in a jet transport, could demonstrate more conclusively the ignition, burning, and extinguishing phenomena. Further null gravity tests are particularly needed to evaluate the effect of different convection rates on burning rate and ignition flash hazard for pure O<sub>2</sub>, and N<sub>2</sub>-O<sub>2</sub> and He-O<sub>2</sub> mixtures at 5, 7 and 10 psia total pressures. These data can be used to help better understand the fire problem in the selection of an atmosphere and to define analytical techniques that can be used to extrapolate one g data to null gravity conditions.

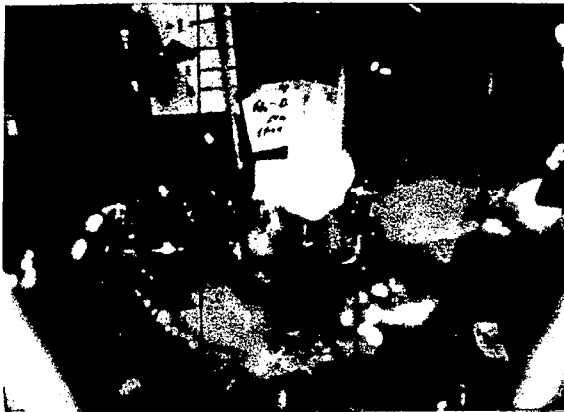
TABLE 8-VIII  
BURNING TRENDS IN ONE G AND NULL GRAVITY

<u>Test Conditions</u>	<u>N<sub>2</sub>-O<sub>2</sub> Atmospheres 7 Psia (50% N<sub>2</sub>-50% O<sub>2</sub>)</u>	<u>He-O<sub>2</sub> Atmospheres 7 Psia (50% He-50% O<sub>2</sub>)</u>
Laboratory one g	At constant power- earlier ignition	Faster propagation rate
	At constant wire tem- perature essentially equal ignition times	At equivalent power much longer ignition time  Shorter burning time
Aero Commander Zero g	Ignition and flame front propagation	Char-front propagation only
One g	Burning above and below cloth  Higher flame	Smaller flame than for N <sub>2</sub> -O <sub>2</sub>
Two g	Higher flame with pulsing effect of flame	Higher flame than for one g He-O <sub>2</sub> but smaller than for N <sub>2</sub> -O <sub>2</sub> at two g





TIME: 5.83  
(SEC) SMOKE BEFORE IGNITION  
AT NULL GRAVITY



6.25  
IGNITION FLASH AT NULL GRAVITY

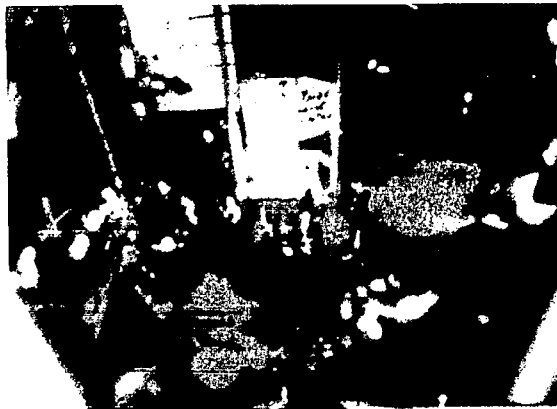


8.98  
NULL GRAVITY BURNING

14.23  
ONE G BURNING

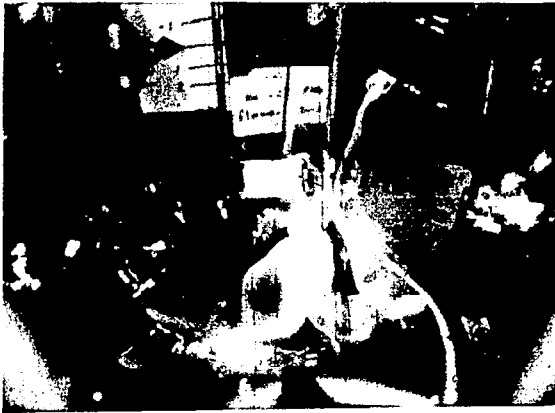


16.38  
TWO G BURNING



RUN NO. 4	ATMOSPHERE:	NITROGEN AND OXYGEN
	PRESSURE:	7 psia TOTAL (3.5 psia N <sub>2</sub> & 3.5 psia O <sub>2</sub> )
	POWER INPUT:	2.4 VOLTS, 8.4 AMPS
	WIRE TEMPERATURE:	870°C

FIGURE 8-27 REPRESENTATIVE NULL GRAVITY TEST OF COTTON CLOTH -  
SELECTED ENLARGED FRAMES FROM RUNS 4 & 12



8.98  
TIME:  
(SEC) SMOKE BEFORE IGNITION  
AT NULL GRAVITY



13.18  
IGNITION FLASH AT NULL GRAVITY



15.28  
CHAR FRONT PROPAGATION  
AT NULL GRAVITY

16.33  
ONE G BURNING



19.48  
TWO G BURNING



RUN NO. 12	ATMOSPHERE:	HELIUM OXYGEN
	PRESSURE:	7 psia TOTAL (3.5 psia He & 3.5 psia O <sub>2</sub> )
	POWER INPUT:	2.4 VOLTS, 8.4 AMPS
	WIRE TEMPERATURE:	750°C

FIGURE 8-27 (Concluded) REPRESENTATIVE NULL GRAVITY TEST OF COTTON CLOTH --  
SELECTED ENLARGED FRAMES FROM RUNS 4 & 12

## CONCLUSIONS AND RECOMMENDATIONS

A cabin atmosphere must be selected following consideration of numerous criteria. A vehicle designer normally selects the cabin atmosphere mixture and pressure level based on a number of requirements such as physiology, low weight penalty, development lead time, cost, hardware availability, compatibility with other vehicles, simplicity of hardware, and fire prevention. Performance during both ground checkout and flight must be considered.

In most instances flammable materials and liquids must be eliminated or, if used, isolated from the cabin atmosphere and ventilation system. Logic indicates that even using the utmost care, the materials, the power source, and ventilation rate aboard a manned spacecraft could potentially cause some material or fluid to ignite and fire to propagate, in any atmosphere.

Some of the analysis and tests on atmosphere selection conducted to date indicate the following:

1. Ignition temperature for a given material is affected very little by gravity and forced convection.
2. The ignition temperature is independent of the amount and nature of atmosphere diluent. The ignition temperature of cotton cloth will decrease in pure oxygen as the oxygen pressure in the atmosphere is increased in the 2.5 psia to 10 psia pressure range.
3. The type of diluent does affect the time to ignition, the energy required to obtain ignition, and the burning rate. Helium-oxygen mixtures require a higher power level or a longer time to ignite than nitrogen-oxygen or pure oxygen, because of the increased heat losses from the ignition source caused by helium's higher thermal conductivity.
4. The presence of an inert diluent in the atmosphere reduces the flame propagation rate for the cotton cloth for the majority of pressures tested. Nitrogen diluent had a greater effect on the reduction of flame propagation rate in one g than helium, with and without forced convection. The burning rate in pure oxygen at 3.5 psia is more than four times faster than in air. Forced ventilation increases the burning rates in all of the atmospheres tested.

5. The insulated wire and wire bundles tested in one g took longer to heat up and the insulation to burn through, in helium-oxygen than in nitrogen-oxygen under all test conditions due to increased heat losses caused by helium's high thermal conductivity. The addition of nitrogen below the 7 psia total pressure condition had a small effect on the time to burn-through as compared to 3.5 psia pure oxygen. The wire when bundled, showed increased time to smoke and burn-through under all atmospheric conditions at constant power input.
6. Flash ignition of the combustible smoke built up during null gravity tests resulted for both mixtures. Tests in  $N_2-O_2$  and others in  $He-O_2$  at 7 psia showed a smaller, more confined flash for a nitrogen-oxygen mixture. In null gravity, the build-up of a smoke cloud could be a problem for pure oxygen and any oxygen-diluent mixture. It can be speculated that because of the tendency of helium to suppress the ignition of the material, more smoke will result and a larger ignition flash could result. A small amount of ventilation could be used to remove excessive smoke. However, ventilation would increase the burning rate after ignition. More null gravity tests are required to evaluate ignition flash in pure  $O_2$ , and  $He-O_2$  and  $N_2-O_2$  mixtures.
7. Moving picture records taken during flight tests at one g, two g and null gravity indicated that the flame was always larger for the  $N_2-O_2$  mixture than for  $He-O_2$ . Only a char front existed for the cotton cloth in null gravity for  $He-O_2$  at 7 psia. Analysis and tests appear to indicate that a fire could extinguish itself in null gravity without forced convection. Helium should be more attractive from an ignition retardation standpoint than nitrogen, since more energy or time-energy is necessary for ignition. The flame if started may also extinguish more readily in null gravity without high ventilation rates. High ventilation rates in most cases should propagate the fire in either diluent. Null gravity tests are required with varying ventilation rates to determine the effect of forced convection on the burning phenomena. The effects on the burning phenomena with different materials should also be tested in null gravity and compared to one g baseline tests.
8. Fire extinguishing techniques that appear promising include (1)  $CO_2$ , cyrogenic nitrogen, or the cabin inert diluent for putting out small fires and (2) inert diluent or vacuum purge for a larger fire (reference 8-10). The crew must use oxygen masks, an alternate compartment or space suits during an inert diluent purge. A vacuum purge would of course require the crewman to be in a space suit or adjacent compartment. It is important to use extinguishing agents that are not toxic to the crewman, unless they are expended at a level below established crew danger levels and may be removed by the onboard life support systems.

For example, CO<sub>2</sub> in small quantities can readily be removed by the onboard life support system. If a regenerative CO<sub>2</sub> removal system is used, CO<sub>2</sub> level in the cabin can be controlled. Cryogenic nitrogen, on the other hand, could well be one of the normal onboard atmospheric supply constituents. Nitrogen and CO<sub>2</sub> are the fire prevention fluids used for the Douglas Space Cabin Simulator Program. A fire was easily put out in a 7 psia N<sub>2</sub>-O<sub>2</sub> atmosphere with CO<sub>2</sub> while the laboratory was operated by a crew of four. The toxins generated by the small fire and CO<sub>2</sub> were successfully controlled by the onboard life support systems.

## REFERENCES

- 8-1. Kimzey, J. H., W. R. Downs, C. H. Eldred, and C. W. Norris, Flammability in Zero-Gravity Environment, NASA Manned Spacecraft Center, Houston, Texas, NASA Technical Report R-246.
- 8-2. Huggett, Clayton, et al., The Combustibility of Materials in Oxygen-Helium and Oxygen-Nitrogen Atmosphere, June 1966, to be released by USAF School of Aerospace Medicine, Brooks Air Force Base, Texas.
- 8-3. Klein, H. A., The Effects of Cabin Atmospheres on Combustion of Some Flammable Aircraft Materials, WADC Technical Report 59-456, April 1960.
- 8-4. Kreith, F., Principles of Heat Transfer, 2nd Edition, International Textbook Co., Scranton, Pa., 1965.
- 8-5. Adelberg, M., S. H. Schwartz, Heat Transfer Domains for Fluids in a Variable Gravity Field with Some Applications to Storage of Cryogens in Space, Advances in Cryogenic Engineering, Vol II, 1966, (K. D. Timmerhaus, Ed.), Plenum Press.
- 8-6. Alvares, N. J., The Effect of Pressure on Ignition by Thermal Radiation, WSCI 66-27, 1966 Spring Meeting, Western States Section The Combustion Institute, Denver Research Institute, April 1966.
- 8-7. Fisher, H. D., M. Gerstein, Investigation of Materials Combustibility and Fire and Explosive Suppression in a Variety of Atmospheres, Summary Report No. SN-6401, Dynamic Sciences Corporation, Monrovia, California, May 1966.
- 8-8. Chianta, Maria A., and A. M. Stoll, Effect of inert Gases on Fabric Burning Rate, presented to Aerospace Medical Association, April 1966, Las Vegas, Nevada.
- 8-9. Frisco, L. J. and Mathes, Evaluation of Thin Wall Spacecraft Electrical Wiring, General Electric Company, Schenectady 5, New York, September 1965, Contract No. NAS 9-4549.
- 8-10. Roth, M. R., M. D., Space Cabin Atmospheres, Part II - Fire and Blast Hazards, NASA Scientific and Technical Information Division, nass SP-48, 1964, Washington, D.C.

